

ResearchOnline@JCU

This file is part of the following reference:

Galbraith, Shaun Colin (2011) *A study of struvite nucleation, crystal growth and aggregation*. PhD thesis, James Cook University.

Access to this file is available from:

<http://researchonline.jcu.edu.au/39332/>

The author has certified to JCU that they have made a reasonable effort to gain permission and acknowledge the owner of any third party copyright material included in this document. If you believe that this is not the case, please contact

*ResearchOnline@jcu.edu.au and quote
<http://researchonline.jcu.edu.au/39322/>*

**A STUDY OF STRUVITE NUCLEATION, CRYSTAL GROWTH
AND AGGREGATION**

Thesis Submitted by

Shaun Colin Galbraith, BE (Hons)

November 2011

For the Degree of Doctor of Philosophy

In the School of Engineering and Physical Sciences

James Cook University

STATEMENT OF ACCESS

I, the undersigned, author of this work, understand that James Cook University will make this thesis available for use within the University Library and, via the Australian Digital Theses network, for use elsewhere

I understand that, as an unpublished work, a thesis has significant protection under the Copyright Act and I do not wish to place any further restriction on this work.

Signature

Date

STATEMENT OF SOURCES

DECLARATION

I declare that this thesis is my own work and has not been submitted in any form for another degree or diploma at any University or other institution of tertiary education. Information derived from the published or unpublished work of others has been acknowledged in the text and a list of references is given.

Signature

Date

STATEMENT ON THE CONTRIBUTION OF OTHERS

This research was conducted under the supervision of Dr. Philip A. Schneider and he therefore has made significant contributions to all areas of the project. The co-supervisor was Dr. Madoc Sheehan; his contribution was administrative and not relevant to the content of this dissertation.

Prof. Adrian Flood contributed to the experimental methodology and parameter estimation work in Chapters 6 and 7.

Chapters 1 to 4 were proof-read and edited for grammatical consistency by Ms. Wendy Smith of “Jewel See Editing”.

Financial support was provided from the School of Engineering and Physical Sciences for my scholarship. Incitec Pivot contributed to a collaborative grant with James Cook University that facilitated the purchase of laboratory equipment and modelling software. Travel to conferences and other institutions for research work was paid for by grants from the Graduate Research Scheme.

Signature

Date

ACKNOWLEDGMENTS

The majority of my acknowledgement must go to my supervisor, Dr. Philip A. Schneider. At the end of this process I feel confident as an independent researcher. Acknowledgment is also due to the rest of my supervisory team; my co-supervisor, Dr. Madoc Sheehan and my research student monitor, Dr. Shaun Belward.

A major part of this project was the experimental work conducted during a three month trip to Suranaree University of Technology in Nakhon Ratchasima, Thailand. I am indebted to Prof. Adrian Flood for his guidance and convincing me that the experimental and modelling results I gathered were actually really quite good. Acknowledgement is due for P'Sukanya and P'James for helping me with all my laboratory needs and P'Jack for driving me to campus every day. Acknowledgement unrelated to my PhD work is given to Nikom, Tor and Tle for the many bottles of 'Beer Leo' we consumed. The trip was a highlight of my PhD studies and I count you all as friends.

Many thanks are due to my parents for their continued support. Thank you to Carmen for always being there and offering to help. Thank you to my friends and in particular my old housemates Russ and Bryan.

Finally, a very large thank you to all the funding bodies that contributed to the research: the School of Engineering and Physical Sciences, Incitec Pivot and the Graduate Research Scheme.

ABSTRACT

This research focused on the development of a rigorous process model of struvite crystallisation in order to address the issue of nutrient removal and recovery from wastewater. The model is based on a dynamic mass balance, coupled to a population balance, incorporating nucleation, crystal growth and aggregation rate mechanisms. These rate mechanisms were dependent on the thermodynamic driving force known as the saturation index. Non-ideal solution thermodynamics were employed to accurately describe the synthetic solutions employed in the experimental studies, enabling determination of the saturation index. Each rate mechanism had two uncertain parameters, namely the rate coefficient and the order of the power-law relationship. The model incorporated a discretised population balance that enabled the simultaneous coupling of nucleation, growth and aggregation mechanisms to the material balance.

The model equations were solved using gPROMS process simulation software.

A series of seeded, batch experiments covering a saturation index range of 0.75-0.25 was carried out to generate a data set that was used to regress the unknown kinetic rate parameters, thus completing the model description. The regressed parameters are presented below. Where, k_i is the rate coefficient for mechanism i and n_i is the order of the power-law relationship to saturation index. The parameters apply to atmospheric pressure and the temperature at which the experiments were conducted, being $29.3 \pm 0.6^\circ\text{C}$.

Mechanism	k_i	n_i
Aggregation	$(3.72 \pm 0.014) \times 10^{-7} L/min$	5.26 ± 0.004
Crystal Growth	$12.49 \pm 0.061 \mu m/min$	5.06 ± 0.005
Nucleation	$(8.50 \pm 0.076) \times 10^7 1/L.min$	1.68 ± 0.014

A number of innovations and novel contributions resulted from this work.

Innovations:

- Application of rigorous process modelling to the issue of nutrient recovery, leading to;
 - embedded rigorous thermodynamics within a process modelling framework
 - improved understanding of the dynamic performance of nutrient recovery systems, based on struvite precipitation
 - a better understanding of the interplay of the mechanisms of nucleation, crystal growth and aggregation
 - performance assessment of nutrient recovery
- A framework is now in place to refine the model, through the addition of extra experimental data and/or to consider additional effects, such as hydrodynamics

Novelty:

- A hybridisation of the two-term and three-term discretised growth rate equation used in the DPB (Discretised Population Balance), leading to;
 - a solution method for a dynamic MSMPR (Mixed Suspension Mixed Product Removal) crystalliser that conserves particle volume without requiring an adjustable discretisation scheme
 - a description of the true nucleation rate, removing the need to guess a source function

This research provides a modelling framework for designing struvite crystallisation systems from the position of understanding the kinetic mechanisms responsible for producing the crystal product. Using this approach will result in a better understanding of currently employed struvite crystallisers so that improvements can be made. More importantly, new designs can be tested and optimised through process modelling, instead of through the construction and operation of costly pilot plants.

TABLE OF CONTENTS

STATEMENT OF ACCESS	i
STATEMENT OF SOURCES	ii
STATEMENT ON THE CONTRIBUTION OF OTHERS.....	iii
ACKNOWLEDGMENTS.....	iv
ABSTRACT.....	v
TABLE OF CONTENTS.....	ix
LIST OF FIGURES.....	xvii
LIST OF TABLES.....	xxv
Chapter 1 - Introduction	1
1.1 Research Background.....	1
1.1.1 Phosphorus Recovery.....	2
1.1.2 Struvite Crystallisation	3
1.2 Research Objectives.....	4
1.3 Structure of Thesis	5
Chapter 2 - Struvite Nucleation Studies	9
2.1 Introduction	9
2.2 Solution Thermodynamics	9
2.2.1 Supersaturation	10
2.2.2 Speciation.....	12

2.2.3	<i>pH</i> specification or Charge Balance.....	15
2.2.4	Activity Models and Ionic Strength.....	15
2.2.5	Numerical Implementation.....	17
2.2.5.1	Numerical Difficulties.....	18
2.3	Nucleation.....	18
2.3.1	Induction Time.....	19
2.3.2	Previous Work.....	21
2.4	Experimental Method.....	22
2.5	Results and discussion.....	24
2.6	Conclusions.....	27
2.7	Key Points from Chapter Two.....	27
Chapter 3 - A Description of Struvite Nucleation, Growth and Aggregation using the Population Balance.....		
3.1	Introduction.....	29
3.2	Previous Work on Precipitation Kinetics.....	30
3.3	Previous Work on Crystal Growth Kinetics.....	31
3.4	The Population Balance.....	32
3.4.1	Struvite Precipitation and the Population Balance.....	33
3.4.2	Moments of the Particle Size Distribution.....	36
3.4.3	Population Balance with Aggregation.....	37
3.5	Discretised Population Balance Equation.....	38

3.5.1	Uniform Discretisation	39
3.5.2	Geometric Discretisation	40
3.5.3	Importance of the First Interval	43
3.5.4	Uniform Discretisation Performance	44
3.5.5	Extracting the Rates	45
3.6	Results and Discussion	47
3.7	Conclusions	55
3.8	Key Points from Chapter Three.....	55
Chapter 4 – Development of a Struvite MSMPR Process Model.....		57
4.1	Introduction	57
4.2	Development of the Process Model	58
4.2.1	Solution Thermodynamics	59
4.2.2	Kinetics.....	60
4.2.2.1	Nucleation Rate.....	61
4.2.2.2	Crystal Growth Rate.....	62
4.2.2.3	Aggregation Kernel.....	63
4.2.3	Population Balance	65
4.2.3.1	Adjustable Discretised Population Balance	65
4.2.3.2	A Hybrid Approach to the DPB.....	66
4.2.4	Mass Balance.....	70

4.3	Results and Discussion	71
4.3.1	Solution Thermodynamics Validation	71
4.3.2	Dynamic Operation	73
4.3.3	Importance of non-ideal thermodynamic behaviour	75
4.3.4	Implications for Process Design	77
4.4	Conclusions	80
4.5	Key Points for Chapter Four	81
Chapter 5 - Stochastic Simulation of a Struvite Crystallisation Model and its Application to Uncertainty Propagation and Control.....		83
5.1	Introduction	83
5.2	Deterministic Uncertainty Propagation	84
5.3	Stochastic Simulations	85
5.3.1	Variables Investigated in the Stochastic Simulations	85
5.3.2	Probability Distributions used in Stochastic Simulations.....	86
5.4	Results and Discussion	87
5.4.1	Base Case Results	88
5.4.2	Number of Stochastic Simulations	88
5.4.3	Kinetic Uncertainty Results	90
5.4.4	Nutrient Load Uncertainty Results.....	94
5.4.5	<i>pH</i> Control	99
5.5	Conclusions	101

5.6	Key Points from Chapter Five.....	102
Chapter 6 - Experimental Methodology		103
6.1	Introduction	103
6.2	Review of Experimental Methods.....	103
6.2.1	Particle Size Distribution (PSD) Measurement.....	104
6.2.2	<i>pH</i> Measurement	105
6.2.3	Concentration Measurement.....	106
6.2.4	Reactor Configuration	107
6.2.4.1	Using Batch Experimental Data to Predict Continuous Crystallisation.....	107
6.3	Experimental Methodology	108
6.3.1	Goals of the Experimental Methodology.....	109
6.3.2	Experimental Setup.....	110
6.3.3	Seed Preparation.....	111
6.3.4	The Electrical Sensing Zone Method.....	112
6.3.5	Initial Saturation Index.....	113
6.3.6	Sampling Procedure	114
6.4	Results and Discussion	115
6.4.1	Hydrodynamic Considerations.....	116
6.4.2	PSD Accuracy.....	117
6.4.3	<i>pH</i> Repeatability	119

6.4.4	PSD Repeatability	122
6.4.5	Total Magnesium Concentration	125
6.4.6	Preliminary analysis of the PSD data	126
6.5	Conclusions	128
6.6	Key Points from Chapter Six.....	128
Chapter 7 - Parameter Estimation of Struvite Crystal Nucleation, Growth and Aggregation Kinetic Parameters.....		
		131
7.1	Introduction	131
7.2	Background to Parameter Estimation.....	132
7.3	Limitations to the Parameter Estimation.....	134
7.3.1	Choice of $L1$ used in Estimations.....	135
7.3.2	Constraints on the Parameters	135
7.4	Parameter Estimation Results.....	136
7.4.1	Initial Saturation Index of 0.37.....	139
7.4.2	Initial Saturation Index of 0.54.....	146
7.4.3	Initial Saturation Index of 0.74.....	152
7.5	Discussion of Parameter Estimation Results.....	152
7.5.1	Initial Size Distribution below the Limit of Detection	154
7.5.2	Nucleation Rate vs. Source Function	157
7.5.3	Nucleation	160
7.5.4	Crystal Growth	163

7.5.5	Aggregation.....	166
7.5.6	Correlation of parameters	167
7.6	Conclusions	170
7.7	Key Points from Chapter 7	171
Chapter 8 - Conclusions and Recommendations		173
8.1	Conclusions	173
8.1.1	Solution Thermodynamics	174
8.1.2	Discretised Population Balance.....	174
8.1.3	Struvite Crystallisation Process Model.....	175
8.1.4	Parameter Estimation	176
8.1.5	Final Thoughts on the Research.....	177
8.2	Recommendations	177
REFERENCES.....		181
NOMENCLATURE.....		189
APPENDICES		197
Appendix A - EES Model.....		197
Appendix B - gPROMS Model.....		201
Appendix C - Raw Data.....		219
Appendix E - Experimental Procedure		265

LIST OF FIGURES

Figure 2.1: Sensitivity of the SI to uncertainty in the K_{sp} shown with %relative uncertainty.....	11
Figure 2.2: EES and PHREEQC thermodynamic solutions at 0.0025M equimolar total analytical concentration of magnesium, ammonium and phosphate against solution pH	18
Figure 2.3: Categorisation of nucleation mechanisms (Mullin, 1993).	19
Figure 2.4: Schematic diagram of experimental apparatus.	23
Figure 2.5: Light intensity versus the time stamped file number; the subfigure shows the light scintillations as nucleation onsets.	24
Figure 2.6: Logarithm of the induction time versus the inversed square logarithm of the supersaturation ratio for the previous studies.....	25
Figure 2.7: Induction time curves obtained by this study and predictions using previous studies.....	26
Figure 3.1: Population density of a steady-state MSMPR crystalliser with nucleation and size-independent crystal growth.....	33
Figure 3.2: Pictures of struvite aggregates, from top-left and moving clockwise; Adnan et al., (2003), This work, Koralewska et al., (2007), Regy et al., (2002).	36
Figure 3.3: Discretised size distribution along the length domain.	39
Figure 3.4: Relationship between the lower bound on the first interval of the discretised length domain and the third moment of the PSD.....	43
Figure 3.5: Population density results for experiment 1, DPB model and SDG model.....	50
Figure 3.6: Population density results for experiment 2, DPB model and SDG model.....	50
Figure 3.7: Population density results for experiment 3, DPB model and SDG model.....	51
Figure 3.8: Population density results for experiment 4, DPB model and SDG model.....	51

Figure 3.9: Population density results for Experiment 2, DPB model with extracted rates, SDG model and DPB model with adjusted kinetic rates.....	54
Figure 4.1: Diagram of process modelling philosophy used for the struvite MSMPR crystalliser.....	58
Figure 4.2: Process flow diagram of the MSMPR struvite crystalliser modelled and its nominal operating conditions.....	59
Figure 4.3: gPROMS solution thermodynamics verified against PHREEQC at 0.0025M equimolar total analytical concentration of magnesium, ammonium and phosphate and varying solution <i>pH</i>	60
Figure 4.4: Sigmoid function as a function of interval number and length.	68
Figure 4.5: The analytical solution for a steady state MSMPR where $B = 1.0 \times 10^6$ [1/L.min], $G = 1.0\mu\text{m}$ and $\tau = 12.5$ min and the numerical solution using the hybrid approach.	69
Figure 4.6: Validation of solution thermodynamics by comparison of measured and predicted <i>pH</i>	72
Figure 4.7: Dynamic response of <i>SI</i> at three initial conditions and three operating conditions; nominal caustic flow, reduced caustic flow and increased caustic flow.	74
Figure 4.8: Particle size distribution under nominal operating conditions shown at 0.1, 0.5, 1, 2 and 10 residence times.....	75
Figure 4.9: Predicted mass of struvite within the simulated MSMPR crystalliser under ideal and non-ideal thermodynamic conditions.....	76
Figure 4.10: Activity coefficients calculated during the simulation.....	77
Figure 4.11: Thermodynamic yield of struvite shown as the percentage of available phosphorus recovered as a function of residence time.	79
Figure 4.12: Reactor saturation index shown as a function of residence time.	80
Figure 5.1: Uniform distribution bounded by $\pm 10\%$ of the mean (μ).	87
Figure 5.2: Sample average <i>SI</i> as a function of the number of simulations for both nutrient load uncertainty and kinetic parameter uncertainty.....	89

Figure 5.3: Sample average pH as a function of the number of simulations for both nutrient load uncertainty and kinetic parameter uncertainty.....	89
Figure 5.4: Sample average L as a function of the number of simulations for both nutrient load uncertainty and kinetic parameter uncertainty.....	90
Figure 5.5: The effect of uniformly-distributed kinetic parameter uncertainties on key process variables under nominal operating conditions expressed as $\%CV$	92
Figure 5.6: Contribution of the individual mechanisms to the total uncertainty found using the deterministic uncertainty analysis.	94
Figure 5.7: Distribution of saturation index produced from the uniform distribution of nutrient load. ...	96
Figure 5.8: The effect of uniformly-distributed nutrient load uncertainties on key process variables under nominal operating conditions expressed as $\%CV$	96
Figure 5.9: Coefficient of variation in the steady state SI for a 1-L, 10-L and 100-L MSMPR crystallizer having a uniform distribution of kinetic rate coefficients.	98
Figure 5.10: Relative contributions of individual nutrient loads on total uncertainty in key process variables in deterministic uncertainty analysis.....	99
Figure 5.11: Frequency distribution of steady-state SI with nutrient load variability for uncontrolled and controlled pH	100
Figure 5.12: Frequency distribution of steady-state $\%PRecoveryT$ with nutrient load variability for uncontrolled and controlled pH	101
Figure 6.1: Schematic diagram of the experimental apparatus.	111
Figure 6.2: Typical PSD from the seed solution used in the batch crystallisation experiments.	112
Figure 6.3: Dynamic pH response during crystallisation in a batch reactor with and without baffles. ...	116
Figure 6.4: PSD produced for a sample from the same batch using the ESZ method and LD method. ...	117
Figure 6.5: Struvite crystals produced using the experimental procedure developed for this work.....	119

Figure 6.6: The pH response for all experiments with an initial SI of 0.37 with experimental group as parameter.	121
Figure 6.7: The pH response for all experiments with an initial SI of 0.54 with experimental group as parameter	122
Figure 6.8: The PSD of three samples taken from the same seed solution at time zero.....	123
Figure 6.9: The PSD of three samples taken after 10 minutes	123
Figure 6.10: The PSD of three samples taken after 20 minutes.	124
Figure 6.11: The PSD of three samples taken after 35 minutes.	124
Figure 6.12: The PSD of three samples taken after 60 minutes.	125
Figure 6.13: Total magnesium concentration through batch time for two initial saturation indices using ICP-AES.....	126
Figure 6.14: Zeroth moment in the measurable size domain during an experiment with an initial $SI = 0.37$	127
Figure 6.15: Third moment as measured during an experiment with an.....	128
Figure 7.1: Conceptual diagram for the parameter estimation process in gPROMS.....	137
Figure 7.2: Seed particle size distribution from the 29/09/10b $SI = 0.37$ experiment.....	140
Figure 7.3: Measured and model-predicted particle size distribution at 3 minutes using the estimated parameters and data from the 29/09/10b $SI = 0.37$ experiment.	140
Figure 7.4: Measured and model-predicted particle size distribution at 10 minutes using the estimated parameters and data from the 29/09/10b $SI = 0.37$ experiment.	141
Figure 7.5: Measured and model-predicted particle size distribution at 20 minutes using the estimated parameters and data from the 29/09/10b $SI = 0.37$ experiment.	141
Figure 7.6: Measured and model-predicted particle size distribution at 35 minutes using the estimated parameters and data from the 29/09/10b $SI = 0.37$ experiment.	142

Figure 7.7: Measured and model-predicted particle size distribution at 60 minutes using the estimated parameters and data from the 29/09/10b $SI = 0.37$ experiment. 142

Figure 7.8: Measured and model-predicted particle size distribution at 120 minutes using the estimated parameters and data from the 29/09/10b $SI = 0.37$ experiment. 143

Figure 7.9: Measured and model-predicted pH over the course of the 29/09/10b $SI = 0.37$ experiment using the estimated parameters..... 143

Figure 7.10: Measured and model-predicted third moment over the course of the 29/09/10b $SI = 0.37$ experiment using the estimated parameters. 144

Figure 7.11: Measured and model-predicted zeroth moment over the course of the 29/09/10b $SI = 0.37$ experiment using the estimated parameters..... 145

Figure 7.12: Measured and model-predicted average particle size over the course of the experiment using the 29/09/10b $SI = 0.37$ estimated parameters. 145

Figure 7.13: Measured and model-predicted total magnesium concentration over the course of the 26/10/10 $SI = 0.37$ experiment using the estimated parameters..... 146

Figure 7.14: Seed particle size distribution from the 26/10/10 $SI = 0.54$ experiment..... 147

Figure 7.15: Measured and model-predicted particle size distribution at 3 minutes using the estimated parameters and data from the 26/10/10 $SI = 0.54$ experiment. 147

Figure 7.16: Measured and model-predicted particle size distribution at 6 minutes using the estimated parameters and data from the 26/10/10 $SI = 0.54$ experiment. 148

Figure 7.17: Measured and model-predicted particle size distribution at 10 minutes using the estimated parameters and data from the 26/10/10 $SI = 0.54$ experiment. 148

Figure 7.18: Measured and model-predicted particle size distribution at 15 minutes using the estimated parameters and data from the 26/10/10 $SI = 0.54$ experiment. 149

Figure 7.19: Measured and model-predicted pH over the course of the 26/10/10 $SI = 0.54$ experiment using the estimated parameters.....	149
Figure 7.20: Measured and model-predicted third moment over the course of the 26/10/10 $SI = 0.54$ experiment using the estimated parameters.	150
Figure 7.21: Measured and model-predicted zeroth moment over the course of the 26/10/10 $SI = 0.54$ experiment using the estimated parameters.	151
Figure 7.22: Measured and model-predicted average particle size over the course of the 26/10/10 $SI = 0.54$ experiment using the estimated parameters.....	151
Figure 7.23: Measured and model-predicted pH over the course of the 30/09/10 $SI = 0.74$ experiment using the estimated parameters.....	152
Figure 7.24: The zeroth moment determined with different initial distributions of sub two micron particles using the estimated parameters.	155
Figure 7.25: The zeroth moment determined with different initial distributions of sub two micron particles and repeated parameter estimation for each initial condition.	156
Figure 7.26: pH with the different initial distributions using the estimated parameters.....	157
Figure 7.27: Third moment with the different initial conditions using the estimated parameters.	157
Figure 7.28: Source function for particles entering the discrete interval at $2\mu m$ as determined from the process model and the regressed exponential function.	159
Figure 7.29: pH response for the estimated parameters compared to nucleation parameters that have been multiplied or divided by a factor of 10.	160
Figure 7.30: pH response for the estimated parameters compared to nucleation parameters that have been multiplied or divided by a factor of 10.	161
Figure 7.31: PSD over the whole size domain demonstrating the effect of multiplying or dividing the estimated nucleation parameters by a factor of 10.	162

Figure 7.32: Growth rate versus saturation index based on the estimated parameters, $kG = 12.49$ and $nG = 5.06$ 164

Figure 7.33: Growth rate versus saturation index using the estimated parameters and a second-order approximation..... 165

Figure 7.34: Representation of the two aggregation scenarios; particle area conservation and particle coalescence..... 168

Figure 7.35: Ratio of conserved and coalesced aggregate surface area against the ratio of particle volumes involved in forming the aggregate. 170

LIST OF TABLES

Table 1.1: General information on struvite.	2
Table 2.1: Thermodynamic equilibria and their governing equations.....	14
Table 2.2: Variations of the Debye-Hückel equation and their applicable conditions (Mullin, 1993).	16
Table 2.3: Clarification of variables used in Equation 2.16-2.18.	21
Table 2.4: Summary of experimental conditions and techniques.	22
Table 3.1: Uniform discretisation performance in terms of dimensionless third moment and CPU time.	45
Table 3.2: Experimental methods and conditions used to compare with DPB equation predictions.....	47
Table 3.3: Constants for SDG and DPB models.	49
Table 3.4: Comparison of the measured solids concentration and calculated solids concentration from the transformed number-size distribution.	53
Table 3.5: Adjusted kinetic rates for DPB model.	55
Table 4.1: Steady state third moment calculated with the analytical solution, ADPB with various values of q and the sigmoidal approach.	70
Table 4.2: % <i>PRec</i> and <i>SI</i> under nominal operating conditions and variable reactor volume.	79
Table 5.1: Base case for the stochastic simulations, based on nominal operating conditions.	88
Table 5.2: Uniformly distributed kinetic parameter uncertainty in a 10-L MSMPR reactor and their effect on key variables at steady state.....	91
Table 5.3: Uniformly distributed nutrient load uncertainty in a 10-L MSMPR reactor and their effect on key variables at steady state.....	95
Table 6.1: Sample times for the two experimental conditions.....	115
Table 6.2: Groups of experiments that used the same seed solution having an initial $SI = 0.37$	120
Table 6.3: Groups of experiments that used the same seed solution having an initial $SI = 0.54$	120

Table 7.1: Summary of unknown parameters to be estimated and experimentally measured variables.	132
Table 7.2: Constant variance models used for the measured variables in the parameter estimation	134
Table 7.3: Constraints placed upon the parameters to be estimated.....	136
Table 7.4: Parameter estimation results from gPROMS reported with 95% confidence interval.....	137
Table 7.5: Nomenclature for naming experiments.....	138
Table 7.6: Range of initial saturation indices covered by struvite crystal growth rate studies.....	163
Table 7.7: Range of aggregation kernels used in different studies using the DPB	167
Table 7.8: Correlation matrix of the parameters estimated by gPROMS.	168

Chapter 1 - Introduction

This chapter introduces the background and motivations for research into struvite crystallisation. The research objectives are stated and the structure of the thesis is given.

The logical narrative of the thesis chapters is summarised.

1.1 Research Background

The research background will provide general information on the mineral struvite and a history of research on nutrient recovery. Understanding the history and importance of this field places this work in context.

Struvite is the common name for the mineral magnesium ammonium phosphate hexahydrate which is formed from equimolar proportions of magnesium, ammonium and phosphate with six water of hydration molecules via Equation 1.1. Some general information on struvite is presented in Table 1.1.



Table 1.1: General information on struvite.

Crystallography	White, inorganic crystal with orthorhombic morphology
Hardness	1.5-1.7 on the Mohs scale (Carballa et al., 2009)
Thermal decomposition	Water loss begins at 55°C and completely lost at 250°C (Bhuiyan et al., 2008c)
Specific gravity	1.71
Molecular weight	245.5 g/mol

1.1.1 Phosphorus Recovery

Phosphorus is a nutrient essential for all life as it is used in metabolic reactions. As the human population increased post industrial revolution, naturally occurring phosphorus in the soils could not support growing food demands (Brinck, 1977). Guano and phosphate rock were mined and used to produce fertilisers to support agricultural needs (Brinck, 1977). At the beginning of the 21st century approximately 85% of global phosphorus demand was supplied by mined phosphate rock (Cordell et al., 2009).

In the late 1990s, a number of studies were published warning of the exhaustion of global phosphate rock reserves by 2050-2100 (Driver et al., 1999, Durrant et al., 1999, Steen, 1998). More recent research suggests a peak in phosphorus production will be reached in 2033 (Cordell et al., 2009). This calculation was based on U.S. geological survey and industry data (Buckingham, 2006, Jasinski, 2007, Association, 2000, Association, 2006). While the riots and food shortages seen in 2007-2008 were not a direct result of phosphorus scarcity, they do offer a potential view of the future, if phosphorus prices were to increase.

Phosphorus recovery is an important means of supplementing phosphorus demand from otherwise wasted sources, alleviating the pressures of mining a finite resource. Methods of recovery can be as simple as ploughing crop residues back into the soil, composting food waste and using human and animal excreta for application to soils (Cordell et al., 2009). However, these are low-grade sources when compared to commercial fertilisers produced from phosphate rock.

One promising method of phosphorus recovery involves the crystallisation of higher grade compounds such as calcium phosphate, hydroxyapatite and struvite (Driver et al., 1999) from wastewater process streams. Struvite crystallisation is a particularly promising option, since it can be used directly as a slow-release fertiliser (Bridger, 1962, Gaterell et al., 2000) and has lower heavy metal contamination than fertilisers produced from phosphate rock (Morse et al., 1998, Uysal et al., 2010). The heavy metal content of struvite is limited because of the low concentrations found in wastewater when compared to mined phosphate rocks (Driver et al., 1999). Along with phosphorus it also contains nitrogen, another important nutrient.

1.1.2 Struvite Crystallisation

Struvite crystallisation research falls into three broad categories: reactor performance studies; thermodynamics studies and kinetics studies. Reactor performance studies involve the design of a struvite crystalliser and testing its operation. These studies are conducted at different scales: laboratory scale (Battistoni et al., 2000, Wu et al., 2005, Fujimoto et al., 1991); pilot scale (Ohlinger et al., 2000, Münch and Barr, 2001, Adnan et al., 2003, Seco et al., 2008, Ali, 2007) and full scale (Battistoni et al., 2005, Jaffer et al., 2002). These studies use a number of methods of agitation, reactor configuration and both synthetic and real solutions. For example, the struvite product may be fluidised with pumps or suspended with mechanical stirrers. Batch, fed-batch and continuous reactors have all been used in struvite reactor design.

Thermodynamic studies are important to understand the conditions under which struvite will form. This information is used to design reactors for phosphorus recovery and/or to develop strategies for mitigating precipitation in process equipment at wastewater treatment plants where struvite accumulation is an issue. Research into struvite crystallisation without a thermodynamic description is nothing more than the mixing of chemicals and observing the results without any understanding of what is really happening in solution. Refer to §2.2 for a detailed review of struvite thermodynamics.

Kinetic studies are used to determine the rate of struvite precipitation. This has a direct impact on process design through batch time/residence time and reactor volume. Previous approaches to struvite kinetic studies can be broadly separated into two groups:

1. Measuring the rate of consumption of magnesium, ammonium or phosphate
2. Measuring the rates of mechanisms affecting precipitation

These approaches are discussed in §2.3, 3.2, 3.3, 3.4 and 4.2.2.

1.2 Research Objectives

In developing the research objectives, two areas were identified for particular focus in this work: aggregation kinetics and process modelling. Aggregation has only been investigated through the addition of different coagulants and measuring the increase in particle size (Levenspiel, 1999) as well as zeta-potential measurements (Bouropoulos and Koutsoukos, 2000, Liu and Warmadewanthi, 2009). These studies did not attempt to describe aggregation or consider its implications on process design.

There is a paucity of process models in the struvite crystallisation literature. To address this shortfall, solution thermodynamics and kinetics are combined into a process model describing particle dynamics. This means designs can be evaluated and optimised via simulations instead of experiments, thus reducing economic risks and ultimately resulting in a better process. The process modelling approach to

struvite crystallisation has only been used by one research group (Ali and Schneider, 2008), where solution thermodynamics and crystal growth kinetics were used to model a fed-batch struvite crystallisation process.

The overarching objective of this research is to develop an approach to modelling the struvite crystallisation process that incorporates solution thermodynamics, kinetics of mechanisms affecting particle dynamics and mass balance relations. A number of individual objectives were identified to complete this project:

1. Develop descriptions for mechanisms that affect particle dynamics and couple them to mass balance relations.
2. Combine struvite solution thermodynamics and kinetic relations into a process model that describes struvite crystallisation.
3. Demonstrate how a struvite crystallisation process model can be used for process design, control and optimisation.
4. Determine the kinetic parameters for struvite nucleation, crystal growth and aggregation using the process model.

1.3 Structure of Thesis

This thesis is structured to provide a logical narrative on how the research objectives were addressed. The purpose of the individual chapters and how they are related to each other is discussed in the following paragraphs. It should be noted that a traditional literature review is omitted in place of addressing specific aspects of the literature in the relevant chapters.

Chapter 1 introduces the background of the research undertaken and gives the research objectives and the structure of the thesis. A stand-alone literature review chapter is not presented in this thesis; instead detailed reviews of previous work are presented in the relevant chapters throughout the thesis.

Chapter 2 presents a review of struvite nucleation studies and experimental results on struvite induction times at low supersaturation. A description of struvite solution thermodynamics is first developed to facilitate the review. The review informs how to best model nucleation. Outcomes of this chapter form the basis for developing approaches to model struvite kinetics. Aspects of this work were published under the title, *A Review of Struvite Nucleation Studies*, in the peer-reviewed conference proceedings of the International Conference on Nutrient Recovery from Wastewater Streams held in Vancouver, Canada, 2009.

Chapter 3 investigates the population balance and its application to struvite nucleation, crystal growth and aggregation. The approach implemented a discretised population balance (DPB) and included the mechanisms of crystal nucleation, crystal growth and particle aggregation. This was compared to a similar approach that included nucleation and size-dependent crystal growth as well as experimental data. The DPB was found to satisfactorily represent the experimental data and the inclusion of aggregation resulted in a more accurate account of real struvite crystallisation behaviour. From this position, a process model can now be developed using this approach to describing the kinetics mechanisms.

Chapter 4 details the development of a process model that describes struvite crystallisation. The model incorporates solution thermodynamics, mechanism kinetics of nucleation, growth and aggregation, population and mass balances. The model successfully describes the solution thermodynamics dynamically and therefore allows the mechanism kinetics to be a direct function of solution thermodynamics. Aspects of this work were published under the title, *Dynamic Simulation of a Struvite*

MSMPR Crystalliser with Crystal Nucleation, Growth and Aggregation, in the peer-reviewed conference proceedings of CHEMECA held in Adelaide, Australia, 2010.

Chapter 5 illustrates how the process model can be applied to process design and control. This is done by using stochastic simulations to show how a struvite crystalliser would respond to various sources of uncertainty. A *pH* control scheme is then implemented to demonstrate how process control can be used to improve reactor behaviour.

Chapter 6 details the experimental method used to regress the kinetic parameters for struvite nucleation, growth and aggregation. The repeatability of the experimentally measured process variables is assessed. Quantitative experimental evidence is shown to justify the use of nucleation, crystal growth and aggregation in the process model.

Chapter 7 details the parameter estimation results. A set of data that covers three experimental conditions is used to maximise the confidence in the estimated parameters. The agreement between model-predictions and measured *pH*, total particle number, total particulate volume and particle size distribution are acceptable given the methods used.

Chapter 8 discusses the conclusions made from the work undertaken as part of this PhD thesis. Recommendations are also made.

The appendices contain input files for the modelling software used (Appendix A - EES Model, Appendix B - gPROMS Model), raw data from experiments (Appendix C - Raw Data) and detailed experimental procedures (Appendix E - Experimental Procedure).

Chapter 2 - Struvite Nucleation Studies

This chapter details the description of struvite solution thermodynamics and provides a review of past struvite nucleation studies. Experiments conducted at low supersaturation addressed a gap in the literature in relation to induction time of this system. Aspects of this chapter were published at the International Conference on Nutrient Recovery from Wastewater Streams, Vancouver 2009.

2.1 Introduction

This chapter focuses on struvite crystal nucleation by reviewing contributions to this field and conducting a nucleation study. It considers how experimental studies on nucleation can be used in a process model. In order to carry out any study of nucleation, solution thermodynamics must first be clearly understood and appropriately described. The first goal of this chapter is to detail the thermodynamic framework used throughout this work, since this is the foundation for the rest of the study.

2.2 Solution Thermodynamics

The precipitation of any solid phase from an aqueous solution is, eventually, governed by solution thermodynamics. Therefore a description of solution thermodynamics is central to any crystallisation process. It determines if crystallisation would proceed and calculates the thermodynamic driving force that would see the process go to equilibrium. The key variable that any thermodynamic description must describe is solute supersaturation. Supersaturation describes a solution where the solute

concentration is greater than its equilibrium value. Supersaturation is a necessary condition for crystallisation.

2.2.1 Supersaturation

Struvite crystallisation involves the integration of three ionic species into the crystal lattice of an existing crystal (crystal growth) or a cluster which has not yet changed phase (nucleation). In cases like this, defining solute concentration can be troublesome, owing to the multiple ions involved. To handle multi-ionic systems, the solute concentration is conveniently defined in terms of the ion activity product (*IAP*), as per Equation 2.1 (Snoeyink and Jenkins, 1980). When the *IAP* is greater than the equilibrium solubility product, K_{sp} , the system is supersaturated and nucleation and/or crystal growth may occur, ultimately returning the system to equilibrium. This work uses the saturation index, or *SI*, given by Equation 2.2 as a representation of solution supersaturation (Abbona et al., 1982, Ali and Schneider, 2006), unless otherwise stated. The equilibrium solubility product used in this work is $pK_{sp} = 13.26 \pm 0.04$ (Ohlinger et al., 1998), where pK_{sp} is the negative base ten logarithm of K_{sp} .

$$IAP = \{Mg^{2+}\}\{NH_4^+\}\{PO_4^{3-}\} \quad 2.1$$

$$SI = \log \left(\frac{IAP}{K_{sp}} \right) \quad 2.2$$

The calculated saturation index will be sensitive to the K_{sp} value used. It is therefore prudent to analyse the sensitivity of the saturation index to the solubility product. The 95% probable error technique is used to show how uncertainty in the K_{sp} used in this work propagates through to *SI*. Figure 2.1 shows that the sensitivity of *SI* to K_{sp} increases as the *SI* decreases.

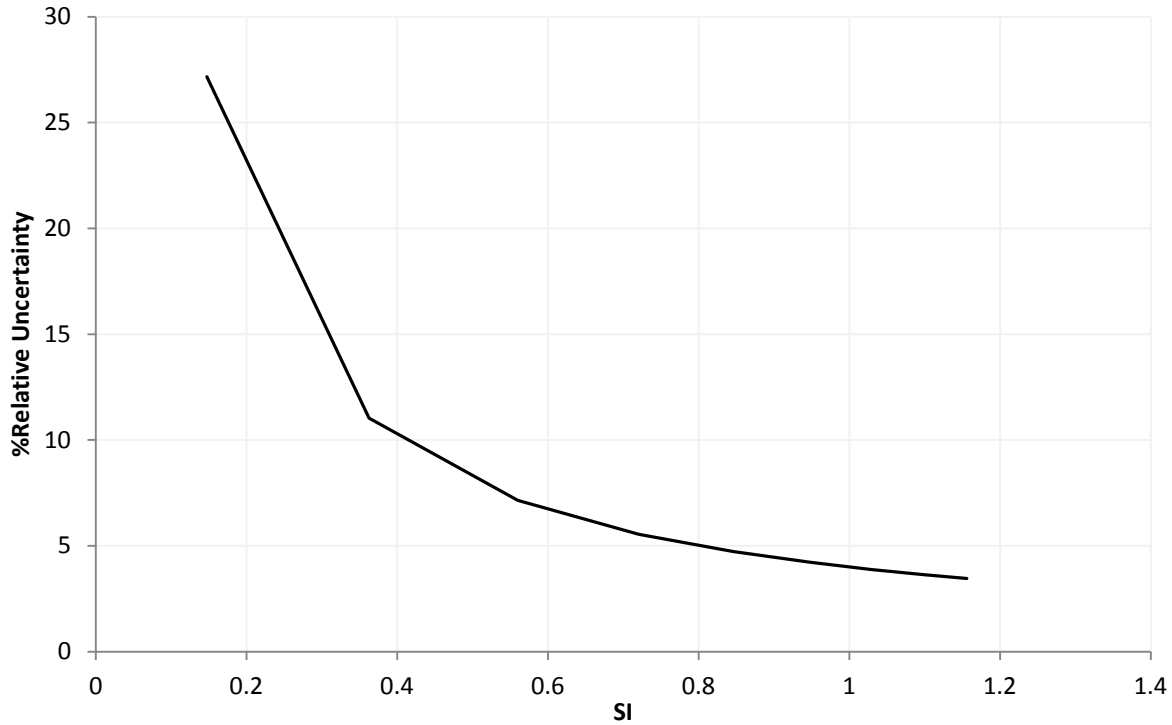


Figure 2.1: Sensitivity of the SI to uncertainty in the K_{sp} shown with %relative uncertainty.

A number of definitions of struvite supersaturation have been used by other researchers. These include the saturation ratio, S_a , defined in Equation 2.3 (Ohlinger et al., 1999) and supersaturation ratio, SSR , as defined by Equation 2.4 (Bhuiyan et al., 2009, Qu, 2007, Fattah et al., 2008). Both of these expressions are variations on the saturation index, incorporating the ion activity product and the minimum solubility product.

$$S_a = \left(\frac{IAP}{K_{sp}} \right)^{1/\nu} \quad 2.3$$

$$SSR = \left(\frac{IAP}{K_{sp}} \right) \quad 2.4$$

Where ν is the number of constituent ions. In the case of struvite, $\nu = 3$.

A more simplified expression for supersaturation, S , based on the concentration of one component, usually phosphorus, is also used (Nelson et al., 2003, Le Corre et al., 2007, Quintana et al., 2005, Harrison et al., 2011). This expression is defined by Equation 2.5 or a variation. The appeal of this approach is that it can be measured experimentally, *i.e.* one component's concentration can be measured both in the equilibrium (C_i^*) and non-equilibrium condition (C_i), negating the need for a full description of the solution thermodynamics. However, this is an incorrect representation of supersaturation, suggesting the concentration of only one component influences crystallisation behaviour.

$$S = C_i - C_i^* \quad 2.5$$

As stated previously, the solubility product of struvite used in this research is that published by Ohlinger et al.,(1998). However, many other pK_{sp} values have been published, such as; 12.60 (Bube, 1910), 13.15 (Taylor et al., 1963b), 9.40 (Borgerding, 1972), 13.12 (Burns and Finlayson, 1982), 12.36 (Buchanan et al., 1994), 12.95 (Aage et al., 1997), 13.36 (Mavinic et al., 2007). The value reported by Ohlinger et al., (1998) is used for the following reasons: it accounts for non-ideal thermodynamics where others do not (Bube, 1910, Borgerding, 1972, Aage et al., 1997); it was found using synthetic and real experimental solutions and it was found using a sound methodology where the difference between experimental measurements and theoretical predictions were minimised using a least squares parameter estimation approach where others do not (Taylor et al., 1963b, Burns and Finlayson, 1982).

2.2.2 Speciation

To determine solute supersaturation, the ion activity product must be determined, which requires knowledge of the free Mg^{+2} , NH_4^+ and PO_4^{-3} activities. As such, the concentration of all ionic species in solution must be known. Therefore, the total concentration of all master elements and spectator ions must be quantified. The concentrations of the master elements are equal to the sum of all species

containing the master elements, as defined by Equations 2.6-2.8, where square brackets represent the concentration of the species in question, taking into account stoichiometry. The species considered in this analysis are based upon the work of Ohlinger et al. (1998).

$$C_{Mg}^T = [Mg^{2+}] + [MgOH^+] + [MgPO_4^-] + [MgHPO_4] + [MgH_2PO_4^+] \quad 2.6$$

$$C_N^T = [NH_4^+] + [NH_3] \quad 2.7$$

$$C_P^T = [PO_4^{3-}] + [HPO_4^{2-}] + [H_2PO_4^-] + [H_3PO_4] + \dots \quad 2.8$$

$$[MgPO_4^-] + [MgHPO_4] + [MgH_2PO_4^+]$$

The total concentrations of the master elements, C_i^T , are known from chemical additions. Spectator ions do not participate in speciation but must also be accounted for. Their concentrations are always known from their chemical additions. The spectator ions considered in this work are chloride, which is added with magnesium in the form of $MgCl_2 \cdot 6H_2O$, and sodium in the form of $NaOH$. The spectator ions can be written in terms of their master elements also, as shown in Equations 2.9 and 2.10.

$$C_{Cl}^T = [Cl^-] \quad 2.9$$

$$C_{Na}^T = [Na^+] \quad 2.10$$

Performing a degrees of freedom analysis at this point presents 5 equations and 13 unknowns, resulting in an underspecified system of equations

The equilibria considered in this work are listed in Table 2.1 and are based on the work of Ohlinger et al. (1998). It is important to note the equilibria equations are defined in terms of species activity and not concentration, which takes into account the hydrated radius effects (Harris, 2010).

Table 2.1: Thermodynamic equilibria and their governing equations.

Compound	Equilibria equation and constant	Reference
HPO_4^{2-}	$\frac{\{H^+\}\{PO_4^{3-}\}}{\{HPO_4^{2-}\}} = 10^{-12.35}$	(Morel and Hering, 1993)
$H_2PO_4^-$	$\frac{\{H^+\}\{HPO_4^{2-}\}}{\{H_2PO_4^-\}} = 10^{-7.20}$	(Morel and Hering, 1993)
H_3PO_4	$\frac{\{H^+\}\{H_2PO_4^-\}}{\{H_3PO_4\}} = 10^{-2.15}$	(Martell and Smith, 1989)
$MgPO_4^-$	$\frac{\{Mg^{2+}\}\{PO_4^{3-}\}}{\{MgPO_4^-\}} = 10^{-4.80}$	(Martell and Smith, 1989)
$MgHPO_4$	$\frac{\{Mg^{2+}\}\{HPO_4^{2-}\}}{\{MgHPO_4\}} = 10^{-2.91}$	(Martell and Smith, 1989)
$MgH_2PO_4^+$	$\frac{\{Mg^{2+}\}\{H_2PO_4^{3-}\}}{\{MgH_2PO_4^+\}} = 10^{-0.45}$	(Martell and Smith, 1989)
$MgOH^+$	$\frac{\{Mg^{2+}\}\{OH^-\}}{\{MgOH^+\}} = 10^{-2.56}$	(Childs, 1970)
NH_4^+	$\frac{\{H^+\}\{NH_3\}}{\{NH_4^+\}} = 10^{-9.25}$	(Taylor et al., 1963a)
H_2O	$\frac{\{H^+\}\{OH^-\}}{\{H_2O\}} = 10^{-14}$	(Harris, 2010)

Performing a degrees of freedom analysis at this point presents 14 equations and 26 unknowns. To simplify the system of equations, ideal thermodynamics could be assumed at the cost of reduced accuracy. If ideal thermodynamics were assumed, species activities would equal species concentrations. Applying this assumption, a degrees of freedom analysis results in 14 equations and 15 unknowns. To fully specify the system the pH must be set or a charge balance must be defined.

2.2.3 *pH* specification or Charge Balance

If the *pH* of the system is known, Equation 2.11 provides the extra equation needed to fully specify the system. Alternatively, the condition of electroneutrality could be applied by adding a charge balance, Equation 2.12. Since the valancy of each and every species is known, the charge balance provides the extra equation to produce zero degrees of freedom.

The advantage of the charge balance is that solution *pH* becomes a dependent variable, subject to the total elemental amounts and the distribution of the ionic species. Thus, model predictions of *pH* can be made, which can then be compared against measurements for validation (or invalidation) purposes. This is further detailed in §4.3.1.

$$pH = -\log (a_{H^+}) \quad 2.11$$

$$0 = \sum C_i Z_i \quad 2.12$$

It is important to note that while spectator ions may not participate in chemical equilibria, they must be included in Equation 2.12. Otherwise the charge balance would incorrectly calculate the hydrogen and hydroxide ion concentrations in order to satisfy the condition of electroneutrality.

The degrees of freedom analysis shows that the concentration of the distribution of master element's species can be determined. To more accurately model solution thermodynamics, real solution effects can be considered.

2.2.4 Activity Models and Ionic Strength

Species activity is related to concentration via the activity coefficient (Equation 2.13). This introduces an unknown activity coefficient for every charged species. The activity coefficients are evaluated with some

variant of the Debye-Hückel equation, depending on the solution ionic strength in question (see Table 2.2).

Table 2.2: Variations of the Debye-Hückel equation and their applicable conditions (Mullin, 1993).

Equation	Conditions
Unmodified Debye-Hückel equation	$I < 0.005\text{mol/L}$
Debye-Hückel equation with Güntelberg approximation	sparingly soluble electrolytes
Debye-Hückel equation with Davies approximation	$I < 0.2\text{mol/L}$
Bromley equation	$I > 0.2\text{mol/L}$

The Davies approximation is used in this work, due to its use in comparable studies to those undertaken in this thesis (Ohlinger et al., 1998, Bouropoulos and Koutsoukos, 2000, Ali and Schneider, 2008) and is given by Equation 2.14.

The ionic strength is defined by Equation 2.15 and is a measure of the concentration of all ions in solution. It is central to all variations of the Debye-Hückel equation and therefore must be calculated to describe non-ideal thermodynamics. Using these equations, the degrees of freedom remains zero and the system of equations is specified for non-ideal conditions.

$$a_i = \gamma_i C_i \quad 2.13$$

$$-\log \gamma_i = AZ_i^2 \left(\left[\frac{\sqrt{I}}{1 + \sqrt{I}} \right] - 0.3I \right) \quad 2.14$$

$$I = \frac{1}{2} \sum C_i Z_i^2 \quad 2.15$$

Where I = Ionic Strength, C_i = Concentration of species i , Z_i = Valency of species i , γ_i = Activity coefficient of species i , A = Debye-Hückel constant (0.509 at 25°C (Mullin, 1993)).

2.2.5 Numerical Implementation

The system of equations described in §2.2.2 must be solved using a numerical approach, owing to its complexity and non-linear nature. There are a number of specialised water chemistry computational solvers, specifically designed to solve the solution thermodynamic equations presented above, predicting either the non-equilibrium states or the solution's equilibrium including potential solid phase formation. These have been used by numerous researchers in the field of nutrient recovery, such as PHREEQC (Ronteltap et al., 2010, Liu and Warmadewanthi, 2009, Maurer et al., 2007, Bhuiyan et al., 2008b), MINTEQA2 (Turker and Celen, 2007, Pastor et al., 2008b, Nelson et al., 2003, Pastor et al., 2010, Münch and Barr, 2001, Doyle and Parsons, 2002), MINEQL+ (Ohlinger et al., 1998, Ohlinger et al., 1999), VisualMINTEQ (Ali and Schneider, 2005) and ChemEQL (Bouropoulos and Koutsoukos, 2000).

These programs use the total analytic concentration of the master and spectator elements in the system and a database of equilibria constants to calculate the concentration of all species in solution. In this study, Engineering Equation Solver¹ (EES) was used to solve the solution thermodynamics specified above. EES solutions were verified by comparing the ionic concentrations of Mg^{2+} , NH_4^+ and PO_4^{3-} against the PHREEQC² solution, as seen in Figure 2.2. The solutions from both solvers are essentially identical (within numerical tolerance), suggesting that EES can adequately manage these complex thermodynamic calculations.

¹Klein, S.A., f-Chart Software, www.fchart.com

²U.S. Geological Survey, Hydrologic Analysis Software Support Program

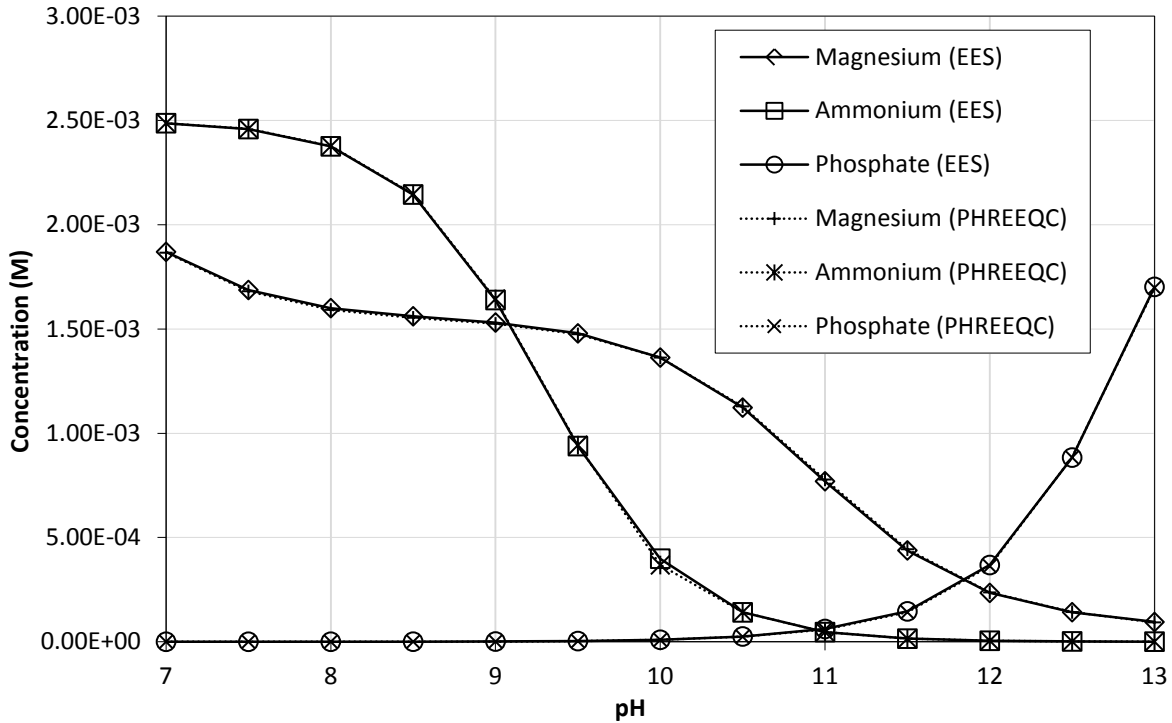


Figure 2.2: EES and PHREEQC thermodynamic solutions at 0.0025M equimolar total analytical concentration of magnesium, ammonium and phosphate against solution pH .

2.2.5.1 Numerical Difficulties

Because this system of equations contains logarithm functions, exponentials and non-linear algebraic equations with constants ranging from $10^{-0.45}$ – 10^{-14} , the equations can be modified, or variables scaled, to avoid numerical difficulties. PHREEQC employs logarithmic concentrations and logarithmic activities as the unknown variables, so that addition and subtraction operations can be used in place of multiplication and division (Parkhurst and Appelo, 1999). Interestingly, the solver used in EES was capable of solving the equations without any such transformation.

2.3 Nucleation

Nucleation is the first step in the crystallisation process. It occurs when solute molecules come together in clusters and grow by accretion. They then coalesce until a critical size is reached, resulting in a new,

stable phase (Mullin, 1993). Nuclei form by either a primary or secondary mechanism. The term 'primary' is reserved for all cases of nucleation in systems that do not contain crystalline matter. Nuclei that are generated in the vicinity of crystals present in the system will have formed by 'secondary' nucleation. A diagram of the scheme used to define nucleation mechanisms is presented below in Figure 2.2.

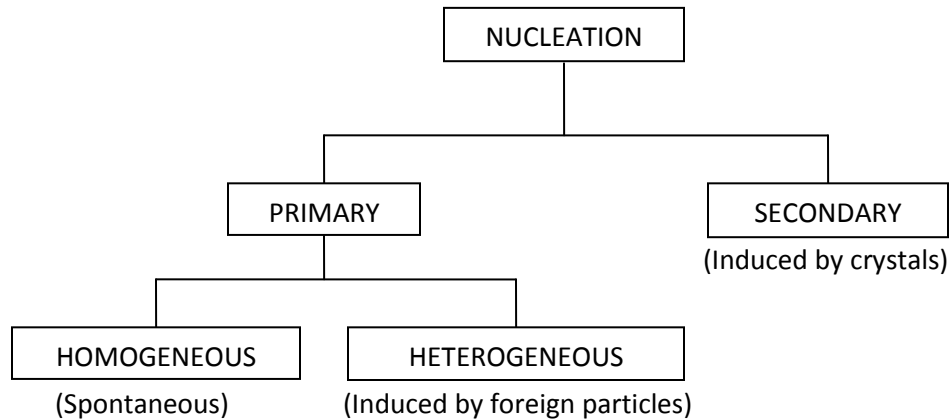


Figure 2.3: Categorisation of nucleation mechanisms (Mullin, 1993).

A period of time usually passes between the achievement of supersaturation and the appearance of primary crystal nuclei; this is called the induction time.

2.3.1 Induction Time

A common approach in nucleation studies, and the one taken by the four studies being reviewed here, is measuring the induction time and applying classical nucleation theory, which is based on primary homogeneous nucleation (Mullin, 1993). This produces a relationship between induction time and supersaturation given by Equation 2.16-2.18. The derivation of this equation can be found in Mullin (1993).

$$\log t_{ind} = \frac{A_{ind}}{(\log S_a)^2} - B_{ind} \quad 2.16$$

$$A_{ind} = \frac{\eta(\gamma^S)^3 v^2}{[(2.3kT)^3 v^2]} \quad 2.17$$

$$B_{ind} = \log \left[\left(\frac{D}{d^5 N^*} \right) \left(\frac{4\Delta G^*}{3\pi k_B T} \right)^{1/2} \right] \quad 2.18$$

Definitions of the terms in the above equations are found in Table 2.3.

It should be noted that primary homogeneous nucleation is practically impossible to achieve in real solutions, due to the presence of dust in even the most meticulously prepared solutions. However, the assumption of homogeneous nucleation is valid under conditions of high supersaturation (Mullin, 1993).

A problem emerges in the application of these data to struvite reactor design. Suspension reactors designed for crystal growth aim to operate within the metastable zone where crystal growth is favoured over nucleation, this traditionally occurs at low supersaturation (Myerson, 1993). This is an important point as struvite reactors can encounter fouling of process equipment, poor product quality, handling difficulties and loss of product due to fines resulting from excess nucleation (Münch and Barr, 2001, Battistoni et al., 2005, Adnan et al., 2003). Therefore it is a major aim of this work to gather nucleation data at low levels of supersaturation, which is relevant to reactor design. A comparison is then made by extrapolating predictions from other studies.

Table 2.3: Clarification of variables used in Equation 2.16-2.18.

Variable	Clarification
d	Interplanar distance in the crystal lattice (m)
D	Diffusion coefficient (m ² /s)
ΔG^*	Gibbs' free energy change to form critical nucleus (J)
k	Boltzmann constant (J/K)
N^*	Number of molecules comprising a critical size nucleus
t_{ind}	Induction time (sec)
T	Absolute temperature (K)
ν	Number of ions into which a molecule dissociates
η	Geometric factor = $\frac{4k_a^3}{27k_v^2}$ Where: k_a = Area shape factor k_v = Volume shape factor
γ^s	Surface energy (J)
v	Molecular volume (m ³)

2.3.2 Previous Work

Because of the complex nature of struvite thermodynamics, it can be difficult to compare the experimental results of previous work. There are different species included in the thermodynamic descriptions used by the studies reviewed here (Ohlinger et al., 1999, Bouropoulos and Koutsoukos, 2000, Kabdaşli et al., 2006, Bhuiyan et al., 2008a). This means that identical initial conditions would give three different supersaturation outputs making comparisons impossible. In order to perform a valid comparison, the raw data from the four previous studies were processed using the EES solver described

in §2.2. A summary of the experimental conditions and techniques used by all studies reviewed here is detailed in Table 2.4.

Table 2.4: Summary of experimental conditions and techniques.

	Ohlinger et al., (1999)	Bouropoulos and Koustoukus (2000)	Kabdaşli et al., (2006)	Bhuyian et al., (2008)
Concentration	4.0 – 20.0 mM	2.75 – 4.0 mM	2.45 mM	56, 70 mg/L at 1:1:10 Mg:PO ₄ :NH ₄
<i>pH</i> range	6.3 – 7.9	8.5	8.44 – 9.17	8.2 – 8.51
Temperature	22 °C	25 °C	23 °C	25 °C
Detection method	Laser scintillations	<i>pH</i> change	Absorption	<i>pH</i> change
Thermodynamic solver	MINEQL+	ChemEQL v2.0	Spreadsheets software	PHREEQC
Induction time (sec)	13 - 2280	360 - 7500	50 - 2520	12 - 500

2.4 Experimental Method

Experiments were conducted at 22 °C with 250 mL solutions at two levels of equimolar concentration (0.001 M [9 induction time measurements] and 0.0025 M [13 induction time measurements]) of magnesium, nitrogen and phosphorus. Supersaturation was established by adjusting the solution *pH* with sodium hydroxide, the range of *pH* covered was 7.8 to 9.2. Induction times were determined by monitoring light scintillations from a HeNe laser directed through the supersaturated solution and recorded with a low-light CCD camera placed perpendicular to the laser. A schematic diagram is shown in Figure 2.4.

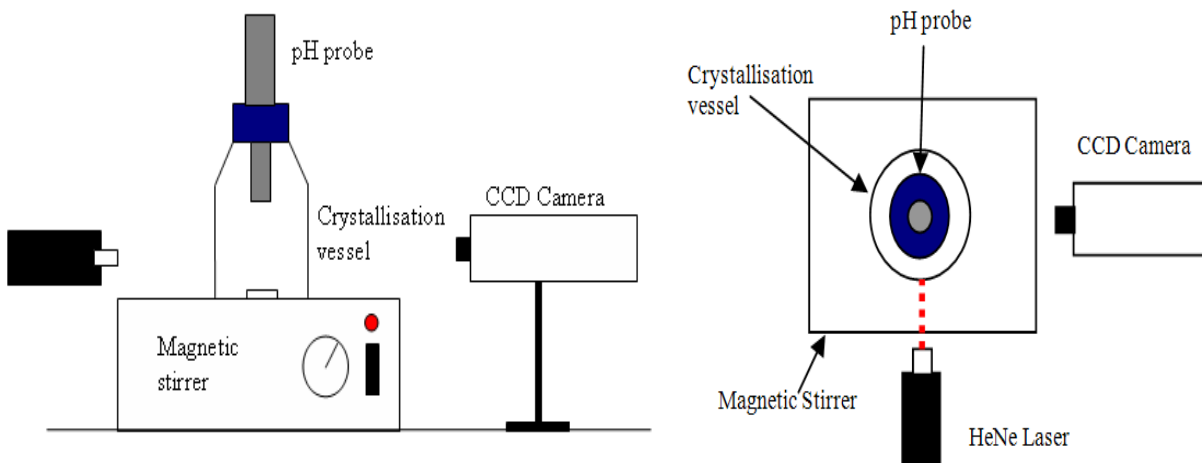


Figure 2.4: Schematic diagram of experimental apparatus.

Prior to nucleation, the solution is clear and therefore no light will be scattered. The induction time is determined by taking images of the solution every three seconds and measuring the time until scintillations are detected. JPEG images from the CCD camera were automatically archived to a high capacity disk drive. Experiments could therefore be conducted unsupervised over extended periods, enabling the investigation of induction time at low solution supersaturation.

Image files were subsequently processed using a MATLAB script, yielding the average red light intensity in the RGB (Red, Blue and Green) JPEG files versus time. Regression of the rate of change of red light intensity was used to determine induction times. A typical plot of light intensity and the pictures responsible are shown in Figure 2.5.

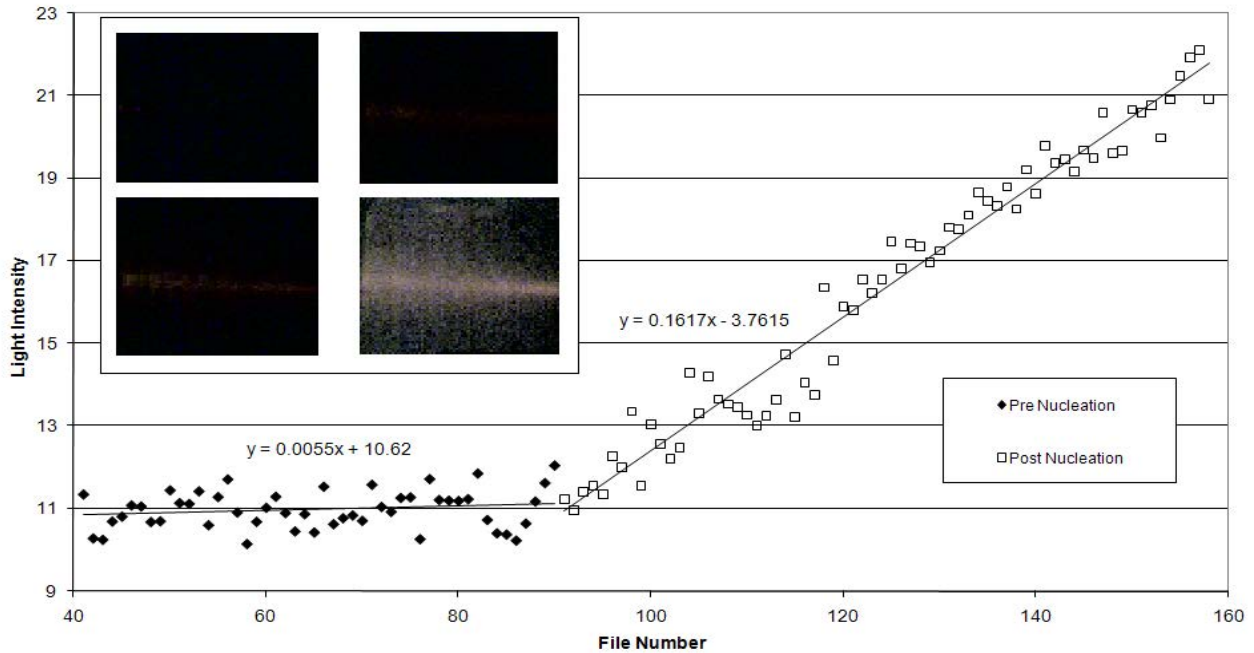


Figure 2.5: Light intensity versus the time stamped file number; the subfigure shows the light scintillations as nucleation onsets.

2.5 Results and discussion

The results from processing the raw data from previous studies through the EES thermodynamic solver are demonstrated in Figure 2.6. The differences between the studies are apparent and none of the studies have overlapping results. This is to be expected due to the different detection methods used and varying hydrodynamic conditions. In two studies (Ohlinger et al., 1999, Kabdaşlı et al., 2006) different detection methods were tested under the same conditions and produced different induction times. It was also found that changes in agitation rates affected induction times. Because it is impossible to quantify the hydrodynamic conditions in the various studies, it cannot be said to what degree the variation in Figure 2.5 is due to hydrodynamics.

The results also support the assumption that homogeneous nucleation is valid at high levels of supersaturation. This is demonstrated by the linear relationship between $\log t_{ind}$ and $\log^{-2} S_a$. The idea

that this assumption is no longer valid at lower levels of supersaturation is also supported by the results. Bouropoulos and Koutsoukos (2000) decreased supersaturation to see where the assumption of homogeneous nucleation no longer applies. This can be clearly seen in Figure 2.6 by the change in gradient. Furthermore, it can be seen that the Ohlinger et al. (1999) and Kabdasli et al. (2006) data points begin to deviate further away from the regressed line as supersaturation decreases.

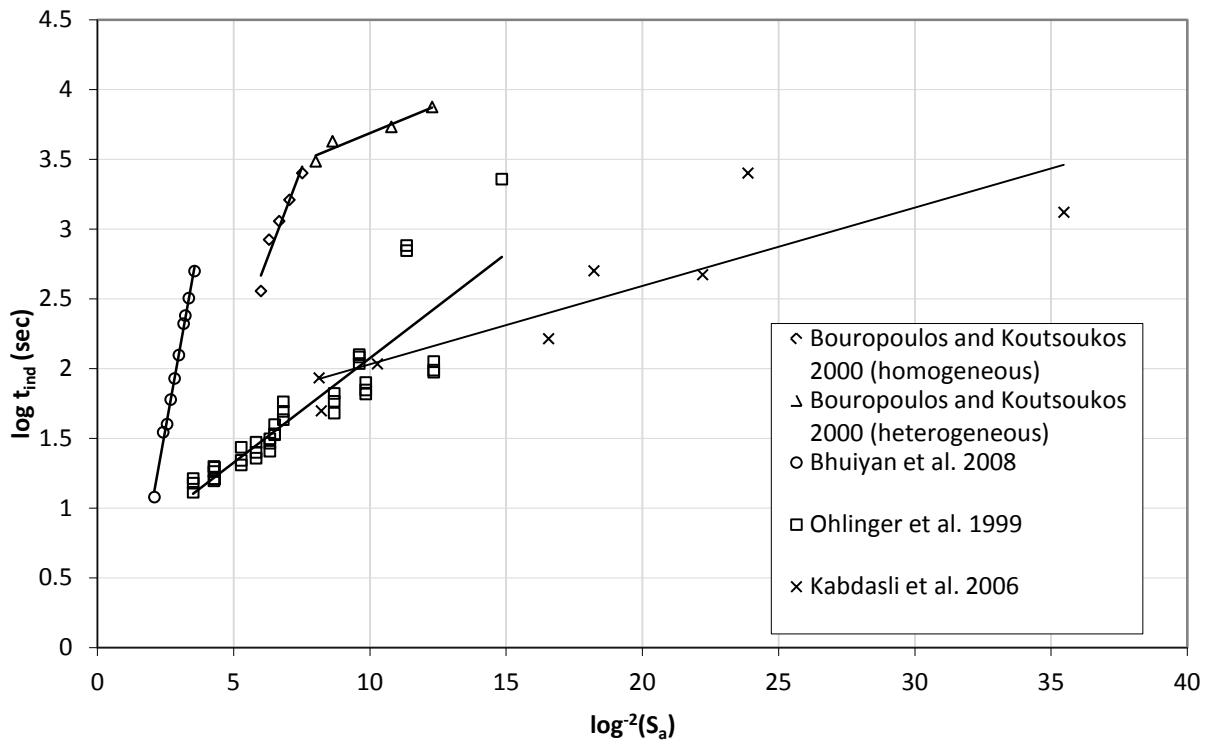


Figure 2.6: Logarithm of the induction time versus the inversed square logarithm of the supersaturation ratio for the previous studies.

The experiments conducted investigated nucleation behaviour at low supersaturation; the results can be seen in Figure 2.7, each data point corresponds to a single induction time experiment and measurement. It is clearly shown that concentration influences induction time at low supersaturation, this is contrary to classical theory which states induction time is only a function of supersaturation. This

is likely a result of the low supersaturation condition violating the assumption of primary homogenous nucleation which is only valid at high supersaturation.

Further evidence supporting this can be found by using the results of previous studies to predict the induction times at the levels of supersaturation used in this study. These predictions can be made by using Equation 2.16 which can be solved using the gradient and y-intercept of the lines in Figure 2.6. The results from these predictions were overlaid with the results from this experimental study in Figure 2.7.

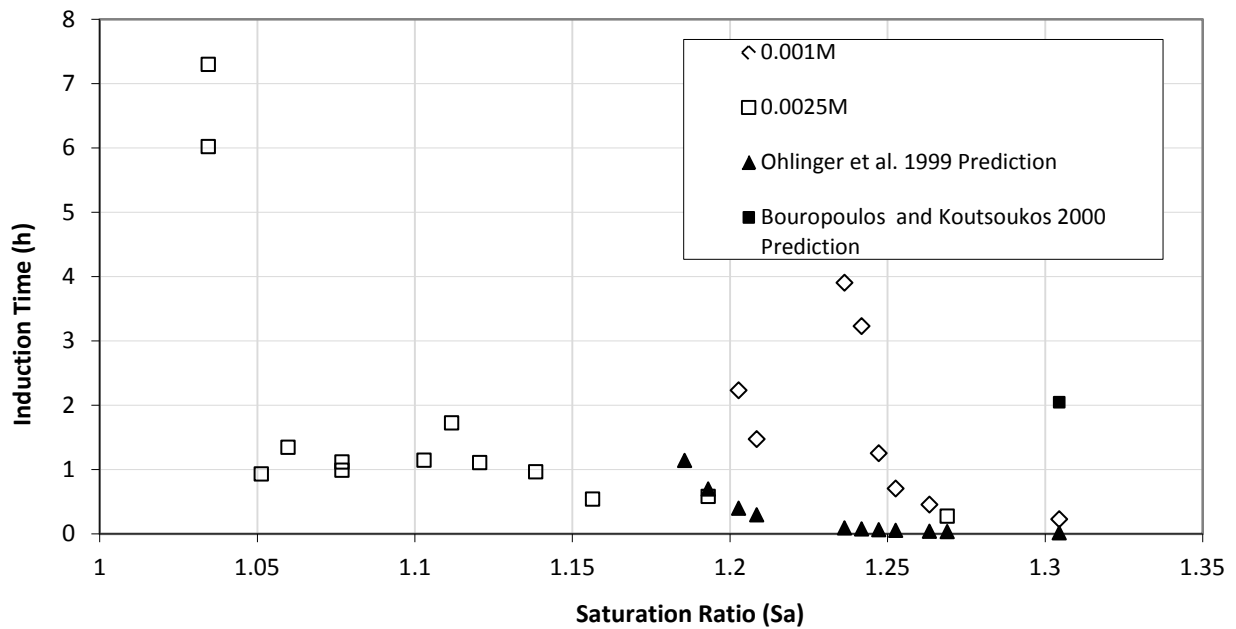


Figure 2.7: Induction time curves obtained by this study and predictions using previous studies.

It can be seen that the Ohlinger et al. (1999) predictions are in reasonable agreement at high supersaturation. Below $S_a = 1.2$, the induction time quickly approaches infinity, though it is apparent in Figure 2.7 that onset of nucleation occurs between 1 to 8 hours below $S_a = 1.2$. The Bouropoulos and Koutsoukos (2000) predictions only appear in Figure 2.7 at the highest level of supersaturation and the Bhuyian et al. (2008) predictions do not appear at all, demonstrating predictions of infinite induction

time at higher supersaturation levels than Ohlinger et al. (1999). The induction time curves themselves show clearly that, even at very low supersaturation, nucleation cannot be avoided indefinitely.

2.6 Conclusions

The solution thermodynamics description implemented in EES proved successful in calculating struvite supersaturation and produced results verified against the well established software package PHREEQC. The method of image capture and analysis can be used to determine induction times at low supersaturation and the results produced with this method indicate that nucleation of struvite could not be avoided indefinitely at low supersaturation. The comparison of previous studies in a common thermodynamic solver demonstrated that hydrodynamic conditions and detection methods may account for variations in observed induction times.

The variation seen in the previous studies and the low supersaturation experiments conducted as part of this work suggest measuring induction time for to describe primary nucleation is a poor approach to apply to process design. Therefore, any description of nucleation kinetics in a process model should not be derived from induction time experiments because of the inherent uncertainty and assumptions required to use induction time data validly.

2.7 Key Points from Chapter Two

- Solution thermodynamics description implemented in EES was verified against the widely used software package PHREEQC.
- Induction time data is highly variable and only valid at high supersaturation, making it unsuitable for use in process design.
- Nucleation cannot be avoided indefinitely at low supersaturation, this is confirmed in §6.4.6, so prudent process design approaches should include this mechanism instead of avoiding it.

- Therefore, another method apart from induction time studies is required for this.

Chapter 3 - A Description of Struvite Nucleation, Growth and Aggregation using the Population Balance

In this chapter an approach describing struvite crystallisation kinetics is used to address the weaknesses of other, previously-used modelling efforts. The discretised population balance (DPB) is employed to frame struvite nucleation, crystal growth and aggregation kinetics. The DPB is found to satisfactorily describe the experimental data obtained from the literature.

3.1 Introduction

Over the course of research on struvite crystallisation there have been a number of kinetic studies conducted. These studies generally take one of two approaches:

1. Precipitation approach
2. Semi-mechanistic approach

The precipitation approach employs a de-supersaturation approach, measuring the rate of consumption of magnesium, ammonium or phosphate from the aqueous phase to determine an overall precipitation rate equation. This approach neglects the mechanisms responsible for precipitation, namely nucleation and crystal growth.

The semi-mechanistic approach involves the incorporation of various mechanisms in order to describe the process kinetics. This entails experimental designs that favour one mechanism over the other, such as labile crystallisation for nucleation or metastable crystallisation for growth (Mullin, 1993, Myerson, 1993), in order to gain resolution of the particular mechanism in question.

Neither approach, however, accounts for phenomena that affect the particle size distribution (PSD) such as aggregation and breakage. While aggregation and breakage do not directly affect overall crystallisation kinetics, since they both conserve mass, they do have significant, indirect effects on nucleation and growth by changing the size and number of particles (Randolph and Larson, 1988).

3.2 Previous Work on Precipitation Kinetics

Precipitation kinetics are described by measuring the rate at which one of the struvite constituents (magnesium, ammonium or phosphate) is consumed and then determining a rate coefficient and order dependency of reaction that best describes the experimental observations, as in Equation 3.1. The limiting reactant is most often chosen, which in the case of struvite, is typically phosphate. This approach has been used by many researchers to describe struvite precipitation kinetics (Nelson et al., 2003, Quintana et al., 2005, Le Corre et al., 2007, Turker and Celen, 2007, Borja et al., 2008).

$$\frac{dC_i}{dt} = -k_{prec}C_i^{n_{prec}} \quad 3.1$$

Where k_{prec} is the rate coefficient of the precipitation rate equation and n_{prec} is the order-dependency of the apparent rate of precipitation.

One weakness of this approach is that the consumption of reactants is dependent on both nucleation and crystal growth (Mullin, 1993), which may be subject to confounding effects. For example, consider a population of crystals undergoing a constant growth rate. The more crystals present, the faster the

overall reaction will proceed. Any precipitation rate equation is, therefore, an unknown combination of the nucleation and growth rate effects. This uncertainty is seen in the literature by the fact that both first order (Nelson et al., 2003, Quintana et al., 2005, Le Corre et al., 2007, Borja et al., 2008) and second order (Bouropoulos and Koutsoukos, 2000, Turker and Celen, 2007) kinetics have been reported to best describe struvite precipitation using this approach.

3.3 Previous Work on Crystal Growth Kinetics

Crystal growth is commonly investigated by growing a population of seed crystals within the metastable zone where crystal growth is the dominant mechanism (Ali and Schneider, 2008, Bhuiyan et al., 2008a). The change in mass or concentration can then be attributed to a linear growth rate (Bhuiyan et al., 2008a) or the change in particle size distribution (PSD) can be compared (Ali and Schneider, 2008, Harrison et al., 2011). This approach assumes that changes in mass, concentration and/or PSD occur solely due to the growth of the seed population, and that other effects, such as nucleation, aggregation and breakage are minimal.

The requirement of operating in the metastable zone is difficult (Ali and Schneider, 2005, Bouropoulos and Koutsoukos, 2000, Battistoni et al., 2006). Testing experimental findings by reproducing experiments can also be challenging, since inorganic salts have highly variable metastable zones (Mullin, 1993). It has also been demonstrated that operating in the metastable zone does not prevent primary nucleation, but only delays its onset by extending induction times, §2.5 (Galbraith and Schneider, 2009). The presence of seed crystals would also increase the likelihood of secondary nucleation (Myerson, 1993) and any nucleation would violate the assumptions necessary to divine the true crystal growth rate. However, if the secondary nucleation rate is much less than the growth rate it could be considered zero but the practicalities of achieving metastable operation with struvite are difficult because of the

lack of a distinct struvite metastable zone (Ali and Schneider, 2005, Bouropoulos and Koutsoukos, 2000, Battistoni et al., 2006).

3.4 The Population Balance

Rather than neglect or seek to silence all but one mechanism (which is likely impossible), the population balance approach can be used to examine all mechanisms simultaneously. The population balance describes how the particle size distribution (PSD) changes with time as a function of a number of mechanisms, such as crystal nucleation, growth and so on. Furthermore, by experimentally measuring the PSD, kinetic information on the mechanisms that affect it can be determined (Randolph and Larson, 1988). The simplest version of the population balance is the steady state MSMPR (Mixed Suspension Mixed Product Removal) crystalliser with nucleation and size-independent crystal growth, as demonstrated by Equation 3.2.

$$n(L) = n^0 \exp\left(\frac{-L}{G\tau}\right) \quad 3.2$$

Where n is the population density, n^0 is the population density of nuclei, L is the crystal length, G is the linear growth rate and τ is the residence time.

It can be seen from Equation 3.2 that a plot of L versus $\ln [n(L)]$ would be linear, allowing G to be regressed from the gradient, and the nucleation rate (B_0) determined from the y-intercept and Equation 3.3, see Figure 3.1.

$$B_0 = n^0 G \quad 3.3$$

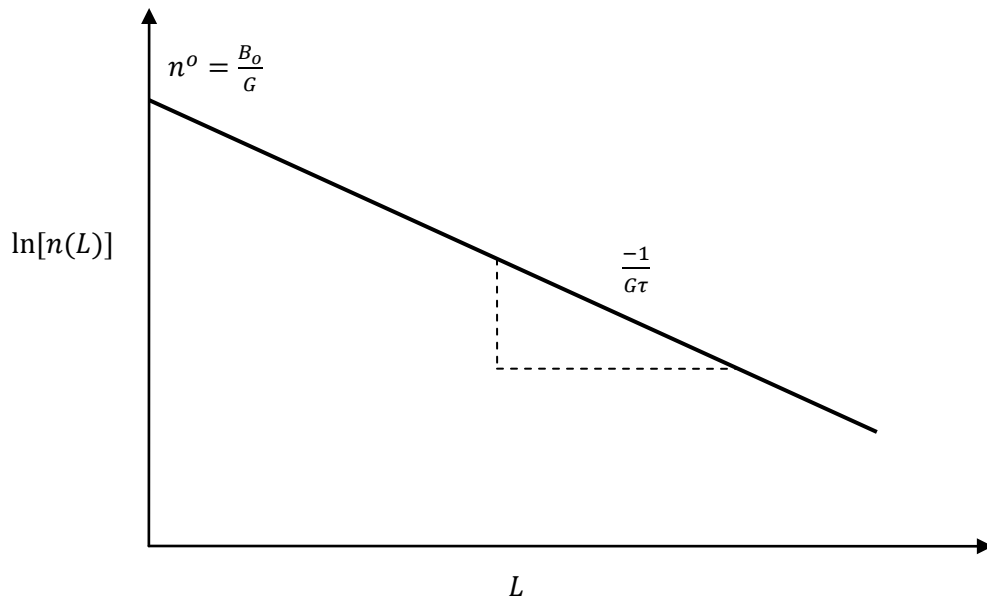


Figure 3.1: Population density of a steady-state MSMPR crystalliser with nucleation and size-independent crystal growth.

3.4.1 Struvite Precipitation and the Population Balance

The population balance approach has been used to investigate struvite crystallisation kinetics (Matynia et al., 2006, Koralewska et al., 2007, Piotrowski et al., 2009, Lobanov, 2009). However, when plotting L versus $\ln [n(L)]$, they did not find the expected linear relationship. The non-linearity suggests that one or more of the assumptions necessary for this approach are flawed. The following reasons can explain the relationship found in the previous research (Randolph and Larson, 1988):

- The reactor may not have satisfied MSMPR
- There may have been size dependent growth or growth rate dispersion
- There may have been another mechanism affecting the PSD, *i.e.* aggregation and/or breakage

In order to address this non-linear behaviour, previous researchers assumed a size-dependant growth (SDG) rate. By assuming SDG, Equation 3.2 can still be used by replacing the size-independent growth rate, G , with an appropriate function of L . A series of SDG models were tested to determine which could best fit the experimental data including: Canning and Randolph model (Canning and Randolph, 1967); Abegg, Stevens and Larson model (Abegg et al., 1968); Rojkowski Exponential model (Rojkowski, 1977); Rojkowski Hyperbolic model I (Rojkowski, 1978b) and the Rojkowski Hyperbolic model II (Rojkowski, 1978a). It was found that the Rojkowski Hyperbolic model I shown in Equation 3.4 (Rojkowski, 1978b) provided the best fit for struvite crystallisation in a number of cases (Matynia et al., 2006; Koralewska et al., 2007; Koralewska et al., 2009; Lobanov, 2009).

$$n = n^o \exp \left[- \left(\frac{G_\infty - G_0}{\tau a G_\infty^2} \ln \left(\frac{a G_\infty L + G_0}{G_0} \right) + \frac{L}{\tau G_\infty} + \ln \left(\frac{G_0 + a G_\infty L}{(1 + aL)G_0} \right) \right) \right] \quad 3.4$$

This model has been used to investigate the effects of magnesium concentration, pH , residence time and different reactor configurations on struvite nucleation and growth rates (Matynia et al., 2006, Koralewska et al., 2007, Piotrowski et al., 2009, Lobanov, 2009).

It should be noted that none of the work that uses the SDG model suggests that SDG is a real mechanism affecting struvite crystallisation. It is chosen for mathematical convenience and goodness of fit. This means that without physical evidence of SDG, the model is, at best, an empirical model for predicting the population density function at steady state. Thus, other possible explanations for the non-linear L versus $\ln [n(L)]$ relationship should be considered.

Firstly, satisfaction of the MSMPR condition is assumed in all published results because of the small crystal sizes reported in the literature (Matynia et al., 2006, Koralewska et al., 2007, Piotrowski et al., 2009, Lobanov, 2009). The largest particles reported (approximately 200 μm) would have a Stokes

settling velocity of 0.0172 m/s , so difficulty in suspension of the crystal population is not an issue. Randolph and Larson (1988) cite the importance of isokinetic sampling to ensure mixed product removal. The achievement of this was not mentioned in the previous studies and it is difficult to verify. The sampling procedure is therefore assumed to satisfy the mixed product removal requirement of isokinetic withdrawal.

Next, it has been suggested that SDG may not be a real phenomenon (Randolph and Larson, 1988) and there is experimental evidence to suggest that observed size-dependant growth is just a manifestation of growth rate dispersion (GRD) (Ginter and Loyalka, 1996, Ulrich, 2003). For that reason SDG will not be pursued as part of this research.

Non-linearity in the L versus $\ln [n(L)]$ relationship could also arise because of aggregation which is often neglected, because it complicates the population balance making analytical solutions intractable (Ramkrishna, 2000). However, aggregation can be an important size enlargement mechanism having a significant impact on the PSD (Randolph and Larson, 1988). Furthermore, qualitative experimental evidence of struvite aggregation from various sources is demonstrated by optical microscopy and scanning electron microscopy, as shown in Figure 3.2.

The photographic evidence in Figure 3.2, and work of Ginter and Loyalka (1996), suggest that aggregation provides a more realistic explanation of the observed MSMPR behaviour. As such, this chapter explores the use of the population balance equation, incorporating nucleation, size-independent crystal growth and aggregation. This approach will be used to extract kinetic information from the experimental results of Matynia et al., (2006). Prior to addressing the population balance equation incorporating aggregation, it is important to elaborate on the moments of the size distribution.

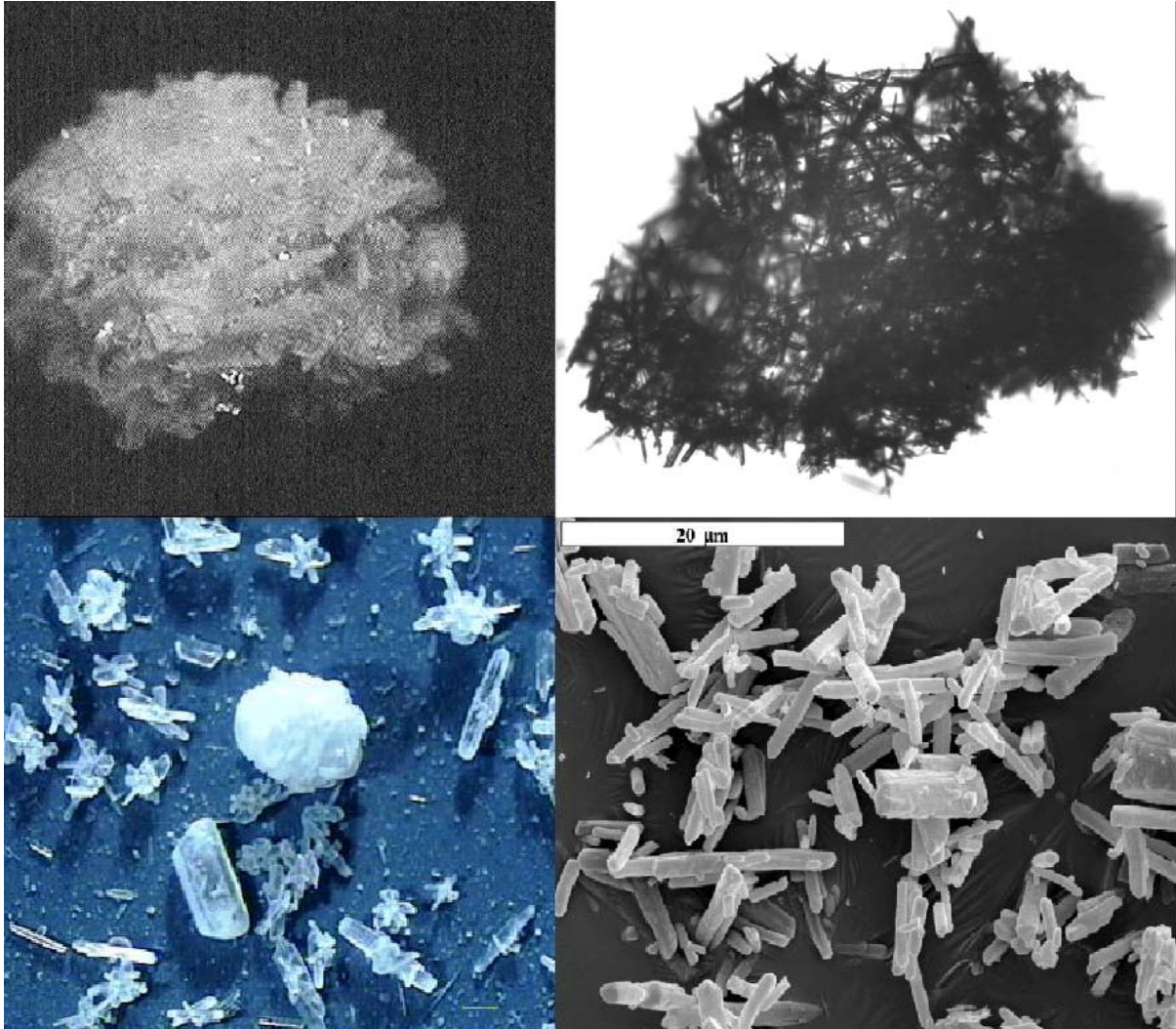


Figure 3.2: Pictures of struvite aggregates, from top-left and moving clockwise; Adnan et al., (2003), This work, Koralewska et al., (2007), Regy et al., (2002).

3.4.2 Moments of the Particle Size Distribution

When a PSD is based on particle length, the moments of the distribution take on a special significance. The first four moments are related to total properties of the suspended population. The zeroth moment is equal to the total number of particles in the system. The first, second and third moments are directly proportional, respectively, to the total length, total area and total volume of the particulate population.

The moments of the distribution are given by Equation 3.5, the so-called moment generating function, where m_j is the j^{th} moment of the distribution.

$$m_j = \int_0^{\infty} L^j n(L) dL \quad 3.5$$

The moments of the distribution provide mean particle size, \bar{L} (Equation 3.6), variance of particle size, σ^2 (Equation 3.7) and the coefficient of variation, CV , which is given by Equation 3.8.

$$\bar{L} = \frac{m_1}{m_0} \quad 3.6$$

$$\sigma^2 = \frac{m_2}{m_0} - \left(\frac{m_1}{m_0}\right)^2 \quad 3.7$$

$$CV = \left(\frac{m_0 m_2}{m_1^2} - 1\right)^{1/2} \quad 3.8$$

3.4.3 Population Balance with Aggregation

The population balance equation for a continuous MSMPR crystalliser with negligible volume change including nucleation, size-independent crystal growth and aggregation is given by Equation 3.9 (Randolph and Larson, 1988).

$$\frac{\partial n}{\partial t} + G \frac{\partial n}{\partial L} = B(L) - D(L) - \sum_k \frac{n_k Q_k}{V} \quad 3.9$$

Where $B(L)$ and $D(L)$ are the birth and death functions, respectively, n_k is the number density in stream k and Q_k is the flow rate of stream k .

The number density is given at an instant of time by the number of particles per unit volume, N , appearing within the size range $L \rightarrow L + dL$ and is given by Equation 3.10.

$$n(L) = \frac{dN}{dL} \quad 3.10$$

Equation 3.9 has no tractable solution because of the birth and death functions. Under the assumption of binary collisions, the aggregation model posits that a particle of size L , aggregating with a particle of size λ , produces the birth and death functions shown in Equations 3.11 and 3.12 (Hulburt and Katz, 1964). Where, β is the aggregation kernel, a detailed treatment is given to the aggregation kernel in §4.2.2.3.

$$B(L) = \frac{L^2}{2} \int_0^L \frac{\beta \left((L^3 - \lambda^3)^{\frac{1}{3}}, \lambda \right) n \left((L^3 - \lambda^3)^{\frac{1}{3}} \right) n(\lambda)}{(L^3 - \lambda^3)^{\frac{2}{3}}} d\lambda \quad 3.11$$

$$D(L) = n(L) \int_0^\infty \beta(L, \lambda) n(\lambda) d\lambda \quad 3.12$$

Numerical methods are therefore necessary to solve Equation 3.9. Approaches taken to solve Equation 3.9 include the collocation of finite elements (Gelbard and Seinfeld, 1978) and cubic spline methods (Steemson and White, 1988). However, this work uses a discretised population balance (DPB) approach, given its success in modelling calcium oxalate precipitation with simultaneous growth and aggregation (Hounslow, 1990, Bramley, 1994).

3.5 Discretised Population Balance Equation

The DPB divides the relevant size domain into discrete intervals where some form of n is assumed (piecewise constant, for example), an example of a discrete size distribution is shown in Figure 3.3. The

result of this is a set of ordinary differential equations which can be solved with the aid of computer software packages. This work uses gPROMS³ to solve the DPB.

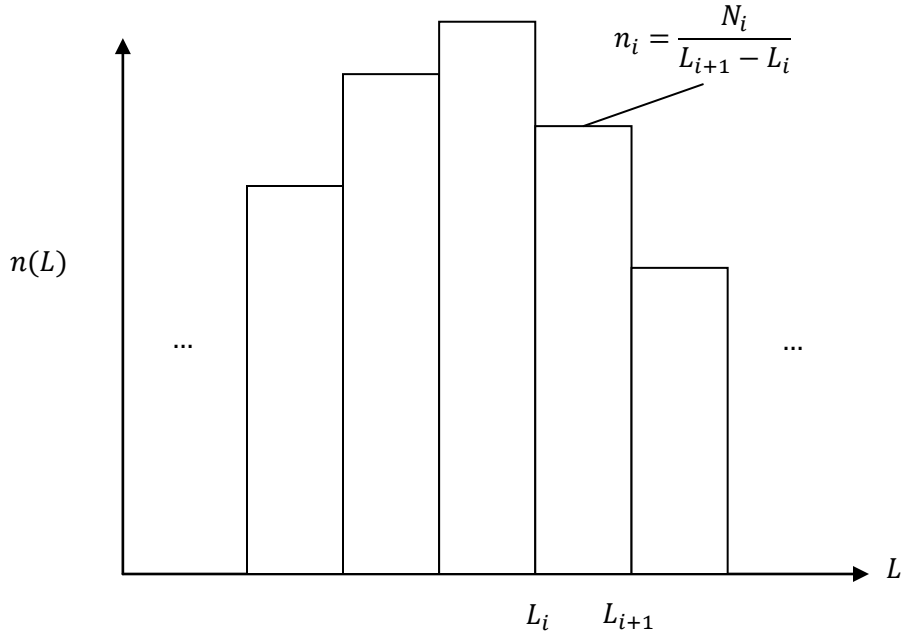


Figure 3.3: Discretised size distribution along the length domain.

3.5.1 Uniform Discretisation

The simplest approach to the DPB with aggregation is a uniformly discretised volume domain, so that $v_{i+1} - v_i = \Delta v$, where Δv is constant. This means the volume of a newly aggregated particle is simply the sum of its original intervals. The coagulation of aerosols was modelled with this approach using Equation 3.13 (Sutugin and Fuchs, 1970).

$$\left. \frac{dN_i}{dt} \right|_{AGG} = \sum_{j+k=i} \varepsilon_{jk} \beta N_j N_k - \sum_{j=1}^{\infty} \varepsilon_{ij} \beta N_i N_j; \quad \varepsilon_{ij} = \begin{cases} 1 & i \neq j \\ \frac{1}{2} & i = j \end{cases} \quad 3.13$$

³ Process Systems Enterprise Limited, Bridge Studios, 107a Hammersmith Bridge Road, London, W69DA, U.K., www.psenderprise.com

Where ϵ is a coefficient used to avoid counting particle interactions more than once.

A weakness in this approach is its inability to accurately describe the length domain. *“One problem with such a model is the necessity of splitting the range of sizes of interest (from 0.065 mm to 30 mm diameter) into a reasonable number of equispaced volume sizes. As each size requires its own equation, it is numerically convenient to limit the number of sizes to less than 30. For a diameter range from 0.065 to 30 mm the volume ranges by a factor of 10^8 which, when divided into 30 equal steps, contains virtually no information about the smaller sizes”* (Batterham et al., 1981). However, modern computing power vastly outstrips that of the 1980s, making this much less of an issue in this work. The ability of the uniform volume discretisation to accurately describe details in the length domain is investigated in §3.5.4.

3.5.2 Geometric Discretisation

Alternatively, a geometric discretisation can be used, so that the ratio in volume of adjoining intervals, v_{i+1}/v_i , is constant. This approach describes the behaviour of small particles more accurately, since the intervals are concentrated towards the start of the domain. This work uses the DPB developed by Hounslow (1990), where $v_{i+1}/v_i = 2$.

The discretisation constant, r , is more conveniently presented on a length basis, Equation 3.14, owing to the crystal growth kinetics being described as a linear growth rate and not a volumetric growth rate.

$$r = \frac{L_{i+1}}{L_i} = \sqrt[3]{2} \quad 3.14$$

Once the discretisation is known, it becomes a matter of developing the appropriate equations for nucleation, crystal growth and aggregation effects. An equation for nucleation and crystal growth can be

developed from first principles. For size-independent growth alone, the population balance is given by Equation 3.15.

$$\frac{\partial n}{\partial t} = G \frac{\partial n}{\partial L} \quad 3.15$$

Integrating with respect to size from L_i to L_{i+1} gives Equation 3.16.

$$\frac{dN_i}{dt} = G(n(L_i) - n(L_{i+1})) \quad 3.16$$

Applying Equation 3.10 results in Equation 3.17.

$$\frac{dN_i}{dt} = G \left(\frac{N_{i-1}}{L_i - L_{i-1}} - \frac{N_i}{L_{i+1} - L_i} \right) \quad 3.17$$

Since nuclei can only appear in the first interval, Equation 3.18 represents the discretised equation for nucleation and crystal growth.

$$\left. \frac{dN_i}{dt} \right|_{NCG} = \begin{cases} B_o - \frac{GN_1}{(r-1)L_1} & i = 1 \\ \frac{G}{(r-1)L_i} (rN_{i-1} - N_i) & i \neq 1 \end{cases} \quad 3.18$$

Where, the subscript, NCG, refers to Nucleation and Crystal Growth.

However, the discretisation of a continuous equation results in the “leakage” of particles into higher size intervals (Hounslow, 1990). While the error in particle numbers may be small, when propagated to the third moment of the distribution, the total particle volume can be over-predicted by as much as 100% (Hounslow, 1990). Clearly, this is an unacceptable situation. To address this, Hounslow (1990) introduced a three-term growth equation of the form shown in Equation 3.19.

$$\frac{dN_i}{dt} = \frac{G}{L_i} (aN_{i-1} + bN_i + cN_{i+1}) \quad 3.19$$

Where the coefficients a , b and c could be chosen to minimise the error incurred through the use of a DPB. After testing 11 different cases of coefficients, Equation 3.20 was found to be the optimal case.

$$\left. \frac{dN_i}{dt} \right|_{NCG} = \begin{cases} B_o + \frac{2G}{(1+r)L_1} \left(\left(1 - \frac{r^2}{r^2-1} \right) N_1 - \frac{r}{r^2-1} N_2 \right) & i = 1 \\ \frac{2G}{(1+r)L_i} \left(\frac{r}{r^2-1} N_{i-1} + N_i - \frac{r}{r^2-1} N_{i+1} \right) & i \neq 1 \end{cases} \quad 3.20$$

It is important to note since all nuclei formed are assumed to be of infinitesimal size, strictly they cannot be included in the DPB because L_1 must be non-zero. Therefore the nucleation rate used in the DPB is actually the rate at which particles appear in the first interval. However, if $L_1 \ll G$, the time required for nuclei to grow into the first interval, $\Delta t = \Delta LG$, can be neglected making the difference between the discretised nucleation rate and real nucleation rate negligible.

The discretised equation, which gives the rate of change of particles in size interval i due to size-independent aggregation (, is given by Equation 3.21, where β_o is the size-independent aggregation kernel. Again, this equation was derived by Hounslow (1990) specifically for $r = \sqrt[3]{2}$ and therefore cannot be applied to a different geometric constant.

$$\left. \frac{dN_i}{dt} \right|_{AGG} = N_{i-1} \beta_o \sum_{j=1}^{i-2} 2^{j-i+1} N_j + \frac{1}{2} \beta_o N_{i-1}^2 - N_i \beta_o \sum_{j=1}^{i-1} 2^{j-i} N_j - N_i \beta_o \sum_{j=i}^{N_{eq}} N_j \quad 3.21$$

Where, the subscript, AGG, represents aggregation.

This form of the DPB has been used successfully by a number of researchers (Hounslow, 1990, Bramley, 1994, Hostomsky and Jones, 1991, Litster et al., 1995, Ilievski, 1991)

3.5.3 Importance of the First Interval

Since nuclei are assumed to have zero size, a DPB violates this assumption because the first size interval of a geometrically discretised size domain cannot be zero. However, if the first interval is small enough, the effect of violating the zero nuclei size assumption should be negligible. To verify this, the third moment of an MSMPR reactor with nucleation and size-independent growth is plotted against the lower bound of the first interval in Figure 3.4. The variables are made dimensionless using Equation 3.22 and 3.23. Arbitrary values for nucleation rate (10^6 $1/L \cdot min$), growth rate ($1 \mu m/min$) and residence time ($12.5 min$) are used.

$$\tilde{m}_3 = \frac{m_3^{numerical}}{m_3^{analytical}} = \frac{\sum_i \left(\frac{1+r}{2} L_i\right)^3 N_i}{6B_0 G^3 \tau^4} \quad 3.22$$

$$\tilde{L}_i = \frac{L_i}{G\tau} \quad 3.23$$

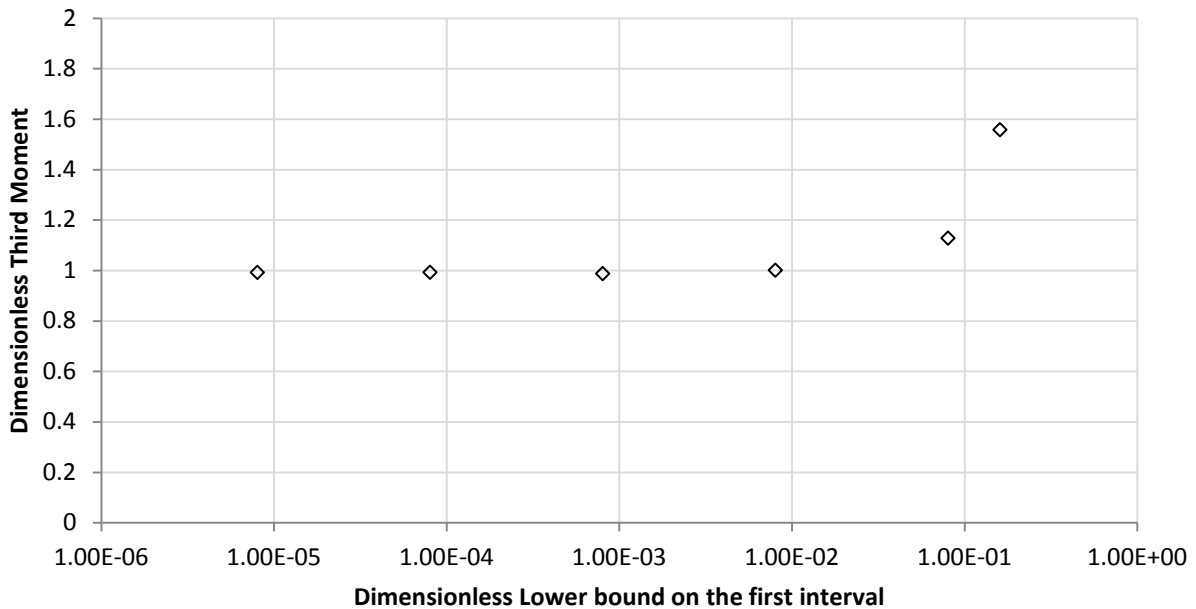


Figure 3.4: Relationship between the lower bound L_i on the first interval of the discretised length domain and the third moment of the PSD.

It can be seen that the third moment is independent of L_1 until the dimensionless length is 0.08 for the arbitrary kinetic parameters used to generate Figure 3.4. Therefore, if the L_1 is chosen so that it has a dimensionless length less than 0.08, the cost of violating the zero-size nuclei assumption is inconsequential to the third moment.

3.5.4 Uniform Discretisation Performance

As discussed in §3.5.1, a uniform discretisation of the volume domain provides simpler equations, describing the aggregation process, but at the cost of an increased number of equations, computational effort and a loss in resolution for smaller particles. Since contemporary computing power is much greater than that in the 1980s, the uniform discretisation is tested at steady state for nucleation and size-independent crystal growth. If model fidelity can be maintained it would provide a basis to further explore the use of the uniform discretisation.

It should be noted that a uniform discretisation of the volume domain cannot be used directly with Equation 3.18, which is based on the length of each interval. Therefore the uniform volume discretisation must be converted to a length discretisation, which is done by taking the cube root of v_i . The length domain covered for this analysis is $0.01 \mu\text{m}$ to $100 \mu\text{m}$ with 1000 intervals. The growth rate used is $1 \mu\text{m}/\text{min}$, the nucleation rate used is 10^6 1/L.min and the residence time is 12.5 min , so dimensionless L_1 is less than 0.08. Table 3.1 shows total number of equations, dimensionless third moment and CPU time required to run the model.

Table 3.1: Uniform discretisation performance in terms of dimensionless third moment and CPU time.

Interval number	Interval volume	Equation number	\tilde{m}_3	CPU time
1000	$1000 \mu m^3$	13055	1.2524	563.078 sec

It can be seen in Table 3.1 that at steady state the numerical third moment found using the uniform discretisation is approximately 25% greater than the analytical result. This is because of the poor resolution of the uniform discretisation in the lower size range. The first interval of the uniform discretisation covers $0.01 \mu m$ to $10 \mu m$, effectively making every particle in the first interval $5 \mu m$. This means the dimensionless length of nuclei birthed into the first interval is 0.4. When examining Figure 3.4, the dimensionless third moment result is not surprising.

The simple solution would be to decrease the size of the first interval so that the dimensionless length is less than or equal to 0.08. However, this greatly increases the number of equations required. If the first interval were small enough to adequately describe nucleation, and the length domain covered is still $0.01 \mu m$ to $100 \mu m$, a total of 10^9 intervals would be required for this uniform discretisation. Assuming that the relationship between number of intervals and CPU time required to solve the system of equations is linear, this would require 6516 days to solve with a commonly available contemporary computer. It is therefore concluded the geometric discretisation is still the best choice.

3.5.5 Extracting the Rates

To use the DPB, the rates of nucleation, growth and aggregation must be known. These are determined from experimentally measuring PSDs and employing relationships derived from the moment form of the population balance equation, which yields two useful equations (3.24 and 3.25) for an MSMR crystalliser operating at steady state (Hounslow, 1990). The moments of the distribution are defined by

Equation 3.26. Two further equations are required to use the Hounslow (1990) rate extraction method, the Aggregation Parameter (K , Equation 3.27) and the Index of Aggregation (I_{AGG} , Equation 3.28).

$$\frac{\beta_0 m_0^2}{2} + \frac{m_0}{\tau} - B_0 = 0 \quad 3.24$$

$$3Gm_2 - \frac{m_3}{\tau} = 0 \quad 3.25$$

$$m_j = \sum_i \bar{L}_i^j N_i \quad 3.26$$

$$K = B_0 \beta_0 \tau^2 \quad 3.27$$

$$I_{AGG} = \frac{K + 1 - \sqrt{1 + 2K}}{K} \quad 3.28$$

The Index of Aggregation was found to have an empirical relationship to the coefficient of variation by Hounslow (1990) when studying experimental data on nickel ammonium sulphate (Tavare et al., 1985). This provides us with the extra equation to extract all three rates from the experimental data. The empirical relationship is given by Equation 3.29.

$$CV = (1 - I_{AGG})^{-0.3} \quad 3.29$$

Equations 3.25 - 3.29 can now be rearranged to yield Equations 3.30 - 3.34 which can be solved with the experimentally determined moments.

$$G = \frac{m_3}{3\tau m_2} \quad 3.30$$

$$I_{AGG} = 1 - CV^{-10/3} \quad 3.31$$

$$K = \frac{2I_{AGG}}{I_{AGG}^2 - 2I_{AGG} + 1} \quad 3.32$$

$$\beta_0 = \frac{\sqrt{1 + 2K} - 1}{m_0\tau} \quad 3.33$$

$$B_0 = \frac{K}{\beta_0\tau^2} \quad 3.34$$

Now that we have the means of extracting the rates from steady-state experimental data and the DPB equation to predict the experimental PSD, we can test the validity of this approach against existing experimental data.

3.6 Results and Discussion

The DPB was tested against four sets of experimental data. The details of the experimental methods, conditions and sources are summarised in Table 3.2.

Table 3.2: Experimental methods and conditions used to compare with DPB equation predictions.

Experiment	Concentration	<i>pH</i>	PSD Analysis Method	Reference	Location of results
1	[Mg] = 0.25 wt% [NH ₄] = 25 wt% [PO ₄] = 25 wt%	9	Laser Diffraction	Matynia et al. (2006)	Figure 3.5
2	[Mg] = 2.0 wt% [NH ₄] = 25 wt% [PO ₄] = 25 wt%	9	Laser Diffraction	Matynia et al. (2006)	Figure 3.6
3	[Mg] = 0.5 wt% [NH ₄] = 25 wt% [PO ₄] = 25 wt%	8	Laser Diffraction	Matynia et al. (2006)	Figure 3.7
4	[Mg] = 0.5 wt% [NH ₄] = 25 wt% [PO ₄] = 25 wt%	11	Laser Diffraction	Matynia et al. (2006)	Figure 3.8

The experiments conducted by Matynia et al. (2006) were performed in a Draft Tube MSMR crystalliser, having a working volume of 0.6 L with identical agitation rates and a constant temperature

of 298 K; the residence time for all experiments was 15 minutes. It should be noted that the concentration is that of the nutrient feed solution to the crystalliser, a sodium hydroxide feed stream is also used. However, the flow rate of the two streams is not given so concentrations in the reactor cannot be calculated. Comparisons between experimental data, SDG model predictions and DPB model predictions is shown in Figure 3.5 to Figure 3.8. The constants used in the SDG model and the nucleation rates, growth rates and aggregation kernel for the DPB are given in Table 3.3.

Table 3.3: Constants for SDG and DPB models.

Expt	DPB			SDG				
	B_0 [$1/m^3 \cdot s$]	G [m/s]	β_0 [m^3/s]	G_0 [m/s]	G_∞ [m/s]	a [$1/m$]	n_0 [$1/m \cdot m^3$]	B_0 [$1/m^3 \cdot s$]
1	2.71×10^{14}	3.83×10^{-9}	1.64×10^{-16}	2.60×10^{-10}	7.74×10^{-9}	124798	2.72×10^{21}	7.09×10^{11}
2	1.95×10^{15}	2.94×10^{-9}	1.17×10^{-17}	3.44×10^{-10}	6.72×10^{-9}	114691	2.09×10^{22}	7.20×10^{12}
3	5.67×10^{15}	1.08×10^{-9}	6.00×10^{-18}	6.71×10^{-10}	5.15×10^{-9}	46933	1.37×10^{22}	9.21×10^{12}
4	7.75×10^{17}	5.94×10^{-9}	9.31×10^{-16}	3.53×10^{-11}	1.21×10^{-8}	83458	1.22×10^{23}	4.33×10^{12}

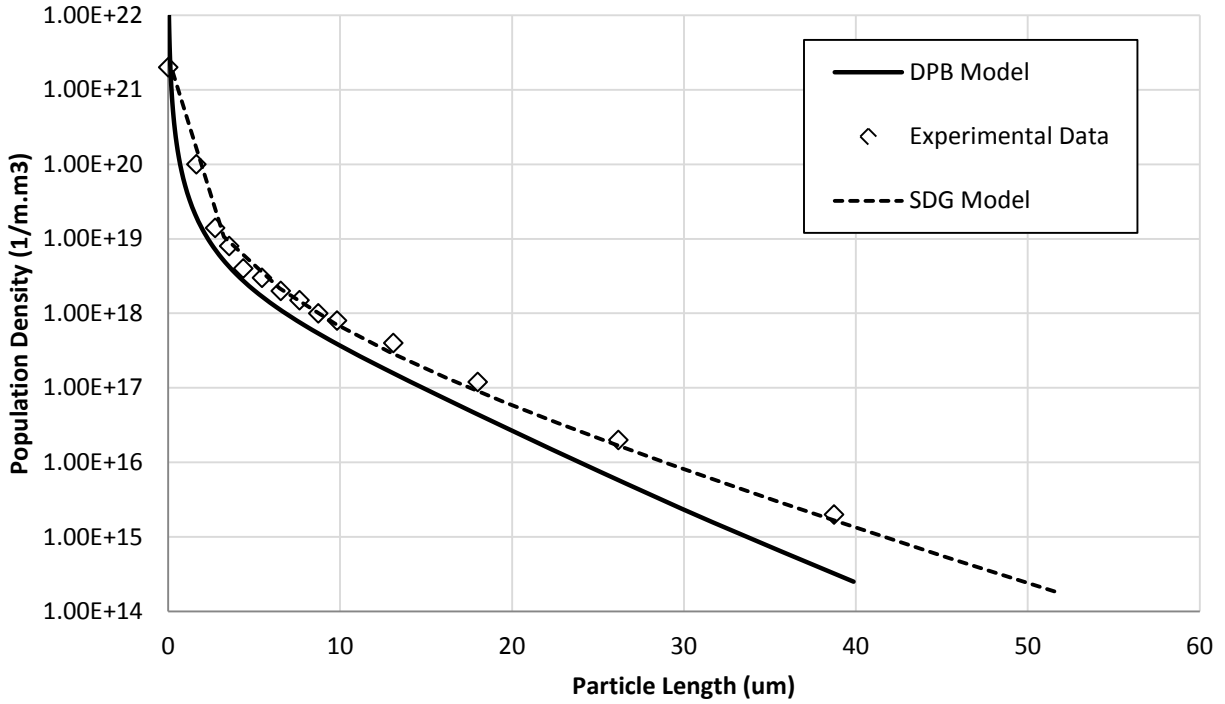


Figure 3.5: Population density results for experiment 1, DPB model and SDG model.

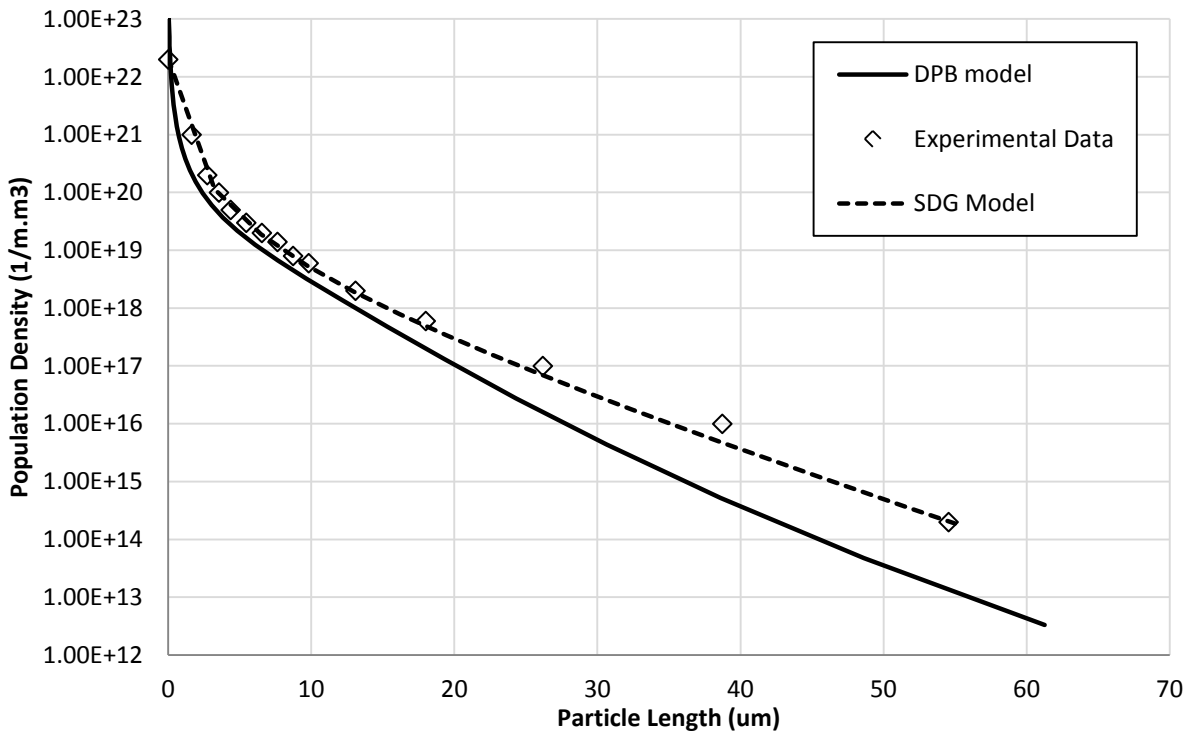


Figure 3.6: Population density results for experiment 2, DPB model and SDG model.

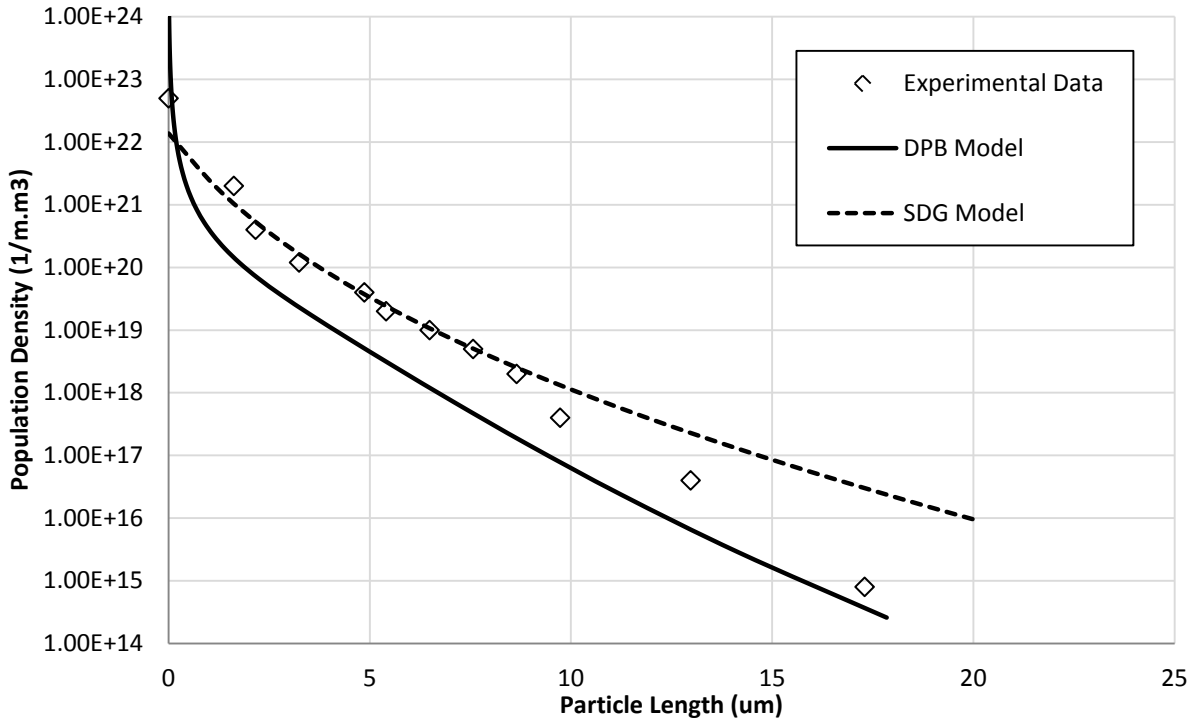


Figure 3.7: Population density results for experiment 3, DPB model and SDG model.

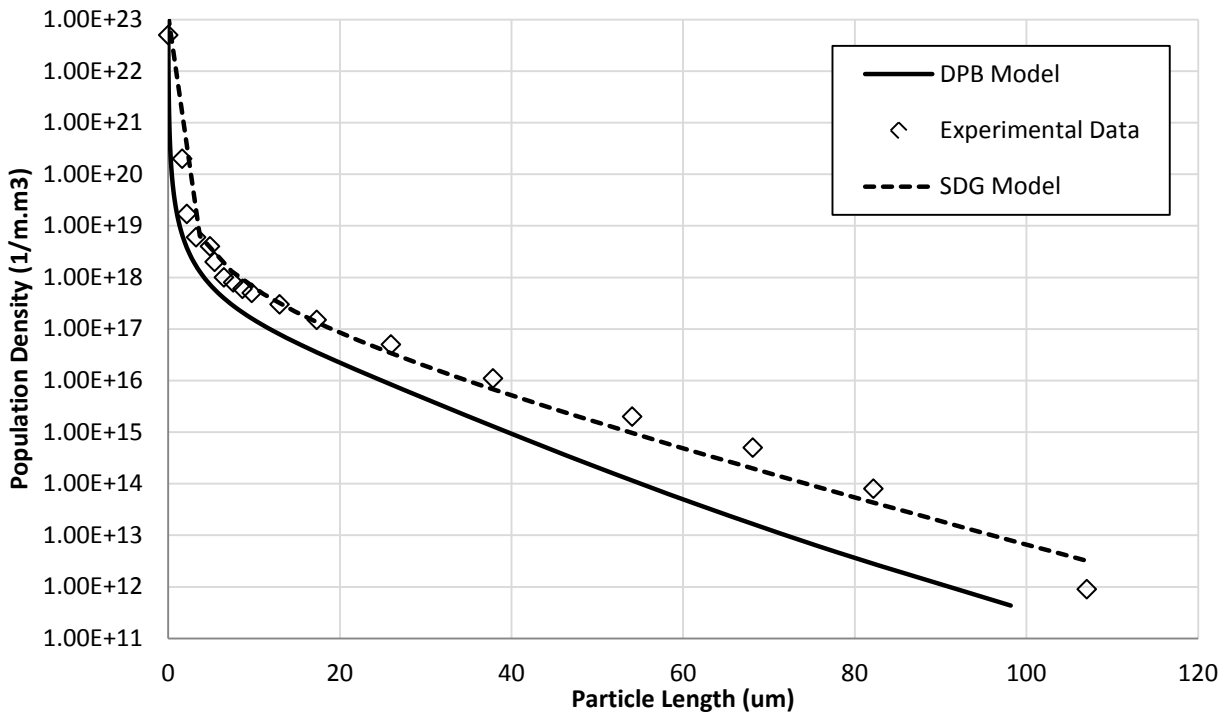


Figure 3.8: Population density results for experiment 4, DPB model and SDG model.

It can be seen in Figure 3.5 to Figure 3.8 that the SDG model appears to provide a better fit than the DPB model, but the scatter of the experimental data must be considered. Unfortunately, Matynia et al. (2006) do not report the uncertainty in their experimental results, making this judgement difficult. However, considering the experimental methods used to collect this data may be of some help. As stated in Table 3.2, all PSD data from Matynia et al. (2006) was collected using a Laser Diffraction size analysis method (*Beckman Coulter LS-230*). Laser Diffraction sizing cannot count particles in order to produce the number-size distribution needed to use both SDG and DPB models. It can only measure the volume-size distribution, which must be subsequently transformed to a number-size distribution, using Equation 3.35 (Mullin, 1993).

$$n_i = \frac{m_i}{k_v \rho L_i^3 \Delta L_i V} \quad 3.35$$

Where, m_i , is the mass of crystals in interval i , k_v , is the volumetric shape factor, ρ , is particle density and V is the volume of the reactor. This transformation requires that all particles have the same shape factor no matter what their individual size, *i.e.* all particles are spheres, cubes or rectangles with the same aspect ratio (Randolph and Larson, 1988). The shape factor used by Matynia et al. (2006) was $k_v = 1$ (cubic particles). Clearly, from Figure 3.2, struvite particles are not cubic, which weakens their analysis and subsequent conclusions. It can also be seen that the crystals do not share the same aspect ratio; some are needle-like ($k_v \approx 8$), while others are more rectangular ($k_v \approx 2.5$). Their shape factor calculation is based on a square base of length, L , and the shape factor accounts for particle depth (Allen, 1990). This violates the requirement of consistent shape factors.

Another way to quantify the affect that the transformation (from mass distribution to number distribution) has on the experimental data is to compare the difference between the measured solids concentration and the solids concentration calculated from the moments of the transformed number-size distribution. Matynia et al. (2006) provided a measured solids concentration for each experiment

performed, the third moment (total volume of crystals) calculated from the experimental distribution can check if mass was conserved during the transformation. The results of this comparison are located in Table 3.4.

Table 3.4: Comparison of the measured solids concentration and calculated solids concentration from the transformed number-size distribution.

Experiment	Measured Solids Concentration (kg/m³)	Calculated Solids Concentration (kg/m³)	Percentage Difference
1	23.3	33.35	30.12%
2	196.7	208.62	5.71%
3	46.7	57.11	18.23%
4	49.2	63.10	22.03%

It can be seen in Table 3.4 that there is a significant difference between the measured solids concentration and those calculated from the third moment of the experimental number-size distribution. This provides further evidence of the uncertainty in using particle size analysis techniques based on particle volume, rather than particle number. Unfortunately, no struvite PSD data has been reported in the literature based on particle counting and sizing techniques. Therefore, any kinetic parameters retrieved from this experimental data likely contain excessive uncertainty, not to mention systematic errors, to be considered useful. However, it is still instructive to make qualitative comparisons between the results plotted in Figure 3.5 to Figure 3.8

While the SDG model does fit better in Figure 3.5 to Figure 3.8, the DPB model produces the same shape as the experimental data in each case when extracting the rates with Equations 3.30 - 3.34. Furthermore, Equation 3.29 used in the rate extraction process is an empirical relation that has not been tested for struvite crystallisation, and could account for deviation between the measured and predicted

population densities. However, if the extracted rates were adjusted to improve the fit, it would demonstrate the ability of the DPB to achieve the same fit as the SDG model. To test this, the extracted rates were adjusted through trial and error. Figure 3.9 shows that a better fit can be achieved by adjusting the rates, as shown in Table 3.5. This suggests that the DPB model has the ability to predict the population density function as well as the SDG model. Furthermore, the existence of experimental evidence for aggregation suggests the DPB model is a more meaningful model in terms of actual kinetic mechanisms.

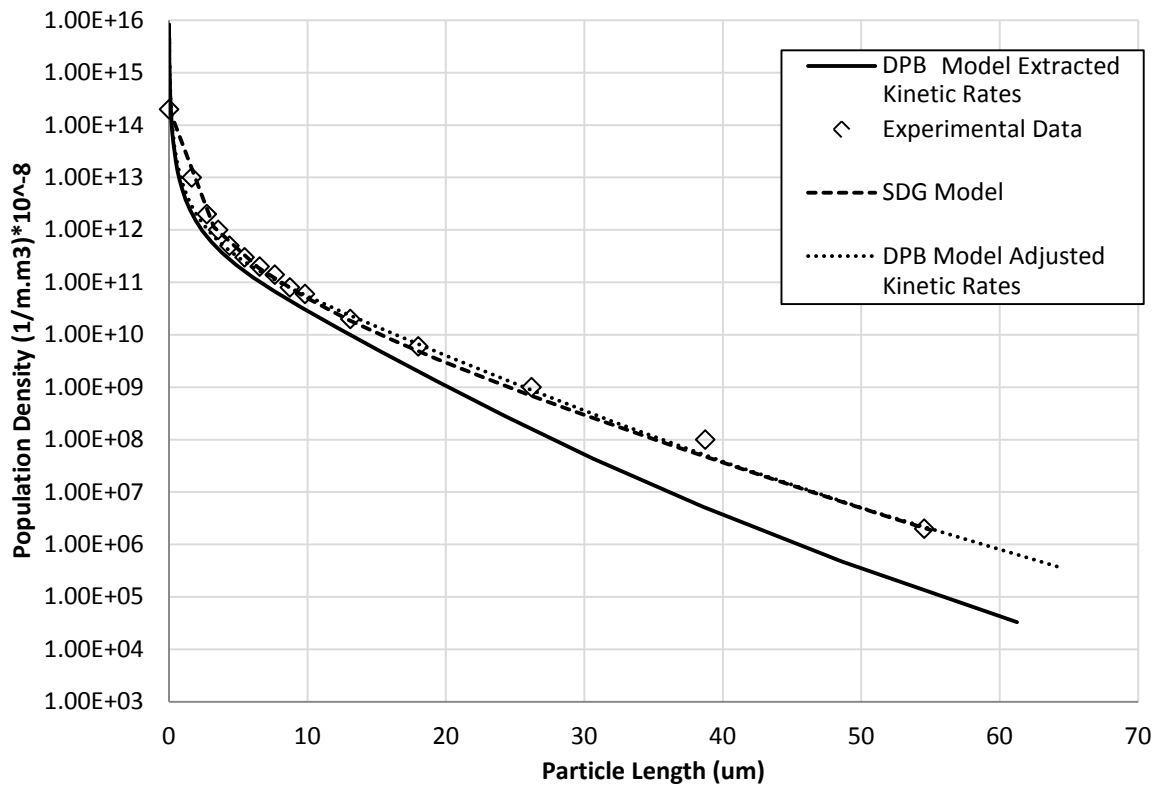


Figure 3.9: Population density results for Experiment 2, DPB model with extracted rates, SDG model and DPB model with adjusted kinetic rates.

Table 3.5: Adjusted kinetic rates for DPB model.

B_0 [$1/m^3 \cdot s$]	G [m/s]	β_0 [m^3/hr]
1.95×10^{15}	3.89×10^{-9}	1.11×10^{-17}

3.7 Conclusions

It was demonstrated that the DPB equation with simultaneous nucleation, growth and aggregation can achieve reasonable agreement with experimentally determined PSDs for struvite precipitation, even though there is considerable uncertainty in the experimental results. The DPB is also more meaningful than the size-dependent growth model, since it describes kinetic mechanisms based on experimental evidence, rather than choosing mechanisms on the basis of mathematical convenience or statistical goodness of fit. On this basis, the DPB with nucleation, crystal growth and aggregation will be used to develop the struvite crystallisation process model. In order to advance the work done to date, experiments should be conducted that utilise a counting method for particle size analysis, limiting uncertainty in the data and increasing the confidence of kinetic parameters determined from those data.

3.8 Key Points from Chapter Three

- Aggregation is a key mechanism influencing struvite crystallisation and has a significant influence on the PSD.
- The DPB allows the investigation of nucleation, crystal growth and aggregation simultaneously.
- The level of agreement between the DPB and experimental data suggests it is capable of modelling struvite nucleation, crystal growth and aggregation during crystallisation.

Chapter 4 – Development of a Struvite MSMPR Process Model

This chapter details the development of a struvite process model incorporating solution thermodynamics, nucleation, growth and aggregation mechanism kinetics, a discretised population balance and mass balance. Dynamic operation of the model is simulated. The importance of non-ideal thermodynamics is clearly shown. The potential of the model for process design is explored by investigating the influence of reactor volume and residence time on phosphorus recovery.

4.1 Introduction

Process modelling is an important tool in better understanding any chemical process. The ability to know how a process will behave under start-up, operation and scheduled (or unscheduled) shut-downs cannot be underestimated. It informs more confident process design, control and optimisation, reducing risk in the deployment of novel processes, such as a nutrient recovery system. Without such risk minimisation strategies, design specifications can be made with poor judgement resulting in unnecessary capital costs or below-capacity process operation. Any experiments that are required at laboratory scale, pilot scale or full scale can be more effectively targeted through process modelling, saving time and money.

4.2 Development of the Process Model

The process model is divided into four separate, yet interconnected components, which, when combined, uniquely describe the operation of a struvite MSMPR crystalliser. These components are: solution thermodynamics (algebraic); nucleation, crystal growth and aggregation kinetics (algebraic); population balance equation (dynamic) and mass balances (dynamic). The way in which these components are used to formulate the process model is represented in Figure 4.1. The resultant model equation set is simulated using gPROMS.

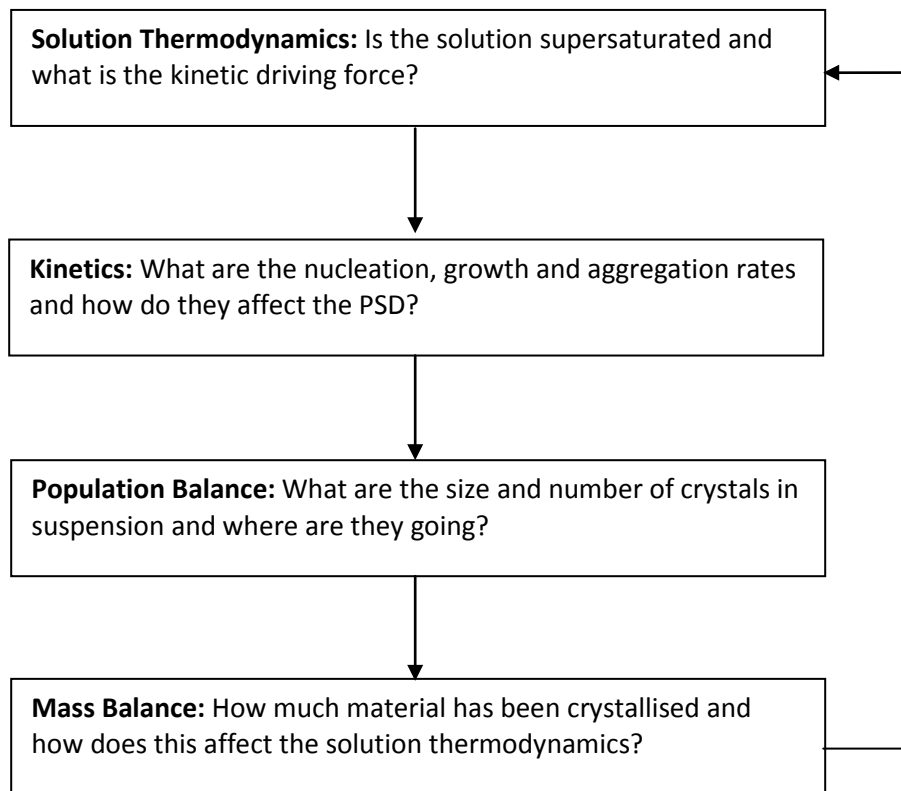


Figure 4.1: Diagram of process modelling philosophy used for the struvite MSMPR crystalliser.

As discussed in §2.2.5 a number of water chemistry software packages exist, which accurately describe non-ideal solution thermodynamics. However, these packages do not easily (or entirely) lend themselves to process modelling or dynamic simulation, which is essential to this study. Therefore, the

description of solution thermodynamics is executed in gPROMS, along with the other mathematical components of the process model.

The MSMPR crystalliser was assumed to be unseeded and starts from arbitrary initial conditions (*i.e.* starting solution concentrations), and achieves a steady-state solution. The process flow diagram and nominal conditions for the MSMPR model are given in Figure 4.2. The struvite constituents are fed by the stream subscripted *MAP* (Magnesium, Ammonium and Phosphate) and the sodium hydroxide, used to adjust *pH*, is fed by the stream subscripted *NaOH*. The input streams, constituent concentrations and flowrates are all specific to struvite crystallisation and based upon the operation of laboratory-scale reactors. However, the number of streams, constituents, flow rates and reactor size could be changed to feasibly model any such system. Batch or fed-batch reactor operation could also be achieved by setting outflow and/or inflow streams to zero.

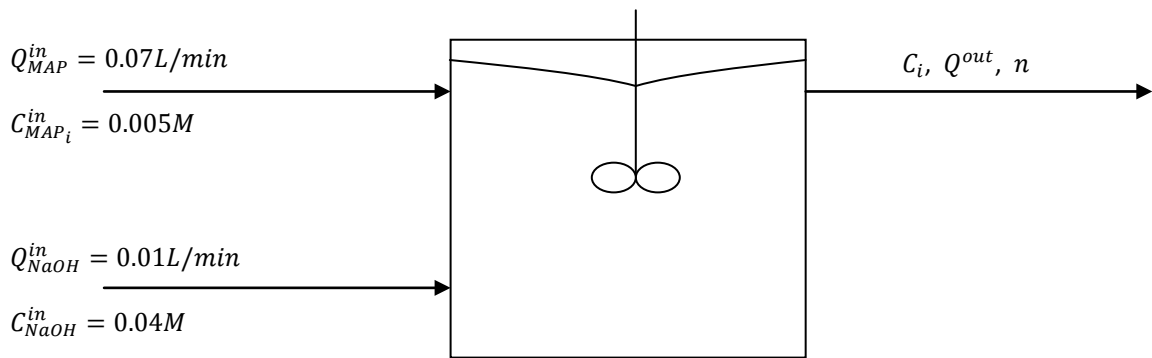


Figure 4.2: Process flow diagram of the MSMPR struvite crystalliser modelled and its nominal operating conditions.

4.2.1 Solution Thermodynamics

The description of struvite solution thermodynamics is detailed in §2.2, so will not be further discussed.

However, this chapter uses gPROMS to implement the solution thermodynamics whereas Chapter 2

used EES. Because of this change in software, the same verification using PHREEQC performed in §2.2.5 is performed for the gPROMS version in Figure 4.3.

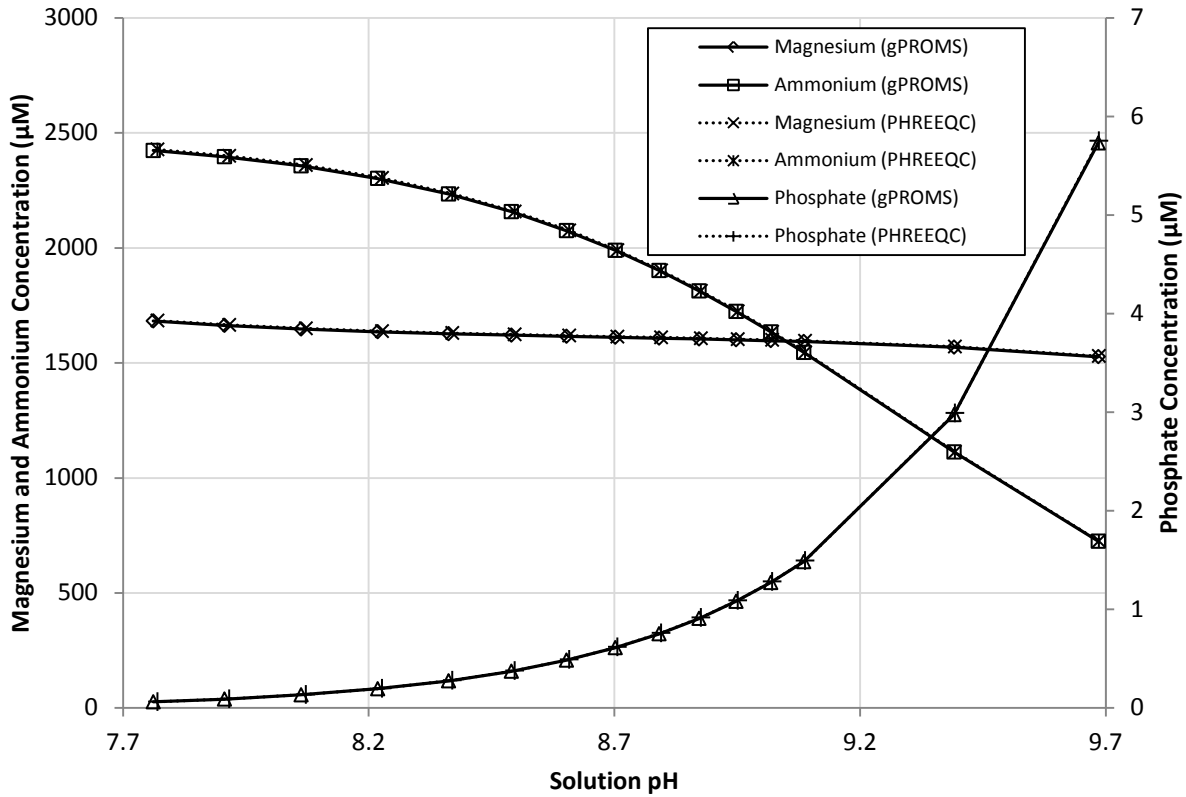


Figure 4.3: gPROMS solution thermodynamics verified against PHREEQC at 0.0025M equimolar total analytical concentration of magnesium, ammonium and phosphate and varying solution pH .

An experimental validation of the solution thermodynamics is included in §4.3.1 of this chapter. This is done by using the charge balance to predict the pH , after a known amount of sodium hydroxide is added to a solution of known concentration. The predicted pH value is then compared to experimental measurements.

4.2.2 Kinetics

The formulation of any rate-based process model requires a description of system kinetics. The kinetics determines batch times for batch configuration and residence times for continuous configuration. It is

tempting to describe a precipitation reaction in the same way one would describe a traditional chemical reaction, however, the influence of physical mechanisms, such as nucleation, crystal growth and aggregation complicate matters, as discussed in §3.2. The modelling equations used in the formulation of the various rate processes are discussed in the following subsections.

4.2.2.1 Nucleation Rate

Primary nucleation and previous research into its kinetics for struvite are reviewed in §2.3. However, the results from those studies are not applicable to the development of a process model, since any operating crystalliser will invariably contain crystals. Thus secondary nucleation is arguably more relevant to developing this mathematical model. Secondary nucleation is the formation of nuclei in the presence of other crystals in the system. There is no universally accepted set of mechanisms responsible for secondary nucleation and a number of potential mechanisms for secondary nucleation abound (Jones, 2002).

One likely important mechanism is *contact nucleation*. This occurs when crystals contact each other or contact crystalliser parts causing the shedding of the boundary layer from the crystal. If the size of the shed boundary layer is greater than the critical nuclei size it becomes a new nucleus itself (Randolph and Larson, 1988). It is now recognised that for systems with high to moderate solubility this is the most significant mechanism in crystallisers (Garside et al., 2002).

Attempts have been made to describe different mechanisms for secondary nucleation theoretically, such as nucleation controlled by: attrition fragments of crystals, cluster formation, surface nucleation, dendritic growth and dendritic coarsening (Mersmann, 1996). However, the precise nucleation mechanism occurring in any particular case is usually contentious (Jones, 2002). In practice, an empirical power law relationship, dependent on supersaturation, crystal mass density and some measure of the

hydrodynamic interactions between crystals and the solution, is sufficient to determine the nucleation rate (Garside et al., 2002).

This work considers the effect of hydrodynamics to be outside of its scope, and thus neglects it. In any event the rate of mixing is held constant in all experiments used to determine kinetic parameters, so even if there were in effect, hydrodynamics need not enter into this analysis. The effect of crystal mass density is also neglected here in the interest of minimising the number of parameters to be estimated. With this in mind, Equation 4.1 is used to describe the nucleation rate in mathematical form.

$$B_o = k_B(SI)^{n_B} = 1.0 \times 10^6(SI)^1 \quad 4.1$$

Here B_o is the nucleation rate (1/L.min), k_B is the nucleation rate coefficient (1/L.min) and its value is chosen based on the order of magnitude reported for similar systems in the literature (Garside and Shah, 1980), n_B is the order of nucleation (unitless).

It should be noted that the inclusion of solution thermodynamics in the process model enables the use of the SI variable (Equation 2.2) – the thermodynamic driving force - in the nucleation rate equation. This is an important contribution, since without it, the approximation described in Equation 2.5 would have to be used.

4.2.2.2 *Crystal Growth Rate*

Crystal growth is understood to be a two-step process where first, solute molecules diffuse to the surface of the crystal, and second, they are integrated into the crystal lattice. It can be assumed that these two processes take place in series, diffusion being driven by the solute concentration difference between the bulk and the boundary layer, and integration being driven by the solute concentration difference between the boundary layer and the equilibrium concentration (Mullin, 1993). These steps

are often lumped together in an empirical equation that relates the crystal growth rate to supersaturation as shown in Equation 4.2 (Garside et al., 2002).

$$G = k_G(SI)^{n_G} \quad 4.2$$

Where G is the size-independent crystal growth rate ($\mu\text{m}/\text{min}$), k_G is the crystal growth rate coefficient ($\mu\text{m}/\text{min}$) and n_G is the order of crystal growth.

Unlike nucleation, there are a number of widely used, theoretical expressions describing the integration process during crystal growth. Two commonly used expressions are those derived from the Burton, Cabrera, Frank (BCF) theory (Burton et al., 1951) and the 'birth and spread' or 'nuclei upon nuclei' model (Ohara and Reid, 1973). One useful feature of the BCF model is that for an integration-controlled growth process, it reduces to the first and second order version of Equation 4.2 for high supersaturation and low supersaturation conditions, respectively (Garside et al., 2002).

However, the use of theoretical models to describe the integration process is considered out of the scope of this work, thus the more empirical power law model will be used. With this in mind, Equation 4.2 describes crystal growth in the mathematical model. A crystal growth coefficient of $1.0\mu\text{m}/\text{min}$ was chosen, somewhat arbitrarily, for the simulations in this chapter. Its order of magnitude is based on the work of Hounslow (1990) and Bramley (1994) on calcium oxalate monohydrate. A first-order growth rate is assumed because it simplifies the mathematics and it corresponds to the high supersaturation degenerate case of the BCF model.

4.2.2.3 Aggregation Kernel

The aggregation kernel was first introduced by Smoluchowski (1917) to describe the collision frequency of dispersed particles due to Brownian motion. Basing his work on Fick's Law of Diffusion, he found the

rate of collisions between particles of size i and j to be given by Equation 4.3 and 4.4 (Smoluchowski, 1917).

$$R_{col} = \beta_{ij}N_iN_j \quad 4.3$$

$$\beta_{ij} = \beta_0 \left(\frac{1}{L_i} + \frac{1}{L_j} \right) (L_i + L_j) \quad 4.4$$

Where R_{col} is the rate of collisions (1/L.min), β_{ij} is the aggregation kernel for particles of size i and j (L/min), β_0 is the size independent aggregation kernel (L/min), N is the number of particles (1/L) and L is the size of the particles.

Since the work of Smoluchowski (1917), other kernels have been developed from a theoretical framework, based on other forces resulting in particle collisions such as, laminar flow, turbulent flow and gravitational forces. Furthermore, other, purely empirical, kernels have also been developed (Jones, 2002). A number of these kernels were tested using Equation 3.21 for calcium oxalate monohydrate (Hounslow, 1990, Bramley, 1994) and aluminium hydroxide (Ilievski, 1991).

It was found that a size-independent kernel provided a better fit than the more complex size-dependent kernels. This is surprising as Smoluchowski (1917) suggests the rate of aggregation, and therefore the kernel, is size dependent. It has been suggested that the increase in aggregation inefficiency and particle disruption with particle size can give rise to apparent size independent aggregation (Jones, 2002). With this in mind, along with the findings of Hounslow (1990), Ilievski (1991) and Bramley (1994), a size-independent kernel will be used to describe struvite aggregation.

Hounslow (1990), Ilievski (1991) and Bramley (1994) also found a relationship between supersaturation and the aggregation kernel that could not be explained by traditional DLVO (Derjaguin, Landau, Verwey and Overbeek) theory of attractive and repulsive forces. It was proposed by Bramley (1994) that the boundary layer surrounding growing crystals results in bridging between colliding particles. The higher

the supersaturation, the larger the boundary layer and the more likely the strength of the bridge would result in a successful aggregate. This proposition has been further supported by further work (Hounslow et al., 2001). It has also been stated that crystals become “stickier” as supersaturation increases (Jones, 2002). With this in mind, Equation 4.5 is used to determine the size-independent aggregation kernel in the process model.

$$\beta_0 = k_\beta (SI)^{n_\beta} = 1.0 \times 10^{-6} (SI)^1 \quad 4.5$$

Where k_β is the aggregation kernel coefficient (L/min) and n_β is the order of the aggregation kernel. The values of k_β and n_β were chosen for the simulations in this chapter, based on the work of Hounslow (1990) on calcium oxalate monohydrate.

4.2.3 Population Balance

Unfortunately the three-term discretised growth equation described in Equation 3.20 cannot be applied to a continuous MSMR model that operates dynamically. The accuracy gained by using the three-term growth equation comes at the cost of numerical stability (Hounslow, 1990). Therefore, applications of the Hounslow (1990) DPB have been limited to batch and steady-state MSMR operation. This is unacceptable as a key objective of this work is a dynamic process model.

Stability can be achieved with the three-term equation if the L_1 chosen is in the same order as the growth rate. However, this means the model nucleation rate is no longer representative of the real nucleation rate, see §3.5.3. One method to address this is to use an adjustable discretised population balance (ADPB).

4.2.3.1 Adjustable Discretised Population Balance

The ADPB can be used to adjust the geometric progression used to discretise the length domain. By refining the discretisation, the accuracy of the more stable two-term growth equation becomes

acceptable. However, this invalidates the discretised aggregation equation that was developed specifically for the case of $r = \sqrt[3]{2}$. An aggregation equation that could be used with the ADPB was developed (Litster et al., 1995) and further improved with Wynn's modification (Wynn, 1996), see Equation 4.6. This introduces a variable, q , which adjusts the geometric constant and therefore the discretisation, so that $r = 2^{1/3q}$. This leads to a rather complex result.

$$\begin{aligned}
\frac{dN_i}{dt} \Big|_{AGG} = & \sum_{j=1}^{i=S_1} \beta_o N_{i-1} N_j \frac{2^{(j-i+1)/q}}{2^{1/q} - 1} + \sum_{p=2}^q \sum_{j=i-S_{p-1}}^{i-S_p} \beta_o N_{i-p} N_j \frac{2^{(j-i+1)/q} - 1 + 2^{-(p-1)/q}}{2^{1/q} - 1} \\
& + \frac{1}{2} \beta_o N_{i-q}^2 + \sum_{p=1}^{q-1} \sum_{j=i+1-S_p}^{i+1-S_{p+1}} \beta_o N_{i-p} N_j \frac{-2^{(j-i)/q} + 2^{1/q} - 2^{-p/q}}{2^{1/q} - 1} \\
& - \sum_{j=1}^{i-S_1+1} \beta_o N_i N_j \frac{2^{(j-i)/q}}{2^{1/q} - 1} - \sum_{j=i-S_1+2}^{\infty} \beta_o N_i N_j
\end{aligned} \tag{4.6}$$

Equation 4.6 introduces the variable S_p which is defined such that the volume, $v = (v_i - v_{i-p})$, falls into the $(i - S_p)^{\text{th}}$ interval. Where p is an array of whole numbers from 1 to q . S_p is given by Equation 4.7.

$$S_p = \text{Int} \left[1 - \frac{q \ln(1 - 2^{-p/q})}{\ln 2} \right] \tag{4.7}$$

While this approach does provide a solution to the inaccuracy of the two-term growth equation, the implementation of Equation 4.6 and 4.7 is difficult. An alternative approach is divided below, using a sigmoid function to allow the $r = \sqrt[3]{2}$ discretisation to be used accurately.

4.2.3.2 A Hybrid Approach to the DPB

The DPB based upon either the two-term or three-term growth equations have the following properties:

1. The two-term growth equation is stable, but over predicts the particle number in the i^{th} interval, translating into unacceptably high errors in the third moment.
2. The three-term growth equation is more accurate but less stable than the two-term model, particularly in the small size intervals, leading to numerical instabilities during solution.

This work proposes that the two approaches be combined, in order to capitalise on their strengths, while limiting their associated weaknesses. It would be ideal if the two-term growth equation could be used for the small size intervals, where the three-term equation is too unstable to offer numerical solutions. The propagation of error to the third moment would be modest, owing to the small size of particles in these intervals. Furthermore, it would also be ideal if the three-term equation were to be used for the larger size intervals, where stability is not an issue, but accuracy is assured for the predicted third moment. This approach was taken in this work. The key was that some form of transition from the two-term to the three-term equation is required.

Eventually, a sigmoid function was employed as a weighting factor, which affected a smooth transition between the two-term and three-term rate equations. The sigmoid function used is given by Equation 4.8 and is applied to the discretised growth equation using Equation 4.9.

$$\alpha_i = \frac{1}{1 + e^{-i+25}} \quad 4.8$$

$$\left. \frac{dN_i}{dt} \right|_{NCG} = (1 - \alpha_i) \left. \frac{dN_i}{dt} \right|_{2term} + \alpha_i \left. \frac{dN_i}{dt} \right|_{3term} \quad 4.9$$

Here α is the weighting factor that displays sigmoidal behaviour and i is the interval number of the discretisation. A constant is required in the Equation 4.8 to shift the function to a position that allows the stable solution of the equation without a significant loss of accuracy. The 25th interval is used in this case which corresponds to a particle length of 2.56 μm . The sigmoid function is based on interval

number rather than particle length, providing a steeper transition from the two-term equation to the three-term equation. This is demonstrated visually by Figure 4.4.

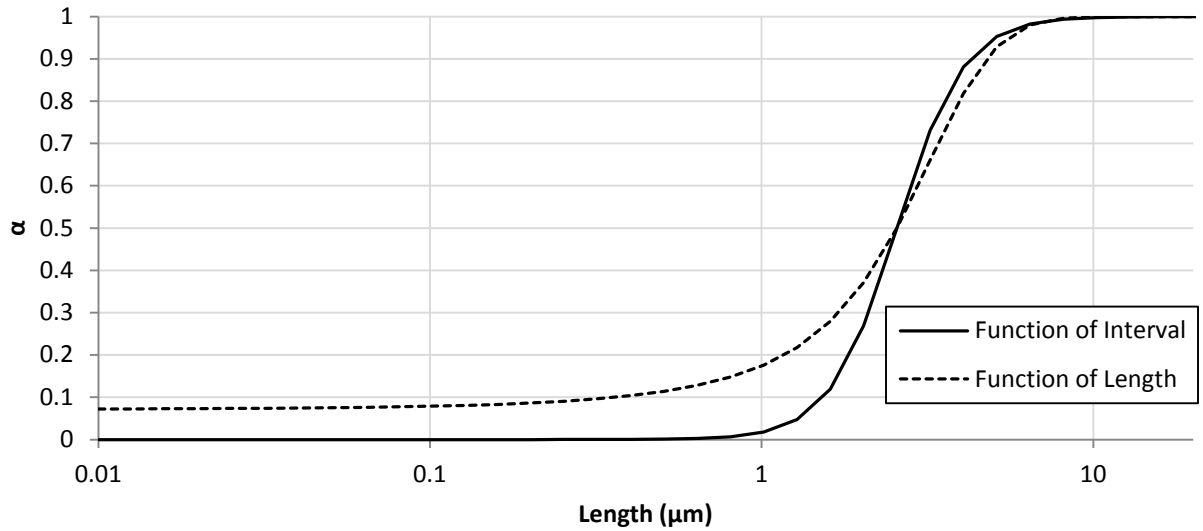


Figure 4.4: Sigmoid function as a function of interval number and length.

Before the hybrid approach can be accepted as valid, it must be verified that it does in fact yield PSD moments with an acceptable degree of accuracy. This was demonstrated by using Equation 3.2 for a steady state MSMPR with nucleation and size-independent crystal growth. By setting the supersaturation to 1 at steady state and using the parameters specified in §4.2.2, the analytic solution for the number density and that calculated using the hybrid approach were compared. These are shown in Figure 4.5.

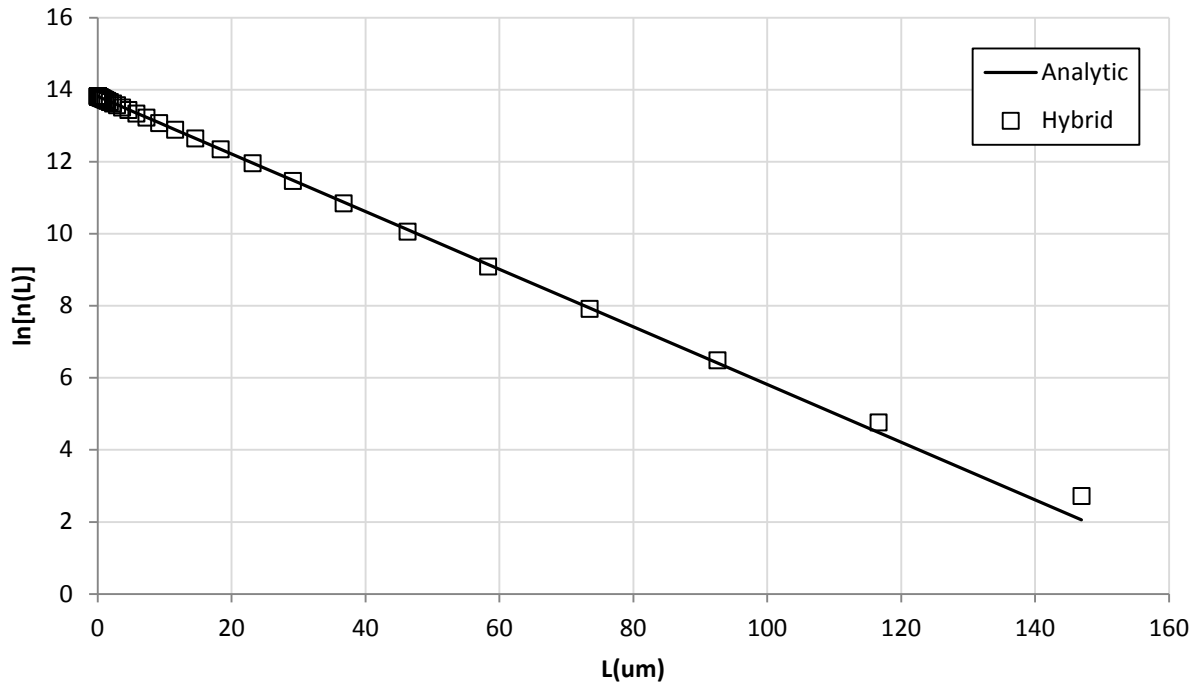


Figure 4.5: The analytical solution for a steady state MSMPR where $B = 1.0 \times 10^6$ [1/L.min], $G = 1.0\mu m$ and $\tau = 12.5$ min and the numerical solution using the hybrid approach.

Clearly, Figure 4.5 shows that the hybrid approach accurately calculates the steady-state population density distribution for an MSMPR. Table 4.1 shows the steady state third moments for the analytical solution, sigmoidal approach and the ADPB for different values of q using the two-term equation. Note that the solution to the ADPB can be easily obtained here as aggregation is omitted for this analysis.

Table 4.1: Steady state third moment calculated with the analytical solution, ADPB with various values of q and the sigmoidal approach.

Solution Method	Third Moment	% Error
Analytical	1.47×10^{11}	0
ADPB ($q = 1$)	3.03×10^{11}	107.03
ADPB ($q = 4$)	1.73×10^{11}	18.23
ADPB ($q = 10$)	1.56×10^{11}	6.21
Hybrid approach	1.45×10^{11}	1.30

Table 4.1 shows that the hybrid approach has quite acceptable accuracy when calculating the steady-state third moment. With this information, the hybrid approach will be used where $r = \sqrt[3]{2}$. This provides acceptable third-moment determination, without introducing the complexities and extra computational load of the ADPB.

4.2.4 Mass Balance

The key purpose of the mass balance is to account for the transfer of material from the aqueous to the solid phase. This is important owing to the influence that the aqueous phase concentrations have on ion speciation and thermodynamic driving forces (see §2.2.2). The total aqueous concentrations of the master elements in terms of all ionic complexes considered are presented again below.

$$C_{Mg}^T = [Mg^{2+}] + [MgOH^+] + [MgPO_4^-] + [MgHPO_4] + [MgH_2PO_4^+] \quad 2.6$$

$$C_N^T = [NH_4^+] + [NH_3] \quad 2.7$$

$$C_P^T = [PO_4^{3-}] + [HPO_4^{2-}] + [H_2PO_4^-] + [H_3PO_4] + [MgPO_4^-] + [MgHPO_4] + [MgH_2PO_4^+] \quad 2.8$$

These equations allow the thermodynamics and mass balance to be coupled. To account for the transfer of magnesium, nitrogen and phosphorus from aqueous to solid phase, Equation 4.10 is used to describe the elemental mass balance in the system.

$$\frac{d(C_i V)}{dt} = C_{MAP_i}^{in} Q_{MAP}^{in} - C_i Q^{out} - \frac{\dot{m}_3 \rho_{struvite} V}{MW_{struvite}} \quad 4.10$$

Where \dot{m}_3 is the rate of change of the third moment (*i.e.* total particle volume) of the PSD, due to precipitation, $\rho_{struvite}$ is the density of struvite and $MW_{struvite}$ is the molecular weight of struvite.

Two other elements that must be balanced are chlorine and sodium, since these are added with magnesium, as $MgCl_2 \cdot 6H_2O$, and with hydroxide, as $NaOH$, used to alter system pH . The mass balances for these can be obtained from Equation 4.10, lacking the consumption-by-crystallisation term. If chlorine and sodium are ignored in the mass balances it will result in a violation of solution electro-neutrality, the importance of this for an accurate description of solution thermodynamics was discussed in §2.2.3.

4.3 Results and Discussion

The results and discussion section is separated into four parts: solution thermodynamics validation, dynamic operation, effect of non-ideal thermodynamics and implications for process design.

4.3.1 Solution Thermodynamics Validation

Because the solution thermodynamics model contains a charge balance, solution pH becomes a dependent variable. This allows experimentally measured pH to be compared against model-predicted solution pH and represents a crucial means of model validation. In one case, three different volumes of $0.5 M NaOH$ were transferred via graduated pipette to a $0.005 M$ solution of $MgCl_2$ and $NH_4H_2PO_4$ in a 1-L baffled beaker. The pH predicted using the solution thermodynamics description, simulated (*i.e.*

solved) in gPROMS was compared against the laboratory measurement taken with a Thermo Orion 8165BNWP Ross Sureflow pH Electrode. The results of this validation study are shown in Figure 4.6.

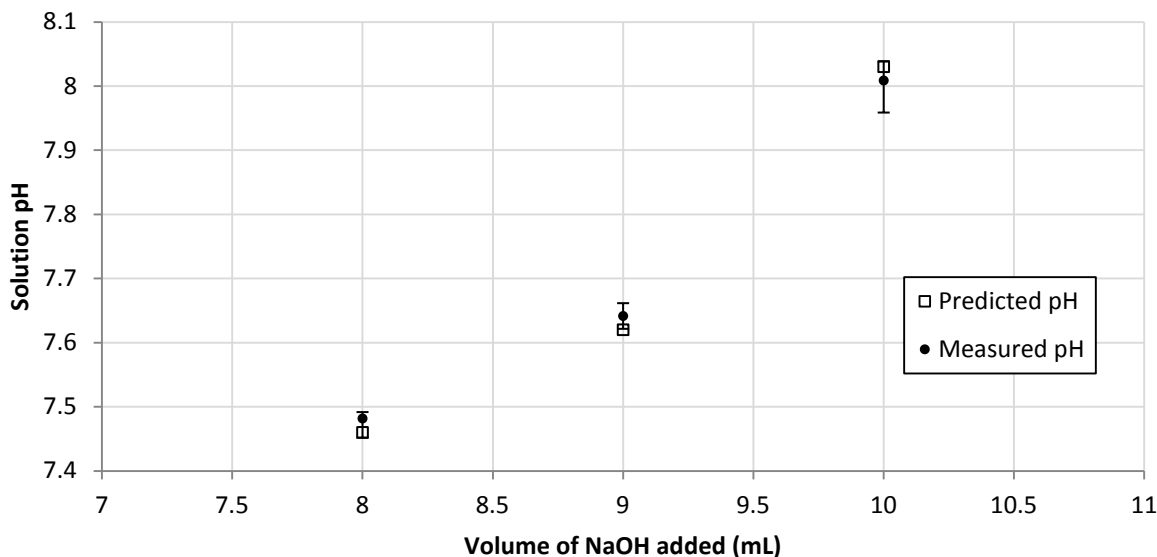


Figure 4.6: Validation of solution thermodynamics by comparison of measured and predicted pH .

The experiments were repeated 6-8 times for each aliquot of $NaOH$ addition. The data point represents the average pH measurement and the error bars correspond to the maximum and minimum pH measurements. It can be seen in Figure 4.6 that all predicted pH points lay within the maximum and minimum pH measurements recorded during the 6-8 repeats. Note that all measurements were taken during the induction time, before any solid struvite appeared, and thus represents a non-equilibrium state.

The results in Figure 4.6 are significant as they confirm the validity of the equilibria constants used in Table 2.1. This approach can be applied to future work aiming to add complexity to struvite solution thermodynamics through the addition of other species found in real wastewater. With each new species added to the thermodynamic model experiments can be performed to confirm model validity. Eventually, sufficient complexity in the thermodynamic model will be achieved to accurately describe

real wastewater. It should be noted that this approach assumes instantaneous kinetics for the equilibria reactions so that the free ions involved are in equilibrium at any given instant of time. This means the solution of the thermodynamic model can be applied to the non-equilibrium condition and dynamically during precipitation.

4.3.2 Dynamic Operation

The dynamic operation of the struvite MSMR crystalliser model is demonstrated by plotting SI dynamic response, starting with a range of different initial conditions and across a range of operating conditions. The initial conditions were changed by altering the concentration of $NaOH$ added to this system at time zero ($C_{NaOH}|_{t=0} = 0.0025; 0.0035; 0.005 \text{ mol/L}$). Changing the operating conditions was achieved by altering the flow of $NaOH$, since this is the method of pH control, and therefore SI control, during operation. Nominal operating conditions were established ($Q_{NaOH}^{in} = 0.01 \text{ L/min}, \tau = 12.5 \text{ min}$), along with the reduced caustic flow case ($Q_{NaOH}^{in} = 0.00833 \text{ L/min}, \tau = 12.766 \text{ min}$) and the increased caustic flow case ($Q_{NaOH}^{in} = 0.01167 \text{ L/min}, \tau = 12.244 \text{ min}$). All other input variables are the same as those used for the nominal operating condition and are given in Figure 4.2.

The SI of struvite is shown for the three initial and operating conditions in Figure 4.7, where the abscissa is reported in normalised time (t/τ). It can be seen that process operation is independent of the initial conditions at steady-state. This is an unsurprising result but its implications should not be overlooked. It illustrates that all components of the process model have been successfully coupled allowing the kinetics to be driven by thermodynamics and changes in the mass balance to be fed back to the thermodynamics dynamically. Since the development of the process model is a major goal of this research, Figure 4.7 is a significant achievement and novel contribution to the field.

All operating conditions reach the same steady-state SI after approximately six residence times, regardless of initial conditions. The first initial condition corresponds to the lowest initial SI , since low concentration of sodium hydroxide leads to a low SI .

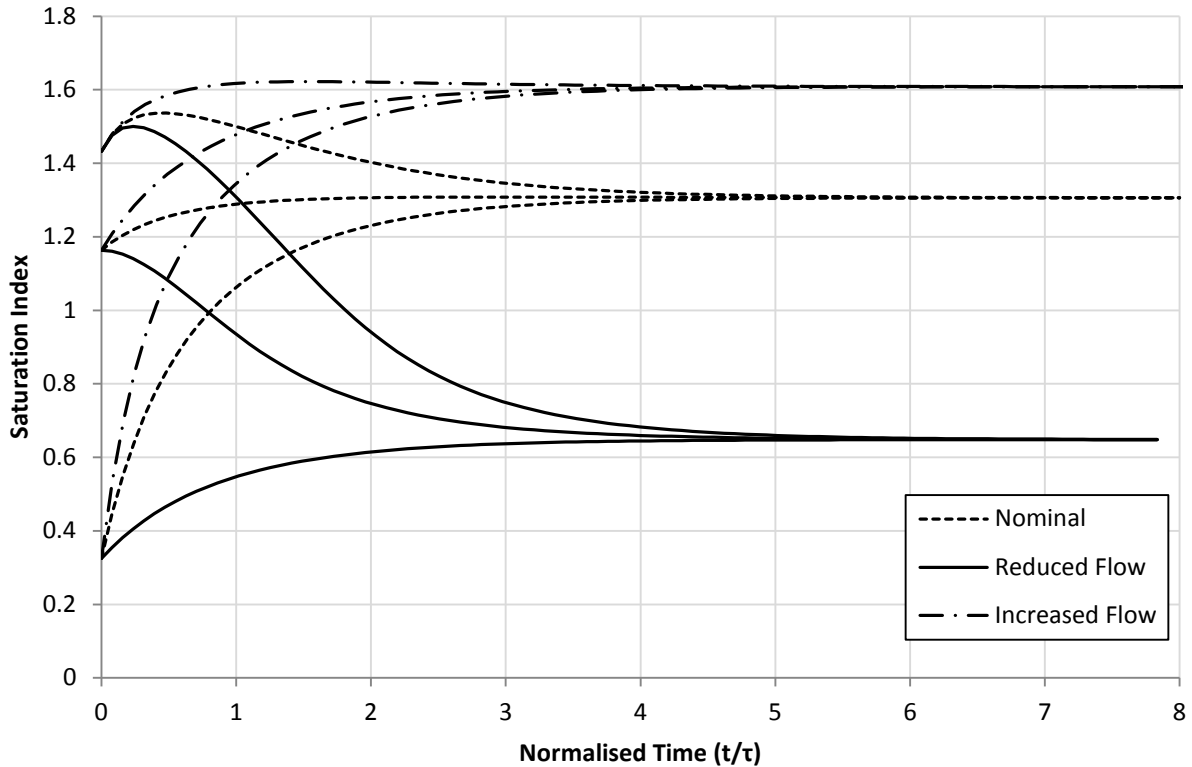


Figure 4.7: Dynamic response of SI at three initial conditions and three operating conditions; nominal caustic flow, reduced caustic flow and increased caustic flow.

A key feature of the process model is the population balance and calculation of the PSD. This is illustrated in Figure 4.8 showing the PSD dynamics under the nominal operating conditions. A large number of small particles can be seen at $t = 0.1 \tau$, which commence growth and aggregation until a steady-state distribution is reached after two residence times. The larger end of the PSD continues to change after two residence times, but only by a small amount as can be seen when comparing the PSD after two and ten residence times. However, this small change in the larger end contributes significantly

to the mass balance, and therefore the system supersaturation, as demonstrated by the steady-state SI being reached after six residence times (*cf.* Figure 4.7).

One feature of Figure 4.8 is the sharp lines connecting points on the distribution. This results from the discrete nature of the distribution, it is especially clear in the large particle sizes where the intervals are larger owing to the geometric progression.

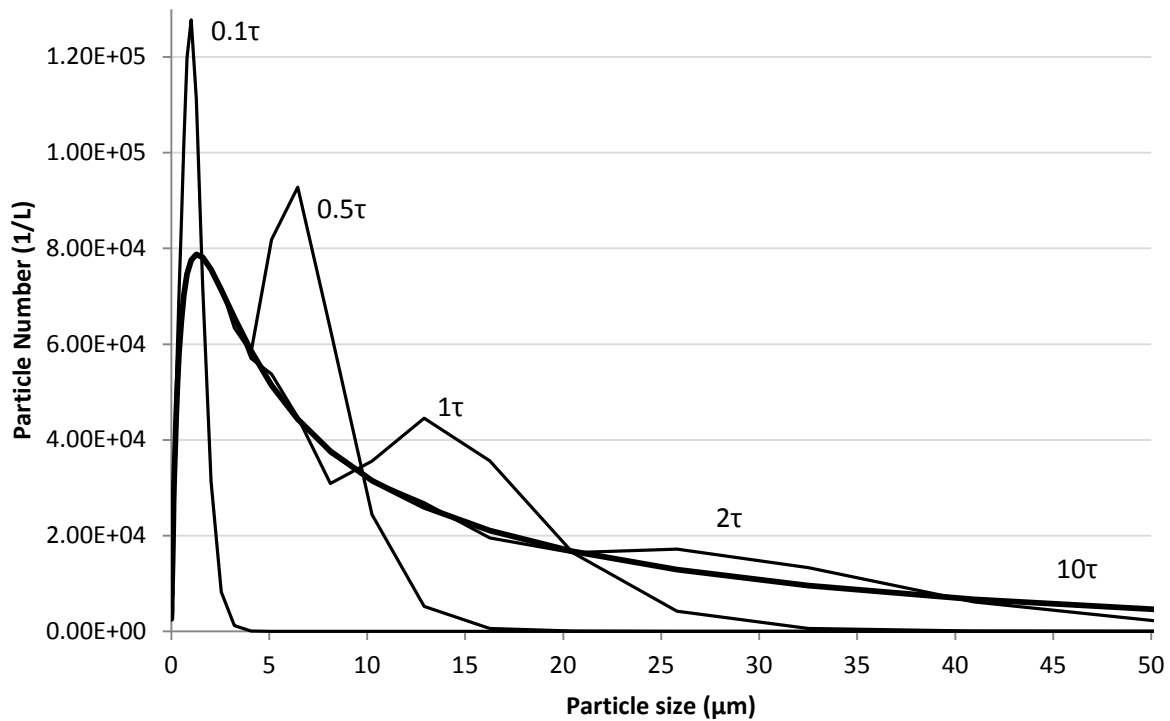


Figure 4.8: Particle size distribution under nominal operating conditions shown at 0.1, 0.5, 1, 2 and 10 residence times.

4.3.3 Importance of non-ideal thermodynamic behaviour

To demonstrate the importance of non-ideal thermodynamic behaviour, the mass of struvite generated within the MSMPR reactor is shown for the case where ideal and non-ideal thermodynamics are presumed to occur (see Figure 4.9). Under ideal behaviour, the mass of struvite produced is over

predicted by 29.3%, compared against the non-ideal case. As such, the simplifying assumption of ideal thermodynamics is therefore unjustified.

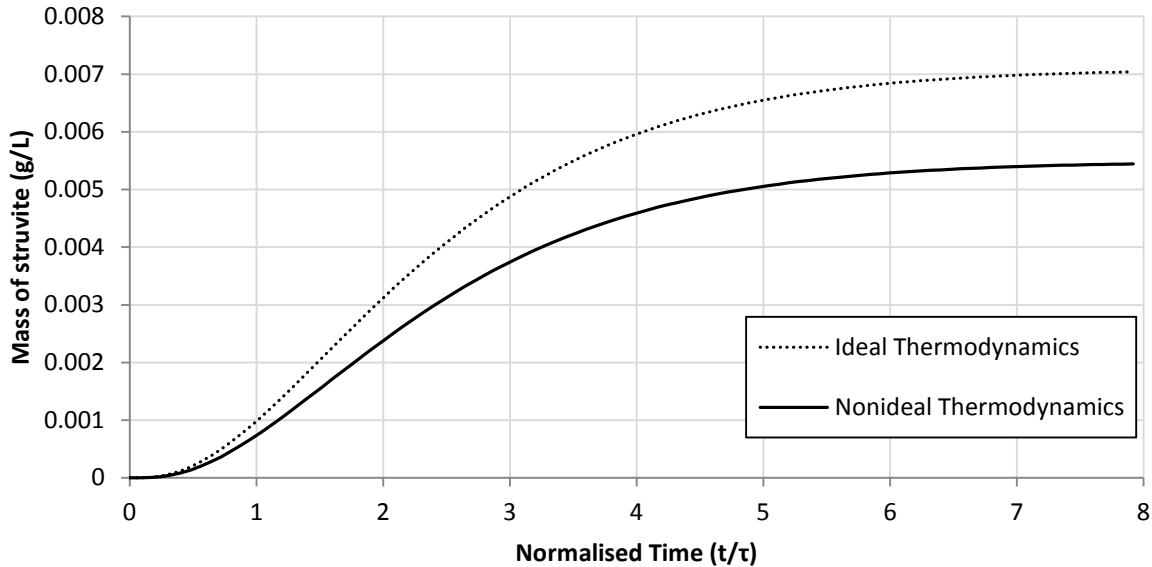


Figure 4.9: Predicted mass of struvite within the simulated MSMPR crystalliser under ideal and non-ideal thermodynamic conditions.

An explanation of the result in Figure 4.9 is given when considering the activity coefficients calculated by the Debye-Hückel equation with Davies approximation (Equation 2.14). The process model can be used to plot the value of the activity coefficients calculated during the dynamic simulation (see Figure 4.10). It can be seen that the activity coefficients for the ± 2 and ± 3 ions are significantly less than one. Therefore, assuming ideal thermodynamics will result in a higher *IAP* and *SI*. With this in mind, the results found in Figure 4.9 are not surprising.

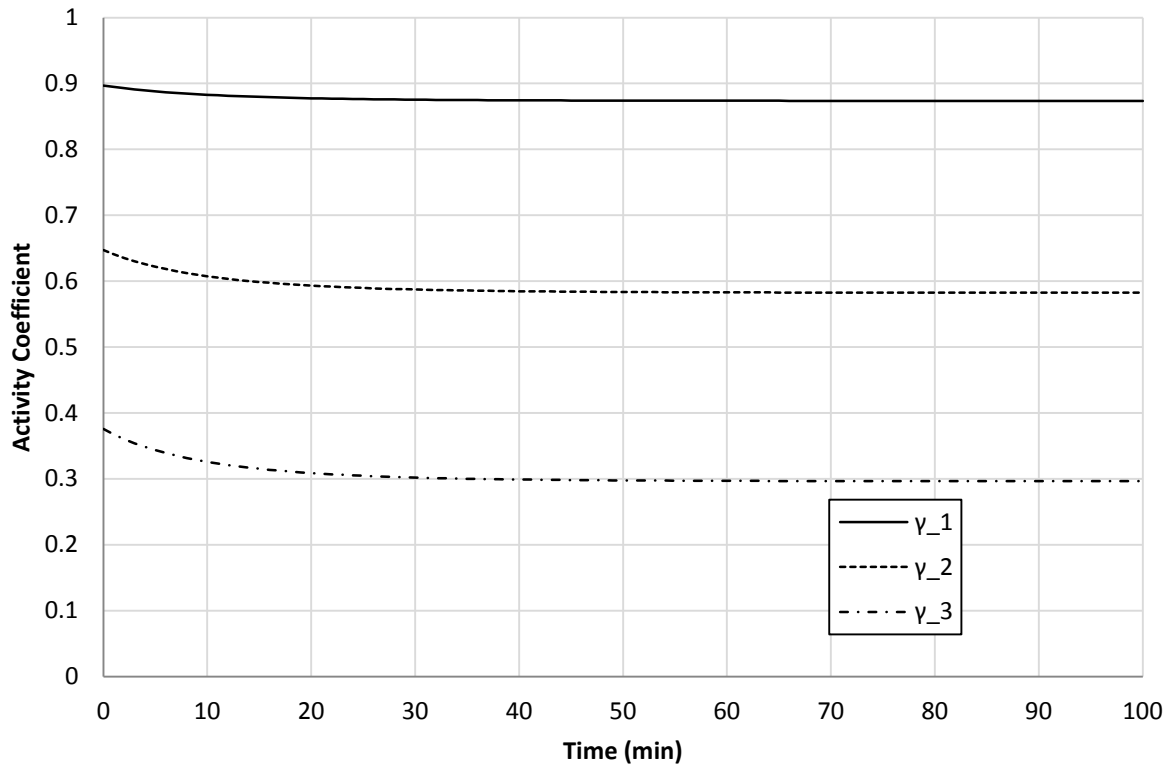


Figure 4.10: Activity coefficients calculated during the simulation.

4.3.4 Implications for Process Design

A key design parameter for any process is the operational volume. The model uses an arbitrary 1-L reactor volume for the nominal case for mathematical convenience. However, the model can be used to investigate the relationship between reactor volume and important variables used in assessing proposed designs. The three variables investigated here are percentage phosphorus recovery ($\%P_{Rec}$), saturation index and mean particle size.

Ultimately any reactor must be designed to recover phosphorus from wastewater streams. Therefore, phosphorus recovery is used to assess reactor performance. Saturation index determines the driving force for the kinetics, making it an important variable to consider in reactor design. While mean particle size does not contain as much information as the PSD, it is still an important parameter that can be used

to assess particle engineering performance. Of course other considerations such as capital cost and product value might be considered when designing a reactor, however, these are neglected in this work for the sake of simplicity.

In this work phosphorus recovery is based on the thermodynamically available phosphorus, rather than the total amount of phosphorus. Some previous studies have reported on phosphorus recovery without considering solution thermodynamics making the distinction between thermodynamic and total recovery impossible (Levenspiel, 1962, Perera et al., 2009). The percentage recovery of thermodynamically available phosphorus ($\%P_{Rec}$) is determined by Equation 4.11.

$$\%P_{Rec} = \frac{C_{MAP}^{in} Q_{MAP}^{in} - C_P Q^{out}}{C_{MAP}^{in} Q_{MAP}^{in} - C_P|_{SI=0} Q^{out}} \times 100\% \quad 4.11$$

Where the numerator in Equation 4.11 is the amount of phosphorus removed by the crystallisation of struvite. The denominator is the phosphorus removed when SI is zero (*i.e.* $C_P|_{SI=0} Q^{out}$) and therefore all available phosphorus has been precipitated. However, this equation cannot be solved *a priori* for all cases, as it requires C_P at two separate operating conditions to be calculated. Because of this, the term $C_P|_{SI=0} Q^{out}$ is calculated by increasing the reactor volume, until SI approaches zero.

The effect of increasing the reactor volume and keeping all other nominal operating conditions constant is shown in Table 4.2. It should be noted that reactor volume is used here as a proxy for residence time. In a real system recovering phosphorus from wastewater, flow rates are determined by the input to the wastewater treatment plant. Therefore, it is preferable to investigate residence time through changes in reactor volume rather than changes in flow.

Table 4.2: % P_{Rec} and SI under nominal operating conditions and variable reactor volume.

V (L)	τ (min)	% P_{Rec}	SI	\bar{L} (μm)
1	12.5	2.02	1.306	4.180
10	125	60.65	0.6239	6.823
15	187.5	71.60	0.4499	6.964
25	312.5	81.72	0.2873	7.077
100	1250	95.04	0.0772	7.207
1000	12500	99.50	0.0007	7.247

As expected, the thermodynamic yield increases with increasing reactor volume/residence time (see Figure 4.11).

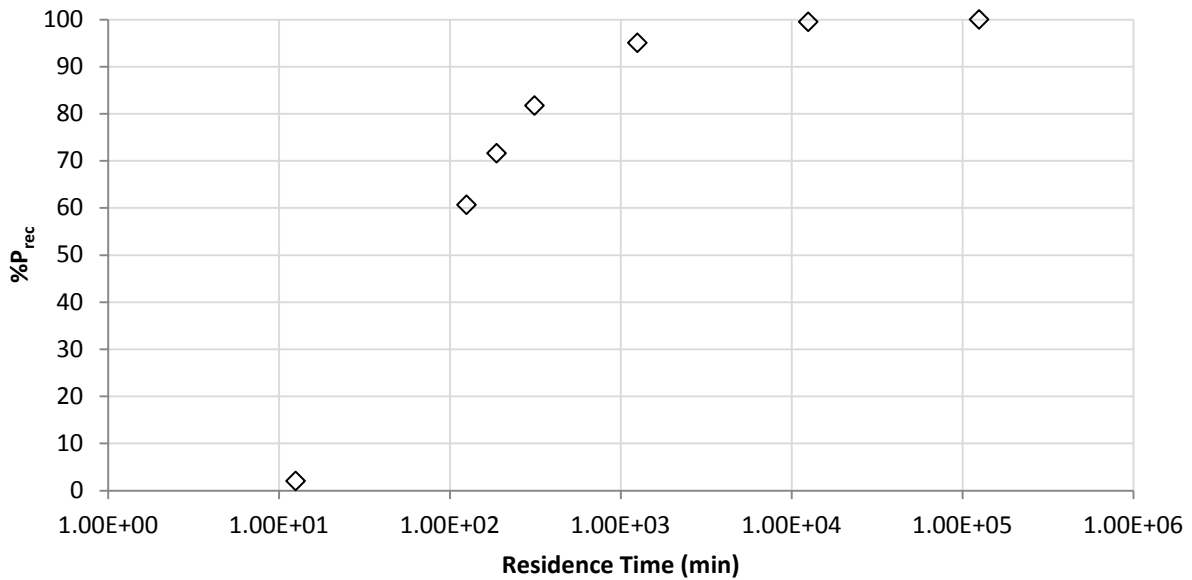


Figure 4.11: Thermodynamic yield of struvite shown as the percentage of available phosphorus recovered as a function of residence time.

This result is mirrored when looking at the saturation index in Figure 4.12.

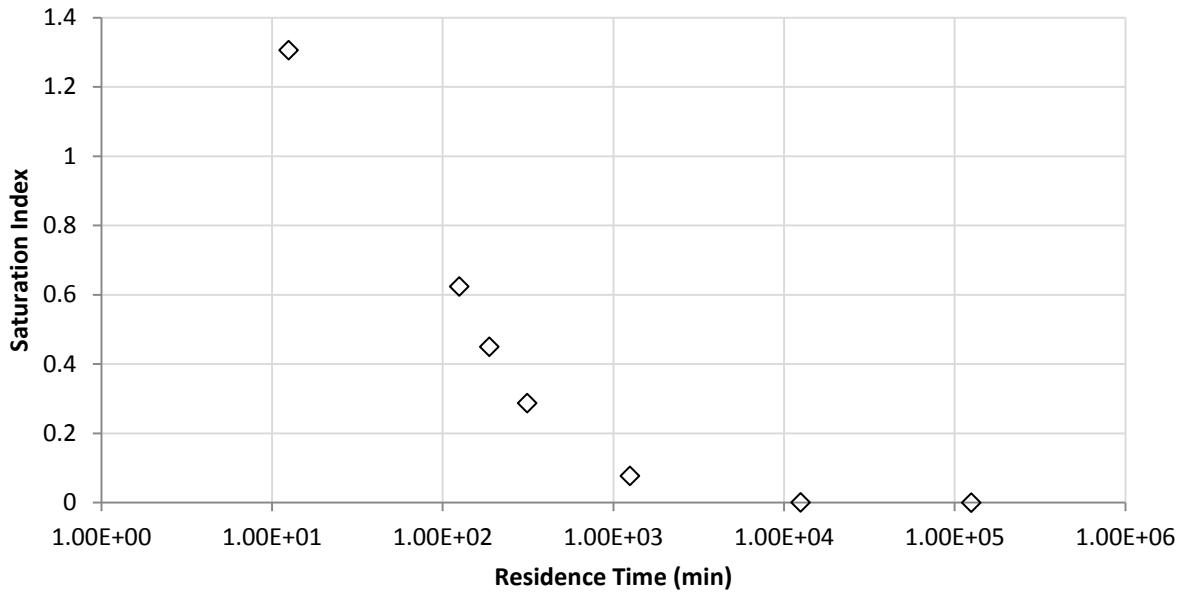


Figure 4.12: Reactor saturation index shown as a function of residence time.

Effectively, 100% thermodynamic recovery occurs when the reactor volume is 10000 L or greater. It can be seen in Figure 4.11 and Figure 4.12 that above a reactor volume of 100 L there are diminishing returns for further increases in reactor volume. If process economics were also included, this information could be used to design a reactor for a real process.

4.4 Conclusions

A model to predict the PSD of struvite produced in an MSMR crystalliser is developed, incorporating solution thermodynamics, mass and population balances and kinetic equations for crystal nucleation, growth and aggregation. It was demonstrated that the solution supersaturation could be computed throughout the simulation for various initial and operating conditions. The use of non-ideal solution thermodynamics in solving the equilibria is shown to be necessary to determine the mass of struvite produced. The thermodynamic recovery of phosphorus can be improved by increasing the reactor

volume but process economics must be first accounted for before an informed design decision can be made.

4.5 Key Points for Chapter Four

- A process model for struvite crystallisation has been developed
- The thermodynamics and kinetics are linked together by the mass balance and the population balance allowing the modelling of the PSD
- Dynamic performance of the process model is demonstrated
- The application of the process model to reactor design is shown

Chapter 5 - Stochastic Simulation of a Struvite Crystallisation Model and its Application to Uncertainty Propagation and Control

This chapter takes the process model developed as part of Chapter 4 and explores the impact of kinetic and process parameter uncertainty propagation with stochastic simulation techniques. It is found that the crystal growth rate coefficient is the most significant kinetic parameter and phosphorus concentration is the most significant nutrient in the feed for uncertainty propagation. A pH control scheme is implemented to limit uncertainty propagation.

5.1 Introduction

The process model developed in Chapter 4 aimed to provide better process design for struvite crystallisation systems. A preliminary application of the model to design was demonstrated by showing the relationship between reactor volume, residence time, saturation index, mean particle size and phosphorus recovery (Table 4.2). Further applications of the model are explored in this chapter. Deterministic and stochastic simulation methods are used to investigate the propagation of uncertainty in key process variables throughout the model.

In a typical wastewater treatment plant the composition of input streams cannot be known for certain, since it is subject to random fluctuations that cannot be anticipated. The ability to assess how uncertainty in the composition propagates through to key output variables such as pH , saturation index, mean particle size and yield would enable more robust process design and operation. Process control and the effect it has on limiting the propagation of uncertainty through the model is also investigated in the chapter.

In §4.3.4 it was found that a 1-L reactor under nominal operating conditions resulted in poor phosphorus recovery and by increasing the reactor volume the recovery could, of course, be significantly improved. For a more realistic demonstration of how the process model could be applied, a 10-L MSMPR reactor under nominal operating conditions is investigated in this chapter.

5.2 Deterministic Uncertainty Propagation

The deterministic approach to uncertainty propagation uses the NIST (National Institute of Standards and Technology [U.S.A.]) method to calculate how uncertainty in measured variables propagates to a calculated quantity (Taylor and Kuyatt, 1994). The equation used to implement the NIST method of uncertainty propagation calculation is shown in Equation 5.1.

$$U_Y = \sqrt{\sum_i \left(\frac{\partial Y}{\partial X_i}\right)^2 U_{X_i}^2} \quad 5.1$$

Where U represents the absolute uncertainty in the variable, Y represents the calculated variable and X_i is the i^{th} measured variable.

One advantage of this approach is its simplicity. The individual terms in the summation can be used to determine the contribution each variable makes to the total uncertainty. The disadvantage is it only considers the maximum and minimum uncertainty. A better, although more complex, representation of

the uncertainty is to use a distribution. The stochastic approach does this, capturing the uncertainty propagation in more detail.

5.3 Stochastic Simulations

Stochastic simulations are used to run the process model many times using stochastically selected values from a probability distribution that covers a range of expected values. In this way error propagation through a non-linear model can be better described and understood. The number of simulations performed should be sufficient to allow the mean of the model output to be independent of the number of simulations.

The standard deviation in the output variables provides a measure of uncertainty propagation by showing how sensitive they are to input variable uncertainties. This approach has been used to assess a range of cellulose hydrolysis models by propagating uncertainty from input variables to output variables (Sin et al., 2010).

5.3.1 Variables Investigated in the Stochastic Simulations

It is not practical to investigate every variable solved in the process model. Therefore, variables that influence key process parameters should be identified so the stochastic simulations can be targeted. The kinetic parameters for nucleation, growth and aggregation are investigated because they are empirical parameters that must be determined from experimental data and therefore contain uncertainty. Because kinetic parameters determine how the PSD changes with time, it is useful to understand how their uncertainty propagates through the model. The kinetic mechanisms will be assumed as first order with respect to the saturation index, only the coefficients k_B , k_G and k_β are subject to uncertainty in this investigation.

The nutrient load (*i.e.* the concentration of P and N in the feed-stream) is investigated because the concentration of real wastewater feeds would be subject to random fluctuations and diurnal characteristics. Furthermore, online measurement of nutrient concentrations is difficult, expensive or both, thus the true nutrient concentrations cannot be known with any confidence in real time. The nutrient load will significantly impact the saturation index through the thermodynamics making it important to investigate. Magnesium and sodium hydroxide concentration also significantly impact the thermodynamics, but, as chemical additions, they can be controlled and are therefore not subject to the same fluctuations as nutrient loads.

The output variables investigated include *SI*, since it is the key thermodynamic driving force for the kinetic mechanisms, and system *pH* because it is the easiest parameter to measure and therefore control. The mean crystal length and the percentage phosphorus recovery are included to describe reactor performance in terms of product size and yield.

5.3.2 Probability Distributions used in Stochastic Simulations

The variables investigated are assumed to have a uniform probability distribution that is bounded by $\pm 10\%$ of the nominal operating conditions. A uniform distribution and its bounds are chosen arbitrarily because, without experimental data or process information, the choice of one distribution and its bounds over another cannot be justified. This is acknowledged as a limitation of the current study because the uncertainty may not be uniformly distributed and the range of possible values may not be $\pm 10\%$ of the mean. However, the purpose of this chapter is to demonstrate how uncertainty propagation can be shown with the model and how this information can be used for process design and control. A uniform distribution bounded by $\pm 10\%$ of the mean, see Figure 5.1, is assumed to be sufficient for this purpose.

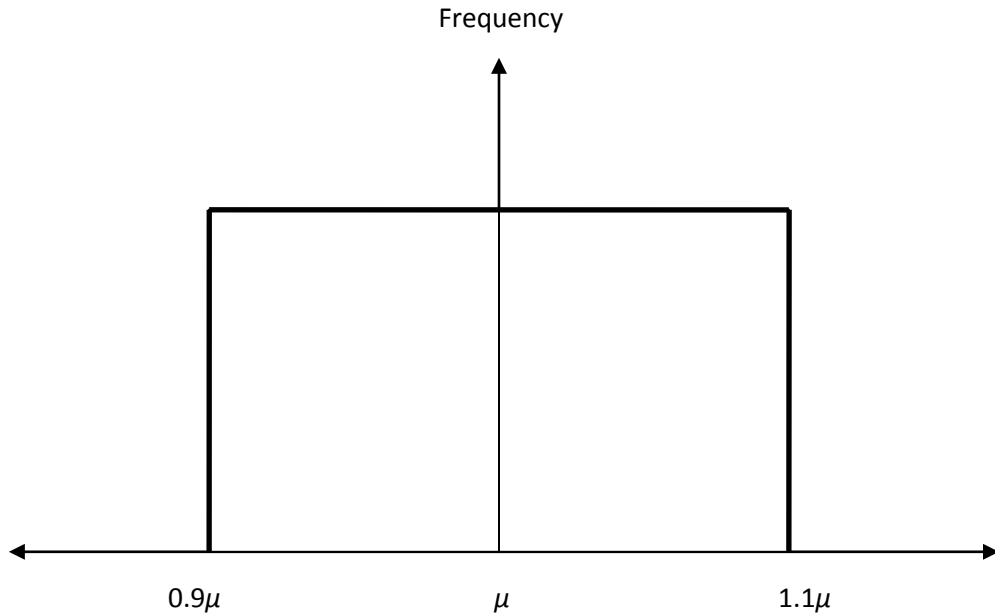


Figure 5.1: Uniform distribution bounded by $\pm 10\%$ of the mean (μ).

5.4 Results and Discussion

To assess the stochastic simulations, a point of reference is required to compare and contrast the simulation results. This 'base case' scenario is calculated using the nominal conditions for the process model detailed in §4.2 applied to the 10-L reactor.

The kinetic parameters and nutrient load were investigated independently, since the source of uncertainty for these variables is different. The uncertainty in the kinetic parameters is derived from their empirical nature and the requirement of experiments to determine their value, while nutrient load uncertainties result from random fluctuations during process operation.

5.4.1 Base Case Results

The base case results are generated for a 10-L crystalliser using the nominal operating conditions defined in §4.2 and are shown in Table 5.1. All simulations are run for ten residence times and assumed to be at steady state; this assumption is considered valid given in results in §4.3.2.

Table 5.1: Base case for the stochastic simulations, based on nominal operating conditions.

<i>SI</i>	<i>pH</i>	\bar{L} (μm)	$\%P_{Rec}$
0.624	7.994	6.823	60.650

5.4.2 Number of Stochastic Simulations

The number of simulations used to assess uncertainty propagation is determined by comparing the mean of the output variables to the number of simulations performed. The number of simulations is deemed sufficient when the mean becomes independent of the number of simulations. This condition is tested independently for both kinetic parameters and nutrient load. The results from this test are shown in Figure 5.2 to Figure 5.4.

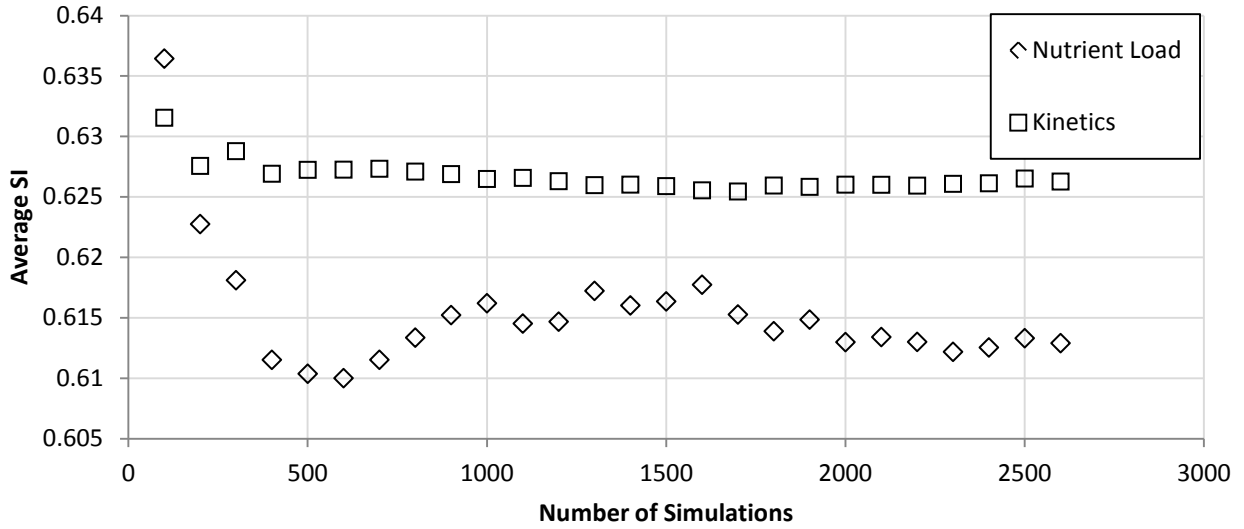


Figure 5.2: Sample average SI as a function of the number of simulations for both nutrient load uncertainty and kinetic parameter uncertainty.

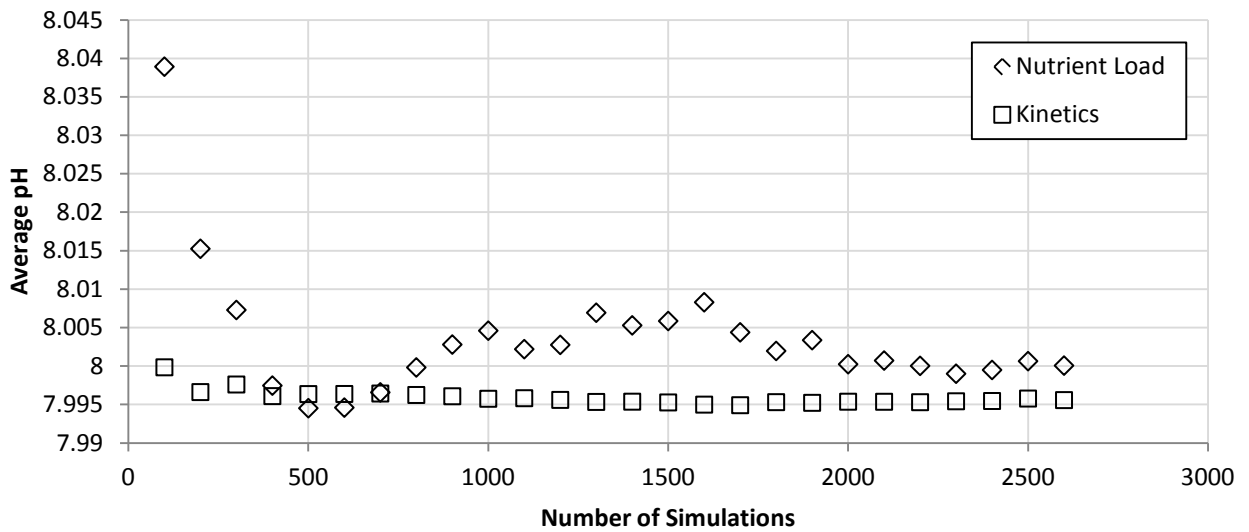


Figure 5.3: Sample average pH as a function of the number of simulations for both nutrient load uncertainty and kinetic parameter uncertainty.

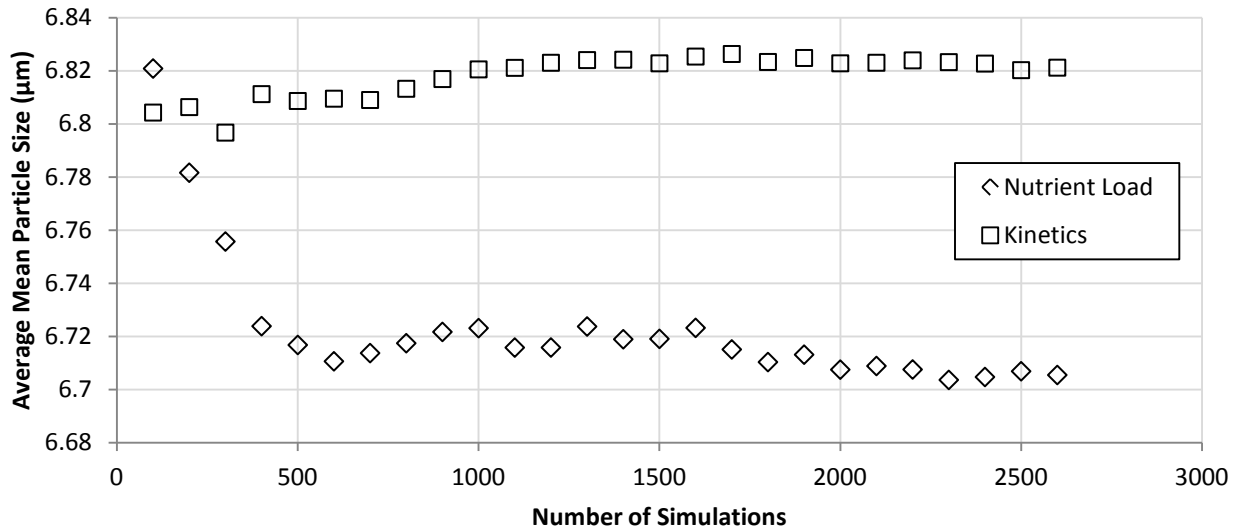


Figure 5.4: Sample average \bar{L} as a function of the number of simulations for both nutrient load uncertainty and kinetic parameter uncertainty.

The results in Figure 5.2 to Figure 5.4 show that 2000 simulations are sufficient to produce a mean that is approximately constant and therefore meaningful for comparisons made between those mean values. As such, 2000 simulations will be used for all stochastic simulations to ensure the uncertainty propagation is appropriately captured.

5.4.3 Kinetic Uncertainty Results

The kinetic uncertainty simulations are performed under two scenarios: individual uncertainty and combined uncertainty. In the individual scenario one parameter is given uncertainty and the others remain constant. In the combined scenario all parameters are given uncertainty. While all parameters would in fact have uncertainty, the individual scenario is used to facilitate comparison between the different parameters. Table 5.2 presents the results from the kinetic uncertainty simulations. The results from the deterministic and stochastic uncertainty analyses are presented together to contrast the two method of analysis.

Deterministic uncertainty is reported as *base case* \pm *absolute error* and the stochastic uncertainty is reported as *mean* \pm *standard deviation*.

Table 5.2: Uniformly distributed kinetic parameter uncertainty in a 10-L MSMPR reactor and their effect on key variables at steady state.

		Uncertainty of $\pm 10\%$ in k_B	Uncertainty of $\pm 10\%$ in k_G	Uncertainty of $\pm 10\%$ in k_β	Combined Uncertainty
<i>SI</i>	<i>base</i> \pm <i>U</i>	0.624 \pm 0.002	0.624 \pm 0.067	0.624 \pm 0.021	0.624 \pm 0.070
	<i>mean</i> \pm σ	0.624 \pm 0.001	0.625 \pm 0.039	0.624 \pm 0.012	0.626 \pm 0.040
<i>pH</i>	<i>base</i> \pm <i>U</i>	7.994 \pm 0.001	7.994 \pm 0.054	7.994 \pm 0.017	7.994 \pm 0.057
	<i>mean</i> \pm σ	7.994 \pm 0.001	7.995 \pm 0.031	7.993 \pm 0.010	7.995 \pm 0.033
<i>L</i>	<i>base</i> \pm <i>U</i>	6.823 \pm 0.252	6.823 \pm 0.480	6.823 \pm 0.186	6.823 \pm 0.573
	<i>mean</i> \pm σ	6.827 \pm 0.144	6.821 \pm 0.275	6.825 \pm 0.107	6.823 \pm 0.329
$\%P_{Rec}$	<i>base</i> \pm <i>U</i>	60.650 \pm 0.099	60.650 \pm 4.333	60.650 \pm 1.345	60.650 \pm 4.538
	<i>mean</i> \pm σ	60.650 \pm 0.057	60.543 \pm 2.480	60.656 \pm 0.773	60.493 \pm 2.592

It can be seen in Table 5.2 that the mean values for all output variables are approximately equal to the base case across all scenarios of uncertainty except for $\%P_{Rec}$. This indicates that error in the kinetic parameters does not skew the output except in the case of $\%P_{Rec}$.

To illustrate how the uncertainty in kinetic parameters propagates to uncertainty in the output variables, the coefficient of variation ($\%CV$) is plotted for each output variable using the results from the stochastic simulations. The results are shown in Figure 5.5.

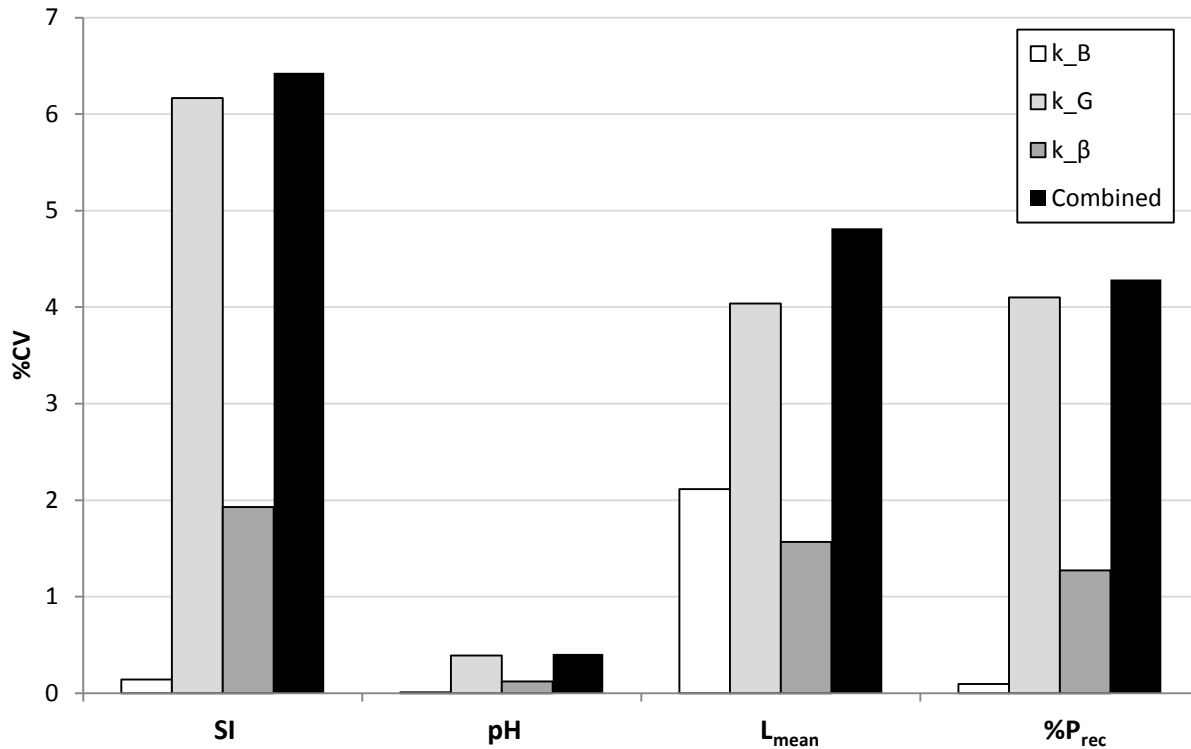


Figure 5.5: The effect of uniformly-distributed kinetic parameter uncertainties on key process variables under nominal operating conditions expressed as %CV.

Figure 5.5 indicates that the uncertainty assigned to the kinetic parameters has little effect on the steady-state pH . The other output variables are more significantly affected by uncertainty propagation from the kinetic parameters. It can be seen clearly in all cases the crystal growth rate coefficient is the most significant parameter in propagating uncertainty, followed by the aggregation kernel coefficient. The nucleation rate coefficient has almost no impact on the output variables except for average particle size.

SI and $\%P_{Rec}$ are both dependent on the mass balance, *i.e.* the amount of struvite that has been crystallised. It is not surprising that the uncertainty in nucleation has the least significance, since the assumed negligible size of nuclei would have a negligible effect on the mass balance. This is not to suggest nucleation can be ignored entirely; a non-zero nucleation rate is essential to a continuous

crystalliser. In the case of mean particle size it is calculated from the first and zeroth moment (Equation 3.6) so the nucleation is more significance.

The importance of particle aggregation to the SI and $\%P_{Rec}$ warrants further discussion. Aggregation is a volume conserving mechanism, so should therefore not contribute to the mass balance. However, it is postulated that an indirect influence on the mass balance may take place through a relationship with the growth rate. This relationship arises because the model formulation is based upon spherical particles in binary collisions that aggregate into one spherical particle. This does not conserve surface area as shown in Equations 5.2-5.4.

$$V_{ij} = V_i + V_j \quad 5.2$$

$$SA_{ij} = 4\pi \left(\sqrt[3]{\frac{3V_{ij}}{4\pi}} \right)^2 \quad 5.3$$

$$4\pi \left(\sqrt[3]{\frac{3V_{ij}}{4\pi}} \right)^2 \neq 4\pi \left(\sqrt[3]{\frac{3V_i}{4\pi}} \right)^2 + 4\pi \left(\sqrt[3]{\frac{3V_j}{4\pi}} \right)^2 \quad 5.4$$

$$\therefore SA_{ij} \neq SA_i + SA_j$$

In reality this does not represent how crystals aggregate, it is perhaps more analogous to bubble or droplet coalescence. However, it is doubtful struvite aggregates also conserve surface area since this would require aggregates to form between points and edges of individual particles, an equally poor representation of reality. It is likely that reality is found somewhere in between these two representations of aggregation. With this in mind it is reasonable to expect an indirect effect from aggregation on the mass balance. Therefore, the results seen in Figure 5.5 are sensible with respect to the model mechanisms and real expectations that struvite aggregates do not conserve surface area.

The conclusions reached by examining the coefficients of variation in the individual mechanisms are strengthened when the contributions to the deterministic uncertainty are investigated. This is done by taking the terms of the summation in Equation 5.1 and determining their percentage contribution to the total uncertainty. The results of this are shown in Figure 5.6.

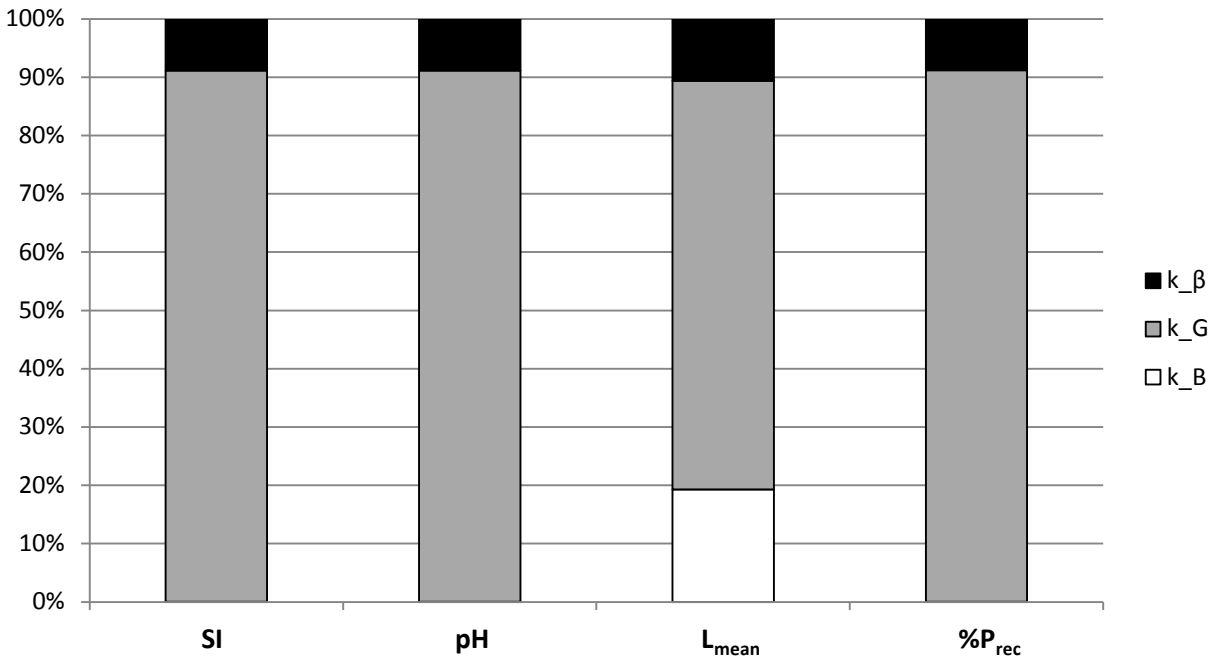


Figure 5.6: Contribution of the individual mechanisms to the total uncertainty found using the deterministic uncertainty analysis.

5.4.4 Nutrient Load Uncertainty Results

The nutrient load simulations are performed under the individual and combined scenarios similarly to the kinetic parameter simulations. Results are shown in Table 5.3 and the deterministic and stochastic uncertainty analyses are presented together, enabling clear comparisons. Deterministic uncertainty is reported as *base case* ± *absolute error* and the stochastic uncertainty is reported as *mean* ± *standard deviation*.

Table 5.3: Uniformly distributed nutrient load uncertainty in a 10-L MSMPR reactor and their effect on key variables at steady state.

		Uncertainty of $\pm 10\% C_{MAP_P}^{in}$	Uncertainty of $\pm 10\% C_{MAP_N}^{in}$	Combined Uncertainty
<i>SI</i>	<i>base</i> $\pm U$	0.624 \pm 0.215	0.624 \pm 0.125	0.624 \pm 0.248
	<i>mean</i> $\pm \sigma$	0.616 \pm 0.125	0.621 \pm 0.072	0.613 \pm 0.142
<i>pH</i>	<i>base</i> $\pm U$	7.994 \pm 0.389	7.994 \pm 0.152	7.994 \pm 0.418
	<i>mean</i> $\pm \sigma$	8.000 \pm 0.224	7.993 \pm 0.088	8.000 \pm 0.238
<i>L</i>	<i>base</i> $\pm U$	6.823 \pm 0.663	6.823 \pm 0.371	6.823 \pm 0.760
	<i>mean</i> $\pm \sigma$	6.764 \pm 0.378	6.803 \pm 0.210	6.707 \pm 0.467
<i>%P_{Rec}</i>	<i>base</i> $\pm U$	60.650 \pm 15.787	60.650 \pm 7.155	60.650 \pm 17.333
	<i>mean</i> $\pm \sigma$	58.999 \pm 9.368	60.231 \pm 4.096	58.581 \pm 10.447

It can be seen in Table 5.3 that the mean values of the output variables have deviated from the base case values reported in Table 5.3. This deviation cannot be disregarded as a random result from the stochastic simulations, since 2000 simulations should be sufficient to make the mean independent of the number of simulations. Therefore it must be a real effect resulting from the uniform distribution of the nutrient load. It is therefore instructive to evaluate the frequency distribution of output *SI* is, as shown Figure 5.7.

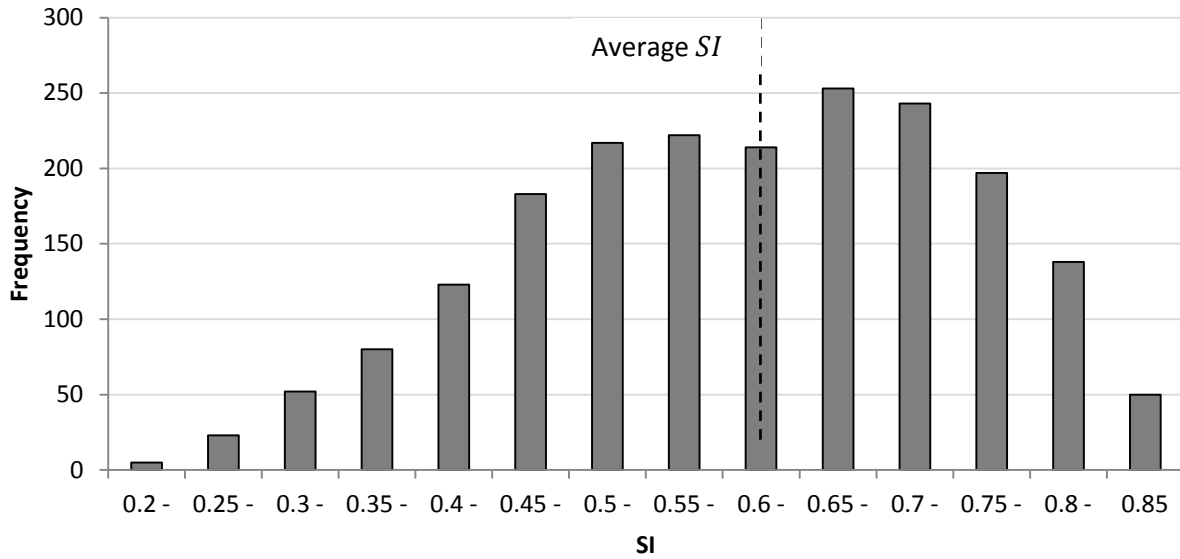


Figure 5.7: Distribution of saturation index produced from the uniform distribution of nutrient load.

Clearly, Figure 5.7 illustrates that the uncertainty/variability in nutrient load does not propagate linearly through the model. This is not surprising owing to the nature of the solution thermodynamics. Figure 5.8 shows this uncertainty propagation using the coefficient of variation.

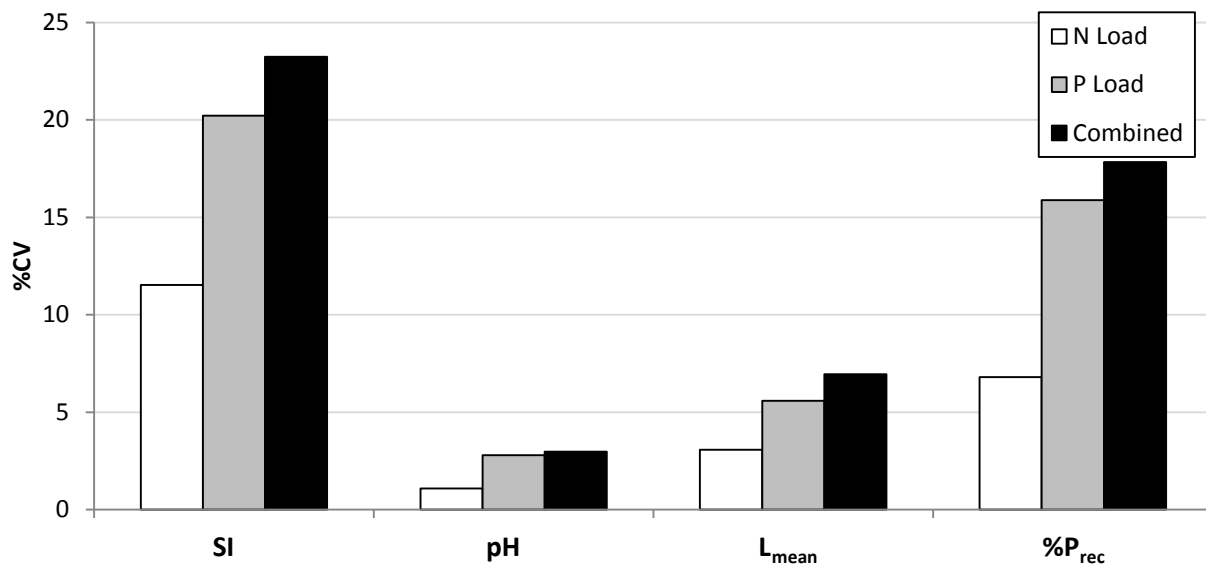


Figure 5.8: The effect of uniformly-distributed nutrient load uncertainties on key process variables under nominal operating conditions expressed as %CV.

Figure 5.8 demonstrates that the uncertainty in the nutrient load results in more variation than the same relative uncertainty in the kinetic parameters. It also shows that uncertainty in the phosphorus load is more significant than the nitrogen load. These results are both due to the influence of thermodynamics on the process.

Uncertainty in the kinetic parameters indirectly affects the thermodynamics by changing the rate at which struvite crystallises, which ultimately feeds back to the thermodynamics through the mass balance. Uncertainty in the nutrient load directly affects the thermodynamics by changing the concentration of nitrogen and phosphorus being fed to the crystalliser.

When comparing the uncertainty propagation from the kinetics to that of the nutrient load, it is important to note that uncertainty in the kinetics becomes more significant as the yield increases. This is because an increased yield leads to increased particle mass which leads to increased surface area for disposition and a heightened sensitivity of the mass balance to changes in the kinetics. Figure 5.9 demonstrates this by showing the coefficient of variation for output SI in a 1-L, 10-L and 100-L MSMPR crystalliser.

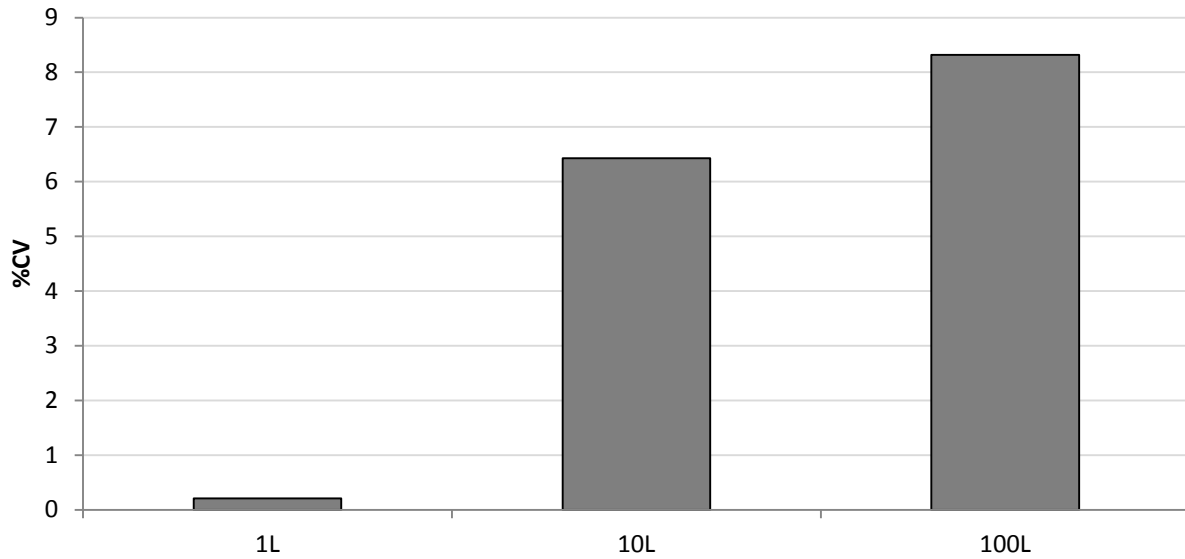


Figure 5.9: Coefficient of variation in the steady state SI for a 1-L, 10-L and 100-L MSMPR crystallizer having a uniform distribution of kinetic rate coefficients.

Figure 5.9 shows the increasing coefficient of variation with increasing reactor volume (the relationship between reactor volume and yield is shown in Figure 4.11). This demonstrates the heightened sensitivity of the thermodynamics to kinetic uncertainty as yield increases.

The finding of phosphorus uncertainty propagation being greater than nitrogen uncertainty propagation in Figure 5.8 is further supported by the analysis of uncertainty contributions from the deterministic uncertainty analysis, outlined in Figure 5.10.

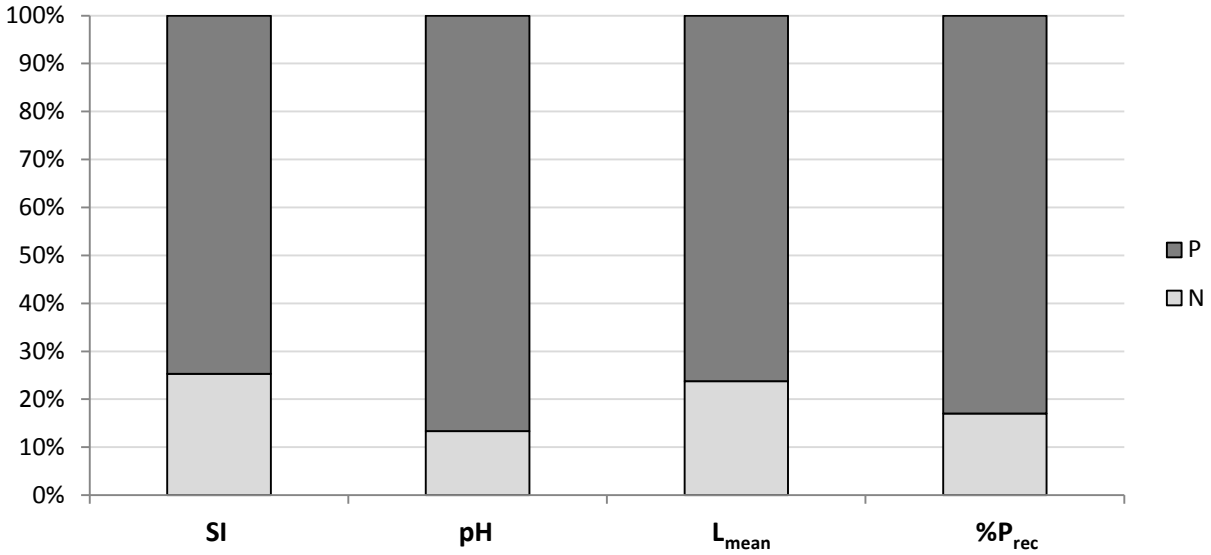


Figure 5.10: Relative contributions of individual nutrient loads on total uncertainty in key process variables in deterministic uncertainty analysis.

The sensitivity of the system to phosphorus uncertainty is greater than nitrogen uncertainty for all output variables. This behaviour results from phosphorus participating in more thermodynamic equilibria reactions compared with nitrogen (see Table 2.1). This makes the concentration of free phosphate and therefore all output variables more sensitive to uncertainty in phosphorus concentration.

5.4.5 *pH* Control

A *pH* control scheme is introduced to the stochastic simulations to assess its ability to limit uncertainty propagation. The control scheme is affected by algebraically fixing the *pH* variable and freeing the flowrate of sodium hydroxide, which maintains zero degrees of freedom in the model. This means the flow of caustic to the reactor will change in order to keep the *pH* constant. This essentially replicates the behaviour of a perfect *pH* controller. The *pH* set point is 8.0, which is based on the base case scenario (*pH* = 7.99).

The controlled pH results will only be reported for the combined nutrient load case where the concentration of both phosphorus and nitrogen are subject to variability. The distribution of SI produced from the controlled pH scenario is compared against the uncontrolled pH scenario in Figure 5.11.

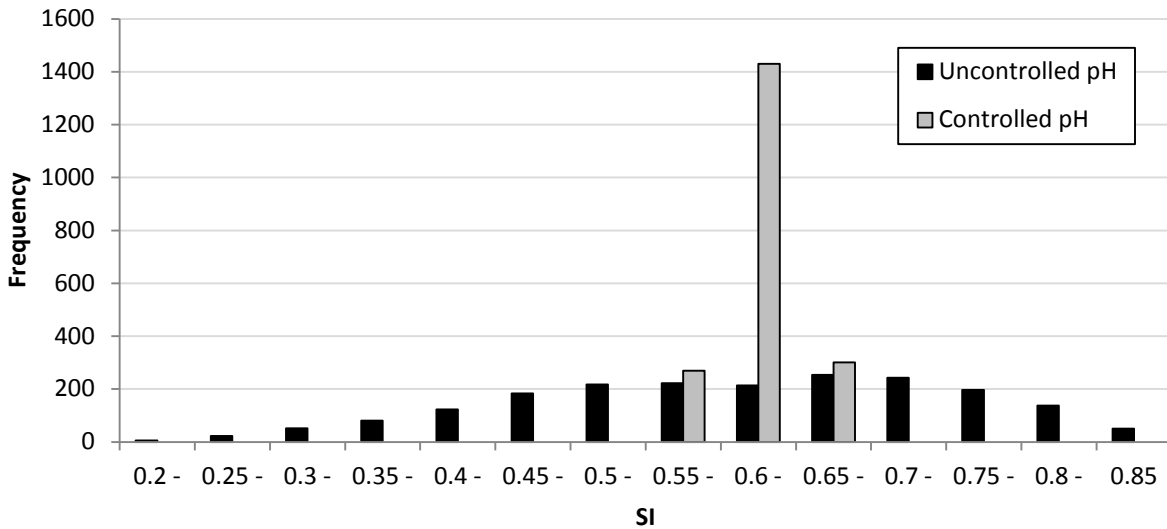


Figure 5.11: Frequency distribution of steady-state SI with nutrient load variability for uncontrolled and controlled pH .

The impact of pH control on phosphorus recovery should also be examined. However, it is difficult to determine the recovery based on thermodynamically available phosphorus if the pH is fixed. This difficulty arises since the pH that corresponds to $SI = 0$ is below the set point. Furthermore, the pH that corresponds to $SI = 0$ changes for each stochastic nutrient load value. To address this, the phosphorus recovery for the controlled pH scenario is based on total phosphorus, $\%P_{Rec}^T$. This is justifiable considering the purpose of this analysis is to demonstrate how a pH control scheme reduces uncertainty propagation and the use of $\%P_{Rec}^T$ accomplishes this. It should be remembered that the total recovery is less than the thermodynamic recovery since it includes phosphorus that is not available

for crystallisation. The $\%P_{Rec}^T$ distribution for the controlled and uncontrolled pH scenarios is location in Figure 5.12.

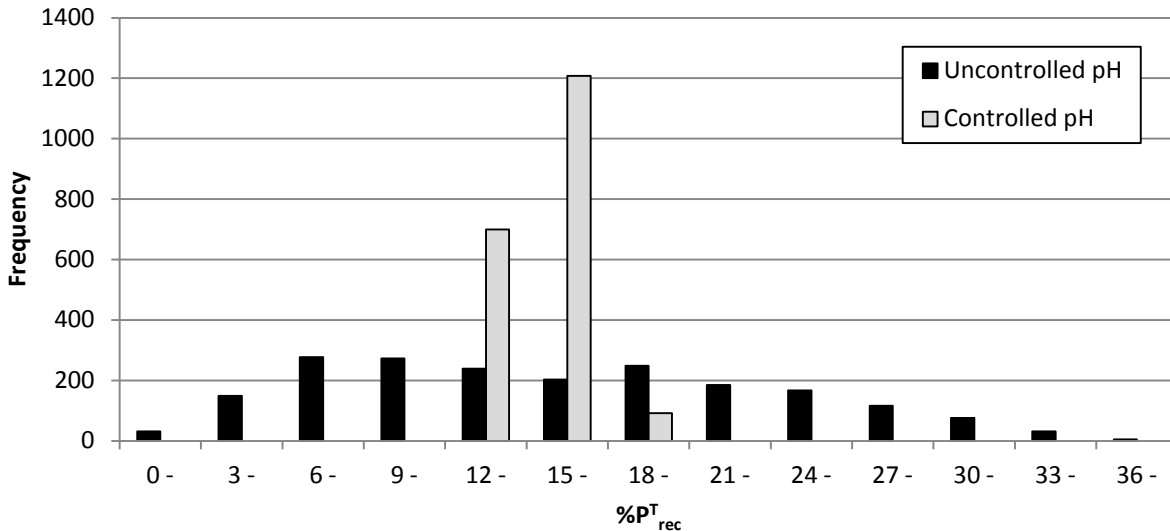


Figure 5.12: Frequency distribution of steady-state $\%P_{Recovery}^T$ with nutrient load variability for uncontrolled and controlled pH .

Figure 5.11 and Figure 5.12 clearly show that a pH control scheme reduces uncertainty propagation through the model. This is important information for an operating crystalliser. It can be seen in Figure 5.12 that the sensitivity of $\%P_{Rec}^T$ to nutrient load uncertainty is improved by introducing pH control. This has economic implications as more consistency in the phosphorus recovery would lead to consistency in revenue generated.

5.5 Conclusions

The sensitivity of key process variables to uncertainty in kinetic parameters and nutrient load is investigated. It was found that uncertainty in crystal growth rate coefficient propagates most significantly to the key output process variables compared to the other kinetic mechanisms. Uncertainty

in the phosphorus load produced greater variability in the model outputs than nitrogen load. The model outputs were found to be more sensitive to nutrient load uncertainty than kinetic parameter uncertainty. However, increasing the yield of the reactor by increasing the reactor volume was found to increase the sensitivity of the model outputs to kinetic parameter uncertainty. A *pH* control scheme was investigated and it greatly reduced uncertainty propagation. This information could be used to design a process that could cope with the uncertainties resulting from running a struvite crystalliser.

5.6 Key Points from Chapter Five

- Deterministic and stochastic methods are used to assess kinetic parameter and nutrient load uncertainty propagation through the process model.
- Uncertainty propagation from the crystal growth rate coefficient is the most significant of the kinetic parameters
- Uncertainty propagation from the phosphorus load is the most significant of the nutrients
- *pH* control greatly reduces uncertainty propagation

Chapter 6 - Experimental Methodology

This chapter outlines the experimental method used to gather data for the parameter estimation of struvite nucleation, crystal growth and aggregation kinetic parameters.

The pH measurement proved to be repeatable and the experimentally measured PSDs demonstrate quantifiable nucleation, crystal growth and aggregation effects, justifying the choice of mechanisms used in the discretised population balances of Chapter 3 and Chapter 4.

6.1 Introduction

A process model for struvite crystallisation was developed in §4.2 and its applications to process design and control were explored in §5.4. However, the kinetic parameters used thus far to describe struvite nucleation, growth and aggregation were not based on the struvite system. Their choice was based on work in similar and comparable crystallisation systems (Hounslow, 1990 and Bramley, 1994). Thus, the model “hardware” is in place, but it remains to add the “software” in order for this model to achieve fidelity. Since no data are available in the literature (see §3.6), an experimental methodology is designed and executed.

6.2 Review of Experimental Methods

For the struvite crystallisation model to be properly utilised it requires kinetic parameters. Experiments must be conducted delivering measurement of variables that can be predicted by the model, subject to the kinetic parameters under evaluation. A review of experimental methods that have been used in the

field of struvite and similar crystallisation systems is conducted before developing the experimental methodology used in this work.

6.2.1 Particle Size Distribution (PSD) Measurement

Arguably, the most important experimental measurement for the population balance is the particle size distribution, or PSD, since it is predicted by the process model. Inaccurate PSD measurements would result in inaccurate kinetic parameters and, commensurately, an inaccurate process model. The most common way of experimentally determining the PSD is with laser diffraction (LD) methods, which indirectly measure the total crystal volume in each size interval by fitting a volume-based PSD to a back-scattering pattern that assumes that all particles are spherical (Xu and Di Guida, 2003). The laser diffraction method of PSD measurement has been applied widely to sizing struvite (Münch and Barr, 2001, Ali and Schneider, 2006, Matynia et al., 2006, Le Corre et al., 2005, Ali and Schneider, 2008, Pastor et al., 2008a, Koralewska et al., 2007, Piotrowski et al., 2009, Ronteltap et al., 2010).

However, because the discrete population balance (DPB) describes changes in particle number, and not volume, a PSD determined with LD methods cannot be used directly and must be converted to give a number density distribution (Randolph and Larson, 1988, Mullin, 1993). This conversion contains significant numerical inaccuracies as demonstrated in §3.6. Therefore LD methods were not used to measure the PSD.

The electrical sensing zone (ESZ) method can be used to directly measure the number and size of particles. ESZ works by drawing particles through an aperture with electrodes on either side of the aperture. When particles disrupt the current through the aperture it changes the impedance and the change in impedance is proportional to the volume of the particle. The number of particles can be determined by counting the number of times the current is disturbed and their size is given by the magnitude of the impedance change. For a more detailed explanation of the ESZ method consult the

literature (Xu and Di Guida, 2003). ESZ methods have been used successfully by Hounslow (1990), Illievksi (1991) and Bramley (1994) to determine crystallisation and size-enlargement kinetic parameters. The advantage of using the ESZ method over laser diffraction is further demonstrated in §6.4.2.

6.2.2 *pH* Measurement

pH measurement is ubiquitous in struvite experimental studies. This is because of the importance that hydrogen and hydroxide ions have on solution thermodynamics as detailed in §2.2.3. Some researchers have even used *pH* measurement to determine the consumption of struvite constituents through reaction equations such as Equation 6.1 (Wang et al., 2005, Turker and Celen, 2007, Stratful et al., 2001, Stratful et al., 2004, Zeng and Li, 2006), Equation 6.2 (Bouropoulos and Koutsoukos, 2000, Matynia et al., 2006, Koralewska et al., 2007, Le Corre et al., 2007).



However, this confuses solution thermodynamics for stoichiometry. The fact that multiple reaction equations can be used suggests that none is correct. Changes in *pH*, due to struvite crystallisation, occur because of changes in the solution thermodynamics as magnesium, ammonium and phosphate ions are removed from the aqueous phase and incorporated into the solid phase. The total concentration of the master elements changes and the speciation changes, the *pH* decreases in order to keep the solution electro-neutral, not because protonated phosphate participates in the crystallisation reaction. Therefore, the reaction equation that uses free phosphate, which is used in this work (Equation 1.1) is the correct one.

The experimentally measured dynamic *pH* response also provides another measurement option for parameter estimation. The experimental procedure developed ensured that the *pH* response of the

system was as repeatable as possible, allowing for higher confidence estimations. While pH has been used experimentally to express kinetics in previous research (Nelson et al., 2003), it has yet to be combined with the PSD in order to elucidate the three kinetic mechanisms of concern in this study.

6.2.3 Concentration Measurement

There are several available methods to measure solution concentration. One commonly used method is colorimetry (Ohlinger et al., 1998, Nelson et al., 2003, Uysal et al., 2010, Lew et al., 2010). Colorimetry is a version of spectrophotometry that is limited to the visible spectrum of electromagnetic radiation. Colorimetric procedures exist to measure the concentration of magnesium, ammonium and phosphate making it the most accessible and widely applicable method. Unfortunately it is impossible to measure the concentration of every species in solution, so an accurate description of the solution thermodynamics is still necessary.

Atomic absorption spectroscopy and atomic emission spectroscopy are also used to measure struvite elemental concentrations (Bouropoulos and Koutsoukos, 2000, Koralewska et al., 2007, Le Corre et al., 2007, Piotrowski et al., 2009, Chimenos et al., 2003, Plaza et al., 2007, Zhao et al., 2006, Li and Zhao, 2003) However, this is limited to magnesium and phosphorus.

The limitation of all concentration measurement techniques used in the literature is they require sampling and further analysis to determine the concentration. Another possible method is the use of ion selective electrodes as they could provide real time measurements of free ionic concentration. However, ion selective electrodes are subject to interference from other ions. This interference is complex and may depend upon the concentration of the primary and competing ions, ionic strength and temperature (Rundle, 2000), making practical implementation difficult.

6.2.4 Reactor Configuration

Previous struvite kinetic studies have been conducted in batch (Nelson et al., 2003, Quintana et al., 2005, Le Corre et al., 2007, Turker and Celen, 2007, Borja et al., 2008, Harrison et al., 2011), fed-batch (Bouropoulos and Koutsoukos, 2000, Le Corre et al., 2007, Ali and Schneider, 2008, Bhuiyan et al., 2008a) and continuous configuration (Matynia et al., 2006, Koralewska et al., 2007, Piotrowski et al., 2009). The process model developed in §4.2 could describe continuous, fed-batch or batch modes, so any reactor configuration could be used to generate the data necessary for parameter estimation.

Batch experiments were chosen for a number of reasons: convenience in setting up the experimental apparatus; shorter, and therefore more, experiments in any given period of time; less reactant required; and reactor engineering techniques can be used to apply the batch parameters to other configurations (Ilievski, 1991).

6.2.4.1 Using Batch Experimental Data to Predict Continuous Crystallisation

Methods for using batch reaction data to predict the operation of a continuous reactor have been developed in chemical reaction engineering (Levenspiel, 1972). These methods are used to derive similar expressions for crystallisers in Ilievski (1991).

The relationship between batch and continuous reactors is based upon the complete segregation limit of micromixing. This means that all volume elements of the same residence time are lumped together into small batches which pass through the system without interacting with other elements of different residence times. With the assumption of complete segregation the following equation can be written (Equation 6.3).

$$\left[\begin{array}{l} \text{Number of crystal} \\ \text{ sized } L \text{ to } L + dL \\ \text{ and aged } t \text{ to } t + dt \\ \text{ in exit} \end{array} \right] = \left[\begin{array}{l} \text{Number sized } L \text{ to } L + dL \\ \text{ expected to be formed} \\ \text{ after } t \text{ to } t + dt \\ \text{ in the system} \end{array} \right] \left[\begin{array}{l} \text{Fraction that spend} \\ \text{ time } t \text{ to } t + dt \\ \text{ in the system} \end{array} \right] \quad 6.3$$

Writing these terms in differential increments produces Equation 6.4.

$$dN(L) = N(L, t)_{batch} E(t) dt \quad 6.4$$

Where $E(t)$ is the residence time distribution. The mean number in the size range L to $L + dL$ is evaluated by integrating Equation 6.4, resulting in Equation 6.5.

$$\bar{N}(L) = \int_0^{\infty} N(L, t)_{batch} E(t) dt \quad 6.5$$

The values of $N(L, t)$ can be obtained directly from batch experiments. Similar expressions can be written for other system variables, such as saturation index (Equation 6.6).

$$\bar{SI} = \int_0^{\infty} SI(t)_{batch} E(t) dt \quad 6.6$$

When applying this approach Ilievski (1991) found it to be a useful tool in predicting the behaviour of continuous precipitation with batch experimental data. However, it is strongly dependent on mixing and flow conditions. If the system cannot be adequately modelled as a completely segregated macrofluid, this approach may not yield reliable results.

6.3 Experimental Methodology

Before elaborating on the experimental methodology it is worth stating the goals so that the approaches and choices made in the development of the experimental methodology can be understood.

6.3.1 Goals of the Experimental Methodology

The ultimate goal of the experimental methodology is to provide accurate and repeatable, and thus reliable, experimental measurements to regress the best possible parameters for the process model. The two principle measurements for this are PSD and pH . This is because PSD is central to the aim of this thesis and pH is the easiest, most straightforward and, as a result, the most widely used real-time measurement in struvite research. An additional measurement of total elemental magnesium concentration will be employed for some experiments to assess mass balance integrity. It should be noted that any one of these measurement types could be used alone to estimate the model parameters in gPROMS. However, using a variety of experimental measurement types ensures higher confidence.

The experiments should also cover the largest possible range of supersaturation. This is because the equations used to describe the kinetics detailed in §4.2.2 are functions of saturation index. For the estimated parameters to be meaningful they must be derived from data that covers a large range of saturation index.

With these factors in mind the goals for the experimental methodology are:

- PSD measurements must be accurate and repeatable
- pH measurements must be accurate and repeatable
- The experiments must cover the largest range of saturation index possible
- Repeatable experimental method

The experimental work aims to determine the particle size distribution (PSD) at various points in time of a batch crystallisation of struvite. These PSDs can then be used to determine kinetic parameters for struvite nucleation, crystal growth and aggregation using the process model discussed in §4.2.

6.3.2 Experimental Setup

The batch experiments were carried out in a 1-L borosilicate glass beaker that was baffled with four removable PVC baffles. Baffles greatly improved the repeatability of the dynamic pH response, owing to more uniform mixing in the system. The reactor was well mixed with a Favorit HS0707V2 hotplate-magnetic stirrer set to a constant mixing rate without heating. The pH was measured using a Thermo Orion 8165BNWP Ross sureflow pH electrode and Thermo Orion 5-star meter. A schematic diagram of the experimental apparatus is given in Figure 6.1.

Temperature was measured with an integrated thermometer, so that the temperature correction of the pH meter could be used. The laboratory was not temperature controlled but remained relatively constant with a mean temperature of 29.3 °C having a standard deviation of 0.6 °C. The pH probe was calibrated at the start of the day with $pH\ 7 \pm 0.02$ and 10 ± 0.05 buffer solutions. All solutions were made using volumetric glassware (pipettes and volumetric flasks), ultra-pure water from a MembraPure Aquinity purifier and ACS reagent grade $NH_4H_2PO_4$, $MgCl_2 \cdot 6H_2O$, $NaOH$ and HCl .

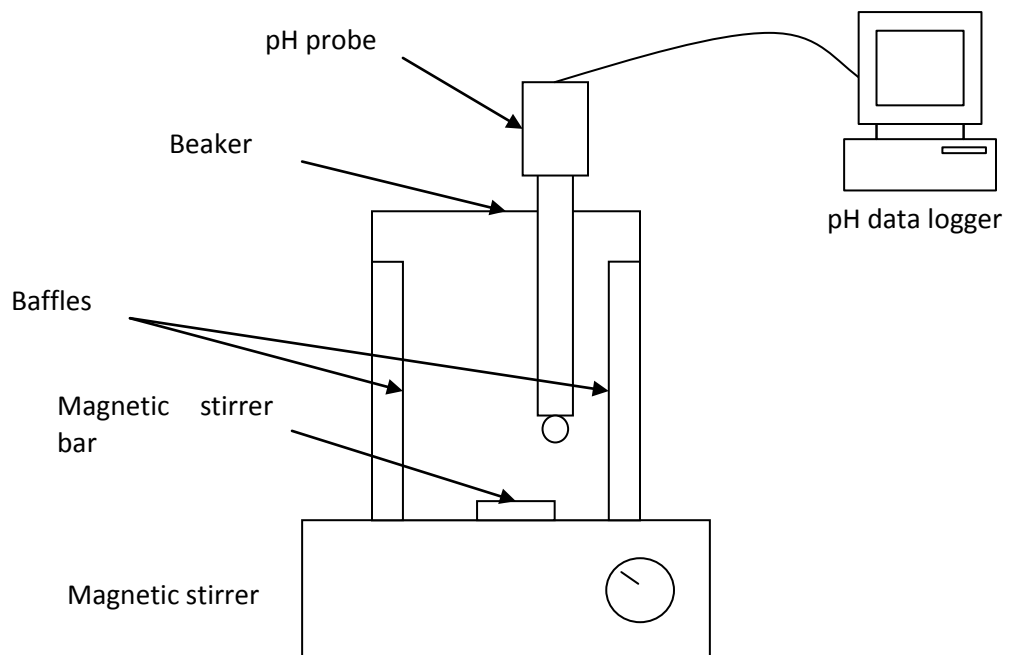


Figure 6.1: Schematic diagram of the experimental apparatus.

6.3.3 Seed Preparation

The experiments were seeded to limit primary nucleation (Mullin, 1993) and improve repeatability in the dynamic pH response by providing a consistent initial PSD that could subsequently grow. Wet seed was chosen to avoid caking and distortion of the PSD due to the drying process. The wet seed slurry was made to have a solids concentration of between 2.5 and 3.5 g/L . To prepare the seeds a 1-L solution of 0.005 M Mg, N and P was prepared to which 10 mL of 0.5 $M NaOH$ was added. The solution was left to crystallise overnight and then allowed to settle. The supernatant solution was decanted until 100 mL remained. The leftover solution was sealed in a Schott bottle and kept on a magnetic stirrer in order to keep the seeds suspended. A typical PSD produced from the seed solution is shown in Figure 6.2.

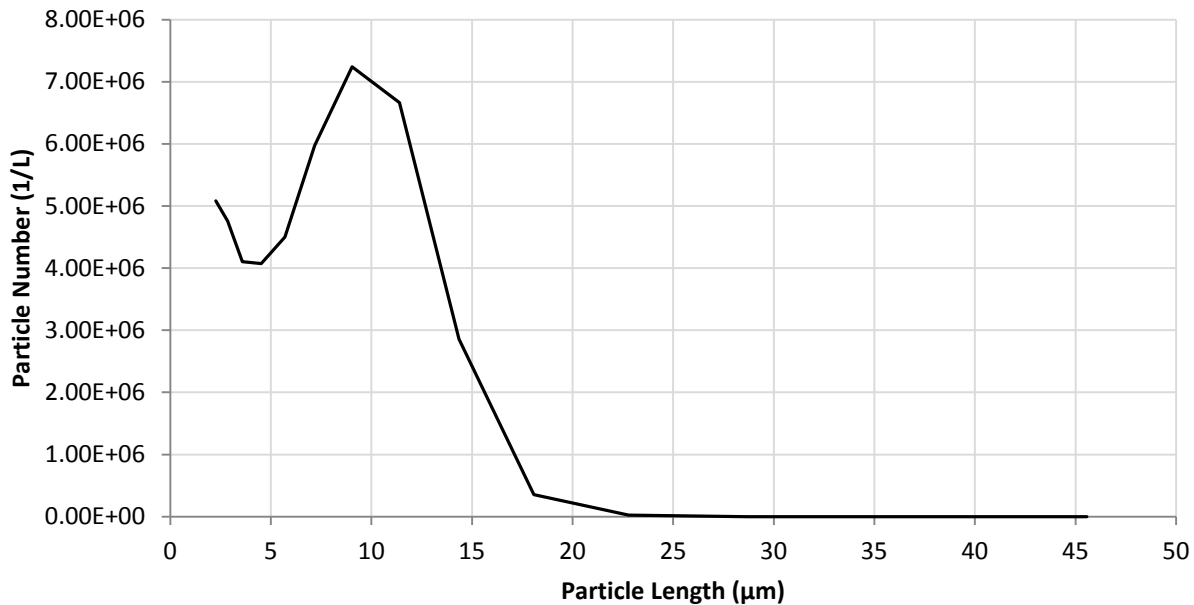


Figure 6.2: Typical PSD from the seed solution used in the batch crystallisation experiments.

6.3.4 The Electrical Sensing Zone Method

The PSD in all experiments was measured with a Beckman Coulter Multisizer 3, which uses the ESZ method. One important consideration when using the ESZ method is the electrolyte in which the particles are suspended. This work used commercially available Beckman Coulter *ISOTON 2*, saturated with struvite. Saturation was achieved by dissolving an excess of struvite in electrolyte. After saturation had been achieved the electrolyte was vacuum filtered with a $0.45 \mu\text{m}$ membrane filter and then stored for later use.

The range of sizes that can be measured during analysis is determined by the size of the aperture through which the particles pass. The choice of aperture size used to measure the PSD is very important and influences the experimental conditions that can be evaluated. The Beckman Coulter Multisizer 3 apertures can detect particles between 2%-60% of the employed aperture size. This immediately introduces a trade-off between resolution of the small particles and aperture blockage.

The available aperture sizes for the apparatus were 50, 100, 560, 1000 and 2000 μm . More aperture sizes are available from the manufacturer. The 560, 1000 and 2000 μm apertures were not considered as they would not measure any particles smaller than 11.2 μm , which were shown to be in significant quantities in preliminary experiments. The 50- μm aperture was also rejected as a possible aperture because its maximum limit is only 30 μm and was easily blocked by larger particles. The 100 μm aperture was chosen because it could still capture the detail in the smaller end of the PSD, without excessive blocking.

6.3.5 Initial Saturation Index

Two values of initial SI were found to be best suited for the experimental method. Firstly, $SI = 0.54$, obtained by adding 9mL of 0.5M NaOH and $SI = 0.37$, obtained by adding 8.5 mL of 0.5 M NaOH to 1 L 0.005 M solution of Mg, N and P. These two conditions gave an SI range of 0.54 to 0.25. While a broader range of SI would produce more confidence in the estimated kinetic parameters, the experimental conditions were limited for the following reasons:

- The duration of each particle size analysis
- Blocking of the aperture tube
- Magnitude of the pH response

The PSD analysis of each sample taken from the batch took approximately three minutes, making the maximum sampling rate for any experiment one sample every three minutes. An experiment with an initial SI of 0.96 was attempted but it was found that approximately 50% of the pH change occurred in the first three minutes and therefore its PSD could not be properly described in that range of pH change.

An experiment with an initial SI of 0.74 was attempted to generate a slower pH response, but aperture blockage occurred, owing to the faster growth rate at this SI . The seed PSD shown in Figure 6.2 shows particles ranging from $2.0\ \mu m$ to $25.0\ \mu m$ so it is unexpected that a $100\ \mu m$ aperture would get blocked in the course of an experiment. However the ESZ method measures particle volume, not length, so the results are reported as the spherical volume equivalent diameter. Since struvite crystals display a needle-like habit with a high aspect ratio (Abbona and Boistelle, 1979, Abbona and Boistelle, 1985, Lind et al., 2000, Wilsenach et al., 2007), these particles are expected to be rather long. For example a particle with an aspect ratio of 8 (used in §3.6) and a $100\ \mu m$ length will have a spherical-equivalent diameter of $31\ \mu m$, assuming a square base. Taking this into account it is not surprising that blockages occur even though the PSD reports particles well within the acceptable range of the aperture tube.

An experiment with an initial SI of 0.22 gave a pH response of 0.06 pH units after 2 hours. Given that the uncertainty in the pH 10 calibration solution is $\pm 0.05\ pH$ units this potential experimental condition was rejected. While it is possible to run the experiment longer to get a greater pH change this may introduce pH “drift” where the pH measurement drifts away from the real value.

6.3.6 Sampling Procedure

In order to analyse the PSD, samples of the crystals produced during the batch reaction had to be taken. It is important that the sample PSD be representative of the reactor and that a consistent and accurate sample volume is taken each time. This is because the Multisizer 3 measures the volume of sample passing through the aperture, leading to an estimation of the number per unit volume in the reactor. Sampling with pipettes gives accurate sample volumes but may lead to classification of the product because of the small inlet of the pipette. A beaker can be used to take a representative sample but are inaccurate when measuring volumes.

To address the problem of representative sampling, a 30-mL beaker was filled with solution from the reactor and a volumetric flask stopper was used to displace a constant volume from the beaker. This method produced a sample volume of $29 \pm 0.5 \text{ mL}$. The sample was then added to 140 mL of saturated *ISOTON 2* electrolyte and then analysed with the Multisizer 3.

The sample times at which the $SI = 0.54$ and $SI = 0.37$ experimental conditions were analysed are presented in Table 6.1.

Table 6.1: Sample times for the two experimental conditions

$SI = 0.37$	$SI = 0.54$
0 minutes	0 minutes
3 minutes	3 minutes
10 minutes	6 minutes
20 minutes	10 minutes
35 minutes	15 minutes
60 minutes	
120 minutes	

The $SI = 0.54$ experiment could only be conducted for 15 minutes owing to aperture blockages. After that time the seed crystals had grown too large (*i.e.* too long), making PSD analysis through the 100- μm aperture infeasible (§6.3.5).

6.4 Results and Discussion

This section will detail the results of preliminary work that was used to develop the experimental procedure.

6.4.1 Hydrodynamic Considerations

To maximize the repeatability of the dynamic pH response the effect of baffling the reactor was investigated. It was found that baffling the reactor made the experimental procedure more repeatable. As such all experiments utilized a set of removable PVC baffles constructed for the 1-L reactor. The four baffles were 10 mm wide and covered the height of the reactor, they were arranged at 90 degrees of each other. It is postulated that the baffles resulted in more consistent hydrodynamic behaviour and therefore a more consistent nucleation rate. Without the baffles nucleation rate variations would change the number of crystals that were growing and therefore change the rate of de-supersaturation. The comparison between pH response from baffled and non-baffled reactors is shown in Figure 6.3.

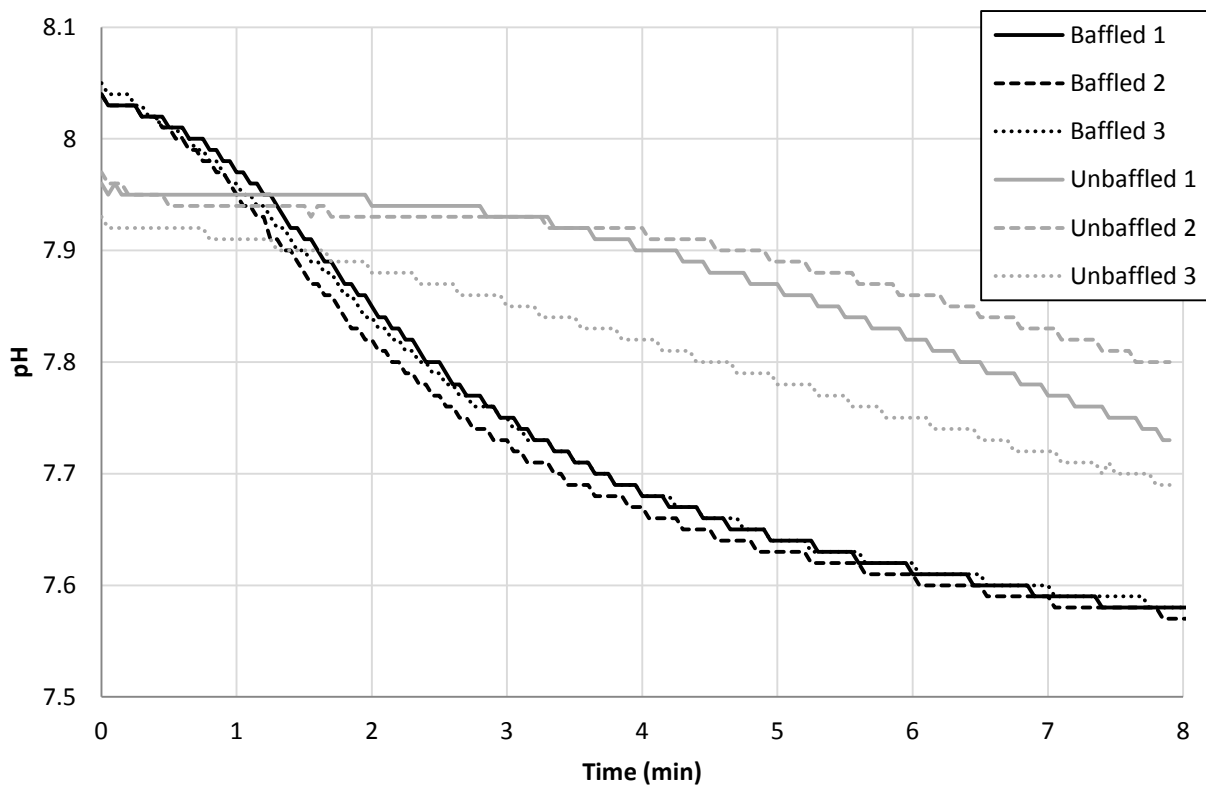


Figure 6.3: Dynamic pH response during crystallisation in a batch reactor with and without baffles.

6.4.2 PSD Accuracy

The reasons for using the ESZ method over LD were briefly discussed in §6.2.1 and §3.6. Both ESZ and LD sizing apparatus were available when the PSD experiments were carried out, so a direct comparison between the two methods could be conducted. The LD sizing was done with a Malvern Mastersizer S using the small volume dispersion unit.

The two samples analysed for the comparison were taken from the same batch and prepared in the same way as a typical sample for the Multisizer 3 analysis to minimise any random errors from using different batches or sample preparation techniques. The PSD produced from the two different sizing methods are shown in Figure 6.4. To allow comparison between the two distributions are plotted using the size intervals generated by the LD analysis. The LD intervals are use seeing as the ESZ intervals do not cover the whole size range of the LD analysis.

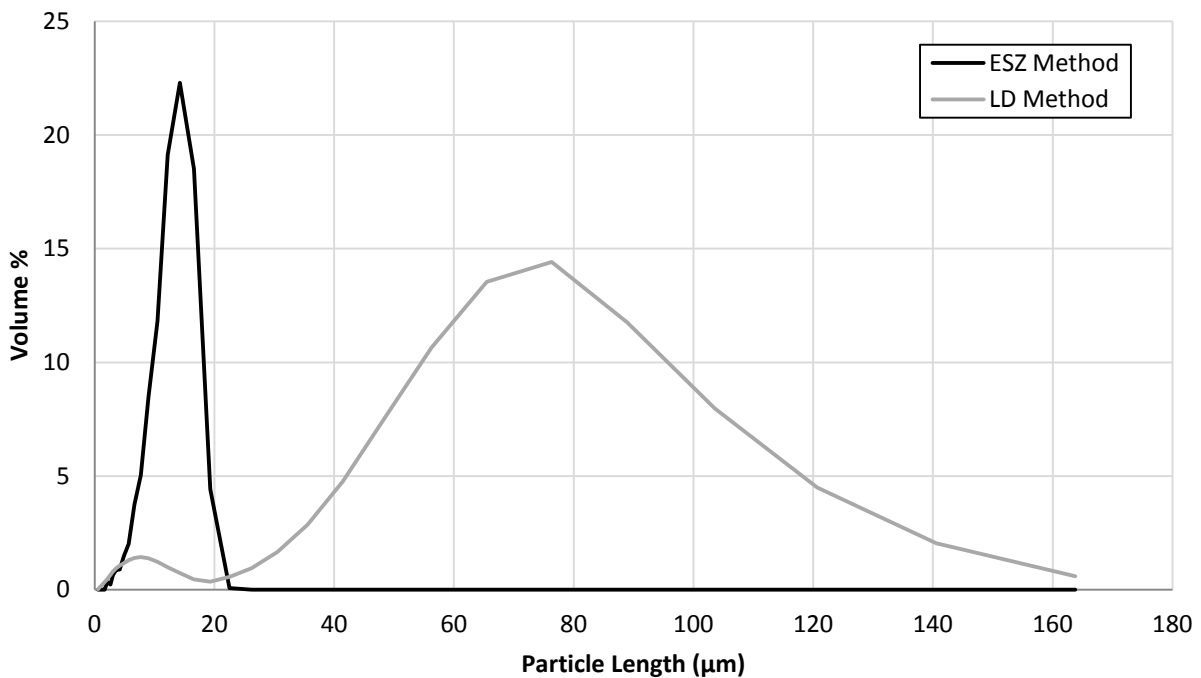


Figure 6.4: PSD produced for a sample from the same batch using the ESZ method and LD method.

It can be seen in Figure 6.4 that the LD method significantly over predicts the size of the particles. When the physical size of the aperture is considered the errors in the LD results are stark. The 100- μm aperture tube was used in the ESZ measurement, which means any particles larger than 100 μm would block the aperture. However, the ESZ analysis did not result in any aperture blockage. The fact that approximately 15% of the particles analysed on a volume basis using LD were reported to be greater than 100 μm highlights the inaccuracy of the method when analysing struvite. It is postulated this is due to the large aspect ratio of the needle-like struvite crystals, causing errors when analysed with the LD method (Xu and Di Guida, 2003).

Microscopy work performed confirms the accuracy of the ESZ method. The struvite produced by this experimental procedure is shown in Figure 6.5. The needles seen in Figure 6.5 are between 14 and 90 μm long which is too large for the ESZ results. However these lengths need to be converted to spherical equivalent diameters. Using a volumetric shape factor of 8 and assuming a square base the size range of particles becomes 4 to 28 μm . This range of particle size is consistent with both Figure 6.2 and Figure 6.4.



Figure 6.5: Struvite crystals produced using the experimental procedure developed for this work.

6.4.3 *pH* Repeatability

When conducting the experiments a number of batches of seed solution were used. This makes comparing *pH* across all experiments difficult, since two different seed distributions will likely result in different *pH* responses. Hence, when comparing the *pH* response the experiments are grouped so that they have a seed solution from a common batch. For the purpose of this comparison a “group” of experiments is defined as experiments having the same initial conditions with regards to *SI* and seed PSD.

Experiments having an initial *SI* of 0.37 are shown in Table 6.2 , while experiments having an initial *SI* of 0.54 are shown in Table 6.3.

Table 6.2: Groups of experiments that used the same seed solution having an initial $SI = 0.37$.

Group	Number of Experiments	Variables Measured
1	3	N_i, pH
2	2	N_i, pH
3	1	N_i, pH, C_{TMg}

Table 6.3: Groups of experiments that used the same seed solution having an initial $SI = 0.54$.

Group	Number of Experiments	Variables Measured
1	2	N_i, pH
2	2	N_i, pH
3	1	N_i, pH
4	1	N_i, pH, C_{TMg}

The pH response for all $SI = 0.37$ experiments is shown in Figure 6.6. It can be seen that there are different pH responses for different seed solutions. However, even with different seed solutions the maximum variance in the pH response ± 0.025 pH units, which, when considering that the uncertainty on the pH 7 buffer solution is ± 0.02 , is a satisfactory result.

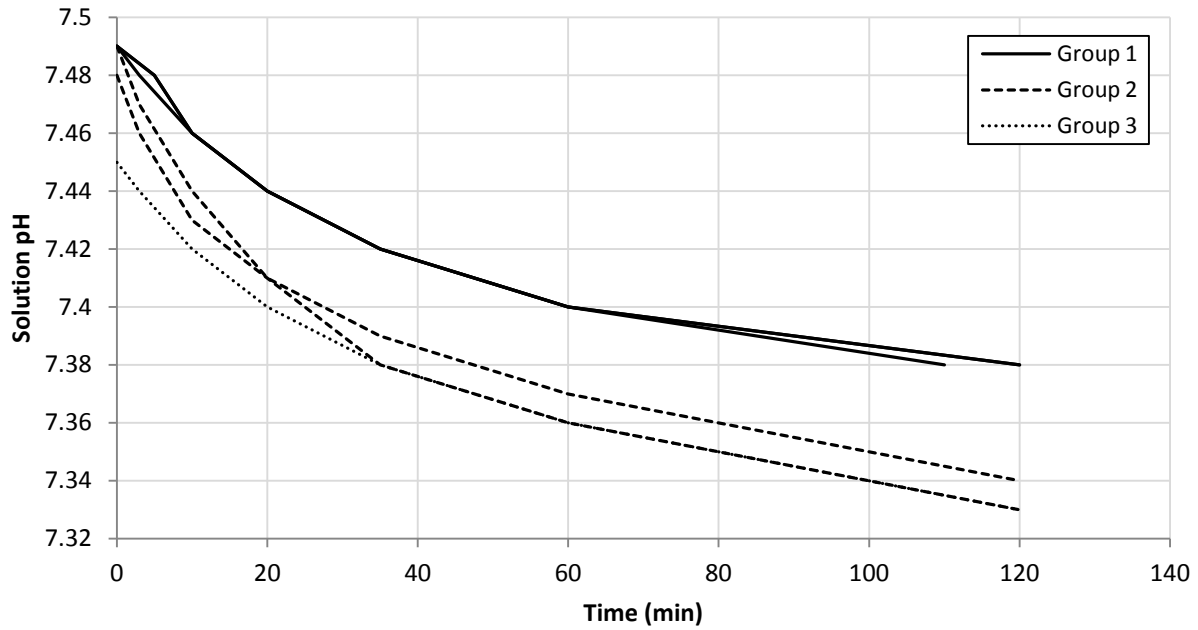


Figure 6.6: The pH response for all experiments with an initial SI of 0.37 with experimental group as parameter.

The pH responses for all $SI = 0.54$ experiments are shown in Figure 6.7. The maximum variation is ± 0.035 pH units which is greater than the $SI = 0.37$ experiments. It is observed that the more rapid pH response and larger gradient of the $SI = 0.54$ experiments result in reduced repeatability.

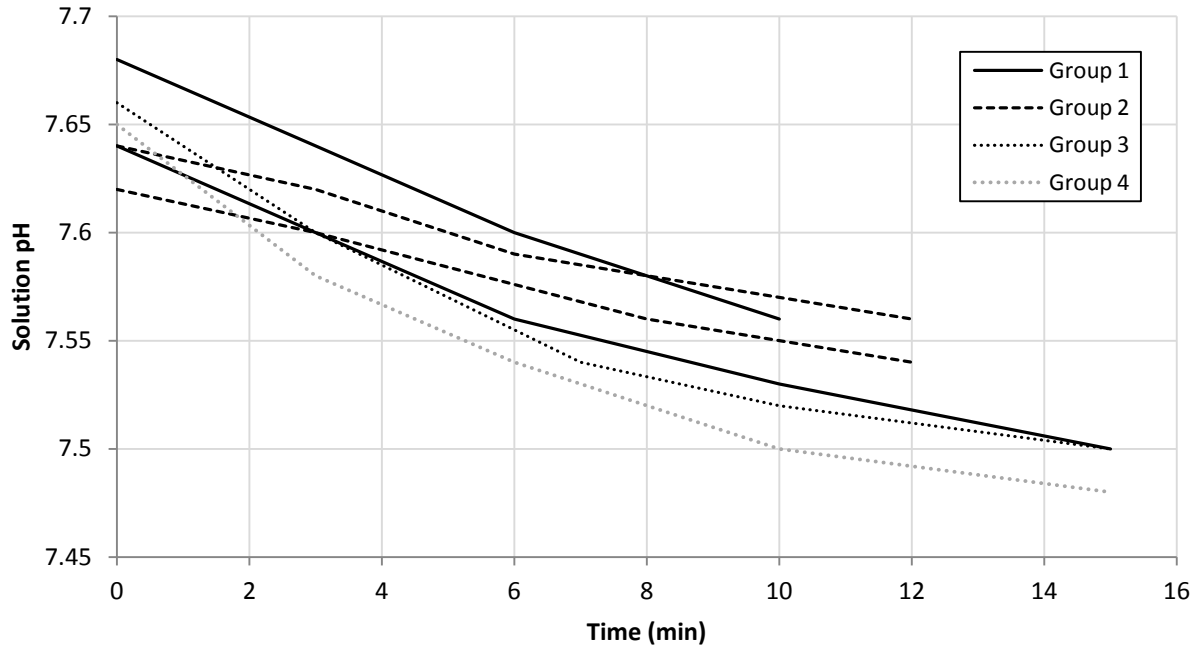


Figure 6.7: The *pH* response for all experiments with an initial *SI* of 0.54 with experimental group as parameter

6.4.4 PSD Repeatability

The PSD results are shown in Figure 6.8 to Figure 6.12. The PSDs shown below are from Group 1 of the $SI = 0.37$ experiments. This is because this group has the highest number of experiments having a common seed size distribution making it the best demonstration of the repeatability of the experimental procedure.

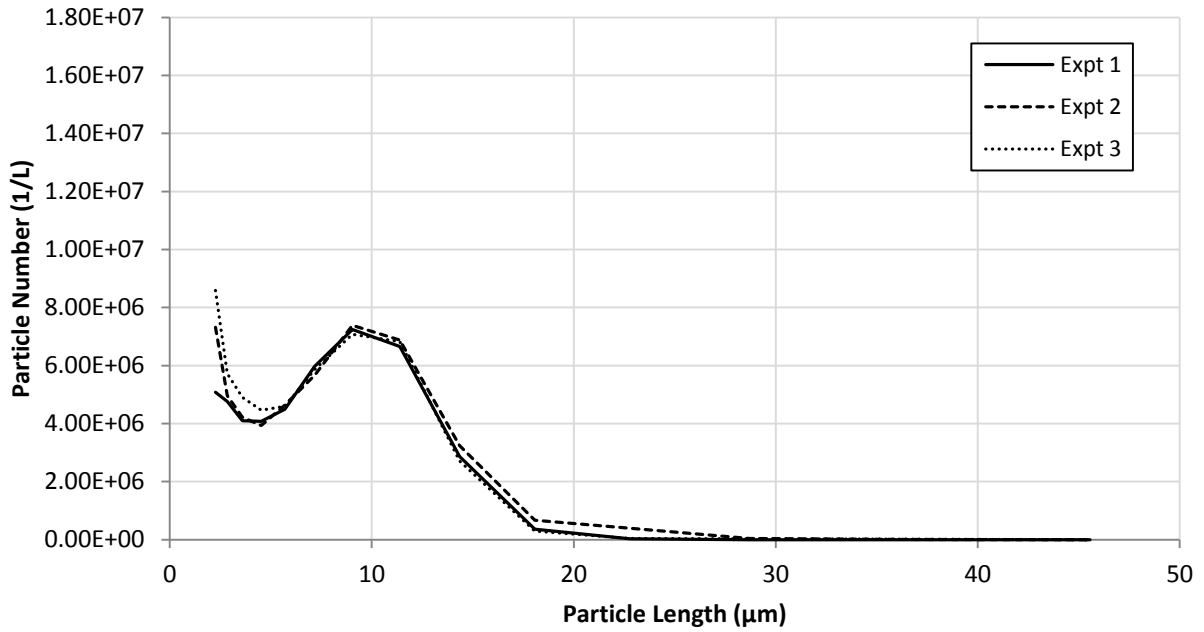


Figure 6.8: The PSD of three samples taken from the same seed solution at time zero.

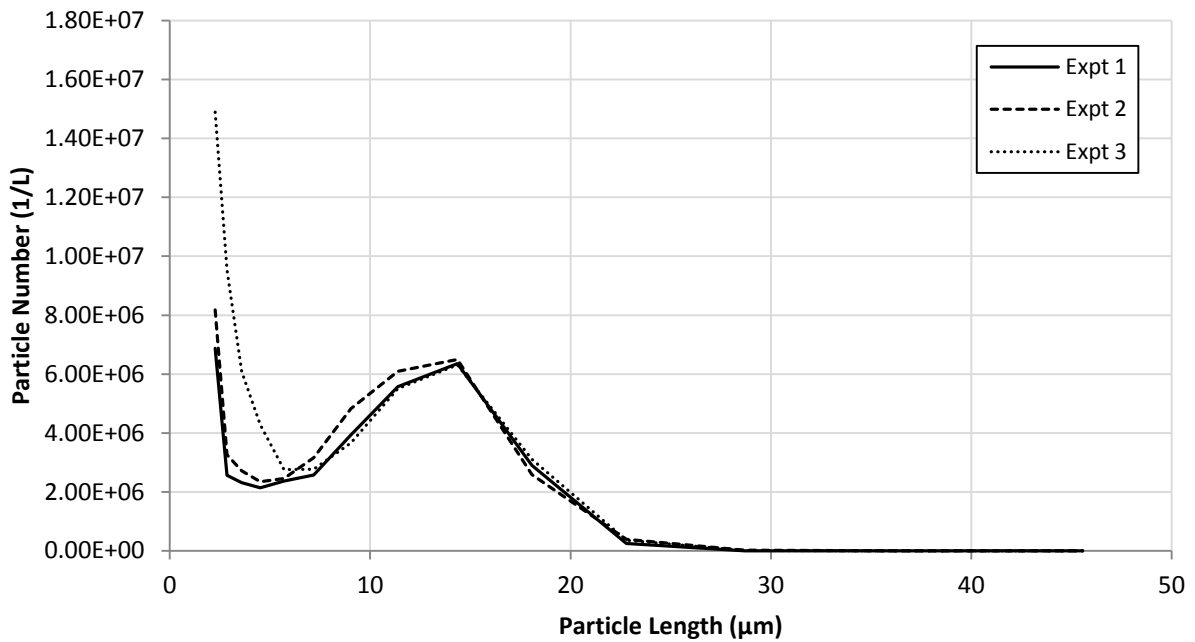


Figure 6.9: The PSD of three samples taken after 10 minutes

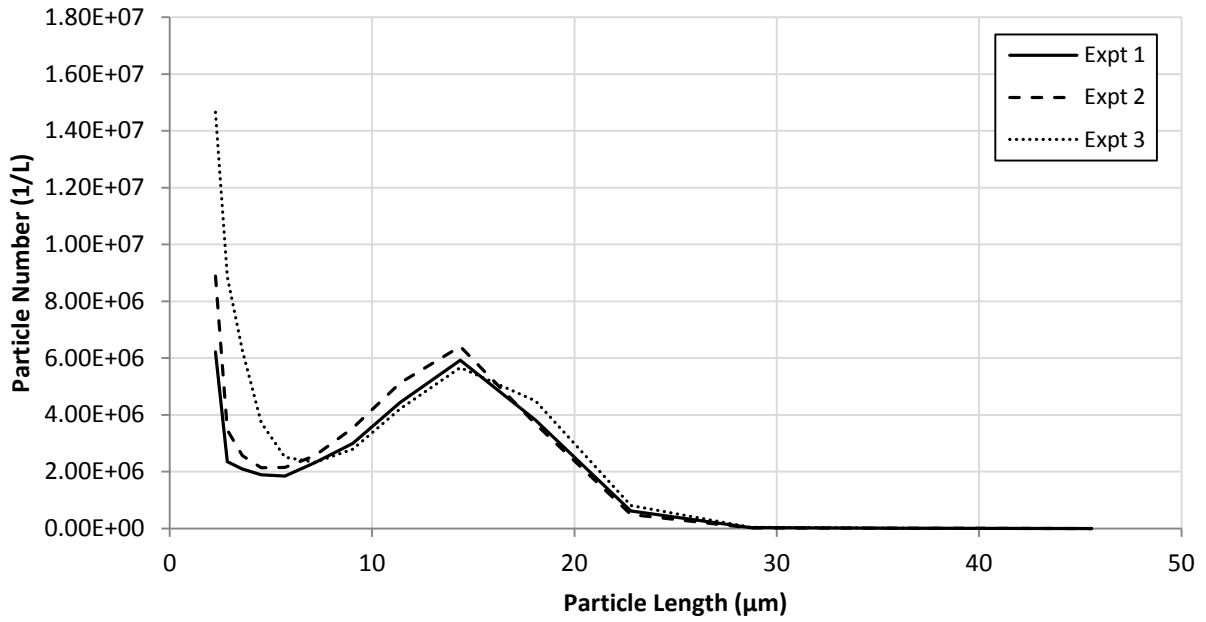


Figure 6.10: The PSD of three samples taken after 20 minutes.

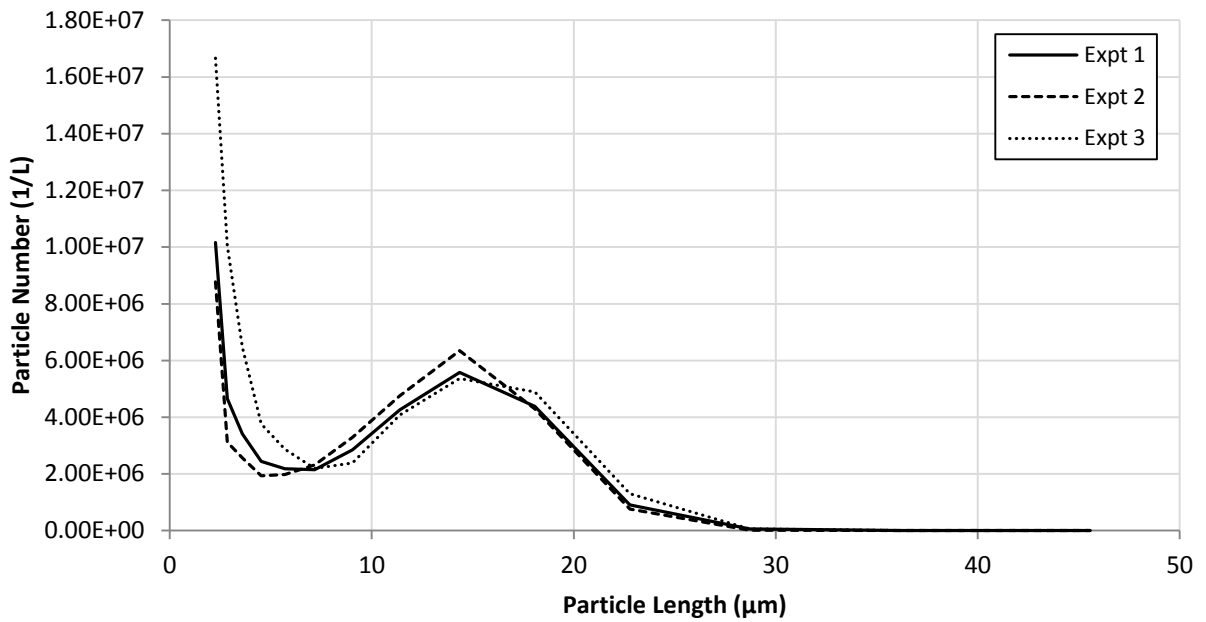


Figure 6.11: The PSD of three samples taken after 35 minutes.

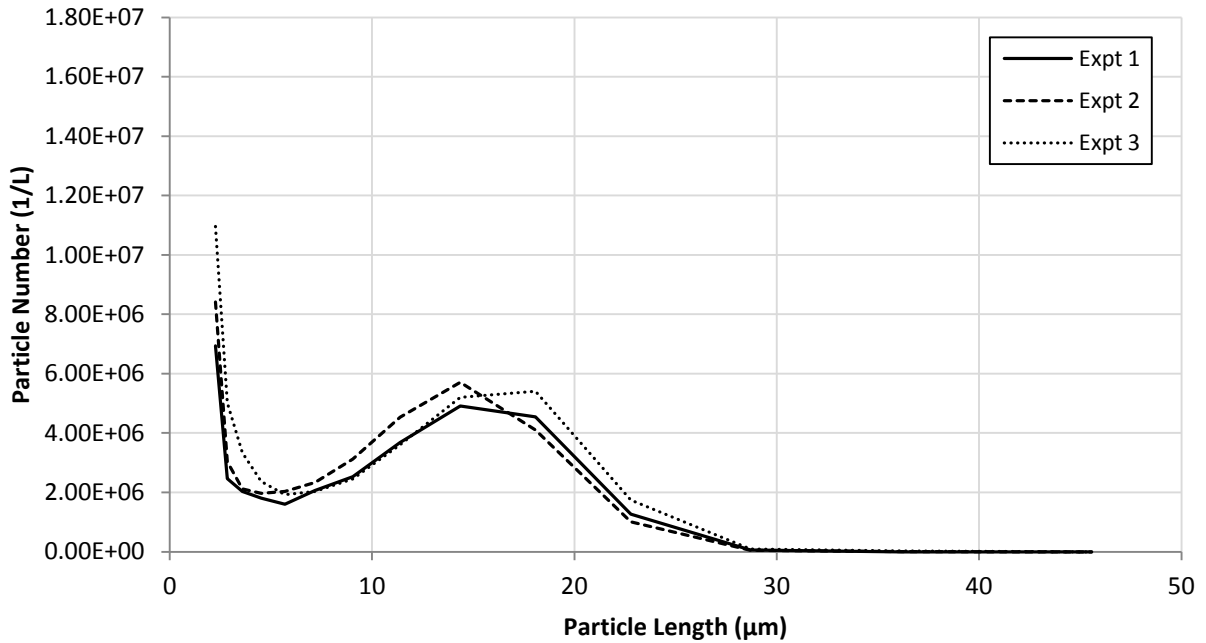


Figure 6.12: The PSD of three samples taken after 60 minutes.

It can be seen in Figure 6.8 to Figure 6.12 that the procedure is highly repeatable given the techniques used for sampling and sizing. This suggests that the sampling procedure developed is consistent across all experiments.

6.4.5 Total Magnesium Concentration

The results from the ICP-AES analysis for total magnesium concentration are shown in Figure 6.13. It can be seen that the rate of consumption of magnesium for the higher initial saturation index condition is much greater than the lower *SI* condition which is expected.

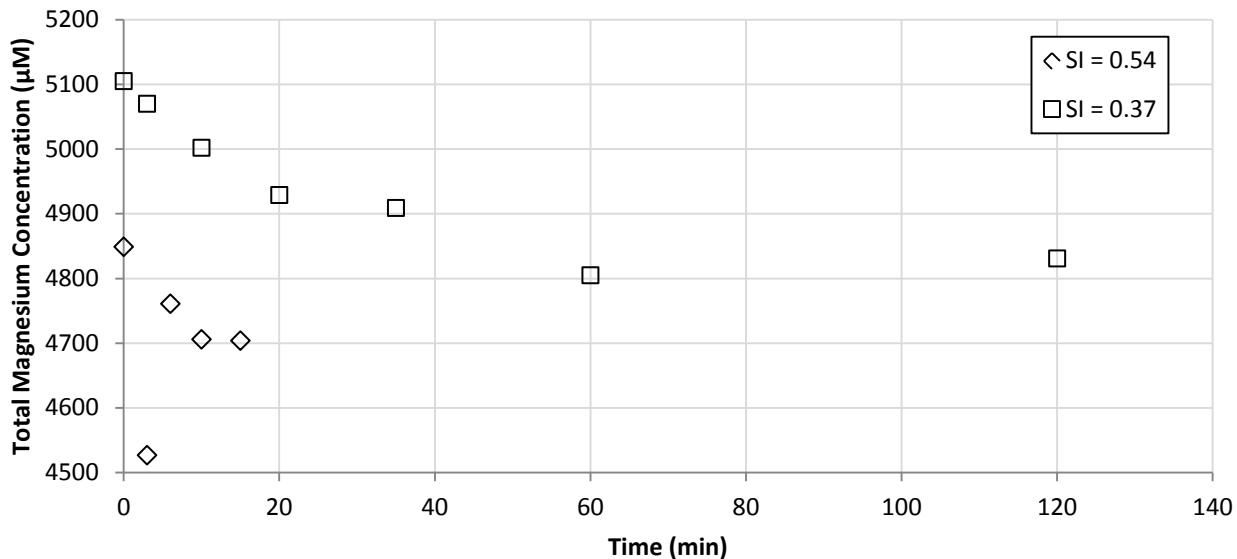


Figure 6.13: Total magnesium concentration through batch time for two initial saturation indices using ICP-AES.

6.4.6 Preliminary analysis of the PSD data

The number-size PSDs generated in this work demonstrate the presence of nucleation through the increase in the number of smaller sized crystals with time and also aggregation by the decrease in number of the peak of the distribution. Figure 6.14 shows the zeroth moment in the measurable size domain, a decrease of total numbers from the original number of seed crystals is seen which is evidence that more particles are aggregating than are entering the lower limit of the aperture. The final data point in Figure 6.14 shows an increase in numbers, which could be due to nucleation dominating aggregation or, possibly, uncertainty in the experimental results.

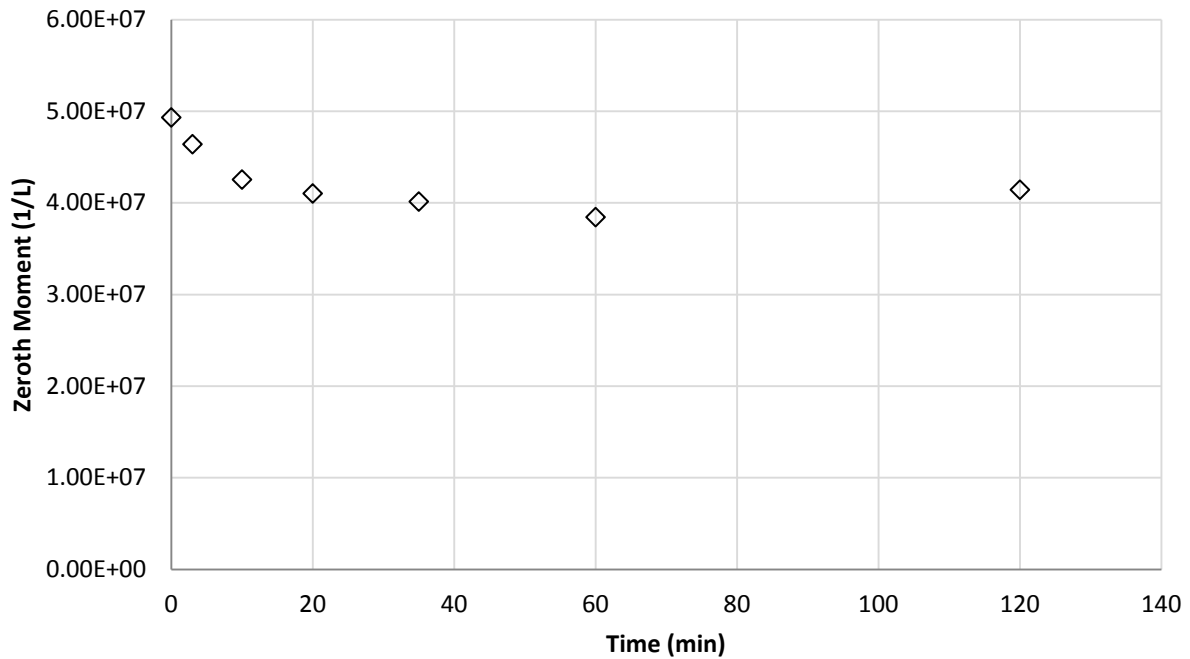


Figure 6.14: Zeroth moment in the measurable size domain during an experiment with an initial $SI = 0.37$.

Figure 6.15 shows the third moment increasing with time. This is expected as crystal growth will always increase the total crystal volume until the thermodynamic limit is reached.

These experimental results provide quantitative evidence that the three mechanisms proposed to describe struvite crystallisation are appropriate. This is further supported by the qualitative micrographs that abound in the literature. Kinetic parameters for these mechanisms can now be estimated using the process model and the parameter estimation functionality of gPROMS.

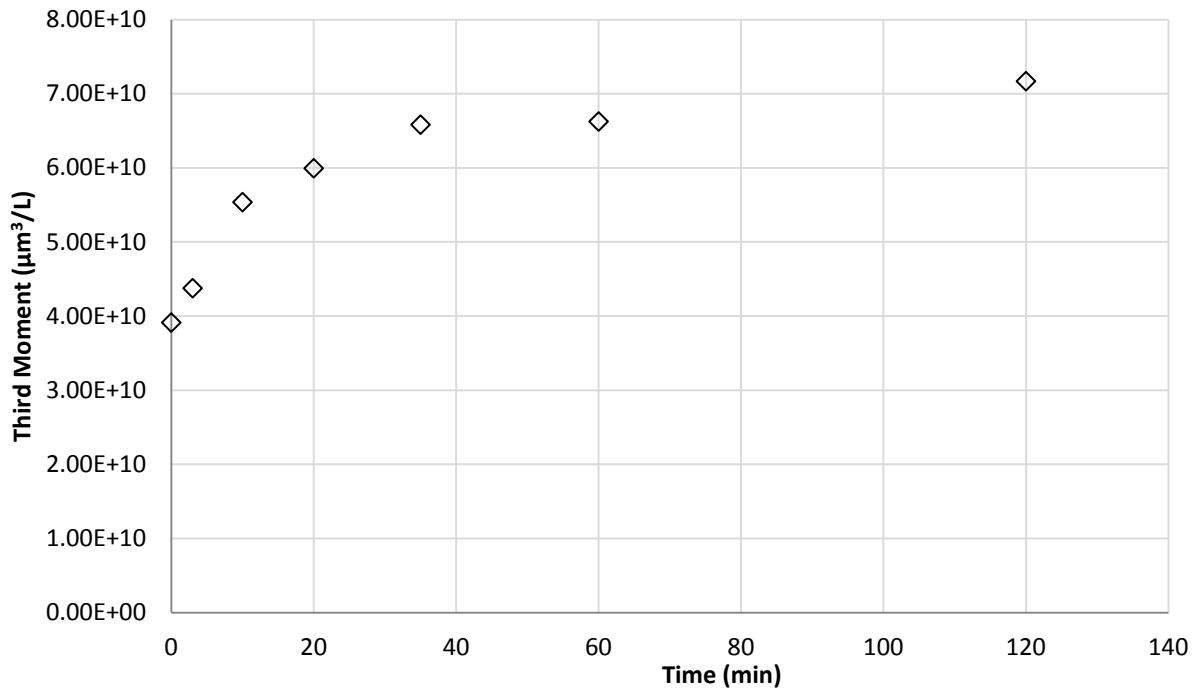


Figure 6.15: Third moment as measured during an experiment with an

6.5 Conclusions

The experimental methodology developed has satisfied the initial $SI = 0.37$ goals stated. The pH and PSD measurements have been demonstrated to be accurate and repeatable and the range of SI covered is as large as possible with the ESZ apparatus. The experimental procedure is repeatable and the results produced clearly demonstrate the phenomena of nucleation, growth and aggregation which are described with the process model.

6.6 Key Points from Chapter Six

- Experimental methodology was developed that satisfied the goals defined.
- Accurate and repeatable pH and PSD measurements were gathered using the methodology.

- Preliminary analysis of the results demonstrates the mechanisms of nucleation, growth and aggregation.

Chapter 7 - Parameter Estimation of Struvite Crystal Nucleation, Growth and Aggregation Kinetic Parameters

This chapter outlines the process used for parameter estimation in order to determine struvite nucleation, growth and aggregation kinetic parameters of the system. A universal set of kinetic parameters enabled the model to predict the pH and particle size distribution dynamic responses for all experiments that contributed to the ensemble data set employed in the regression analysis.

7.1 Introduction

In the previous chapter the methodology for the experiments used in this study were discussed and experimental evidence for the kinetic mechanisms used in the process model was apparent. This suggests that the approach used here for process modelling, at least to this point, is sound. To properly utilise the process model, the kinetic parameters employed must describe the rates of struvite crystallisation encountered in a real system. Prior to that, valid experimental data did not exist to determine these parameters, so approximations were used based on work done on other crystallisation systems (Hounslow, 1990, Bramley, 1994).

The experimental data generated with the procedure outlined in §6.3 were used with the process model developed in gPROMS to utilise its parameter estimation functionality (gPROMS, 2004). This calculates a

set of parameters that minimises the weighted differences between the experimental data and the corresponding model predictions.

7.2 Background to Parameter Estimation

In order to determine parametric values a number of experiments can be conducted and used to estimate parameters from known measurements. The gPROMS parameter estimation functionality aims to determine the value of the unknown parameters in order to maximise the probability that the model will predict the experimental values (gPROMS, 2004). A summary of the unknown parameters to be estimated and the process variables that were measured are given in Table 7.1.

Table 7.1: Summary of unknown parameters to be estimated and experimentally measured variables.

Unknown Model Parameters	Measured Process Variables
k_{β} : Aggregation kernel coefficient	PSD: Particle size distribution pH : Solution pH C_{Mg}^T : Total magnesium concentration*
n_{β} : Aggregation kernel order	
k_G : Crystal growth rate coefficient	
n_G : Crystal growth rate order	
k_B : Nucleation rate coefficient	
n_B : Nucleation rate order	

*Note: Not all experiments have C_{Mg}^T data

The estimation goal of maximizing the probability that the model will predict the experimental measurements is achieved by minimizing the objective function, Φ , given by Equation 7.1.

$$\Phi = \frac{NU}{2} \ln(2\pi) + \frac{1}{2} \min_{\theta} \left\{ \sum_{i=1}^{NE} \sum_{j=1}^{NV_i} \sum_{k=1}^{NM_{ij}} \left[\ln(\sigma_{ijk}^2) + \frac{(\tilde{z}_{ijk} - z_{ijk})^2}{\sigma_{ijk}^2} \right] \right\} \quad 7.1$$

Where,

- NU Total number of measurement taken during all the experiments
- θ Set of model parameters to be estimated. The acceptable values may be subject to given lower and upper bounds, *i.e.* $\theta_L < \theta < \theta_U$
- NE Number of experiments performed
- NV_i Number of variables measured in the i^{th} experiment
- NM_{ij} Number of measurements of the j^{th} variable in the i^{th} experiment
- σ_{ijk}^2 Variance of the k^{th} measurement of the j^{th} variable in the i^{th} experiment
- \tilde{z}_{ijk} k^{th} measured value of the j^{th} variable in the i^{th} experiment
- z_{ijk} k^{th} model-predicted value of the j^{th} variable in the i^{th} experiment

The maximum likelihood objective function (Equation 7.1) allows for a number of variance models describing the experimental measurements, such as constant variance, constant relative variance and heteroscedastic variance. All experimental measurements for this work were given a constant variance model, because it is the simplest variance model and there was no experimental evidence to suggest one of the other more complex variance models would be better suited to the data and therefore the estimation. The variance values used for each measured variable are given in Table 7.2.

Table 7.2: Constant variance models used for the measured variables in the parameter estimation

Measured Variable	Constant Variance
pH	0.05
C_{TMg}	100 (μM^2)
N_i	10000 ($1/L^2$)

The chosen pH variance was based on the uncertainty of the pH 10 buffer solution used to calibrate the pH probe. The magnesium variance is based on two standard deviations of the concentration measurements as reported by the university's advanced analytical centre. The particle number variance was originally based on replicate measurements of the same sample in the ESZ sizer. This led to a constant relative variance of 10% but this proved to be too generous and the estimations were poor. A constant variance model was evaluated and the value of 10000 was settled upon because it was largest value of variance that constrained the estimation process enough to work effectively. It is understood that this is an unrealistic value, as demonstrated by the experimental PSDs in §6.4.4. However, the goal of this work is to produce estimates for kinetic parameters and so long as the estimates result in a reasonable fit against measurement this approach is justified.

7.3 Limitations to the Parameter Estimation

As stated in §6.3.5 the data were collected over two experimental conditions based on two different initial saturation indices. This approach was taken to maximise the range of saturation index over which data could be obtained. Additionally, one result from an experiment attempted at the $SI = 0.74$ initial condition was incorporated into the estimation. While there are no PSD data for this condition, due to aperture blockages (see §6.3.4) there is known initial seed PSD and some pH measurements. This is used to broaden the region of supersaturation that the parameters are tested over.

7.3.1 Choice of L_1 used in Estimations

As discussed in §6.3.4 the experimental measurements of particle size have a detection limit of $2 \mu m$. However, using an L_1 of $2 \mu m$ in the mathematical model violates the assumption that $B_0^{Real} \approx B_0^{Model}$, as demonstrated in Figure 3.4. Therefore, L_1 must be chosen so that it satisfies the assumption made about nucleation rates and also maintains the experimental interval sizes used by the ESZ apparatus. The value used in §3.5.3 ($L_1 = 0.01 \mu m$) is an obvious choice, but does not maintain the experimental intervals when the geometric constant is applied. Consequently, $L_1 = 0.009843 \mu m$ is used considering it is the closest value to $0.01 \mu m$ that maintains the experimental interval sizes.

While changing the model L_1 from $2 \mu m$ to $0.009843 \mu m$ makes the assumption of $B_0^{Real} \approx B_0^{Model}$ justifiable, it does introduce another limitation to the estimation process. The numbers in the intervals less than $2 \mu m$ are unknown and therefore cannot be accurately described in the initial conditions. The initial number in each interval less than $2 \mu m$ is therefore set arbitrarily to $5 \times 10^6 1/L$. It is understood this is unrealistic, but there are not enough data to accurately extrapolate particle numbers below $2 \mu m$ and $5 \times 10^6 1/L$ is a reasonable guess based on the magnitudes of the other intervals. The importance of the sub $2 \mu m$ particles and the impact they have on model predictions is investigated later in §7.5.1.

7.3.2 Constraints on the Parameters

It was found that the constraints placed upon each parameter played an important role during the estimation procedure. If the upper and lower limits are too far apart, poor or failed estimations may result. However, if the constraints are too tight the parameter estimation functionality of gPROMS is not properly utilised. A series of preliminary estimations, using a trial and error method, was conducted before a final set of parameter constraints was found that could direct the estimation to a satisfactory outcome, while allowing gPROMS the freedom to evaluate a range of parameter combinations. Table 7.3 shows the parameter ranges employed for all estimations.

Table 7.3: Constraints placed upon the parameters to be estimated

Estimated Parameter	Initial Guess	Lower Limit	Upper Limit
k_{β}	$1.0 \times 10^{-7} L/min$	$1.0 \times 10^{-8} L/min$	$9.0 \times 10^{-6} L/min$
n_{β}	4.0	1.0	5.0
k_G	$1.0 \mu m/min$	$0.5 \mu m/min$	$15.0 \mu m/min$
n_G	2.0	1.0	6.0
k_B	$8.5 \times 10^7 1/L.min$	$1.0 \times 10^7 1/L.min$	$9.0 \times 10^8 1/L.min$
n_B	3.0	1.0	5.0

7.4 Parameter Estimation Results

Accepting the limitations and constraints presented above, a total of 13 experiments covering 3 different experimental conditions were combined into a single, ensemble data set used in the parameter estimation. This is a critical concept, since it brings a degree of confidence to the estimation that would not be possible if the estimation was performed with data from one experimental condition or even from just one experiment. This was demonstrated in the preliminary estimations carried out to determine the best initial guesses and limits for the unknown parameters. It was found parameters estimated with data from different experimental conditions did not agree. By collating the data into one ensemble set, parameters could be estimated across *all* experimental conditions tested to that point. Data can also be supplemented from additional experiments to further improve the estimates of the kinetic parameters. A conceptual diagram of how the data were incorporated into the gPROMS parameter estimation process is given in Figure 7.1.

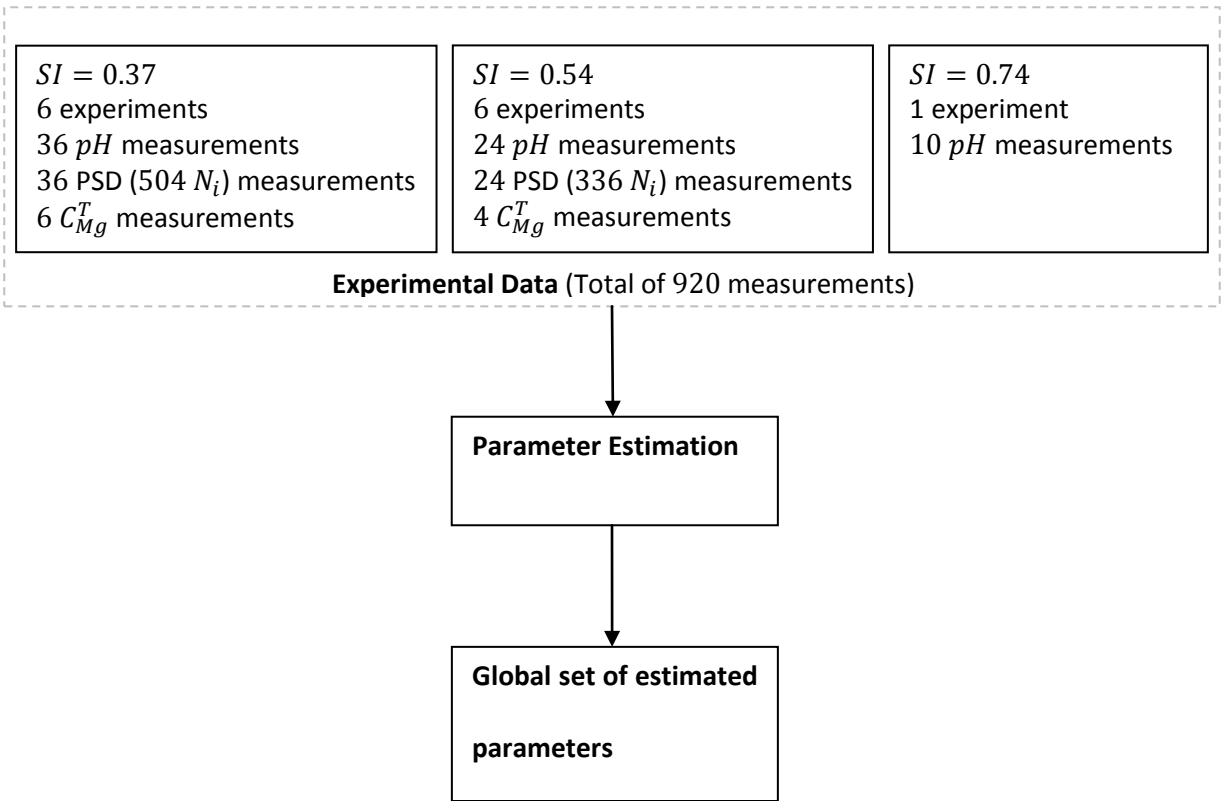


Figure 7.1: Conceptual diagram for the parameter estimation process in gPROMS.

With this in mind, the results of the parameter estimation are shown in Table 7.4. The parameters are reported with their 95% confidence interval as determined by gPROMS.

Table 7.4: Parameter estimation results from gPROMS reported with 95% confidence interval.

Mechanism	k_i	n_i
Aggregation	$(3.72 \pm 0.014) \times 10^{-7} \text{ L/min}$	5.26 ± 0.004
Crystal Growth	$12.49 \pm 0.061 \mu\text{m/min}$	5.06 ± 0.005
Nucleation	$(8.50 \pm 0.076) \times 10^7 \text{ 1/L.min}$	1.68 ± 0.014

Using the results from the parameter estimation, Equations 4.1, 4.2 and 4.5 can be rewritten as Equations 7.2, 7.3 and 7.4.

$$B = 8.50 \times 10^7 (SI)^{1.68} \quad 7.2$$

$$G = 12.49 (SI)^{5.06} \quad 7.3$$

$$\beta = 3.72 \times 10^{-7} (SI)^{5.26} \quad 7.4$$

The ability of these estimated parameters to agree with the experimental measurements is tested in the following sections. The nomenclature for naming the different experiments conducted is shown below in Table 7.5.

Table 7.5: Nomenclature for naming experiments.

<i>SI = 0.37</i>	<i>SI = 0.54</i>	<i>SI = 0.74</i>
29/09/10a	15/09/10	30/09/10
29/09/10b	23/09/10	
30/09/10	28/09/10	
19/10/10a	18/10/10a	
19/10/10b	18/10/10b	
26/10/10	26/10/10	

It should be noted that all experimental data were used in the parameter estimations. Subsets of these data were used to carry out validation checks, in order to give an ongoing assessment of the validity of the regressed parameters. Strictly, validations should be carried out with independent data sets. However, it was felt that this was at odds with the philosophy of the concept of determining a single set of parameters, based on an ensemble data set, which could, from time to time, be updated with new values.

7.4.1 Initial Saturation Index of 0.37

This section contains the results of the parameter estimation for experiments having an initial saturation index of 0.37. It is impractical to show the results for all estimations. The measurements compared to model outputs using the estimated parameters in this section were gathered from the 29/09/10b experiment (see Appendix C - Raw Data).

The measurements used to assess the quality of the estimation are as follows:

- Particle size distribution
- pH
- Third moment
- Zeroth moment
- Average particle size
- Total magnesium concentration (where applicable)

It should be noted that the moments reported and average particle size only consider particles in the measurable size domain of the ESZ device, which spans 2% to 60% of the orifice diameter (*i.e.* 2 to 60 μm). This means that all particles smaller than 2 μm are neglected when the PSD is integrated to determine its moments and number-mean particle size.

The experimental uncertainty is the same as the variance reported in §7.2. For the moments and average particle size the experimental uncertainty is reported as $\pm 20\%$ of the measurement. Given the results from the three repeats reported in §6.4.2 this is considered reasonable. The PSD results are shown in Figure 7.2 to Figure 7.8. Note the seed PSD does not show the model prediction, since it was used as the assumed-known initial condition in the model.

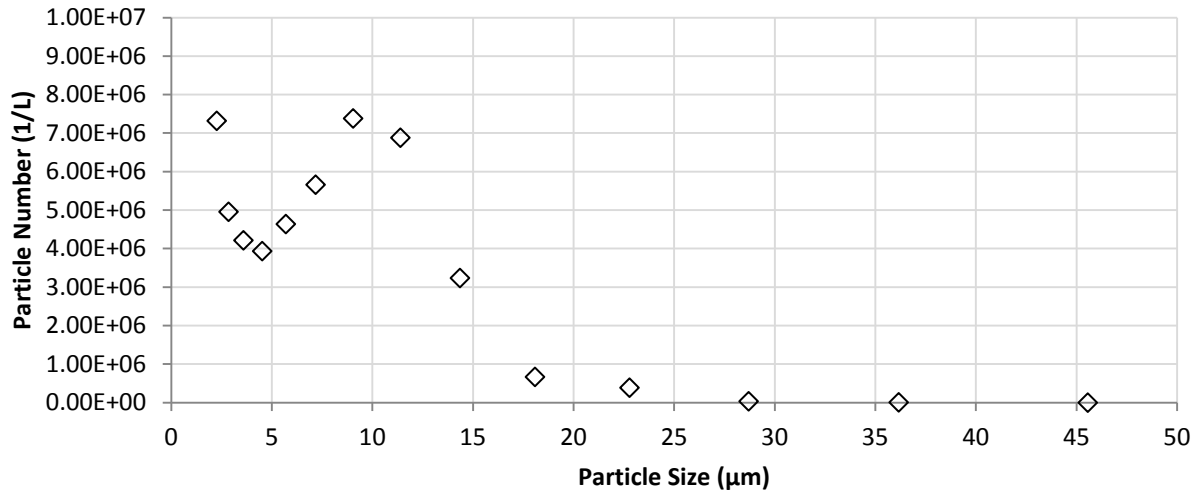


Figure 7.2: Seed particle size distribution from the 29/09/10b $SI = 0.37$ experiment.

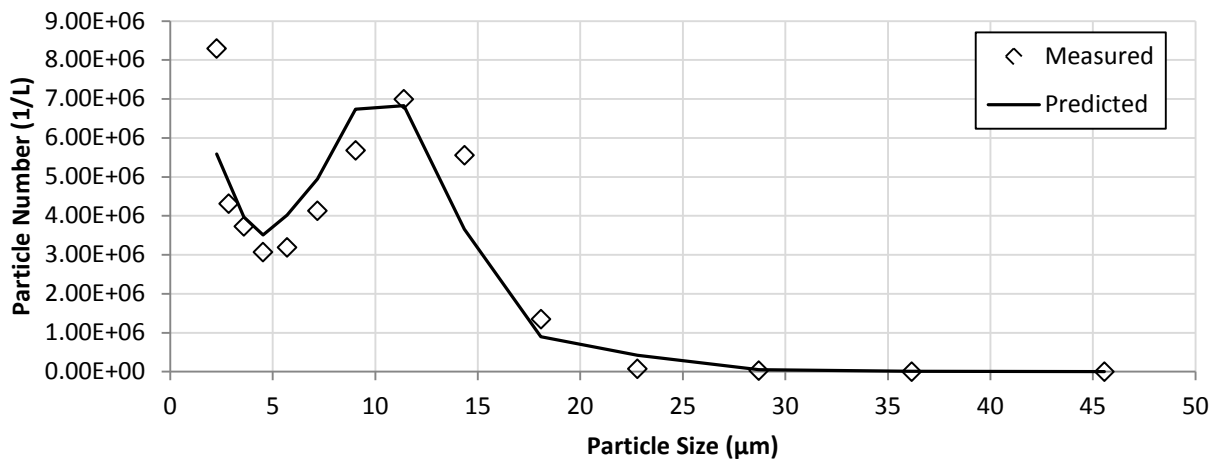


Figure 7.3: Measured and model-predicted particle size distribution at 3 minutes using the estimated parameters and data from the 29/09/10b $SI = 0.37$ experiment.

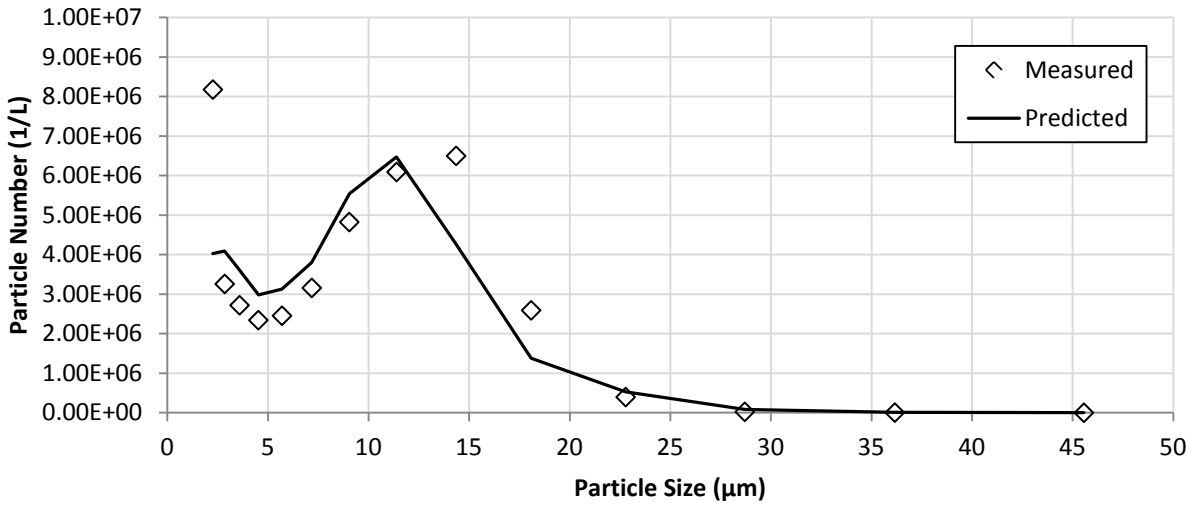


Figure 7.4: Measured and model-predicted particle size distribution at 10 minutes using the estimated parameters and data from the 29/09/10b $SI = 0.37$ experiment.

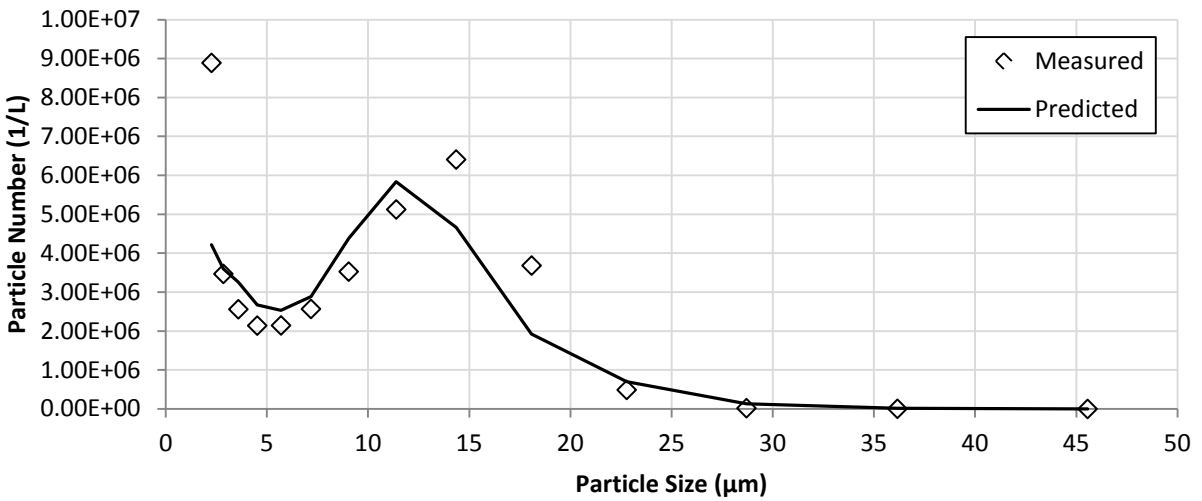


Figure 7.5: Measured and model-predicted particle size distribution at 20 minutes using the estimated parameters and data from the 29/09/10b $SI = 0.37$ experiment.

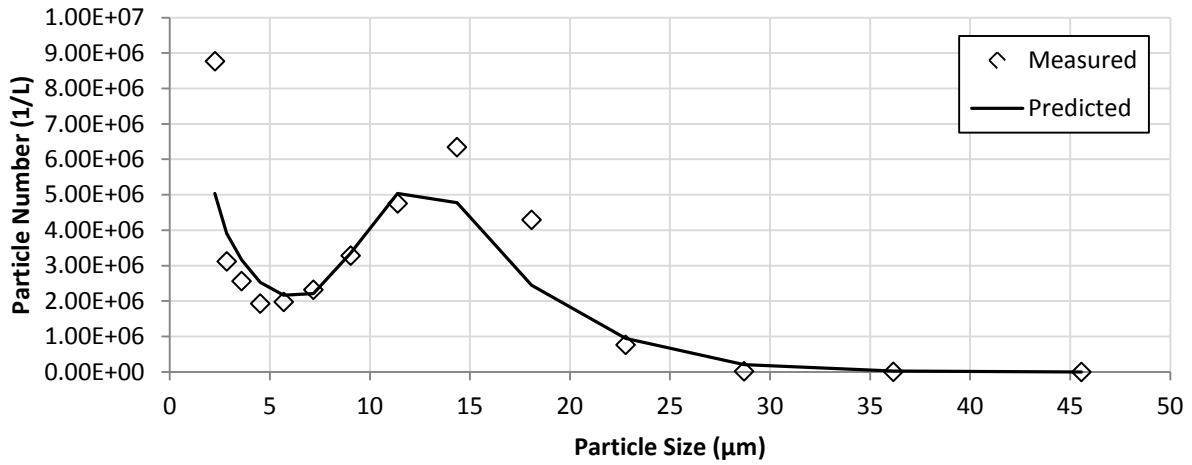


Figure 7.6: Measured and model-predicted particle size distribution at 35 minutes using the estimated parameters and data from the 29/09/10b $SI = 0.37$ experiment.

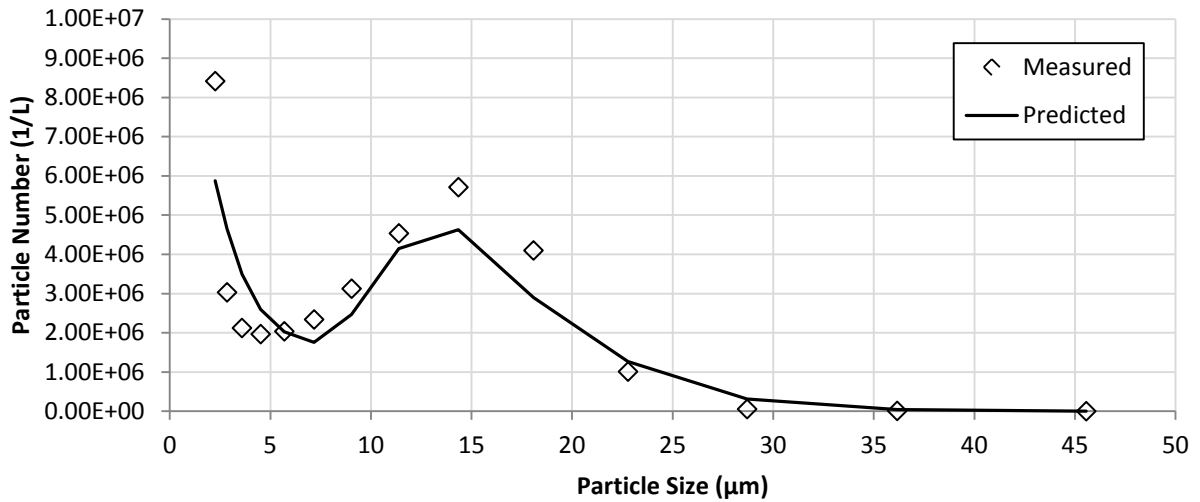


Figure 7.7: Measured and model-predicted particle size distribution at 60 minutes using the estimated parameters and data from the 29/09/10b $SI = 0.37$ experiment.

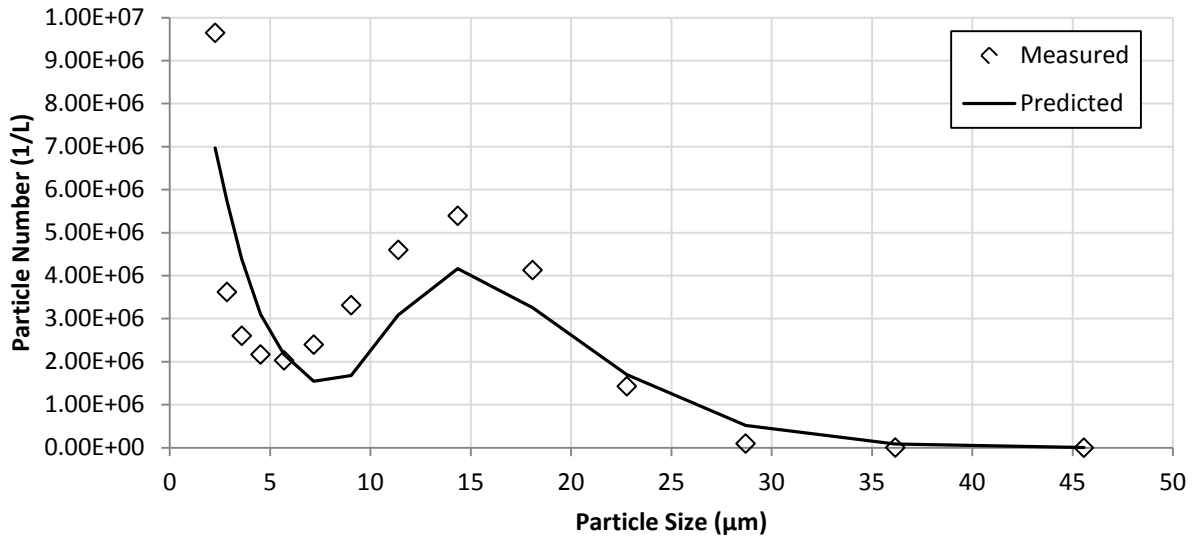


Figure 7.8: Measured and model-predicted particle size distribution at 120 minutes using the estimated parameters and data from the 29/09/10b $SI = 0.37$ experiment.

The measured and model-predicted pH results are shown in Figure 7.9.

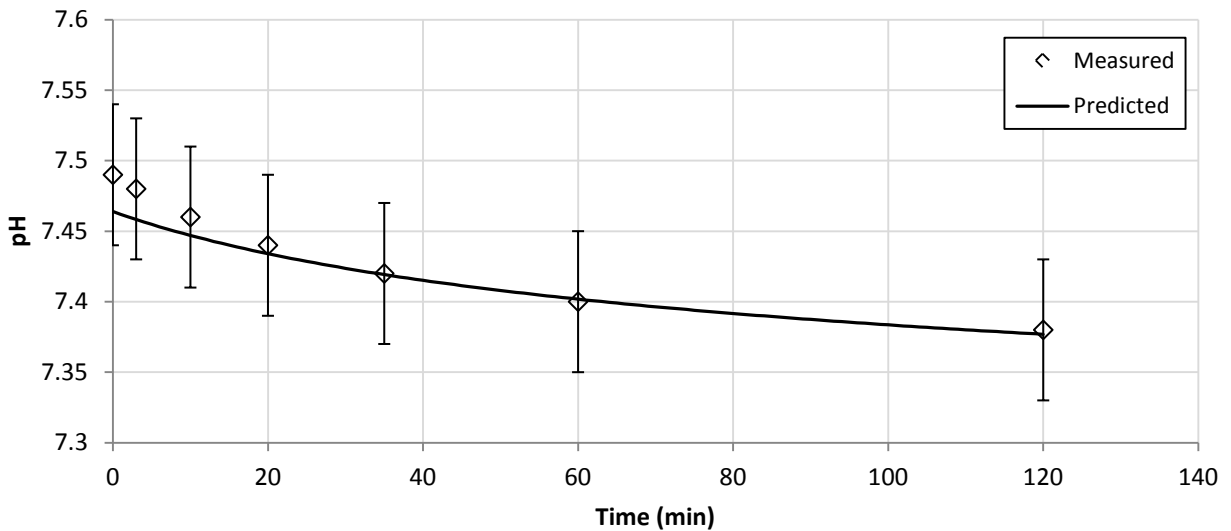


Figure 7.9: Measured and model-predicted pH over the course of the 29/09/10b $SI = 0.37$ experiment using the estimated parameters.

The measured and model-predicted third moment results over the measurable length domain are shown in Figure 7.10.

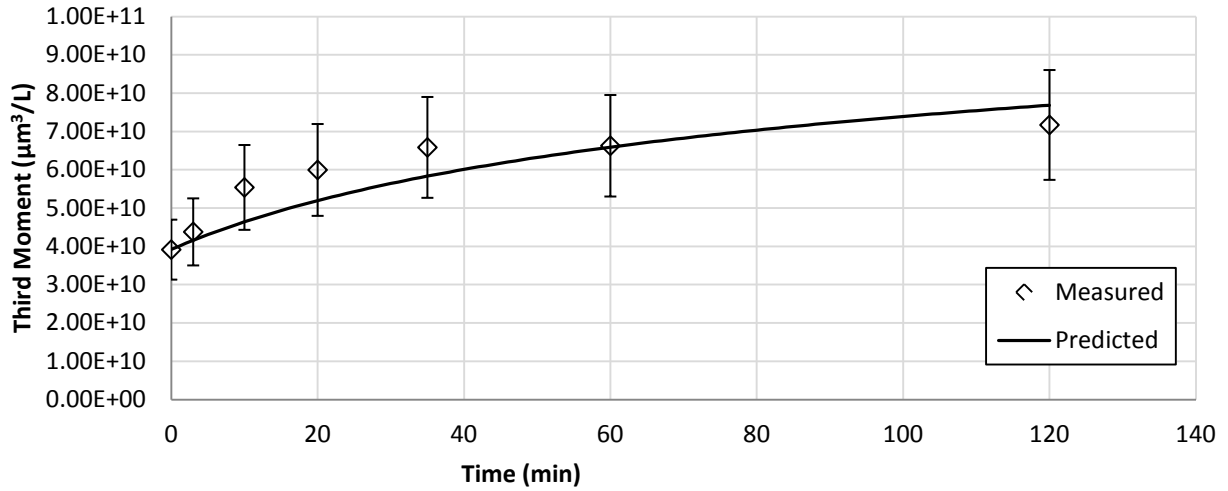


Figure 7.10: Measured and model-predicted third moment over the course of the 29/09/10b $SI = 0.37$ experiment using the estimated parameters.

The measured and model-predicted zeroth moment results over the measurable length domain are shown in Figure 7.11.

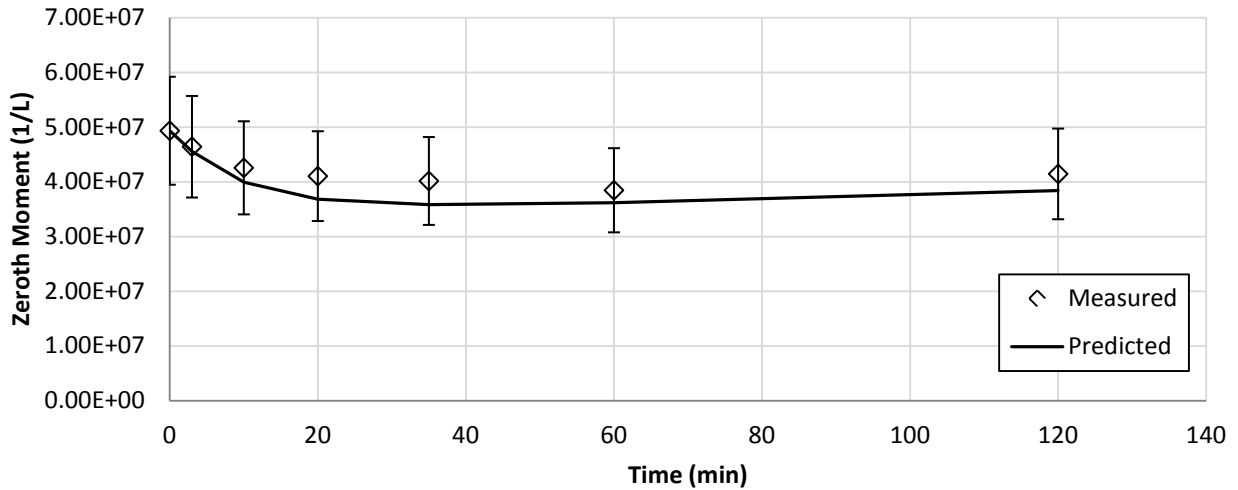


Figure 7.11: Measured and model-predicted zeroth moment over the course of the 29/09/10b $SI = 0.37$ experiment using the estimated parameters.

The measured and model-predicted average particle size results over the measurable length domain are shown in Figure 7.12.

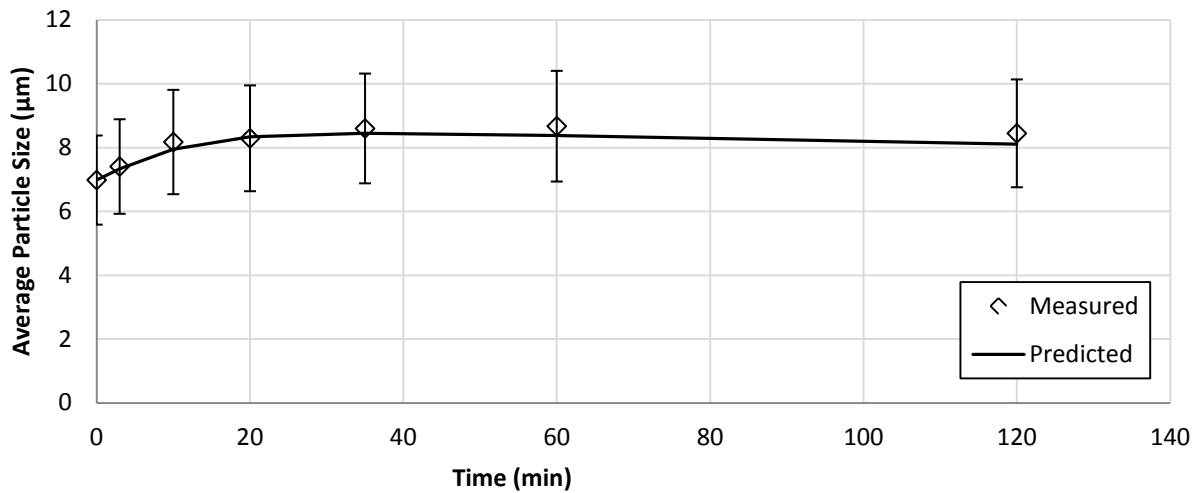


Figure 7.12: Measured and model-predicted average particle size over the course of the experiment using the 29/09/10b $SI = 0.37$ estimated parameters.

The 29/09/10b experiment used in the above plots does not have corresponding magnesium concentration data. In order to demonstrate the quality of the estimation with total magnesium concentration, measurements taken from the 26/10/10 experiment are compared to model prediction below in Figure 7.13.

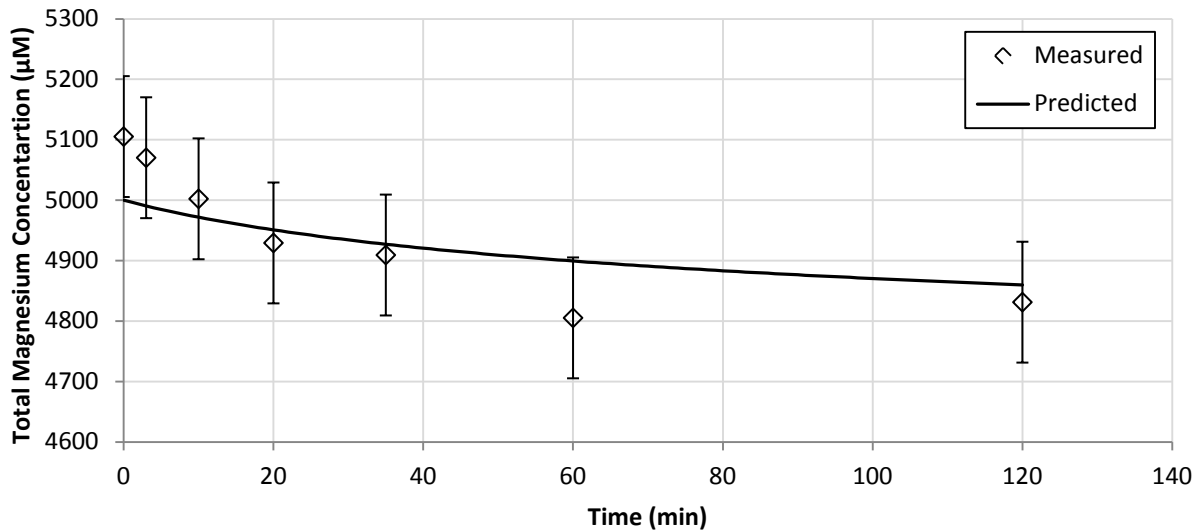


Figure 7.13: Measured and model-predicted total magnesium concentration over the course of the 26/10/10 $SI = 0.37$ experiment using the estimated parameters.

7.4.2 Initial Saturation Index of 0.54

This section contains all the parameter estimation results for experiments having an initial saturation index of 0.54. The results used here for comparison are from the 26/10/10 experiment (see Appendix C - Raw Data, not to be confused with the 26/10/10 experiment which used an initial saturation index of 0.37). The PSD results are shown below in Figure 7.14 to Figure 7.18.

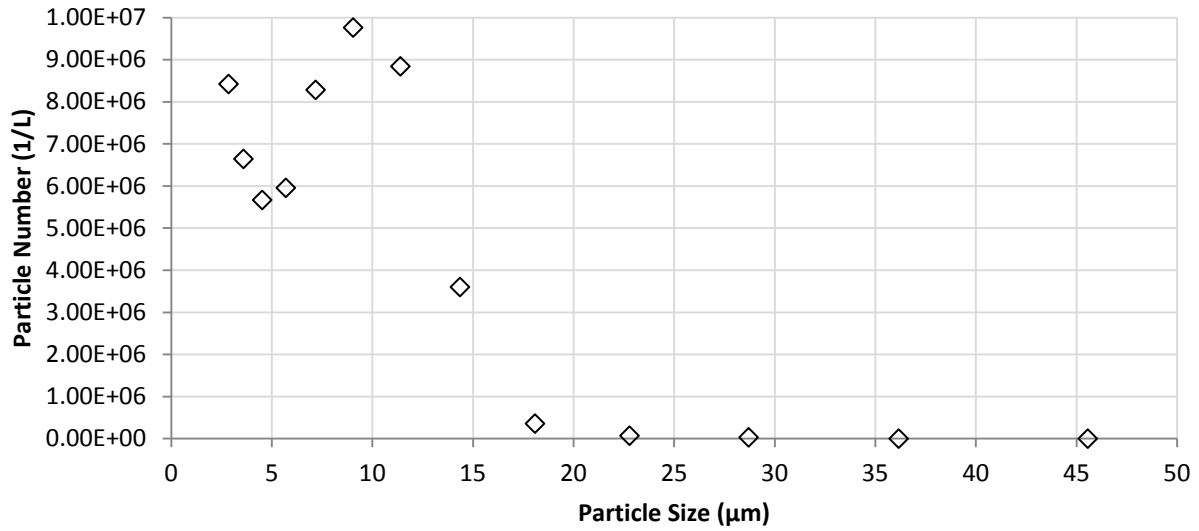


Figure 7.14: Seed particle size distribution from the 26/10/10 $SI = 0.54$ experiment.

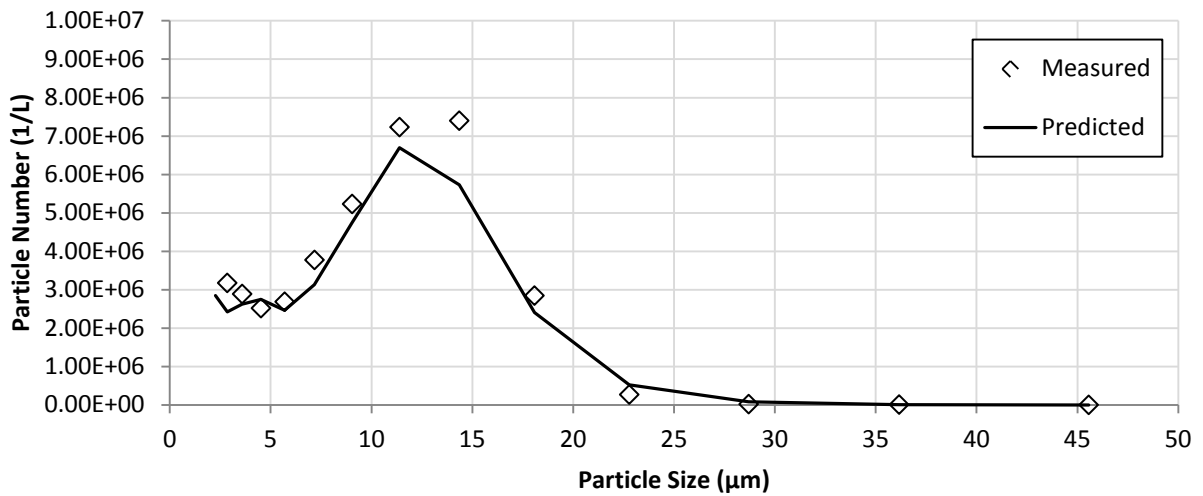


Figure 7.15: Measured and model-predicted particle size distribution at 3 minutes using the estimated parameters and data from the 26/10/10 $SI = 0.54$ experiment.

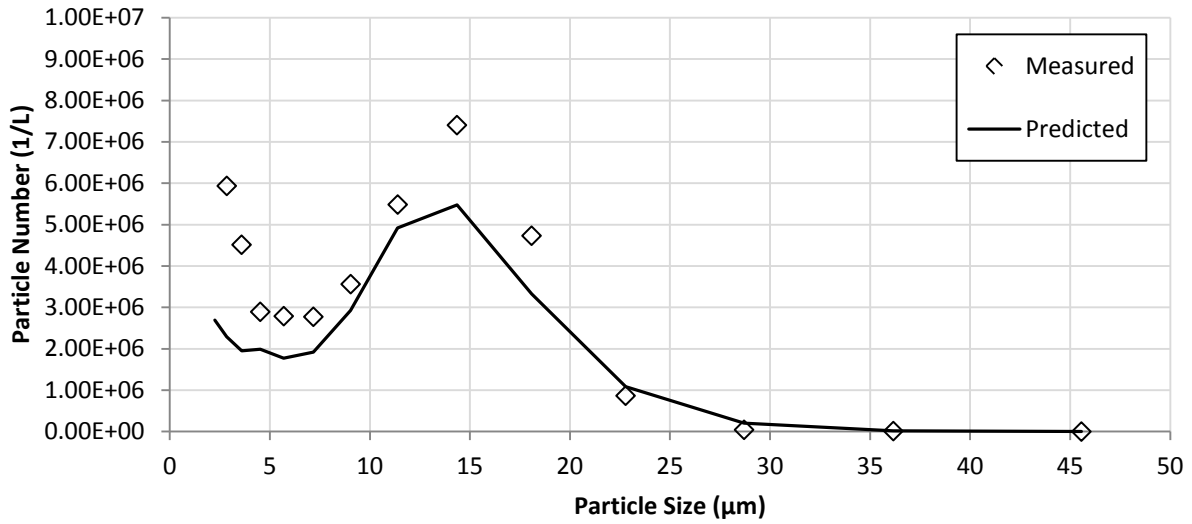


Figure 7.16: Measured and model-predicted particle size distribution at 6 minutes using the estimated parameters and data from the 26/10/10 $SI = 0.54$ experiment.

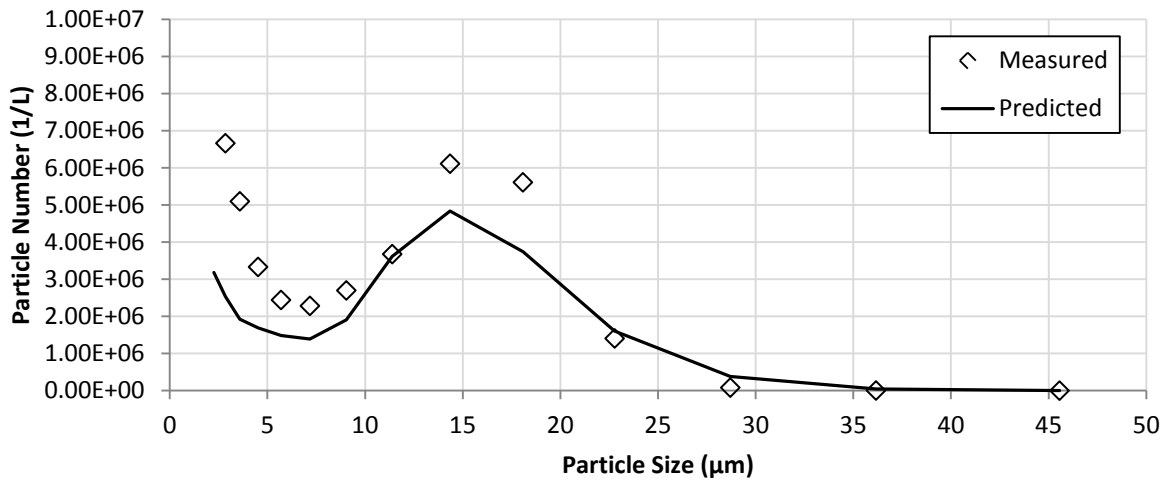


Figure 7.17: Measured and model-predicted particle size distribution at 10 minutes using the estimated parameters and data from the 26/10/10 $SI = 0.54$ experiment.

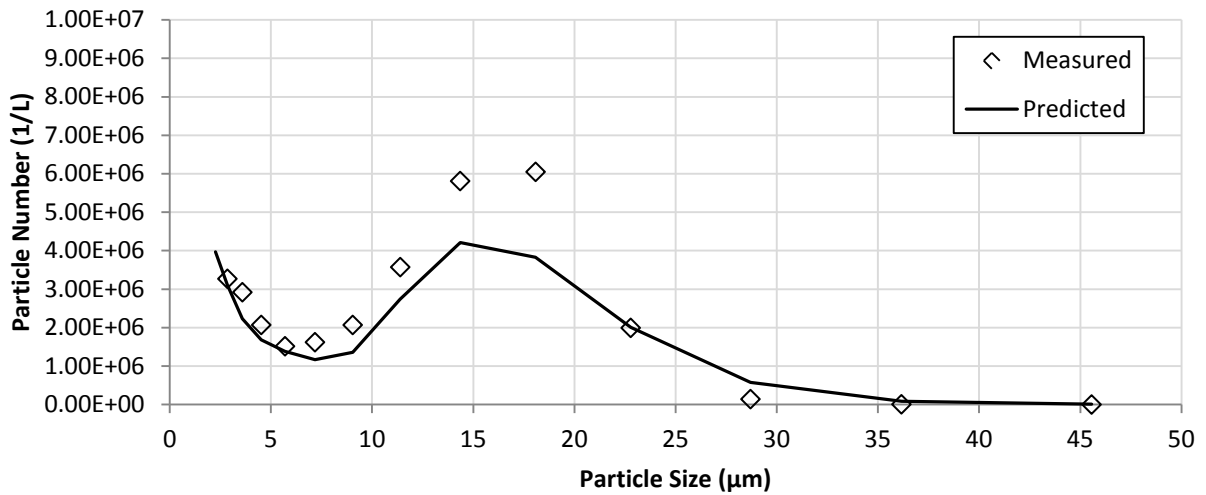


Figure 7.18: Measured and model-predicted particle size distribution at 15 minutes using the estimated parameters and data from the 26/10/10 $SI = 0.54$ experiment.

The measured and model-predicted pH results are shown in Figure 7.19.

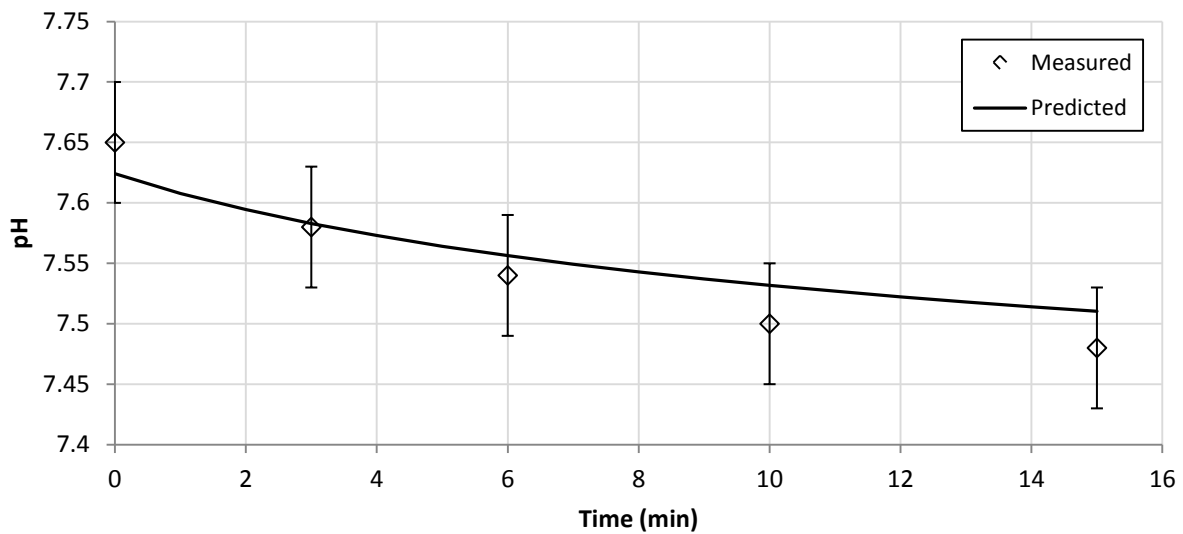


Figure 7.19: Measured and model-predicted pH over the course of the 26/10/10 $SI = 0.54$ experiment using the estimated parameters.

The measured and model-predicted third moment results over the measurable length domain are shown in Figure 7.20.

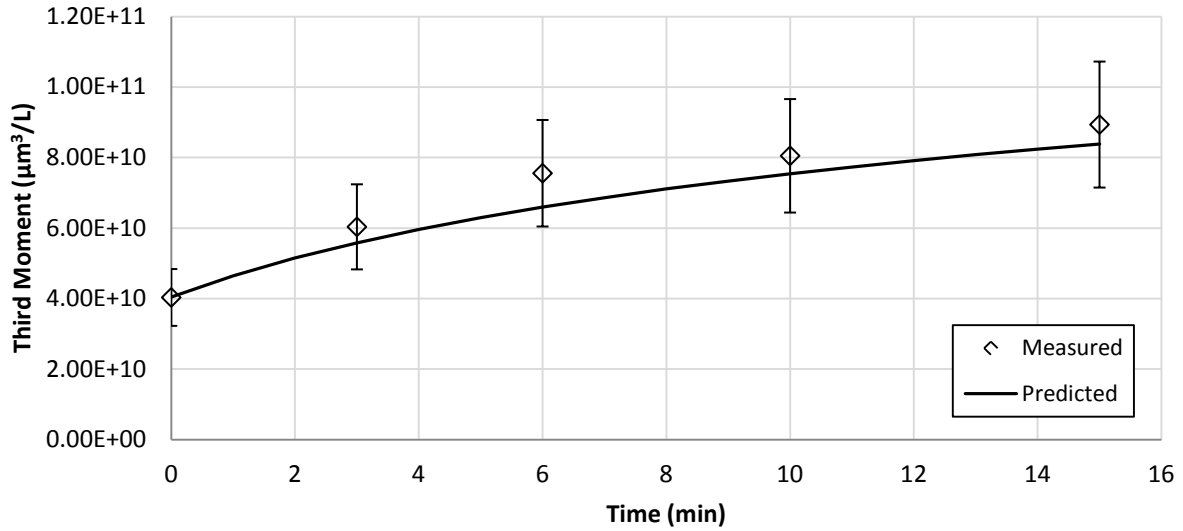


Figure 7.20: Measured and model-predicted third moment over the course of the 26/10/10 $SI = 0.54$ experiment using the estimated parameters.

The measured and model-predicted zeroth moment results over the measurable length domain are shown in Figure 7.21.

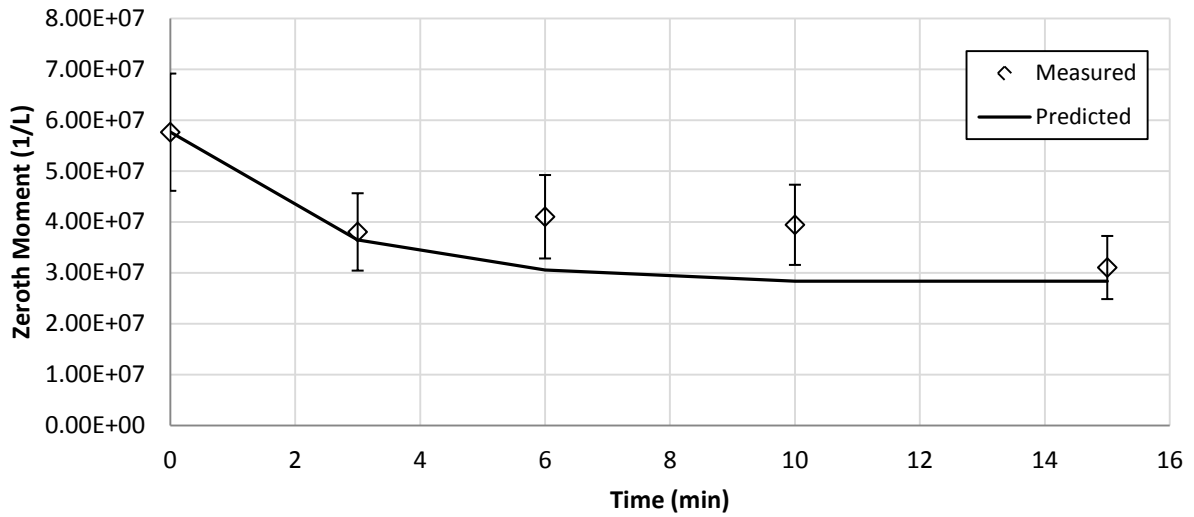


Figure 7.21: Measured and model-predicted zeroth moment over the course of the 26/10/10 $SI = 0.54$ experiment using the estimated parameters.

The measured and model-predicted average particle size results over the measurable length domain are shown in Figure 7.22.

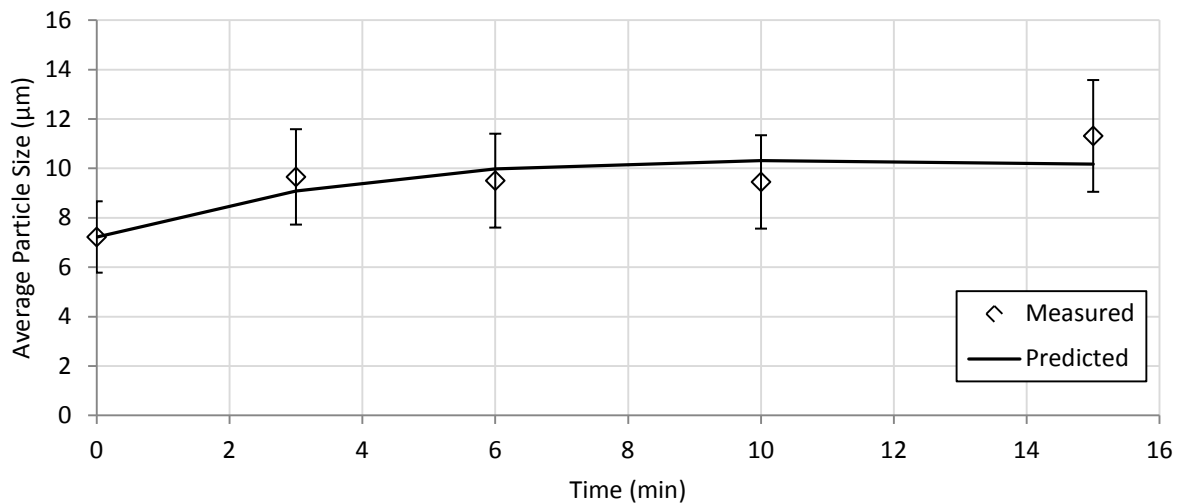


Figure 7.22: Measured and model-predicted average particle size over the course of the 26/10/10 $SI = 0.54$ experiment using the estimated parameters.

7.4.3 Initial Saturation Index of 0.74

This section contains the results of the parameter estimation for experiments having an initial saturation index of 0.74. There are no dynamic PSD measurements for the 0.74 saturation index condition as aperture blockage prevented this (§ 6.3.5). However, the initial PSD and pH data are sufficient to be used in the estimation. While there is no dynamic PSD data, satisfactory agreement of the pH response does increase the confidence in the estimated parameters showing their accuracy over a larger range of SI . This is demonstrated below in Figure 7.23. The data were obtained from the 30/09/10 experiment (see Appendix C - Raw Data).

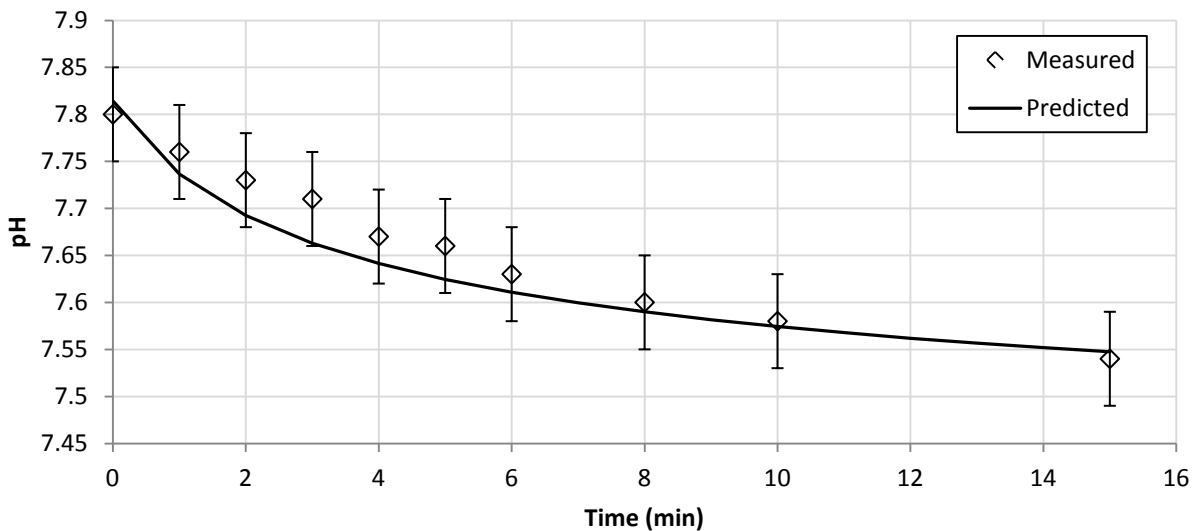


Figure 7.23: Measured and model-predicted pH over the course of the 30/09/10 $SI = 0.74$ experiment using the estimated parameters.

7.5 Discussion of Parameter Estimation Results

The parameter estimation proved successful in a number of areas. Firstly, the model-predicted pH response across the range of tested saturation indices is within experimental uncertainty. This is a key measurement, in addition to the particle size distribution, and provides confidence that the process

model has achieved mass-balance, since it couples the solution thermodynamics to the mechanism kinetics.

Secondly, the predictions of zeroth moment, third moment and average particle size are all within 20% experimental uncertainty, except for two data points in Figure 7.19. The zeroth moment result suggests that the nucleation rate and aggregation kernel being calculated from the kinetic parameters are reasonable over the range of conditions evaluated. However, the zeroth moment is perhaps not the best test for the accuracy of nucleation and aggregation kinetic parameters, since they might confound one another, when predicting the moments of the distribution. Nevertheless, this is an encouraging result.

The third moment result suggests that the model-predicted growth rates from the kinetic parameters are also reasonable. Furthermore, since the third moment is directly coupled to the mass balance (through density and volumetric shape factor), the agreement between measurements and predictions demonstrate that the model conserves mass to within 15%. This is an important result, since a process model that accurately predicts the particle size distribution, but fails to accurately predict crystal mass production rates, is of little use for process design. The average particle size (Equation 3.6) result is also satisfactory, which is important in describing the particulate product's characteristics.

Further to moments of the distribution, the particle size distribution model predictions themselves were successful. While the PSD peak is under predicted in every case, the shape of the model-predicted distribution is similar to the measured distribution. Additionally, over the range of experimental measurements the model is able to produce the tail of the peak below $2 \mu m$, the peak above $2 \mu m$ and the trough that connects them together. While the magnitude of numbers in many bins is outside 20-30% experimental error seen in §6.4.4 the position of these important features along the length domain is comparable. This is considered a positive result given the measurement technique employed and the notorious uncertainty incurred from sampling solids from dilute solutions.

However, it must be acknowledged that there are limitations of the model and estimation process. These are explored in the following sections.

7.5.1 Initial Size Distribution below the Limit of Detection

The most obvious limitation is the shape of the distribution of particles below the measurable limit of the ESZ sizer. These particles cannot be neglected, so assumptions must be made about their distribution. The parameter estimation work assumed a uniform distribution of 5×10^6 1/L below the detection limit of the ESZ device, which, in the face of no other information, seemed like an appropriate guess. The impact of this assumed initial distribution below the limit of detection must be explored. This was done by plotting the zeroth moment against time for different assumed uniform distributions below the limit of detection. The results from the 29/09/10b $SI = 0.37$ experiment is used to test the effect of differing initial distributions. The zeroth moment is tested against two different assumed distributions below $2 \mu m$; a) uniform distribution of 1×10^6 1/L and b) uniform distribution of 2×10^7 1/L. The results are shown in Figure 7.24.

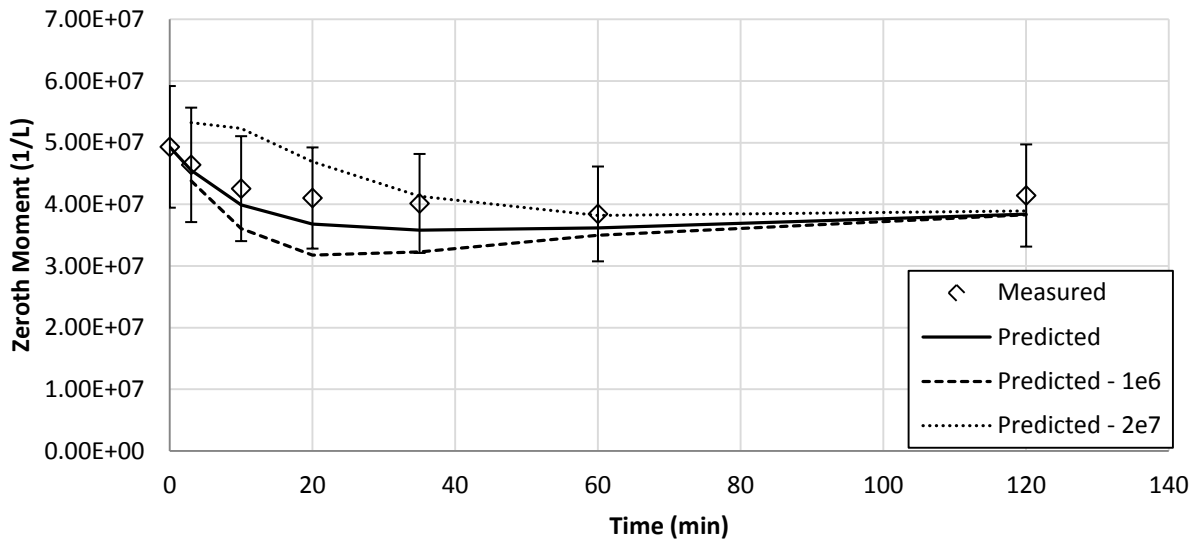


Figure 7.24: The zeroth moment determined with different initial distributions of sub two micron particles using the estimated parameters.

It can be seen that the initial distribution does have an impact on the zeroth moment but it is rather small considering the range of numbers tested. Over the range of 20% and 400% of the assumed value in the estimation the zeroth moment remains within 20% of the experimental values. The effect of the initial distribution is, not surprisingly, seen most starkly in the initial stages of the simulation, but ultimately converges as the system approaches equilibrium. However, if a new set of parameters were estimated using the other initial distributions it is possible the model would produce just as satisfactory agreement. To test this, the estimation process is repeated, using these different initial conditions, see Figure 7.25.

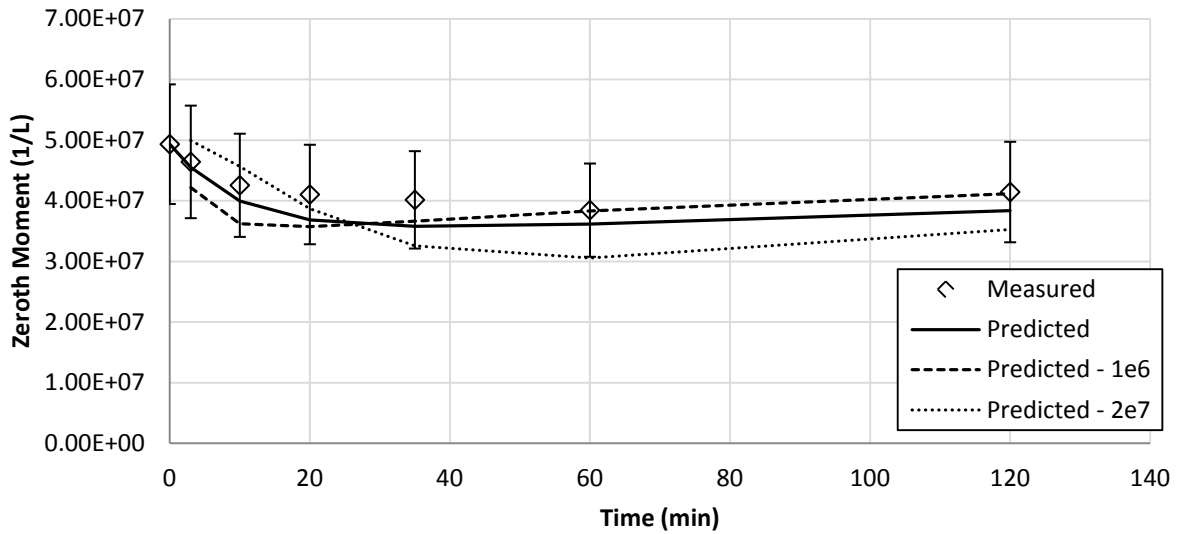


Figure 7.25: The zeroth moment determined with different initial distributions of sub two micron particles and repeated parameter estimation for each initial condition.

Figure 7.25 shows that by using the different initial distributions in the estimation, a set of different parameters cannot reproduce the same model-predicted results. This suggests there is a unique initial distribution that will provide the best agreement. However, the relative insensitivity of the zeroth moment over the measurable length domain suggests the choice of initial distribution below $2 \mu m$ is not critical to the estimation process. It can be seen that the original assumption of a $5 \times 10^6 1/L$ uniform distribution produces a reasonable agreement compared to the others. Given the insensitivity of the zeroth moment to this initial distribution, the improvement to the estimation that would be gained by optimizing the initial distribution is not justifiable. This conclusion is further supported when considering the impact of the initial distribution below the measurable limit on the mass balance (third moment) and pH response, because of their small size, see Figure 7.26 and Figure 7.27.

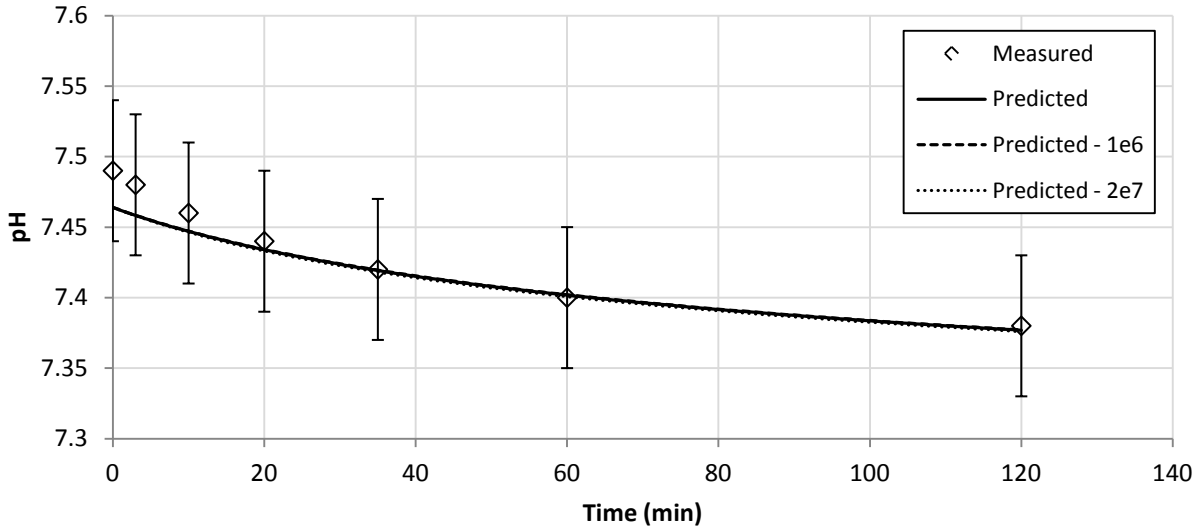


Figure 7.26: *pH* with the different initial distributions using the estimated parameters.

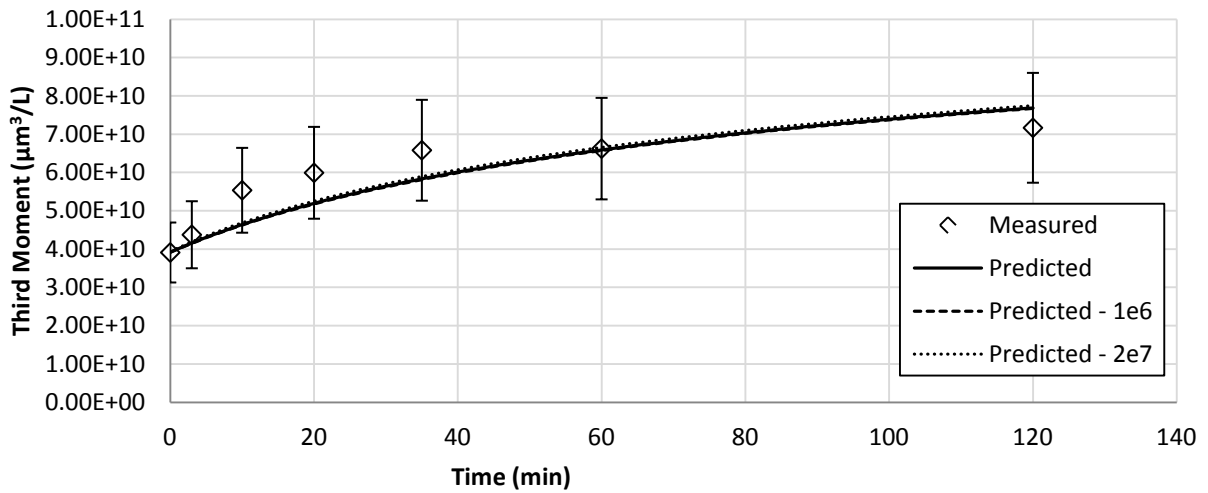


Figure 7.27: Third moment with the different initial conditions using the estimated parameters.

7.5.2 Nucleation Rate vs. Source Function

In discussing the issues with unknown distributions outside the limits of the experimental apparatus, a logical question is; “what did the other researchers who used the DPB do about it?” Simply, they did not try to determine a nucleation rate, rather contrived a source function, B_{μ} . The source function is defined

as the rate of appearance of particles in the first size interval from the region of the particle size domain smaller than the minimum detectable limit of the particle size analyser (Hartel and Randolph, 1986). In the case of Hounslow (1990), and the subsequent work of Illievski (1991) and Bramley (1994), a series of equations derived from the DPB were used to calculate the source function.

Hounslow (1990) found the source function decayed exponentially with time and used an empirical equation to calculate the source function, Equation 7.5. The work of Illievski (1991) and Bramley (1994) was primarily concerned with growth and aggregation rates so the source function was not significantly discussed.

$$B_u = A \exp \left[-\frac{t}{t_u} \right] \quad 7.5$$

The model developed as part of this work can be used to easily determine the source function for any interval. This is simply done by considering only those terms in Equations 3.21 and 4.9 that result in an increase the number of particles in the i^{th} interval, neglecting those terms that remove particles. In this way the validity of the empirical exponential source function can be tested. In Figure 7.28 the source function is determined for the interval that corresponds to the minimum detection limit of the ESZ particle sizer used at $2 \mu m$, and a regressed exponential function is superimposed.

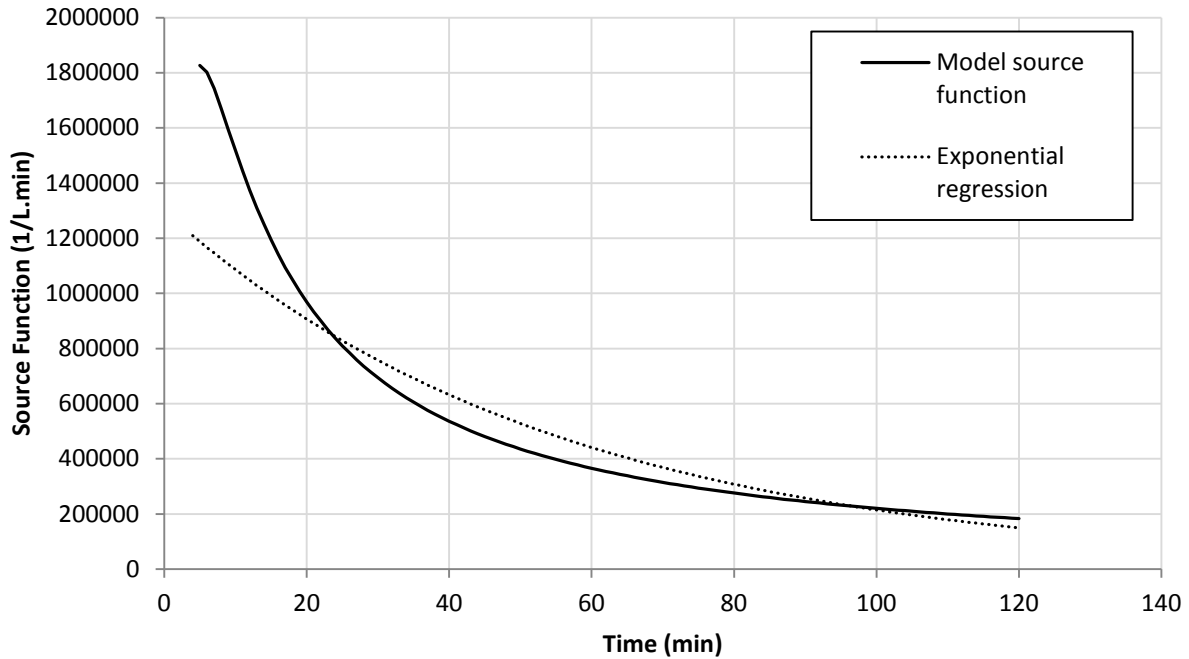


Figure 7.28: Source function for particles entering the discrete interval at $2\mu m$ as determined from the process model and the regressed exponential function.

The regressed equation has an R^2 value of 0.9359 and is given Equation 7.6.

$$B_u = 1.3 \times 10^6 \exp\left[-\frac{t}{55.56}\right] \quad 7.6$$

It can be seen that the exponential source function provides a reasonable approximation of particles entering the $2\mu m$ interval, but cannot match the shape of the source function as predicted by the full DPB model incorporating nucleation. It should be acknowledged that neither approach is without flaws. Equation 7.5 offers no potential to couple the source function to the system properties that drive it, namely supersaturation. The use of a nucleation rate means the estimated nucleation parameters cannot be properly validated with the experimental methodology used here, since the size domain over which nucleation is most significant cannot be measured. At best the experimental PSDs and zeroth moment can be used to suggest only that the nucleation rate and regressed parameters are not

unrealistic. While this is an important statement, the inability to properly validate the findings is a flaw in the method used for this research.

7.5.3 Nucleation

Even though the regressed nucleation parameters cannot be properly validated, they do not significantly affect the model fidelity with regards to pH and m_3 . In §5.4.3, stochastic simulations showed that the mass balance was not strongly dependent on the nucleation rate, owing to the small size of nuclei. This is especially true for the experimental methodology used to regress these parameters, since batch time/driving force is not sufficient to allow nuclei to grow to a size that significantly impacts the mass balance. This is demonstrated in the pH response, Figure 7.29, and the third moment response, Figure 7.30, by varying the estimated nucleation parameters by a factor of 10 in either direction. To maximise the effect when the nucleation rate coefficient is multiplied by 10 the order is divided by 10 and *vice versa*.

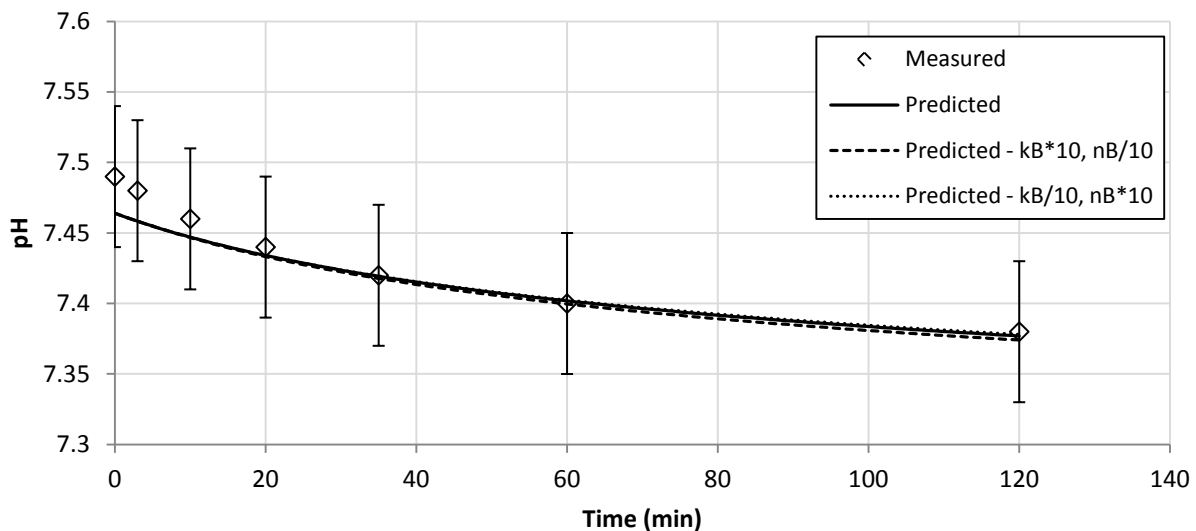


Figure 7.29: pH response for the estimated parameters compared to nucleation parameters that have been multiplied or divided by a factor of 10.

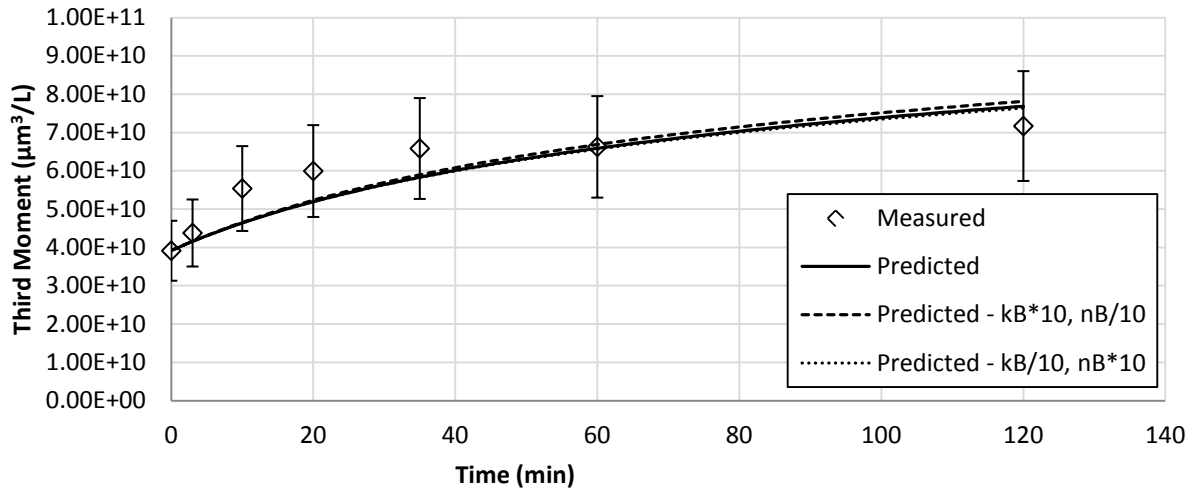


Figure 7.30: pH response for the estimated parameters compared to nucleation parameters that have been multiplied or divided by a factor of 10.

Figure 7.29 and Figure 7.30 show that the changes in nucleation kinetic parameters have almost no effect on the mass balance. That is not to say these parameters have no significance at all, as shown by plotting the PSD over the entire size domain, not just the measurable size domain. Figure 7.31 shows the PSD of a batch having an initial $SI = 0.37$ and the initial seed distribution of the 29/09/10b experiment after 120 minutes.

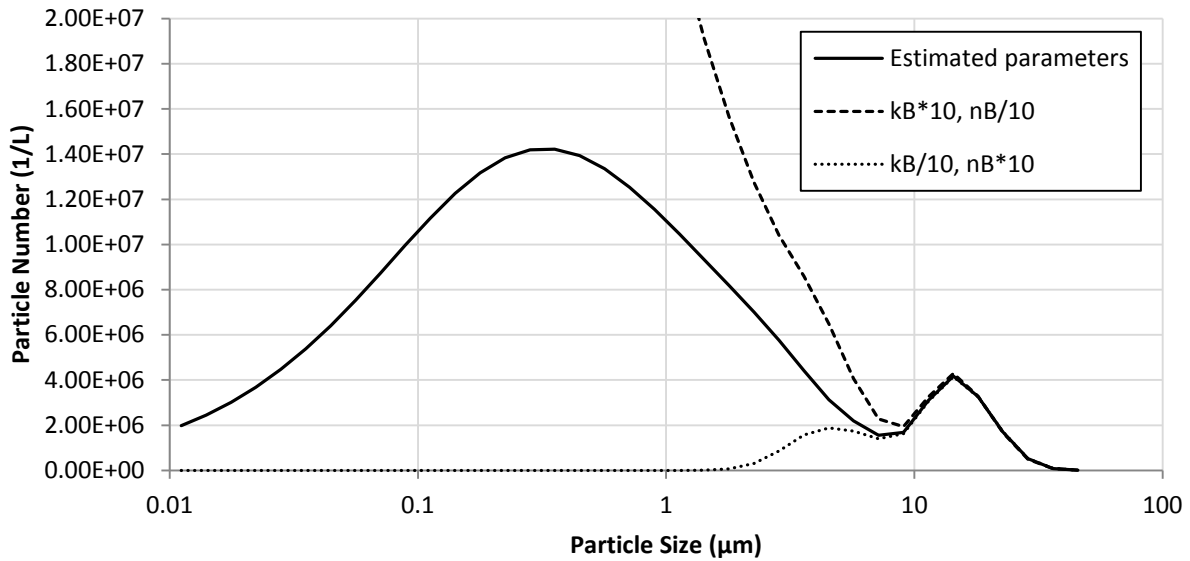


Figure 7.31: PSD over the whole size domain demonstrating the effect of multiplying or dividing the estimated nucleation parameters by a factor of 10.

It can be seen in Figure 7.31 that the numbers below $10 \mu\text{m}$ are vastly different, which is not unexpected. However, these particles are so small that their contribution to the mass balance, and therefore the third moment, is negligible, as demonstrated by Figure 7.29 and Figure 7.30. This suggests that nucleation could essentially be ignored in seeded batch reactors if the model was not concerned with the PSD and was used primarily to predict system pH and amount of struvite produced (*i.e.* mass balance information).

While it is true that the nucleation parameters are not significant for the experimental methodology used here, the effort taken to regress a true nucleation rate should not be understated. In the continuous operation of a struvite crystalliser, an exponential source function could not be used to replace the nucleation rate, since the source function has no capacity to feed a *steady-state* supply of particles into the PSD. Furthermore, a major goal of this work is to develop a modelling approach that could be used for process design, control and optimization. With that goal in mind, it is clearly better to

use an approach that employs the nucleation rate, instead of neglecting it or approximating it with a source function, since this ultimately enhances the model’s functionality.

7.5.4 Crystal Growth

The regressed crystal growth rate parameters were somewhat surprising, owing to the fifth order dependency on saturation index in the power law model. The BCF theory of crystal growth suggests that the growth order should be between second order (at low supersaturation) and first order (at high supersaturation) (Garside et al., 2002). This is supported by the work on struvite growth rates in the literature (Ali and Schneider, 2008, Harrison et al., 2011). However, these studies did not consider aggregation and, thus, a comparison between this work and theirs must consider the range of *SI* used to regress the parameters (see Table 7.6).

Table 7.6: Range of initial saturation indices covered by struvite crystal growth rate studies.

Study	Range of <i>SI</i>
This Work (2011)	0.75 – 0.25
Ali (2008)	0.57 – 0.32
Harrison (2011)	1.84 – 0.82

It can be seen in Table 7.6 that the work most comparable in terms of *SI* is that of Ali (2005). The experimental methodology of Ali (2008) used a constant *SI* and, thus, did not allow for de-supersaturation effects. The *SI* = 0.25 value cover in this work is based on the two-hour batch time for the *SI* =0.37 experiments and the estimated parameters.

One possible explanation for the fifth order regression is the possible existence of a “null supersaturation” or “dead zone”. The dead zone is said to occur at low levels of supersaturation where impurities block the step growth of kink sites (Nadarajah et al., 1995). This phenomenon has been seen

for lysozyme and calcium oxalate monohydrate (Nadarajah et al., 1995, Weaver et al., 2007). In order to make the modelled growth rate sufficiently low in the region of the perceived dead zone, the resultant growth rate order must be of high enough order to produce low growth rates at low SI values, but still be able to give reasonable growth at higher levels of SI . Since SI is less than one, higher orders imply lower growth rates within this region. Plotting the growth rate using the regressed parameters yields Figure 7.32.

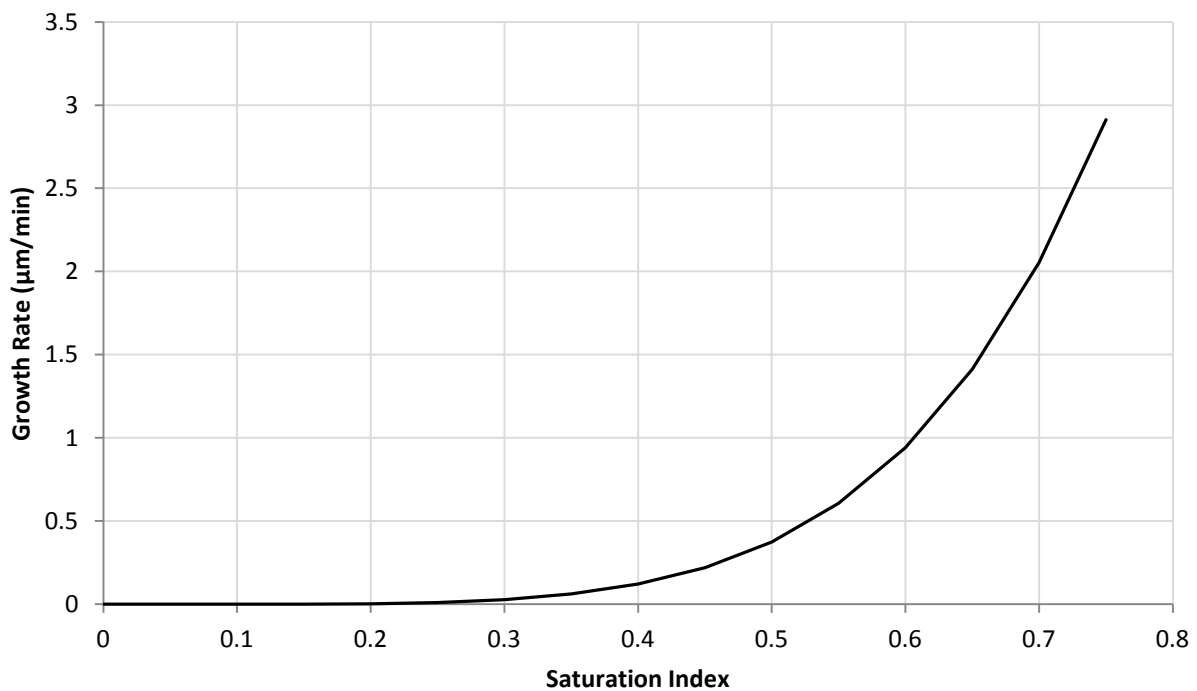


Figure 7.32: Growth rate versus saturation index based on the estimated parameters, $k_G = 12.49$ and $n_G = 5.06$.

Figure 7.30 shows that struvite appears to have a dead zone that could extend all the way to $SI = 0.3$, where crystal growth is, for all intents and purposes, zero. To test if the fifth order growth regression makes sense with respect to the BCF theory of crystal growth, a second-order approximation is considered where the growth rate is zero inside the dead zone and follows Equation 7.7 at higher values

of SI^* , the null saturation index. The results of this second-order approximation are shown in Figure 7.33.

$$G = k_G(SI - SI^*)^2$$

7.7

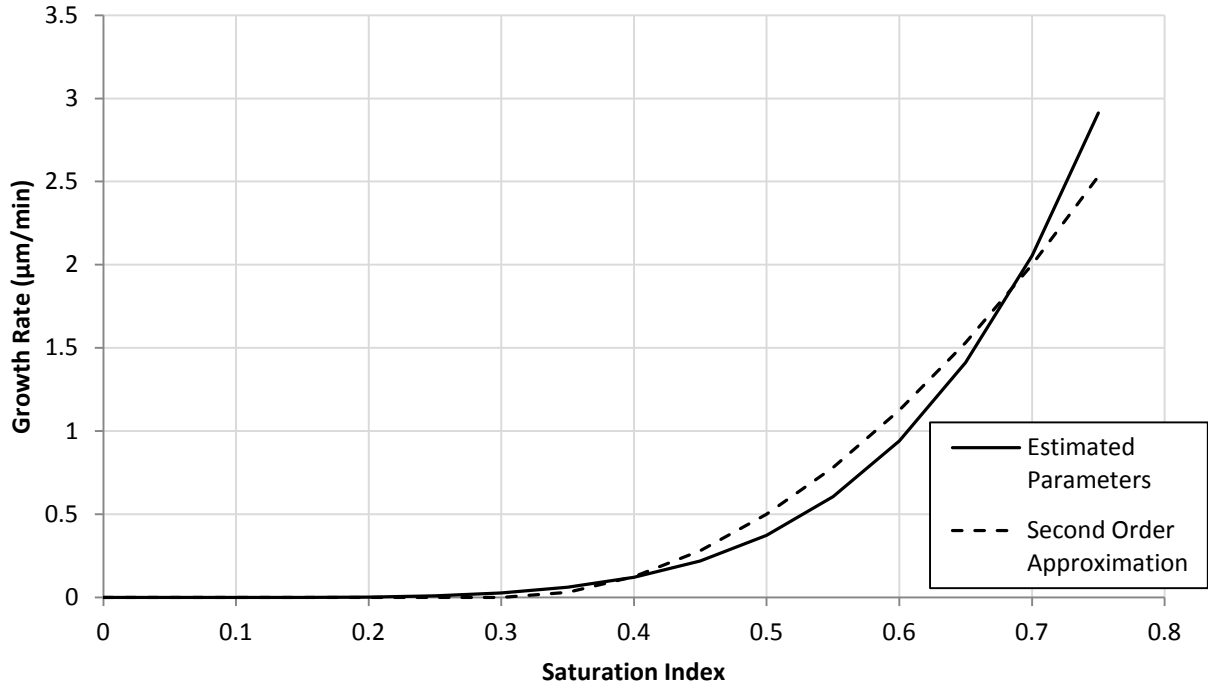


Figure 7.33: Growth rate versus saturation index using the estimated parameters and a second-order approximation

The value of k_G used in the second-order approximation is $12.5 \mu\text{m}/\text{min}$. It can be seen in Figure 7.33 that the second-order growth equation is a reasonable approximation to the growth equation using the estimated parameters, when employing the concept of the dead zone. This presents the possibility of incorporating a dead zone into the process model, employing a second-order growth in the parameter estimation.

While using a second-order growth equation and incorporating a dead zone adheres to the BCF model of crystal growth, it is concluded that keeping the estimated fifth order equation is better for running the

process model. The decision is based on the observation that a small amount of crystal growth was taking place within the dead zone, given observable changes in system pH , which implies that PO_4^{-3} was being converted to struvite.

7.5.5 Aggregation

There is no theoretical description of aggregation that suggests the order between the aggregation kernel and supersaturation. Therefore, comparisons to previous work that used the DPB approach to modelling aggregation were made. The order of aggregation encountered in this work is supported by the work of Ilievski (1991) who used a 4th order relationship between size independent aggregation and supersaturation, which represented 85% of the data within $\pm 70\%$ of the correlation. This relationship was based on a proposed size independent kernel for $Al(OH)_3$ (Halfon and Kaliaguine, 1976).

Furthermore, Bramley (1994) used the same relationship between size-independent aggregation kernel and supersaturation, regressing an order of 3.55. This is contrary to the linear relationship found by Hounslow (1990), but the range of supersaturation investigated in the case of Hounslow (1990) was much smaller. Therefore, the correlation of Bramley (1994) is considered more representative. The regressed order of estimation in this work was 5.26, similar to Ilievski (1991) and Bramley (1994).

Apart from aggregation order, it is important to consider the aggregation kernel coefficient. This was done by considering the range of aggregation kernel calculated using this work's estimated parameters and those by Ilievski (1991) and Bramley (1994). Table 7.7 shows the range of aggregation kernels in those cases.

Table 7.7: Range of aggregation kernels used in different studies using the DPB

Study	Range of aggregation kernel
<i>This work (2011)</i>	$10^{-8} - 10^{-10}$
<i>Bramley (1994)</i>	$10^{-9} - 10^{-11}$
<i>Ilievski (1991)</i>	$10^{-9} - 10^{-11}$

It can be seen in Table 7.7 that the range of aggregation kernels used in this work is comparable to those found in previous studies, further increasing the confidence in the estimated parameters.

7.5.6 Correlation of parameters

The gPROMS parameter estimation process generates a correlation matrix that quantifies correlations between all regressed parameters, shown in Table 7.8. The correlation matrix is calculated using terms from the variance-covariance matrix. Values close to unity indicate strong correlations between the relevant parameters. It can be seen that the coefficient and the order associated with each mechanism are correlated. This is not surprising, since changes in, say, the growth rate coefficient could be offset by changes in the growth rate expression's order. Similar effects would be seen with the power law relationships for nucleation and aggregation.

Table 7.8 also shows that the following parameter pairs $(k_{\beta} : k_G)$, $(k_{\beta} : n_G)$, $(k_G : n_{\beta})$ and $(n_{\beta} : n_G)$ are highly correlated, having elements in the matrix greater than 0.8. This is not surprising because of the way the DPB treats aggregated particles discussed in §5.4.3.

Table 7.8: Correlation matrix of the parameters estimated by gPROMS.

	k_β	k_G	k_B	n_β	n_G	n_B
k_β	1	-	-	-	-	-
k_G	0.855	1	-	-	-	-
k_B	0.0542	-0.276	1	-	-	-
n_β	0.973	0.812	0.0582	1	-	-
n_G	0.847	0.976	-0.273	0.848	1	-
n_B	0.0164	-0.34	0.961	0.0351	-0.357	1

The difference between the aggregation model that conserves surface area and the one that coalesces two spherical particles into a single spherical particle (which is embedded in the DPB) bears further scrutiny. A diagram representing these two modes of aggregation is shown in Figure 7.34

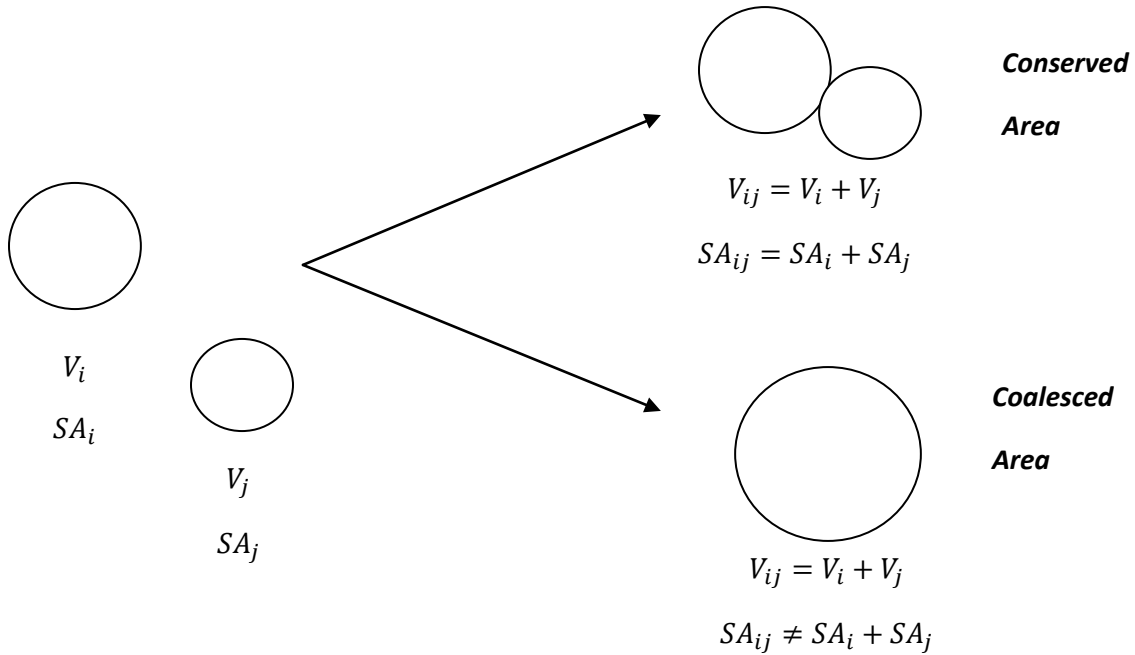


Figure 7.34: Representation of the two aggregation scenarios; particle area conservation and particle coalescence.

Crystal growth and aggregation rates may well be confounded, when one considers the resultant surface area of an aggregate. It has been discussed in §5.4.3 that aggregates formed in the model are single spherical particles, conserving the volume of the two aggregating particles, much like coalescing droplets, so the equation for surface area is given by Equation 5.3. If surface area of the crystal population were conserved, then the area available for crystal growth would not be dependent on aggregation and the correlation in Table 7.8 would not likely occur. Since the reality lies somewhere between these two extremes, is it prudent to consider how this deviation from reality affects the process model and the parameter estimation.

Comparison between the two aggregation scenarios is facilitated by plotting the ratio of conserved surface area to coalesced surface area against the ratio of particle volumes of the two particles involved in the aggregation process. Equation 7.8 gives the aggregate surface area if both particle volume and surface area are conserved. The ratio of the two surface areas shown in Figure 7.35.

$$SA_{ij}^{Coalesced} = 4\pi \left(\sqrt[3]{\frac{3V_{ij}}{4\pi}} \right)^2 \quad 5.3$$

$$SA_{ij}^{Conserved} = 4\pi \left(\sqrt[3]{\frac{3V_i}{4\pi}} \right)^2 + 4\pi \left(\sqrt[3]{\frac{3V_j}{4\pi}} \right)^2 \quad 7.8$$

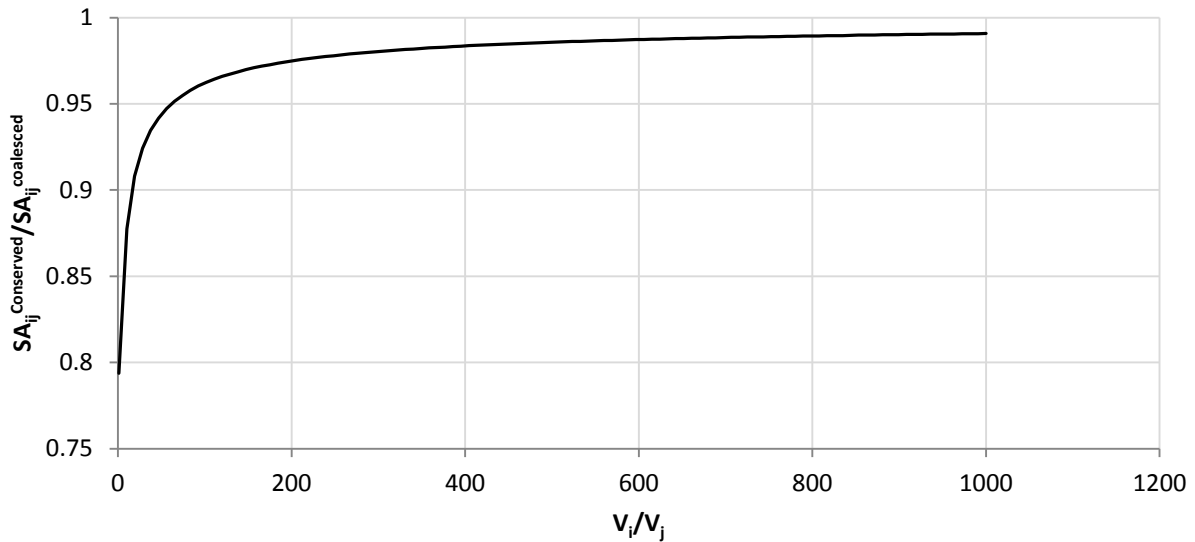


Figure 7.35: Ratio of conserved and coalesced aggregate surface area against the ratio of particle volumes involved in forming the aggregate.

Figure 7.35 shows that the ratio of surface areas approaches unity as the difference between particle size *increases* (which implies a large particle and a small one aggregating). At ratios of particle volume of 65 or greater, there is a less than 5% difference between the two surface areas under the two extreme particle aggregation scenarios. Since a particle that has 65 times more volume is only 4 times larger in spherical-equivalent diameter, this suggests that this is perhaps not that concerning. However, the error would become amplified as aggregates containing error aggregate with other aggregates containing error. It must be conceded that the model has no way of accounting for this. Either way, any systematic errors of this nature will cause the parameter values to be biased away from their true values, although this analysis suggests that this may not be a critical issue.

7.6 Conclusions

A single set of parameters were estimated for all the experiments performed using the methodology developed in Chapter 6. The parameters enabled the model to predict the time-varying *pH* behaviour

and can produce predictions of zeroth and third moment to within 20% of the experimental data. The PSD results are also satisfactory, since the important features of the experimental particle size distribution are well predicted by the model.

It was found that the nucleation rate is not important when modelling a batch reactor, since nuclei do not have either the time, nor the driving force to impact the mass balance. However, if the model were to be applied to a continuous or fed-batch system, nucleation rates would have a greater impact. Until this is done, estimated nucleation parameters cannot be properly validated.

The crystal growth rate power law model was deemed to be of higher order than expected from BCF theory, but a dead zone can explain this result. Using the concept of the dead zone, a second-order regression could still be supported, however, it was not possible to fully clarify this situation in this work. Furthermore, the crystal growth rate and aggregation kernel were found to be correlated through the way the DPB treats aggregating particles.

7.7 Key Points from Chapter 7

- A single set of parameters is found to acceptably predict experimental measurements over all conditions examined
- The nucleation parameters could not be confirmed as representative since the experimental methodology did not allow nuclei to sufficiently impact any experimental measurements
- A fifth-order dependence of the crystal growth rate on saturation index was found suggesting the presence of a supersaturation dead zone, when accommodating this dead zone a second-order dependence could approximate the model results
- The aggregation and crystal growth parameters were found to be correlated, since aggregating particles do not conserve surface area, which tends to confound the two mechanisms.

Chapter 8 - Conclusions and Recommendations

This chapter revisits the work done over the course of this research and offers conclusions that can be drawn from the work. Following this recommendations are made on how to improve the work and directions for further research.

8.1 Conclusions

The research conducted as part of this PhD project successfully fulfilled the research objectives identified in §1.2 which are revisited below:

1. The population dynamics were described with the kinetic mechanisms of nucleation, crystal growth and aggregation through the discretised population balance equation. The third moment of the distribution allowed the population dynamics to be coupled to the mass balance.
2. The solution thermodynamics and other model components were combined into a process model that describes struvite crystallisation in batch, fed-batch or continuous modes.
3. The process model was used to show how design parameters affected reactor performance and how the process behaves when subjected to various sources of uncertainty. The effects of a pH control scheme were also demonstrated.

4. Kinetic parameters for nucleation, crystal growth and aggregation were estimated from a data ensemble covering various experimental conditions. The parameters were able to produce acceptable model predictions compared to experimental measurements.

Additionally, there are particular achievements and conclusions made over the course of this research that bear elaboration.

8.1.1 Solution Thermodynamics

While the inclusion of a charge balance into the solution thermodynamics may seem pedestrian, it is an often overlooked and very important aspect of this work should be acknowledged. The charge balance allows the pH to be calculated from chemical additions to the solution and therefore can be employed for validation purposes. Furthermore, dynamic simulation of the process model would not be possible without a charge balance since pH measurements would have been required at each time step, making those simulations essentially impossible. The charge balance is also fundamental to the parameter estimation, given that pH measurements are used in the estimation process. They are also used to test the success or failure of the estimated parameters. Simply, without the charge balance the work after Chapter 3 would not have been possible. It is suggested to all future researchers in this field that while the charge balance is not necessary in describing struvite solution thermodynamics, it is neglected at their peril.

8.1.2 Discretised Population Balance

The discretised population balance with nucleation, crystal growth and aggregation is an important feature of this research and an important contribution to the ultimate goal of understanding struvite crystallisation. It gives the ability to describe the mechanisms of nucleation, crystal growth and aggregation simultaneously. This is significant, since it removes limiting assumptions that would

otherwise be required. Previous nucleation studies were constrained to operate at high saturation index for the results to be valid. Previous crystal growth studies did not consider nucleation or aggregation. The ability of the DPB to consider all mechanisms of interest was fundamental to the development of the process model.

Furthermore, the approach used to implement the DPB in the process model should be reflected upon. The hybrid approach to the model, wherein the two-term growth expression transitions to the three-term equation affords many advantages. This was a novel approach to addressing instability of the three-term growth equation in the small size intervals and the leakage of crystal numbers from the two-term growth equation in the large size intervals. Previous approaches have either neglected the small size intervals, replacing the nucleation rate with a particle source function or they used an adjustable discretisation where a finer discretisation are used with the two-term growth equation, making its accuracy acceptable. The hybrid approach is not considered superior to either of the alternatives but it does provide a means to describe the true nucleation rate without the increased complexity of the adjustable DPB.

8.1.3 Struvite Crystallisation Process Model

The process model developed as part of this work is novel in combining thermodynamics with a kinetic description of the nucleation, crystal growth and aggregation. It can be used to simulate batch, fed-batch and continuous reactor modes, so is applicable to a variety of design scenarios. The potential of the model for process design was demonstrated by showing the relationship between reactor volume and phosphorus recovery. Furthermore, crystalliser behaviour was assessed when subjected to various sources of uncertainty. The potential of the model to develop control systems was shown by simulating a pH controller that adjusts the flow of caustic to keep pH constant at the set point.

8.1.4 Parameter Estimation

The parameter estimation was the last stage of the research. Experiments were conducted over a range of saturation indices and the ensemble of data was incorporated into gPROMS for the parameter estimation. The experimental methodology developed to achieve this was successful in clearly showing nucleation, crystal growth and aggregation during batch crystallisation. PSD and pH measurements were gathered at $SI = 0.37$ and $SI = 0.54$. Further to this, pH measurements were gathered at $SI = 0.74$. The kinetic parameters estimated from the entire data set are presented again below in Table 7.4.

Table 7.4: Parameter estimation results from gPROMS reported with 95% confidence interval.

Mechanism	k_i	n_i
Aggregation	$(3.72 \pm 0.014) \times 10^{-7} L/min$	5.26 ± 0.004
Crystal Growth	$12.49 \pm 0.061 \mu m/min$	5.06 ± 0.005
Nucleation	$(8.50 \pm 0.076) \times 10^7 1/L.min$	1.68 ± 0.014

Using the estimated parameters, the model could predict the shape and location of the peaks and troughs of the measured PSD. While the fit is not perfect, it is considered acceptable and representative of the system considering challenge of taking PSD measurements. The pH model predictions were within experimental uncertainty for all conditions used in the data ensemble. The model predictions of the integrated properties of the PSD, *i.e.* zeroth moment, third moment and mean particle size, were all within $\pm 20\%$ experimental uncertainty.

However, shortcomings in the experimental methodology used, and, hence, in the estimated parameters were discovered. The nucleation parameters have almost no impact on the system pH or mass of crystallised struvite. This is caused by the small size of crystal nuclei and the batch time being insufficient for the nuclei to grow to a size of significance to the mass balance. Nevertheless, it would be

unwise to ignore nucleation altogether as it is fundamental to continuous operation. The nucleation parameters estimated here produced adequate model predictions of zeroth moment and mean particle size. It must be conceded that the experimental methodology used in this work could not produce nucleation parameters with a high degree of confidence although the m_0 and \bar{L} results suggest they are of realistic orders of magnitude.

The crystal growth rate was found to have a fifth-order dependence on saturation index, which does not fit with the Burton-Cabrera-Frank theory of crystallisation. This high order dependency on the saturation index implies the possibility of a dead zone, where the growth rate approaches zero. When this dead zone is considered, a second-order growth rate dependency can be used to approximate the model predictions. The aggregation parameters were similar to those found by other studies using the same methodology, *i.e.* batch experimental data and DPB.

8.1.5 Final Thoughts on the Research

Substantial progress has been made through this work to understand struvite crystallisation by considering a number of key mechanisms. The combination of solution thermodynamics, population balance and mechanism kinetics in a process model is a novel and a significant contribution, laying the foundation for further work. While some limitations were encountered with the experimental methodology and parameter estimation, a single set of parameters was found that acceptably describes the experimental measurements within the model framework developed.

8.2 Recommendations

After conducting this study of struvite nucleation, crystal growth and aggregation, the following recommendations are made for future work.

- Currently the solution thermodynamics can only accurately describe synthetic solutions containing the constituent molecules struvite in addition to spectator ions, sodium and chlorine. It is recommended that future studies add to the list of elements considered in the thermodynamics using pH measurements to validate each new addition until real wastewater can be accurately described.
- Hydrodynamic effects are not considered in this study as constant mixing conditions are used in all experiments. However, the nucleation rate and aggregation kernel are both dependent on the rate of collisions of particles in the crystalliser (the nucleation rate dependence is due to secondary contact nucleation). Therefore, future studies could improve on the descriptions for nucleation and aggregation, by considering crystalliser hydrodynamics. Crystal growth is less dependent on hydrodynamics, as the second-order approximation outside the dead zone implies integration controlled growth.
- A major shortcoming identified was the inability of the experimental methodology to capture the effects of nucleation. This resulted in nucleation parameters that cannot be properly validated against experimental measurement. Future studies should develop experimental methodologies to address this. Basing the experiments on either fed-batch or continuous operation would be a promising place to start. Seedless experiments may sound tempting to force nucleation to contribute more to the experimental results. However, this would introduce significant primary nucleation which is subject to much greater uncertainty than secondary nucleation. Furthermore, the single nucleation rate equation would need to describe both primary and secondary nucleation which could prove challenging. It is therefore suggested that seeded experiments be retained in future methodologies.
- The major focus of this work was the development of the process model and determination of kinetic parameters for key mechanisms. Unfortunately, this meant the model was underused

and not applied to investigate different operating conditions of different struvite designs for the purpose of increasing phosphorus recovery and improving product quality. It is strongly recommended that the work undertaken here is used for these purposes, for which it was developed.

- The process model required the simplifying assumption of perfect mixing throughout the crystalliser and in any product removal. Future work might consider methods for applying this approach to reactor designs that cannot be properly described by a well mixed batch, fed-batch or continuous reactor. Given that most operating reactor designs do not fit into those categories this is important for implementing the modelling approach in real systems.

REFERENCES

- AAGE, H. K., ANDERSEN, B. L., BLOM, A. & JENSEN, I. 1997. The solubility of struvite. *Journal of Radioanalytical and Nuclear Chemistry*, 223, 213-215.
- ABBONA, F. & BOISTELLE, R. 1979. Growth Morphology and Crystal Habit of Struvite Crystals ($MgNH_4PO_4 \cdot 6H_2O$). *Journal of Crystal Growth*, 46, 339-354.
- ABBONA, F. & BOISTELLE, R. 1985. Nucleation of Struvite ($MgNH_4PO_4 \cdot 6H_2O$) Single-Crystals and Aggregates. *Crystal Research and Technology*, 20, 133-140.
- ABBONA, F., MADSEN, H. E. L. & BOISTELLE, R. 1982. Crystallization of 2 Magnesium Phosphates, Struvite and Newberyite - Effect of Ph and Concentration. *Journal of Crystal Growth*, 57, 6-14.
- ABEGG, C. F., STEVENS, J. D. & LARSON, M. A. 1968. Crystal Size Distribution in Continuous Crystallizers when Growth Rate is Size-Dependent. *Aiche Journal*, 14, 118-122.
- ADNAN, A., KOCH, F. A. & MAVINIC, D. S. 2003. Pilot-scale study of phosphorus recovery through struvite crystallization - II: Applying in-reactor supersaturation ratio as a process control parameter. *Journal of Environmental Engineering and Science*, 2, 473-483.
- ALI, M. I. 2007. Struvite crystallization in fed-batch pilot scale and description of solution chemistry of struvite. *Chemical Engineering Research & Design*, 85, 344-356.
- ALI, M. I. & SCHNEIDER, P. A. 2005. Crystallization of struvite from metastable region with different types of seed crystal. *Journal of Non-Equilibrium Thermodynamics*, 30, 95-111.
- ALI, M. I. & SCHNEIDER, P. A. 2006. A fed-batch design approach of struvite system in controlled supersaturation. *Chemical Engineering Science*, 61, 3951-3961.
- ALI, M. I. & SCHNEIDER, P. A. 2008. An approach of estimating struvite growth kinetic incorporating thermodynamic and solution chemistry, kinetic and process description. *Chemical Engineering Science*, 63, 3514-3525.
- ALLEN, T. 1990. *Particle size measurement*, London ; New York, Chapman and Hall.
- ASSOCIATION, E. F. M. 2000. *Phosphorus: Essential Element for Food Production*, Brussels, European Fertilizer Manufacturers Association (EFMA).
- ASSOCIATION, I. F. I. 2006. *Sustainable Development and the Fertilizer Industry* International Fertilizer Industry Association.
- BATTERHAM, R. J., HALL, J. S. & BARTON, G. 1981. Pelletizing Kinetics and Simulation of Full Scale Balling Circuits. *3rd International Symposium on Agglomeration*. Nuremberg, West Germany.
- BATTISTONI, P., PACI, B., FATONE, F. & PAVAN, P. 2005. Phosphorus removal from supernatants at low concentration using packed and fluidized-bed reactors. *Industrial & Engineering Chemistry Research*, 44, 6701-6707.
- BATTISTONI, P., PACI, B., FATONE, F. & PAVAN, P. 2006. Phosphorus removal from anaerobic supernatants: Start-up and steady-state conditions of a fluidized bed reactor full-scale plant. *Industrial & Engineering Chemistry Research*, 45, 663-669.
- BATTISTONI, P., PAVAN, P., PRISCIANDARO, M. & CECCHI, F. 2000. Struvite crystallization: A feasible and reliable way to fix phosphorus in anaerobic supernatants. *Water Research*, 34, 3033-3041.
- BHUIYAN, M. I. H., MAVINIC, D. S. & BECKIE, R. D. 2008a. Nucleation and growth kinetics of struvite in a fluidized bed reactor. *Journal of Crystal Growth*, 310, 1187-1194.
- BHUIYAN, M. I. H., MAVINIC, D. S. & BECKIE, R. D. 2009. Dissolution kinetics of struvite pellets grown in a pilot-scale crystallizer. *Canadian Journal of Civil Engineering*, 36, 550-558.

- BHUIYAN, M. I. H., MAVINIC, D. S. & KOCH, F. A. 2008b. Phosphorus recovery from wastewater through struvite formation in fluidized bed reactors: a sustainable approach. *Water Science and Technology*, 57, 175-181.
- BHUIYAN, M. I. H., MAVINIC, D. S. & KOCH, F. A. 2008c. Thermal decomposition of struvite and its phase transition. *Chemosphere*, 70, 1347-1356.
- BORGERDING, J. 1972. Phosphate Deposits in Digestion Systems. *Journal Water Pollution Control Federation*, 44, 813-&.
- BORJA, R., QUINTANA, M., COLMENAREJO, M. F., BARRERA, J., SANCHEZ, E., GARCIA, G. & TRAVIESO, L. 2008. Removal of phosphorus through struvite precipitation using a by-product of magnesium oxide production (BMP): Effect of the mode of BMP preparation. *Chemical Engineering Journal*, 136, 204-209.
- BOUROPOULOS, N. C. & KOUTSOUKOS, P. G. 2000. Spontaneous precipitation of struvite from aqueous solutions. *Journal of Crystal Growth*, 213, 381-388.
- BRAMLEY, A. S. 1994. *A Study of the Growth and Aggregation of Calcium Oxalate Monohydrate*. Doctor of Philosophy, University of Adelaide.
- BRIDGER, G. L., SALUTSKY, M.L., STAROTSKA, R.W. 1962. Metal ammonium phosphates as fertilisers. *Journal of Agricultural and Food Chemistry*, 10, 181-188.
- BRINCK, J. W. 1977. World resources of phosphorus. *Ciba Foundation symposium*, 23-48.
- BUBE, K. 1910. Ueber Magnesiumammoniumphosphat. *Zeitschrift für Analytische Chemie*, 49, 525-596.
- BUCHANAN, J. R., MOTE, C. R. & ROBINSON, R. B. 1994. Thermodynamics of Struvite Formation. *Transactions of the Asae*, 37, 617-621.
- BUCKINGHAM, D. A., JASINSKI, S.M., 2006. Phosphate Rock Statistics, Historical Statistics for Mineral and Material Commodities in the United States. In: SURVEY, U. G. (ed.).
- BURNS, J. R. & FINLAYSON, B. 1982. Solubility Product of Magnesium Ammonium Phosphate Hexahydrate at Various Temperatures. *Journal of Urology*, 128, 426-428.
- BURTON, W. K., CABRERA, N. & FRANK, N. C. 1951. The Growth of Crystals and the Equilibrium Structure of their Surfaces. *Philosophical Transactions*, A243, 299-358.
- CANNING, T. F. & RANDOLPH, A. D. 1967. Some Aspects of Crystallization Theory: Systems that Violate McCabes Delta L Law. *Aiche Journal*, 13, 5-10.
- CARBALLA, M., MOERMAN, W., VANDEKERCKHOVE, A., DERYCKE, D. & VERSTRAETE, W. 2009. Phosphate removal in agro-industry: Pilot- and full-scale operational considerations of struvite crystallization. *Water Research*, 43, 1887-1892.
- CHILDS, C. W. 1970. A potentiometric study of equilibria in aqueous divalent metal orthophosphate solutions. *Inorganic Chemistry*, 11, 2465-2469.
- CHIMENOS, J. M., FERNANDEZ, A. I., VILLALBA, G., SEGARRA, M., URRUTICOECHEA, A., ARTAZA, B. & ESPIELL, F. 2003. Removal of ammonium and phosphates from wastewater resulting from the process of cochineal extraction using MgO-containing by-product. *Water Research*, 37, 1601-1607.
- CORDELL, D., DRANGERT, J. O. & WHITE, S. 2009. The story of phosphorus: Global food security and food for thought. *Global Environmental Change-Human and Policy Dimensions*, 19, 292-305.
- DOYLE, J. D. & PARSONS, S. A. 2002. Struvite formation, control and recovery. *Water Research*, 36, 3925-3940.
- DRIVER, J., LIJMBACH, D. & STEEN, I. 1999. Why recover phosphorus for recycling, and how? *Environmental Technology*, 20, 651-662.
- DURRANT, A. E., SCRIMSHAW, M. D., STRATFUL, I. & LESTER, J. N. 1999. Review of the feasibility of recovering phosphate from wastewater for use as a raw material by the phosphate industry. *Environmental Technology*, 20, 749-758.

- FATTAH, K. P., SABRINA, N., MAVINIC, D. S. & KOCH, F. A. 2008. Reducing operating costs for struvite formation with a carbon dioxide stripper. *Water Science and Technology*, 58, 957-962.
- FUJIMOTO, N., MIZUOCHI, T. & TOGAMI, Y. 1991. Phosphorus Fixation in the Sludge Treatment System of a Biological Phosphorus Removal Process. *Water Science and Technology*, 23, 635-640.
- GALBRAITH, S. C. & SCHNEIDER, P. A. 2009. A Review of Struvite Nucleation Studies. In: MAVINIC, D. S., KOCH, F. A. & ASHLEY, K. (eds.) *International Conference on Nutrient Recovery from Wastewater Streams*. Vancouver, Canada: IWA Publishing.
- GARSDIE, J., MERSMANN, A., NÝVLT, J., INSTITUTION OF CHEMICAL ENGINEERS (GREAT BRITAIN) & EUROPEAN FEDERATION OF CHEMICAL ENGINEERING. WORKING PARTY ON CRYSTALLIZATION. 2002. *Measurement of crystal growth and nucleation rates*, Railway Terrace, Rugby, UK, Institution of Chemical Engineers.
- GARSDIE, J. & SHAH, M. B. 1980. Crystallization Kinetics from Msmpr Crystallizers. *Industrial & Engineering Chemistry Process Design and Development*, 19, 509-514.
- GATERELL, M. R., GAY, R., WILSON, R., GOCHIN, R. J. & LESTER, J. N. 2000. An economic and environmental evaluation of the opportunities for substituting phosphorus recovered from wastewater treatment works in existing UK fertiliser markets. *Environmental Technology*, 21, 1067-1084.
- GELBARD, F. & SEINFELD, J. H. 1978. Numerical-Solution of Dynamic Equation for Particulate Systems. *Journal of Computational Physics*, 28, 357-375.
- GINTER, D. M. & LOYALKA, S. K. 1996. Apparent size-dependent growth in aggregating crystallizers. *Chemical Engineering Science*, 51, 3685-3695.
- GPROMS 2004. gPROMS Advanced User Guide. *Process Systems Enterprise Ltd*.
- HALFON, A. & KALIAGUINE, S. 1976. Alumina Trihydrate Crystallisation Part 2: A Model of Agglomeration. *Canadian Journal of Chemical Engineering*, 54, 168-172.
- HARRIS, D. C. 2010. *Quantitative chemical analysis*, New York, NY, W. H. Freeman and Co.
- HARRISON, M. L., JOHNS, M. R., WHITE, E. T. & MEHTA, C. M. 2011. Growth Rate Kinetics for Struvite Crystallisation. *PRES'11 14th International Conference on Process Integration, Modelling and Optimisation for Energy Saving and Pollution Reduction*. Florence, Italy: Italian Association of Chemical Engineering.
- HARTEL, R. W. & RANDOLPH, A. D. 1986. Mechanisms and Kinetic Modeling of Calcium-Oxalate Crystal Aggregation in a Urinelike Liquor .2. Kinetic Modeling. *Aiche Journal*, 32, 1186-1195.
- HOSTOMSKY, J. & JONES, A. G. 1991. Calcium-Carbonate Crystallization, Agglomeration and Form during Continuous Precipitation from Solution. *Journal of Physics D-Applied Physics*, 24, 165-170.
- HOUNSLOW, M. J. 1990. *A Discretized Population Balance for Nucleation, Growth and Aggregation*. Doctor of Philosophy, University of Adelaide.
- HOUNSLOW, M. J., MUMTAZ, H. S., COLLIER, A. P., BARRICK, J. P. & BRAMLEY, A. S. 2001. A micro-mechanical model for the rate of aggregation during precipitation from solution. *Chemical Engineering Science*, 56, 2543-2552.
- HULBURT, H. M. & KATZ, S. 1964. Some Problems in Particle Technology. A Statistical Formulation. *Chemical Engineering Science*, 19, 555.
- ILIEVSKI, D. 1991. *Modelling Al(OH)₃ Agglomeration during Batch and Continuous Precipitation in Supersaturated Caustic Aluminate Solutions*. Doctor of Philosophy, University of Queensland.
- JAFFER, Y., CLARK, T. A., PEARCE, P. & PARSONS, S. A. 2002. Potential phosphorus recovery by struvite formation. *Water Research*, 36, 1834-1842.
- JASINSKI, S. M. 2007. Phosphate Rock, Mineral Commodity Summaries. In: SURVEY, U. S. G. (ed.).
- JONES, A. G. 2002. *Crystallization process systems*, Oxford ; Boston, Butterworth-Heinemann.
- KABDAŞLI, I., PARSONS, S. A. & TUNAY, O. 2006. Effect of major ions on induction time of struvite precipitation. *Croatica Chemica Acta*, 79, 243-251.

- KORALEWSKA, J., PIOTROWSKI, K., WIERZBOWSKA, B. & MATYNIA, A. 2007. Reaction-crystallization of struvite in a continuous liquid et-pump DTM MSM PR crystallizer with upward circulation of suspension in a mixing chamber - an SDG kinetic approach. *Chemical Engineering & Technology*, 30, 1576-1583.
- LE CORRE, K. S., VALSAMI-JONES, E., HOBBS, P. & PARSONS, S. A. 2005. Impact of calcium on struvite crystal size, shape and purity. *Journal of Crystal Growth*, 283, 514-522.
- LE CORRE, K. S., VALSAMI-JONES, E., HOBBS, P. & PARSONS, S. A. 2007. Kinetics of struvite precipitation: Effect of the magnesium dose on induction times and precipitation rates. *Environmental Technology*, 28, 1317-1324.
- LEVENSPIEL, O. 1962. *Chemical reaction engineering; an introduction to the design of chemical reactors*, New York,, Wiley.
- LEVENSPIEL, O. 1972. *Chemical reaction engineering*, New York,, Wiley.
- LEVENSPIEL, O. 1999. *Chemical reaction engineering*, New York, Wiley.
- LEW, B., PHALAH, S., SHEINDORF, C., KUMMEL, M., REBHUN, M. & LAHAV, O. 2010. Favorable Operating Conditions for Obtaining High-Value Struvite Product from Sludge Dewatering Filtrate. *Environmental Engineering Science*, 27, 733-741.
- LI, X. Z. & ZHAO, Q. L. 2003. Recovery of ammonium-nitrogen from landfill leachate as a multi-nutrient fertilizer. *Ecological Engineering*, 20, 171-181.
- LIND, B. B., BAN, Z. & BYDEN, S. 2000. Nutrient recovery from human urine by struvite crystallization with ammonia adsorption on zeolite and wollastonite. *Bioresource Technology*, 73, 169-174.
- LITSTER, J. D., SMIT, D. J. & HOUNSLOW, M. J. 1995. Adjustable Discretized Population Balance for Growth and Aggregation. *Aiche Journal*, 41, 591-603.
- LIU, J. C. & WARMADWANTHI 2009. Recovery of phosphate and ammonium as struvite from semiconductor wastewater. *Separation and Purification Technology*, 64, 368-373.
- LOBANOV, S. 2009. Sewage Treatment to Remove Ammonium Ions by Struvite Precipitation. In: MAVINIC, D. S., KOCH, F. A. & ASHLEY, K. (eds.) *International Conference on Nutrient Recovery from Wastewater Streams*. Vancouver, Canada: IWA Publishing.
- MARTELL, A. E. & SMITH, R. M. 1989. *Critical Stability Constants*, New York, Plenum Press.
- MATYNIA, A., KORALEWSKA, J., WIERZBOWSKA, B. & PIOTROWSKI, K. 2006. The influence of process parameters on struvite continuous crystallization kinetics. *Chemical Engineering Communications*, 193, 160-176.
- MAURER, M., RONTELTAP, M. & GUJER, W. 2007. Struvite precipitation thermodynamics in source-separated urine. *Water Research*, 41, 977-984.
- MAVINIC, D. S., BHUIYAN, M. I. H. & BECKIE, R. D. 2007. A solubility and thermodynamic study of struvite. *Environmental Technology*, 28, 1015-1026.
- MERSMANN, A. 1996. Supersaturation and nucleation. *Chemical Engineering Research & Design*, 74, 812-820.
- MOREL, F. M. M. & HERING, J. G. 1993. *Principles and Applications of Aquatic Chemistry*, New York, John Wiley and Sons.
- MORSE, G. K., BRETT, S. W., GUY, J. A. & LESTER, J. N. 1998. Review: Phosphorus removal and recovery technologies. *Science of the Total Environment*, 212, 69-81.
- MULLIN, J. W. 1993. *Crystallization*, Oxford ; Boston, Butterworth-Heinemann.
- MÜNCH, E. V. & BARR, K. 2001. Controlled struvite crystallisation for removing phosphorus from anaerobic digester sidestreams. *Water Research*, 35, 151-159.
- MYERSON, A. S. 1993. *Handbook of industrial crystallization*, Boston, Butterworth-Heinemann.
- NADARAJAH, A., FORSYTHE, E. L. & PUSEY, M. L. 1995. The Averaged Face Growth-Rates of Lysozyme Crystals - the Effect of Temperature. *Journal of Crystal Growth*, 151, 163-172.

- NELSON, N. O., MIKKELSEN, R. L. & HESTERBERG, D. L. 2003. Struvite precipitation in anaerobic swine lagoon liquid: effect of pH and Mg : P ratio and determination of rate constant. *Bioresource Technology*, 89, 229-236.
- OHARA, M. & REID, R. C. 1973. *Modeling crystal growth rates from solution*, Englewood Cliffs, N.J., Prentice-Hall.
- OHLINGER, K. N., YOUNG, T. M. & SCHROEDER, E. D. 1998. Predicting struvite formation in digestion. *Water Research*, 32, 3607-3614.
- OHLINGER, K. N., YOUNG, T. M. & SCHROEDER, E. D. 1999. Kinetics effects on preferential struvite accumulation in wastewater. *Journal of Environmental Engineering-Asce*, 125, 730-737.
- OHLINGER, K. N., YOUNG, T. M. & SCHROEDER, E. D. 2000. Postdigestion struvite precipitation using a fluidized bed reactor. *Journal of Environmental Engineering-Asce*, 126, 361-368.
- PARKHURST, D. L. & APPELO, C. A. J. 1999. User's guide to PHREEQC (Version2) - A computer program for speciation, reaction-path, advective-transport, and inverse geochemical calculations. *USGS Water-Resources Investigation Report*.
- PASTOR, L., MANGIN, D., BARAT, R. & SECO, A. 2008a. A pilot-scale study of struvite precipitation in a stirred tank reactor: Conditions influencing the process. *Bioresource Technology*, 99, 6285-6291.
- PASTOR, L., MANGIN, D., FERRER, J. & SECO, A. 2010. Struvite formation from the supernatants of an anaerobic digestion pilot plant. *Bioresource Technology*, 101, 118-125.
- PASTOR, L., MARTI, N., BOUZAS, A. & SECO, A. 2008b. Sewage sludge management for phosphorus recovery as struvite in EBPR wastewater treatment plants. *Bioresource Technology*, 99, 4817-4824.
- PERERA, P. W. A., WU, W. X., CHEN, Y. X. & HAN, Z. Y. 2009. Struvite Recovery from Swine Waste Biogas Digester Effluent through a Stainless Steel Device under Constant pH Conditions. *Biomedical and Environmental Sciences*, 22, 201-209.
- PIOTROWSKI, K., KORALEWSKA, J., WIERZBOWSKA, B. & MATYNIA, A. 2009. Kinetics of Reaction-Crystallization of Struvite in the Continuous Draft Tube Magma Type Crystallizers-Influence of Different Internal Hydrodynamics. *Chinese Journal of Chemical Engineering*, 17, 330-339.
- PLAZA, C., SANZ, R., CLEMENTE, C., FERNANDEZ, J. M., GONZALEZ, R., POLO, A. & COLMENAREJO, M. F. 2007. Greenhouse evaluation of struvite and sludges from municipal wastewater treatment works as phosphorus sources for plants. *Journal of Agricultural and Food Chemistry*, 55, 8206-8212.
- QU, X. 2007. *BENCH-SCALE TWO-DIMENSIONAL FLUIDIZED BEDHYDRODYNAMICS AND STRUVITE GROWTH STUDIES*. Master of Applied Science, University of British Columbia.
- QUINTANA, M., SANCHEZ, E., COLMENAREJO, M. F., BARRERA, J., GARCIA, G. & BORJA, R. 2005. Kinetics of phosphorus removal and struvite formation by the utilization of by-product of magnesium oxide production. *Chemical Engineering Journal*, 111, 45-52.
- RAMKRISHNA, D. 2000. *Population balances : theory and applications to particulate systems in engineering*, San Diego, CA, Academic Press.
- RANDOLPH, A. D. & LARSON, M. A. 1988. *Theory of particulate processes : analysis and techniques of continuous crystallization*, San Diego, Academic Press.
- ROJKOWSKI, Z. 1977. New Empirical Equation of Size Dependent Crystal Growth and its use. *Kristall Und Technik-Crystal Research and Technology*, 12, 1121-1128.
- ROJKOWSKI, Z. 1978a. 2 Parameter Kinetic-Equation of Size Dependent Crystal-Growth. *Kristall Und Technik-Crystal Research and Technology*, 13, 1277-1284.
- ROJKOWSKI, Z. 1978b. New Hyperbolic Empirical Model of Size Dependent Crystal-Growth. *Bulletin De L Academie Polonaise Des Sciences-Serie Des Sciences Chimiques*, 26, 265-270.
- RONTELTAP, M., MAURER, M., HAUSHERR, R. & GUJER, W. 2010. Struvite precipitation from urine - Influencing factors on particle size. *Water Research*, 44, 2038-2046.

- RUNDLE, C. C. 2000. A Beginners Guide to Ion-Selective Electrode Measurements. Available: <http://www.nico2000.net/book/Beginners%20Guide.pdf>.
- SECO, A., PASTOR, L., MANGIN, D. & BARAT, R. 2008. A pilot-scale study of struvite precipitation in a stirred tank reactor: Conditions influencing the process. *Bioresource Technology*, 99, 6285-6291.
- SIN, G., MEYER, A. S. & GERNAEY, K. V. 2010. Assessing reliability of cellulose hydrolysis models to support biofuel process design-Identifiability and uncertainty analysis. *Computers & Chemical Engineering*, 34, 1385-1392.
- SMOLUCHOWSKI, M. 1917. Mathematical Theory of the Kinetics of the Coagulation of Colloidal Solutions. *Z. Phys. Chem*, 92, 129-168.
- SNOEYINK, V. L. & JENKINS, D. 1980. *Water chemistry*, New York, Wiley.
- STEEMSON, M. L. & WHITE, E. T. 1988. Numerical Modeling of Steady-State Continuous Crystallization Processes Using Piecewise Cubic Spline Functions. *Computers & Chemical Engineering*, 12, 81-89.
- STEEN, I. 1998. Phosphorus availability in the 21st Century: management of a nonrenewable resource. *Phosphorus and Potassium*, 25-31.
- STRATFUL, I., SCRIMSHAW, M. D. & LESTER, J. N. 2001. Conditions influencing the precipitation of magnesium ammonium phosphate. *Water Research*, 35, 4191-4199.
- STRATFUL, I., SCRIMSHAW, M. D. & LESTER, J. N. 2004. Removal of struvite to prevent problems associated with its accumulation in wastewater treatment works. *Water Environment Research*, 76, 437-443.
- SUTUGIN, A. G. & FUCHS, N. A. 1970. Formation of condensation aerosols under rapidly changing environmental conditions. Theory and method of calculation. *Aerosol Science and Technology*, 1, 287.
- TAVARE, N. S., SHAH, M. B. & GARSIDE, J. 1985. Crystallization and Agglomeration Kinetics of Nickel Ammonium-Sulfate in an Msmpr Crystallizer. *Powder Technology*, 44, 13-18.
- TAYLOR, A. W., FRAZIER, A. W. & GURNEY, E. L. 1963a. Solubility products of di and trimagnesium phosphates and the dissociation of magnesium phosphate solutions. *Trans. Faraday Soc.*, 1585-1589.
- TAYLOR, A. W., GURNEY, E. L. & FRAZIER, A. W. 1963b. Solubility products of magnesium ammonium and magnesium potassium phosphates. *Transactions of the Faraday Society*, 487, 1580-583.
- TAYLOR, B. N. & KUYATT, C. E. 1994. *Guidelines for evaluating and expressing the uncertainty of NIST measurement results*, Gaithersburg, MD, U.S. Department of Commerce, Technology Administration, National Institute of Standards and Technology.
- TURKER, M. & CELEN, I. 2007. Removal of ammonia as struvite from anaerobic digester effluents and recycling of magnesium and phosphate. *Bioresource Technology*, 98, 1529-1534.
- ULRICH, J. 2003. Solution crystallization - Developments and new trends. *Chemical Engineering & Technology*, 26, 832-835.
- UYSAL, A., YILMAZEL, Y. D. & DEMIRER, G. N. 2010. The determination of fertilizer quality of the formed struvite from effluent of a sewage sludge anaerobic digester. *Journal of Hazardous Materials*, 181, 248-254.
- WANG, J., BURKEN, J. G., ZHANG, X. Q. & SURAMPALLI, R. 2005. Engineered struvite precipitation: Impacts of component-ion molar ratios and pH. *Journal of Environmental Engineering-Asce*, 131, 1433-1440.
- WEAVER, M. L., QIU, S. R., HOYER, J. R., CASEY, W. H., NANCOLLAS, G. H. & DE YOREO, J. J. 2007. Inhibition of calcium oxalate monohydrate growth by citrate and the effect of the background electrolyte. *Journal of Crystal Growth*, 306, 135-145.

- WILSENACH, J. A., SCHUURBIERS, C. A. H. & VAN LOOSDRECHT, M. C. M. 2007. Phosphate and potassium recovery from source separated urine through struvite precipitation. *Water Research*, 41, 458-466.
- WU, Q. Z., BISHOP, P. L. & KEENER, T. C. 2005. A strategy for controlling deposition of struvite in municipal wastewater treatment plants. *Water Environment Research*, 77, 199-207.
- WYNN, E. J. W. 1996. Improved Accuracy and Convergence of Discretized Population Balance of Litster et al. *Aiche Journal*, 42, 3.
- XU, R. L. & DI GUIDA, O. A. 2003. Comparison of sizing small particles using different technologies. *Powder Technology*, 132, 145-153.
- ZENG, L. & LI, X. M. 2006. Nutrient removal from anaerobically digested cattle manure by struvite precipitation. *Journal of Environmental Engineering and Science*, 5, 285-294.
- ZHAO, Q. I., LI, W. & YOU, S. J. 2006. Simultaneous removal of ammonium-nitrogen and sulphate from wastewaters with an anaerobic attached-growth bioreactor. *Water Science and Technology*, 54, 27-35.

NOMENCLATURE

Abbreviations

ADPB	Adjustable Discretised Population Balance
AGG	Aggregation
%CV/CV	Percentage Coefficient of Variation/Coefficient of Variation
DPB	Discretised Population Balance
ESZ	Electrical Sensing Zone
GRD	Growth Rate Dispersion
LD	Laser Diffraction
MAP	Magnesium Ammonium Phosphate
MSMPR	Mixed Suspension Mixed Product Removal
NCG	Nucleation and Crystal Growth
PSD	Particle Size Distribution
SDG	Size-Dependent Growth

Latin Symbols

A	Debye-Hückel constant (0.509 at 25°C, (Mullin, 1993)) [-]
A_{ind}	Induction time equation constant [-]

a	Parameter in Rojkowski hyperbolic kinetic model [1/m]
a_i	Activity of species i [mol/L]
B_{ind}	Induction time equation constant [-]
B_o	Nucleation rate [1/L.min]
$B(L)$	Birth Function [1/ $\mu\text{m.L.min}$]
C_i	Concentration of species i [mol/L]
C_i^*	Equilibrium concentration of species i [mol/L]
C_i^T	Total concentration of element i [mol/L]
$C_{MAP_i}^{in}$	Concentration of element i in the <i>MAP</i> feed stream [mol/L]
C_{NaOH}^{in}	Concentration of <i>NaOH</i> in the <i>NaOH</i> feed stream [mol/L]
$D(L)$	Death function [1/ $\mu\text{m.L.min}$]
D	Diffusion coefficient [m^2/s]
d	Interplanar distance in the crystal lattice [m]
$E(t)$	Residence time distribution [1/min]
G	Crystal growth rate [$\mu\text{m}/\text{min}$]
G_∞	Maximum crystal growth rate in Rojkowski hyperbolic kinetic model [$\mu\text{m}/\text{min}$]
G_0	Minimal crystal growth rate in Rojkowski hyperbolic kinetic model [$\mu\text{m}/\text{min}$]
ΔG^*	Gibb's free energy change to form critical nucleus [J]

I	Ionic strength [mol/L]
I_{AGG}	Index of aggregation [-]
IAP	Ion activity product [mol ³ /L ³]
k	Boltzmann constant [J/K]
k_{β}	Rate constant for aggregation [L/min]
k_G	Rate constant for crystal growth [$\mu\text{m}/\text{min}$]
k_B	Rate constant for nucleation [1/L.min]
k_{prec}	Rate constant of precipitation reaction [1/min]
k_a	Surface area shape factor [-]
k_v	Volumetric shape factor [-]
K	Aggregation parameter (Hounslow, 1990) [-]
K_{sp}	Equilibrium solubility product [mol ³ /L ³]
L	Particle size [μm]
\tilde{L}	Dimensionless length [-]
L_i	Lower bound on the i^{th} size interval [μm]
\bar{L}_i	Mean size of the i^{th} interval [μm]
\bar{L}	Average particle size [μm]
ΔL_i	Size of the i^{th} interval [μm]

m_j	j^{th} moment of the distribution [$\mu\text{m}^j/\text{L}$]
\widetilde{m}_j	Dimensionless j^{th} moment of the distribution [-]
m_i	Mass of particles in the i^{th} interval [kg]
\dot{m}_j	Rate of change of the j^{th} moment of the distribution [$\mu\text{m}^j/\text{L}\cdot\text{min}$]
$MW_{Struvite}$	Molecular weight of struvite (245.5 g/mol)
n	Number density function [$1/\mu\text{m}\cdot\text{L}$]
n^0	Number density function of nuclei [$1/\mu\text{m}\cdot\text{L}$]
n_k	Number density function of stream k [$1/\mu\text{m}\cdot\text{L}$].
n_β	Order of aggregation [-]
n_G	Order of crystal growth [-]
n_B	Order of nucleation [-]
n_{prec}	Order of precipitation reaction [-]
N	Number of particles [$1/\text{L}$]
N_i	Number of particles in interval i [$1/\text{L}$]
N^*	Number of molecules comprising a critical size nucleus [-]
NE	Number of experiments performed [-]
NM_{ij}	Number of measurements of the j^{th} variable in the i^{th} experiment [-]
NU	Total number of measurement taken during all the experiments [-]

NV_i	Number of variables measured in the i^{th} experiment [-]
pH	Negative logarithm of hydrogen activity [-]
$\%P_{Rec}$	Percentage recovery of available phosphorus [-]
$\%P_{Rec}^T$	Percentage recovery of total phosphorus [-]
Q_{MAP}^{in}	Volumetric flow rate of feed stream <i>MAP</i> [L/min]
Q_{NaOH}^{in}	Volumetric flow rate of feed stream <i>NaOH</i> [L/min]
Q^{out}	Volumetric flow rate of outlet stream [L/min]
Q_k	Volumetric flow rate of stream <i>k</i> [L/min].
r	Discretisation constant L_{i+1}/L_i [-]
R_{col}	Rate of collisions [1/L.min]
SA	Surface area [μm^2]
S	Supersaturation [mol/L]
S_a	Saturation ratio [-]
SI	Saturation index [-]
SI^*	Saturation index limit of growth dead zone [-]
SSR	Supersaturation ratio [-]
T	Absolute temperature [K]
t	Time [min]

t_{ind}	Induction time [sec]
U	Uncertainty in of a variable in the NIST uncertainty propagation equation [-]
V	Reactor volume [L]
v	Particle volume [μm^3]
X	Measured variable in the NIST uncertainty propagation equation [-]
Y	Calculated variable in the NIST uncertainty propagation equation [-]
Z_i	Valency of species i [-]
z_{ijk}	k^{th} predicted value of the j^{th} variable in the i^{th} experiment.
\tilde{z}_{ijk}	k^{th} measured value of the j^{th} variable in the i^{th} experiment.

Greek Symbols

β	Aggregation kernel [L/min]
β_o	Size independent aggregation kernel [L/min]
$\beta_{i,j}$	Aggregation kernel for particles of size i and size j [L/min]
γ_i	Activity coefficient of species i [-]
γ^s	Surface energy [J]
ε	Variable for linear DPB (Sutugin and Fuchs, 1970) [-]
η	Geometric factor in Equation Error! Reference source not found. [-]
θ	Set of model parameters to be estimated

λ	Variable of integration (length)
μ	Arithmetic mean
ν	Number of ions into which a molecule dissociates [-]
$\rho_{Struvite}$	Density of struvite (1710 kg/m ³)
ρ	Density of crystal [kg/m ³]
σ	Standard Deviation [-]
σ^2	Variance [-]
τ	Residence time [min]
v	Molecular volume [m ³]
Φ	Objective function used by gPROMS [-]

Brackets

$\{i\}$	Activity of species i [mol/L]
$[i]$	Concentration of species i [mol/L]

APPENDICES

Appendix A - EES Model

"Struvite Thermodynamic Calculator"

"CONSTANTS"

"These are the constants used throughout the thermodynamic calculator. They include the Debye-Huckel constant,..."

"...valancies of the species in soluion, equilibrium constants for the species in solution and the solubility product of..."

"...struvite."

A = 0.509

"Debye-Huckel constant at 25 degrees C, from

Mullin (1993)"

Z_1 = 1

"Absolute charge for +/- 1 ions"

Z_2 = 2

"Absolute charge for +/- 1 ions"

Z_3 = 3

"Absolute charge for +/- 1 ions"

K_HPO4 = 10^(-12.35)

"HPO4 <---> H + PO4"

K_H2PO4 = 10^(-7.2)

"H2PO4 <---> H + HPO4"

K_H3PO4 = 10^(-2.15)

"H3PO4 <---> H + H2PO4"

K_HNH3 = 10^(-9.25)

"NH4 <---> H + NH3"

K_MgHPO4 = 10^(-2.91)

"MgHPO4 <---> H + MgPO4"

K_MgOH = 10^(-2.56)

"MgOH <---> OH + Mg"

K_MgPO4 = 10^(-4.8)

"MgPO4 <---> Mg + PO4"

K_MgH2PO4 = 10^(-0.45)

"MgH2PO4 <---> H + MgHPO4"

K_w = 10⁽⁻¹⁴⁾

"H2O <---> H + OH"

K_so = 10^(-13.26)

"Minimum solubility product of struvite"

"ADDITIONS"

"These are the concentrations of reactants added to solution. They are based on magnesium chloride, ammonium..."

"...dihydrogen phosphate, sodium hydroxide and sodium chloride."

C_MgCl2 = 0.005 "mol/L"

"Concentration of magnesium chloride in the

initial volume"

C_NH4H2PO4 = 0.005 "mol/L"

"Concentration of ammonium dihydrogen

phosphate in inital volume"

C_NaOH = 0.5 "mol/L"

"Concentration sodium hydroxide in solution to

be added"

C_NaCl = 0.0 "mol/L"

"Concentration of sodium chloride in initial

volume"

"VOLUMES"

"Defines the initial volume of solution, added volume of sodium hydroxide and the total volume of solution."

V_o = 1 "L"

V_NaOHadded = 0.00 "L"

V = V_o + V_NaOHadded "L"

"TOTAL CONCENTRATION"

"These determine the total concentration of master elements and spectator ions in solution, accounting for any volume addition."

C_T_Mg = (C_MgCl2*V_o)/V "mol/L"

$C_{T_P} = (C_{NH_4H_2PO_4} * V_o) / V$ "mol/L"
 $C_{T_N} = (C_{NH_4H_2PO_4} * V_o) / V$ "mol/L"
 $C_{Cl} = ((2 * C_{MgCl_2} + C_{NaCl}) * V_o) / V$ "mol/L"
 $C_{Na} = ((C_{NaOH} + C_{NaCl}) * V_{NaOHadded}) / V$ "mol/L"

"SPECIES BALANCES"

"These balances equate the total amount of each master element in the aqueous phase to the sum of all species in solution..."

"...containing the master element."

$C_{T_Mg} - C_{struvite} = C_{Mg} + C_{MgOH} + C_{MgH_2PO_4} + C_{MgHPO_4} + C_{MgPO_4}$
 $C_{T_N} - C_{struvite} = C_{NH_3} + C_{H_2NH_3}$
 $C_{T_P} - C_{struvite} = C_{H_3PO_4} + C_{H_2PO_4} + C_{HPO_4} + C_{PO_4} + C_{MgH_2PO_4} + C_{MgHPO_4} + C_{MgPO_4}$ "Phosphorus balance"

"Magnesium
"Nitrogen ba

"CHARGE BALANCE"

"This makes sure the concentration of anions equals the cations. Note that there are no balances for H and OH. Depending on the..."

"...concentration of master elements and spectator ions the concentration of H and OH will be set to satisfy the charge balance and..."

"...the equilibrium equation. If the pH is specified, i.e. C_H is defined, then the term 'TotalCharge = 0' must be commented out to..."

"...maintain degrees of freedom"

$TotalCharge = (2 * C_{Mg} + C_{MgOH} + C_{MgH_2PO_4} + C_{H_2NH_3} + C_H + C_{Na}) - (3 * C_{PO_4} + 2 * C_{HPO_4} + C_{H_2PO_4} + C_{MgPO_4} + C_{OH} + C_{Cl})$

TotalCharge = 0

"Comment this out if the pH is set"

{pH = 7}
calculated"

"Comment this out the pH is unknown or to be

"IONIC STRENGTH"

"Because of the non-ideal thermodynamics the ionic strength is required to calculate the activity coefficients for the species."

$I = 0.5 * ((C_{H_2PO_4} * (Z_{-1})^2) + (C_{HPO_4} * (Z_{-2})^2) + (C_{PO_4} * (Z_{-3})^2) + (C_{MgH_2PO_4} * (Z_{-1})^2) + (C_{MgPO_4} * (Z_{-1})^2) + (C_{Mg} * (Z_{+2})^2) + (C_{MgOH} * (Z_{+1})^2) + (C_{H_2NH_3} * (Z_{+1})^2) + (C_{OH} * (Z_{-1})^2) + (C_H * (Z_{+1})^2) + (C_{Cl} * (Z_{-1})^2) + (C_{Na} * (Z_{+1})^2))$

"ACTIVITY COEFFECIENTS"

"The activity coefficients are calculated using the Debye-Huckel equation with Davies Approximation. Note the unity values of..."

"...activity coefficient are commented out below the equations. Using the unity values is useful for troubleshooting the code and ..."

"...finding bugs."

$-\text{LOG}_{10}(\gamma_1) = (A * Z_{-1}^2) * (I^{0.5} / (1 + (I^{0.5}))) - 0.3 * I$ "Activity coefficient for ions with positive or negative charge of 1"

$-\text{LOG}_{10}(\gamma_2) = (A * Z_{-2}^2) * (I^{0.5} / (1 + (I^{0.5}))) - 0.3 * I$ "Activity coefficient for ions with positive or negative charge of 2"

$-\text{LOG}_{10}(\gamma_3) = (A * Z_{-3}^2) * (I^{0.5} / (1 + (I^{0.5}))) - 0.3 * I$ "Activity coefficient for ions with positive or negative charge of 3"

{gamma_1 = 1

gamma_2 = 1

gamma_3 = 1}

"ACTIVITIES"

"This multiplies all ions in solution by there corresponding activity coefficient. Note that species without a charge are not included..."

"...as they are not subject to the hydrated radius effect."

$Act_{H_2PO_4} = (\gamma_1) * (C_{H_2PO_4})$

$Act_HPO4 = (\gamma_2) \cdot (C_HPO4)$
 $Act_PO4 = (\gamma_3) \cdot (C_PO4)$
 $Act_MgH2PO4 = (\gamma_1) \cdot (C_MgH2PO4)$
 $Act_MgPO4 = (\gamma_1) \cdot (C_MgPO4)$
 $Act_Mg = (\gamma_2) \cdot (C_Mg)$
 $Act_MgOH = (\gamma_1) \cdot (C_MgOH)$
 $Act_H2NH3 = (\gamma_1) \cdot (C_H2NH3)$
 $Act_H = (\gamma_1) \cdot (C_H)$
 $Act_OH = (\gamma_1) \cdot (C_OH)$

"EQUILIBRIA"

"These equations determine the activity of species participated in equilibrium reactions defined by their equilibrium constants."

$(Act_HPO4) \cdot K_HPO4 = ((Act_H) \cdot (Act_PO4))$
 $(Act_H2PO4) \cdot K_H2PO4 = ((Act_H) \cdot (Act_HPO4))$
 $(C_H3PO4) \cdot K_H3PO4 = ((Act_H) \cdot (Act_H2PO4))$
 $(Act_MgPO4) \cdot K_MgPO4 = ((Act_Mg) \cdot (Act_PO4))$
 $(C_MgHPO4) \cdot K_MgHPO4 = ((Act_Mg) \cdot (Act_HPO4))$
 $(Act_MgH2PO4) \cdot K_MgH2PO4 = ((Act_Mg) \cdot (Act_H2PO4))$
 $(Act_MgOH) \cdot K_MgOH = ((Act_Mg) \cdot (Act_OH))$
 $(Act_H2NH3) \cdot K_H2NH3 = ((Act_H) \cdot (C_NH3))$
 $K_w = (Act_H) \cdot (Act_OH)$

"pH AND SUPERSATURATION"

"These equations calculate the pH and supersaturation of struvite once the speciation has been determined by solving the above equations"

$pH = -\text{LOG}_{10}(Act_H)$	"Definition of pH"
$IAP = Act_Mg \cdot Act_H2NH3 \cdot Act_PO4$	"Ion Activity Product - used to define struvite solute concentration"
$Sa = (IAP/K_so)^{(1/3)}$	"Saturation ratio"
$SI = \text{LOG}_{10}(IAP/K_so)$	"Saturation index"
$SSR = (IAP/K_so)$	"Supersaturation ratio"

"EQUILIBRIUM OR NON-EQUILIBRIUM"

"This sets either the equilibrium or nonequilibrium condition. $C_struvite = 0$ means there is no struvite in solution so the ..."

"...saturation index must be non zero, i.e. non-equilibrium. $SI = 0$ means equilibrium has been reached and the necessary..."

"...amount of struvite has been precipitated or dissolved."

$C_struvite = 0$

"SI = 0"

Appendix B - gPROMS Model

Variable Types

All variables used in gPROMS must have defined *variable types* which have a lower and upper bound and a default value used in numerical iterations. The table below shows the variable types defined by the author in formulating the gPROMS model.

Name	Lower bound	Default value	Upper bound
CONCENTRATION	0.0	0.5	1.0E20
FLOWRATE	0.0	1.0	1.0E20
GAMMA	1.0E-10	0.5	1.1
IONICSTRENGTH	1.0E-5	0.5	5.0
NDASH	-1.0E20	20.0	1.0E20
NOTYPE	-1.0E30	1.0	1.0E50
NUMBERS	0.0	1.0	1.0E20
pH	1.0	1.0	14.0
RATE	-1.0E20	1.0	1.0E20
SIZE	0.0	1.0	1.0E40
VOLUME	0.0	1.0	1.0E20

Model Entities

There are three model entities used in the gPROMS model: (1) Thermodynamic entity which describes the solution thermodynamics; (2) Conservation entity which describes the mass balance and population balance; (3) Stochastic entity which is used to do a large number of simulations using stochastic model inputs.

```
# Thermodynamic model for struvite crystallisation
```

PARAMETER

```
# The parameter section defines constants that are not subject to change  
# during the model simulation.
```

```
# Equilibrium constants determining the speciation for a synthetic solution  
# containing magnesium, ammonium and phosphate. Includes the solubility  
# constant of struvite and the sources for the constants.
```

```
K_MgOH          AS REAL # Childs 1970  
K_NH4           AS REAL # Taylor et al. 1963  
K_HPO4         AS REAL # Morel and Hering 1993  
K_H2PO4        AS REAL # Morel and Hering 1993  
K_H3PO4        AS REAL # Morel and Smith 1989  
K_MgH2PO4      AS REAL # Morel and Smith 1989  
K_MgHPO4       AS REAL # Morel and Smith 1989  
K_MgPO4        AS REAL # Morel and Smith 1989  
K_w            AS REAL # Snoeyink and Jenkins 1980  
K_so          AS REAL # Ohlinger 1998
```

```
# Constants concerning the non-ideal nature of the thermodynamics. Including  
# Debye-Huckel coefficient, absolute valencies and charge balance.
```

```
DebyeCoefficientA AS REAL # Debye-Huckel coefficient  
Z1              AS REAL # Absolute valency for +/- 1 ions  
Z2              AS REAL # Absolute valency for +/- 2 ions  
Z3              AS REAL # Absolute valency for +/- 3 ions  
CB              AS REAL # Charge balance  
Gamma0         AS REAL
```

```
# Conversion factors to change units of concentration for improved numerical  
# behaviour. Includes, molar, millimolar and micromolar
```

```
MICROMOLAR AS REAL DEFAULT 1E6 # Micromolar conversion factor  
MILLIMOLAR AS REAL DEFAULT 1E3 # Millimolar conversion factor  
MOLAR AS REAL DEFAULT 1E0 # Molar conversion factor  
ConcentrationConversion AS REAL
```

VARIABLE

```
# The variable section defines the names for variables that are subject to  
change during the simulation.
```

```
# Variables for non-ideal conditions, pH and supersaturation.
```

```
C_H          AS Concentration # Concentration of hydrogen, +1  
C_OH        AS Concentration # Concentration of hydroxide, -1
```

```

pH                AS pH                # pH of solution
IonicStrength     AS IONICSTRENGTH    # Ionic strength of solution
Gamma1            AS Gamma             # Activity coefficient for +/- 1 ions
Gamma2            AS Gamma             # Activity coefficient for +/- 2 ions
Gamma3            AS Gamma             # Activity coefficient for +/- 3 ions
IAP               AS NOTYPE            # Ion Activity Product
SI                AS NOTYPE            # Saturation Index

```

```

# Variables for the total concentration of the master elements involved in
# speciation.

```

```

C_T_Mg            AS Concentration    # Total concentration of magnesium
C_T_NH4           AS Concentration    # Total concentration of ammonium
C_T_PO4           AS Concentration    # Total concentration of phosphate
C_Cl              AS Concentration    # Total concentration of chloride
C_Na              AS Concentration    # Total concentration of sodium

```

```

# Variables for the individual ions involved in speciation.

```

```

C_Mg              AS Concentration    # Magnesium, +2
C_MgOH            AS Concentration    # Magnesium hydroxide, +1
C_MgH2PO4         AS Concentration    # Magnesium dihydrogen phosphate, +1
C_MgPO4           AS Concentration    # Magnesium phosphate, -1
C_NH3             AS Concentration    # Ammonia, 0
C_NH4             AS Concentration    # Ammonium, +1
C_H3PO4           AS Concentration    # Trihydrogen phosphate, 0
C_H2PO4           AS Concentration    # Dihydrogen phosphate, -1
C_HPO4            AS Concentration    # Hydrogen phosphate, -2
C_PO4             AS Concentration    # Phosphate, -3
C_MgHPO4          AS Concentration    # Magnesium hydrogen phosphate, 0

```

```

# Activities for the ions involved in speciation.

```

```

Act_H2PO4         AS Concentration
Act_HPO4          AS Concentration
Act_PO4           AS Concentration
Act_MgH2PO4       AS Concentration
Act_MgPO4         AS Concentration
Act_Mg            AS Concentration
Act_MgOH          AS Concentration
Act_NH4           AS Concentration
Act_H             AS Concentration
Act_OH            AS Concentration
Act_NH3           AS Concentration
Act_MgHPO4        AS Concentration
Act_H3PO4         AS Concentration

```

SET

```

# The set section is where the values for the parameters are set for use
# during the simulation.

```

```

ConcentrationConversion := MICROMOLAR;
K_MgOH                  := (10^(-2.56))*ConcentrationConversion;
K_NH4                   := (10^(-9.25))*ConcentrationConversion;
K_HPO4                  := (10^(-12.35))*ConcentrationConversion;
K_H2PO4                 := (10^(-7.20))*ConcentrationConversion;
K_H3PO4                 := (10^(-2.15))*ConcentrationConversion;
K_MgH2PO4               := (10^(-0.45))*ConcentrationConversion;
K_MgHPO4                := (10^(-2.91))*ConcentrationConversion;
K_MgPO4                 := (10^(-4.80))*ConcentrationConversion;
K_w                     := (10^(-14))*ConcentrationConversion^2;

```

```

K_so          := (10^(-13.26))*ConcentrationConversion^3;
Z1           := 1;
Z2           := 2;
Z3           := 3;
DeByeCoefficientA := 0.509; # Coefficient for assumed constant T 298.13K
CB           := 0;         # Charge balance is set to zero
Gamma0       := 1;         # Species without charge

EQUATION
# The equation section is where all the equations for the model are written.

# The total concentrations are the sum of their free ions and complexes
C_T_Mg = C_Mg + C_MgOH + C_MgH2PO4 + C_MgPO4 + C_MgHPO4;
C_T_NH4 = C_NH3 + C_NH4;
C_T_PO4 = C_H3PO4 + C_H2PO4 + C_HPO4 + C_PO4 + C_MgH2PO4 + C_MgPO4 +
C_MgHPO4;

# The relationship between pH and the concentration of hydrogen ions. The
# negative log equation results in integration errors during fixed pH
# stochastic simulations. Using the alternative equation solves this
# problem.
pH=-LOG10(Act_H/ConcentrationConversion); #Use this equation for free pH
#10^(-pH)= Act_H/ConcentrationConversion; #Use this equation for fixed pH

# Defining the ionic strength of the solution.
IonicStrength*ConcentrationConversion =
0.5*((C_H2PO4*(Z1^2))+(C_HPO4*(Z2^2))+(C_PO4*(Z3^2))+(C_MgH2PO4*(Z1^2))+(C_Mg
PO4*(Z1^2))+(C_Mg*(Z2^2))+(C_MgOH*(Z1^2))+(C_NH4*(Z1^2))+(C_OH*(Z1^2))+(C_H*(
Z1^2))+(C_Cl*(Z1^2))+(C_Na*(Z1^2)));

# Calculating activity coefficients using the Debye Hucke equation with
# Davies approximation. Setting the activity coefficients to unity can be
# helpful when troubleshooting the code.
-LOG10(Gamma1) =
DeByeCoefficientA*(Z1^2)*(IonicStrength^(1/2))/(1+IonicStrength^(1/2))-
(0.3*IonicStrength); # Calculating activity coefficients for ions with
positive or negative charge of 1
-LOG10(Gamma2) =
DeByeCoefficientA*(Z2^2)*(IonicStrength^(1/2))/(1+IonicStrength^(1/2))-
(0.3*IonicStrength); # Calculating activity coefficients for ions with
positive or negative charge of 2
-LOG10(Gamma3) =
DeByeCoefficientA*(Z3^2)*(IonicStrength^(1/2))/(1+IonicStrength^(1/2))-
(0.3*IonicStrength); # Calculating activity coefficients for ions with
positive or negative charge of 3
#Gamma1 = 1;
#Gamma2 = 1;
#Gamma3 = 1;

# Calculating ion activity by multiplying the concentration by the ion
# activity.
Act_H2PO4 = (Gamma1)*(C_H2PO4);
Act_HPO4 = (Gamma2)*(C_HPO4);
Act_PO4 = (Gamma3)*(C_PO4);
Act_MgH2PO4 = (Gamma1)*(C_MgH2PO4);
Act_MgPO4 = (Gamma1)*(C_MgPO4);
Act_Mg = (Gamma2)*(C_Mg);

```

```

Act_MgOH      = (Gamma1)*(C_MgOH);
Act_NH4       = (Gamma1)*(C_NH4);
Act_H         = (Gamma1)*(C_H);
Act_OH        = (Gamma1)*(C_OH);
Act_NH3       = (Gamma0)*(C_NH3);
Act_MgHPO4    = (Gamma0)*(C_MgHPO4);
Act_H3PO4     = (Gamma0)*(C_H3PO4);

# Equilibria equations.
(Act_H2PO4)*K_H2PO4      = ((Act_H)*(Act_HPO4));
(Act_HPO4)*K_HPO4       = ((Act_H)*(Act_PO4));
(Act_H3PO4)*K_H3PO4     = ((Act_H)*(Act_H2PO4));
(Act_MgPO4)*K_MgPO4     = ((Act_Mg)*(Act_PO4));
(Act_MgHPO4)*K_MgHPO4   = ((Act_Mg)*(Act_HPO4));
(Act_MgH2PO4)*K_MgH2PO4 = ((Act_Mg)*(Act_H2PO4));
(Act_MgOH)*K_MgOH       = ((Act_Mg)*(Act_OH));
(Act_NH4)*K_NH4         = ((Act_H)*(Act_NH3));
(K_w)                   = ((Act_H)*(Act_OH));

# Calculating the Ion Activity Product
IAP = Act_Mg*Act_NH4*Act_PO4;

# Calculating the saturation index
SI = LOG10(IAP/K_so);

# Definition of the charge balance charge balance
CB = Z2*C_Mg + Z1*C_MgOH - Z1*C_MgPO4 + Z1*C_MgH2PO4 + Z1*C_NH4 - Z3*C_PO4 -
Z2*C_HPO4 - Z1*C_H2PO4 - Z1*C_OH + Z1*C_H - Z1*C_Cl + Z1*C_Na;

```

#Discretised population balance model

PARAMETER

NEQ AS INTEGER DEFAULT 100 #The number of discrete size domains
r AS REAL #Discretisation factor
RHO AS REAL DEFAULT 1710 #Density, kg/m3
MW AS REAL DEFAULT 245.5 #Molecular Weight, g/mol
Kv AS REAL DEFAULT 3.14159265/6 #Shape factor for spheres
PI AS REAL DEFAULT 3.14159265 #Pi

VARIABLE

#NOTE: The variables are defined for a continuous MSMR reactor
#The model equations can still be used for other reactor configurations
#by changing reactor in and out flows to appropriate values
VOL AS VOLUME #Volume of the reactor, L
FLOW_MAP_IN, FLOW_NaOH_IN, FLOW_OUT AS FLOWRATE #Flowrate of streams in and out of the reactor, L/min

CONCENTRATION_Mg_IN, CONCENTRATION_N_IN, CONCENTRATION_P_IN, CONCENTRATION_NaOH_IN AS CONCENTRATION #Concentration of master elements and caustic into reactor, mol/L

CONCENTRATION_Mg, CONCENTRATION_N, CONCENTRATION_P, CONCENTRATION_Cl, CONCENTRATION_Na AS CONCENTRATION #Concentration of master and spectator elements in the reactor, mol/L
TAU AS NOTYPE #Hydraulic residence time of the reactor

Bo AS NOTYPE #Nucleation rate, 1/L.min
Go AS NOTYPE #Size Independent Growth Rate, um/min
BETAo AS NOTYPE #Size Independent Aggregation Kernel, L/min

A, B, C AS NOTYPE #Coefficients for 3term growth equation
LBAR AS SIZE #Average particle size (first moment divided by zeroth moment), um
L AS ARRAY(NEQ) OF SIZE #Lower bound on the ith interval, um
LINT AS ARRAY(NEQ) OF SIZE #Mean size of interval i, um
N AS ARRAY(NEQ) OF NUMBERS #Number of crystals flowing in the reactor, 1/L
MOM AS ARRAY(4) OF NOTYPE #Moments of the particle size distribution

NDASH AS ARRAY(NEQ) OF RATE #Total rate of change of crystals of L(i), 1/L.min
NDASH_NCG2term AS ARRAY(NEQ) OF RATE #Contribution of Nucleation and Crystal Growth found with the 2 term equation, 1/L.min
NDASH_NCG3term AS ARRAY(NEQ) OF RATE #Contribution of Nucleation and Crystal Growth found with the 3 term equation, 1/L.min

#There are four terms of the discretised aggregation equation derived by Hounslow (1990)
#Each term describes particular binary interactions that result in the birth or death
#of particles in the ith interval. Complications arise when combining the terms in one
#equation, therefore a variable is created for each term of the equation making it easier
#to calculate the rate of change of crystals in each size interval due to nucleation

```

#crystal growth and aggregation.
NDASH_BIRTH_1 AS ARRAY(NEQ) OF RATE #First term for birthing particles in the
ith interval
NDASH_BIRTH_2 AS ARRAY(NEQ) OF RATE #Second term for birthing particles in
the ith interval
NDASH_DEATH_1 AS ARRAY(NEQ) OF RATE #First term for killing particles in the
ith interval
NDASH_DEATH_2 AS ARRAY(NEQ) OF RATE #Second term for killing particles in the
ith interval

#These multipliers are used in the first birth and death mechanism. Separate
variables are
#created because of complications arising from the indexes used in the for
loops.
MULTIPLIER_BIRTH_1 AS ARRAY(NEQ) OF NOTYPE
MULTIPLIER_DEATH_1 AS ARRAY(NEQ) OF NOTYPE

k_NUC,k_CG,k_AGG AS NOTYPE #Rate constants nucleation, crystal growth and
aggregation
n_NUC,n_CG,n_AGG AS NOTYPE #Order of the kinetics for nucleation, crystal
growth and aggregation

MOLES_STRUVITE AS NOTYPE #Moles of struvite in reactor, mol
P_RECOVERY AS NOTYPE #Percentage of P recovered based on total
P
N_RECOVERY AS NOTYPE #Percentage of N recovered based on total
N
VOLUME_PRODUCTION_RATE AS NOTYPE #Volumetric rate of struvite produced,
um^3/L.min
MOLES_PRODUCTION_RATE AS NOTYPE #Molar rate of struvite produced, mol/min
SIG_2term AS ARRAY(NEQ) OF NOTYPE #Sigmoidal function to stabilise three
term growth equation
SIG_3term AS ARRAY(NEQ) OF NOTYPE #Sigmoidal function to stabilise three
term growth equation

SET
#For the current form of the DPB the geometric discretisation constant must
be
#the cube root of two or the aggregation equation will be invalid. If a
different
#constant is desired the DPB must be re-derived based on the new constnat.
#An adjustable DPB has been developed by Litster et al. (1995) and Wynn
(1996)
r := 2^(1/3); #r = L(i+1)/Li

EQUATION
#Number balance where NDASH is the sum rate of change of numbers in the ith
#interval due to nucleation, crystal growth and aggregation
$N = NDASH - (N*FLOW_OUT)/VOL; #1/L.min

#Equations used to determine the configuration of the reactor
FLOW_MAP_IN + FLOW_NaOH_IN = FLOW_OUT; #This equations makes this a
continuous reactor with no accumulation
TAU = VOL/FLOW_OUT; #The calculates the residence
time for the reactor
$VOL = (FLOW_MAP_IN + FLOW_NaOH_IN) - FLOW_OUT; #This equation accounts for
any any accumulation if the flow in does

```

#not equal the flow out,
it is also necessary for fed-batch simulations

#Element Balances

#Because of the 1:1:1 molar ratio of Mg, N and P in struvite the variable
"MOLES_PRODUCTION_RATE" can be used as the consumption term

#for all three elements, i.e. consumption of Mg = consumption of N =
consumption of P = production of struvite

$VOL * \$CONCENTRATION_Mg + CONCENTRATION_Mg * \$VOL =$
 $FLOW_MAP_IN * CONCENTRATION_Mg_IN - FLOW_OUT * CONCENTRATION_Mg -$
 $MOLES_PRODUCTION_RATE * 1E6;$

$VOL * \$CONCENTRATION_N + CONCENTRATION_N * \$VOL = FLOW_MAP_IN * CONCENTRATION_N_IN$
 $- FLOW_OUT * CONCENTRATION_N - MOLES_PRODUCTION_RATE * 1E6;$

$VOL * \$CONCENTRATION_P + CONCENTRATION_P * \$VOL = FLOW_MAP_IN * CONCENTRATION_P_IN$
 $- FLOW_OUT * CONCENTRATION_P - MOLES_PRODUCTION_RATE * 1E6;$

#These mass balances account for the spectator elements introduced through
caustic and magnesium addition

#without these balances the thermodynamic model will not operate accurately.
Magnesium is commonly added in

#the form of MgCl₂, hence the "2" in the inflow term for Cl.

$VOL * \$CONCENTRATION_Na + CONCENTRATION_Na * \$VOL =$
 $FLOW_NaOH_IN * CONCENTRATION_NaOH_IN - FLOW_OUT * CONCENTRATION_Na;$
 $VOL * \$CONCENTRATION_Cl + CONCENTRATION_Cl * \$VOL =$
 $2 * FLOW_MAP_IN * CONCENTRATION_Mg_IN - FLOW_OUT * CONCENTRATION_Cl;$

#Calculate the average particle size

$LBAR * MOM(1) = MOM(2);$ #um

#Discretized size domain with geometric discretisation

$L(1) = 0.01;$ #L(1) is chosen to be small enough to approximate
nuclei

FOR i := 1 TO NEQ-1 DO
r = L(i+1)/L(i);

END

#To calculate the mean size of each interval. This is used when calculating
#the moments of the PSD - it is assumed all particles in the ith interval
#have this size.

FOR i := 1 TO NEQ-1 DO
LINT(i) = (L(i) + L(i+1))/2;

END

LINT(NEQ) = (L(NEQ) + r*L(NEQ))/2;

$A = 2 * r / ((1 + r) * (r^2 - 1));$

$B = 2 / (1 + r);$

$C = -2 * r / ((1 + r) * (r^2 - 1));$

#Discretized population balance with Nucleation and Growth #

$NDASH_NCG2term(1) = 0.5 * (Bu - SIG_2term(1) * ((Go * N(1)) / ((r-1) * L(1))));$

FOR i := 2 TO NEQ DO

$NDASH_NCG2term(i) = SIG_2term(i) * ((Go * (r * N(i-1) - N(i))) / ((r-1) * L(i)));$

END

$NDASH_NCG3term(1) = 0.5 * (Bu - SIG_2term(1) * ((Go * N(1)) / ((r-1) * L(1))));$

FOR i := 2 TO NEQ-1 DO

```

        NDASH_NCG3term(i) = SIG_3term(i)*((Go/L(i))*(A*N(i-1) + B*N(i) +
C*N(i+1)));
END
NDASH_NCG3term(NEQ) = SIG_3term(NEQ)*((Go/L(NEQ))*(A*N(NEQ-1) + B*N(NEQ)));

#Discretized population balance for the 1st mechanism of birth
NDASH_BIRTH_1(1) = 0; #Crystals cannot be birthed into the first interval
NDASH_BIRTH_1(2) = 0; #Crystals cannot be birthed into the second interval
FOR i := 1 TO NEQ DO
    MULTIPLIER_BIRTH_1(i) = 2^(i-NEQ+1);
END
FOR i := 3 TO NEQ DO
    NDASH_BIRTH_1(i) = N(i-1)*BETAo*SIGMA(MULTIPLIER_BIRTH_1(NEQ-(i-1):NEQ-
2)*N(1:i-2));
END

#Discretized population balance for the 2nd mechanism of birth
NDASH_BIRTH_2(1) = 0; #Crystals cannot be birthed in the first interval
FOR i := 2 TO NEQ DO
    NDASH_BIRTH_2(i) = 0.5*BETAo*(N(i-1)^2);
END

#Discretized population balance for the 1st mechanism of death
NDASH_DEATH_1(1) = 0; #Crystals cannot leave the first interval because of
this term
FOR i := 1 TO NEQ DO
    MULTIPLIER_DEATH_1(i) = 2^(i-NEQ);
END
FOR i := 2 TO NEQ DO
    NDASH_DEATH_1(i) = N(i)*BETAo*SIGMA(MULTIPLIER_DEATH_1(NEQ-(i-1):NEQ-
1)*N(1:i-1));
END

#Discretized population balance for the 2nd mechanism of death
FOR i := 1 TO NEQ DO
    NDASH_DEATH_2(i) = N(i)*BETAo*SIGMA(N(i:NEQ));
END

#Net rate of change in interval i due to nucleation, growth and aggregation
NDASH = NDASH_NCG + NDASH_BIRTH_1 + NDASH_BIRTH_2 - NDASH_DEATH_1 -
NDASH_DEATH_2;

#Calculate the numerical moments based on the PSD
$MOM(1) = SIGMA($N); #ZEROTH MOMENT, 1/L.min
$MOM(2) = SIGMA(LINT*$N); #FIRST MOMENT, um/L.min
$MOM(3) = SIGMA((LINT^2)*$N); #SECOND MOMENT, um^2/L.min
$MOM(4) = SIGMA((LINT^3)*$N); #THIRD MOMENT, um^3/L.min
$MOLES_STRUVITE = (($MOM(4)*RHO*Kv*VOL)/MW)*1E-15; #Moles of struvite,
mol/min

#Conversion factor: [um^3/L.min]*[kg/m^3 = g/L]*[L]*[mol/g]
#after cancelling units we are left with [um^3.mol/L.min]
#therefore a conversion factor for L/um^3 is required
#1L = 1dm^3; 10dm = 1000000um; 10^3dm^3 = 1000000^3um^3 = 10^-15L/um^3

#Volume and molar production rates. These must be based on the NDASH varibale
#for the mass balances to be valid.

```

```

VOLUME_PRODUCTION_RATE = SIGMA((LINT^3)*NDASH); #um^3/L.min
MOLES_PRODUCTION_RATE = ((VOLUME_PRODUCTION_RATE*RHO*Kv*VOL)/MW)*1E-15;
#mol/min

#Phosphorus and nitrogen recovery percentage. Note that these are based on
#the total amount of P and N in the system NOT the amount thermodynamically
#available. To calculate the recovery based on the available P and N the
#concentration at SI=0 must be known.
P_RECOVERY = ((CONCENTRATION_P_IN*FLOW_MAP_IN -
CONCENTRATION_P*FLOW_OUT)/(CONCENTRATION_P_IN*FLOW_MAP_IN))*100;
N_RECOVERY = ((CONCENTRATION_N_IN*FLOW_MAP_IN -
CONCENTRATION_N*FLOW_OUT)/(CONCENTRATION_N_IN*FLOW_MAP_IN))*100;

FOR i := 1 TO NEQ DO
    SIG_3term(i) = 1/(1 + exp(-i + 25));
    SIG_2term(i) = 1 - SIG_3term(i);
END

```

#Stochastic simulations for struvite crystallisation model

PARAMETER

#NoSimulations is the number of simulations to be performed with

#stochastically chosen variable values

NoSimulations AS INTEGER

UNIT

#Because the deterministic simulations use two model entities units must be

#defined for both these entities. They are defined as arrays because the

#stochastic variables are placed in an array and then the deterministic

#simulation is performed for each number in that array

SimulationPB AS ARRAY(NoSimulations) OF Conservation #SimulationPB

relates to the conservation model

SimulationT AS ARRAY(NoSimulations) OF Thermo #SimulationT

relates to the thermodynamic model

VARIABLE

#Input Uncertainty. These are the input variables that will be stochastically

#chosen from a range of possible values

#The kinetic rate constants for nucleation, crystal growth and aggregation

#are chosen because they are determined from experiment and therefore have

#a degree of uncertainty. Performing multiple simulations with stochastic

#kinetic constants allows us to see the sensitivity of the model outputs to

#uncertainty in the rate constants.

k_AGG AS ARRAY(NoSimulations) OF NOTYPE

k_CG AS ARRAY(NoSimulations) OF NOTYPE

k_NUC AS ARRAY(NoSimulations) OF NOTYPE

#The concentration of P and N being fed to the reactor are also

stochastically

#chosen because in a real reactor the P and N source is wastewater which is

#subject to random variation. The other key components being fed (Mg and

NaOH)

#can be controlled.

CONCENTRATION_P_IN AS ARRAY(NoSimulations) OF CONCENTRATION

CONCENTRATION_N_IN AS ARRAY(NoSimulations) OF CONCENTRATION

#Output uncertainty. These are the key output variables identified.

SI AS ARRAY(NoSimulations) OF NOTYPE

pH AS ARRAY(NoSimulations) OF NOTYPE

LBAR AS ARRAY(NoSimulations) OF NOTYPE

P_RECOVERY AS ARRAY(NoSimulations) OF NOTYPE

N_RECOVERY AS ARRAY(NoSimulations) OF NOTYPE

#Statistical information can be retrieved from the stochastic simulations

#the mean of all simulations and the variance in the output variables are

#calculated in this model.

SImean AS NOTYPE

SIVariance AS NOTYPE

pHmean AS NOTYPE

pHVariance AS NOTYPE

LBARmean AS NOTYPE

LBARvariance AS NOTYPE

P_RECOVERYmean AS NOTYPE

P_RECOVERYvariance AS NOTYPE

```
N_RECOVERYmean      AS NOTYPE
N_RECOVERYvariance  AS NOTYPE
```

EQUATION

```
#This for loop to to assign each element of the array to a variable in the
#deterministic model.
```

```
FOR i := 1 TO NoSimulations DO
  k_AGG(i)           = SimulationPB(i).k_AGG;
  k_CG(i)            = SimulationPB(i).k_CG;
  k_NUC(i)           = SimulationPB(i).k_NUC;
  CONCENTRATION_P_IN(i) = SimulationPB(i).CONCENTRATION_P_IN;
  CONCENTRATION_N_IN(i) = SimulationPB(i).CONCENTRATION_N_IN;
  SI(i)              = SimulationT(i).SI;
  pH(i)              = SimulationT(i).pH;
  LBAR(i)            = SimulationPB(i).LBAR;
  P_RECOVERY(i)      = SimulationPB(i).P_RECOVERY;
  N_RECOVERY(i)      = SimulationPB(i).N_RECOVERY;
END
```

END

```
#Here are the equations for the mean and variance of all the key output
#variables.
```

```
SImean = SIGMA(SI)/NoSimulations;
SIVariance = SIGMA((SI - SImean)^2)/NoSimulations;
pHmean = SIGMA(pH)/NoSimulations;
pHvariance = SIGMA((pH - pHmean)^2)/NoSimulations;
LBARmean = SIGMA(LBAR)/NoSimulations;
LBARvariance = SIGMA((LBAR - LBARmean)^2)/NoSimulations;
P_RECOVERYmean = SIGMA(P_RECOVERY)/NoSimulations;
P_RECOVERYvariance = SIGMA((P_RECOVERY - P_RECOVERYmean)^2)/NoSimulations;
N_RECOVERYmean = SIGMA(N_RECOVERY)/NoSimulations;
N_RECOVERYvariance = SIGMA((N_RECOVERY - N_RECOVERYmean)^2)/NoSimulations;
```

```

#This is the process for the deterministic struvite crystalliser
UNIT
#The unit section defines which model entities will be used in the process
#to simulate a struvite crystalliser both thermodynamics and conservation
#discriptions must be used.
MSMPR AS CONSERVATION
THERMO AS THERMO

EQUATION
#These equations use the SI calculated from thermodynamics in the
#kinetic equations.
MSMPR.Bo = MSMPR.k_NUC*(THERMO.SI)^MSMPR.n_NUC;
MSMPR.Go = MSMPR.k_CG*(THERMO.SI)^MSMPR.n_CG;
MSMPR.BETAo = MSMPR.k_AGG*(THERMO.SI)^MSMPR.n_AGG;

#Mass Balances. This equates the concentration of master elements calculated
#from the mass balance in the CONSERVATION entity with the total aqueous
#concentration used the THERMO entity
THERMO.C_T_Mg = MSMPR.CONCENTRATION_Mg;
THERMO.C_T_NH4 = MSMPR.CONCENTRATION_N;
THERMO.C_T_PO4 = MSMPR.CONCENTRATION_P;

THERMO.C_Na = MSMPR.CONCENTRATION_Na;
THERMO.C_Cl = MSMPR.CONCENTRATION_Cl;

ASSIGN
#Assigning values to known variables
WITHIN MSMPR DO
    FLOW_MAP_IN := 0.07;           #L/min
    FLOW_NaOH_IN := 0.01;         #L/min
    CONCENTRATION_Mg_IN := 5000;  #uM
    CONCENTRATION_N_IN := 5000;   #uM
    CONCENTRATION_P_IN := 5000;   #uM
    CONCENTRATION_NaOH_IN := 40000; #uM

#Kinetic parameters for nucleation, crystal growth and aggregation
    k_NUC := 1E6;   #1/min.L
    k_CG := 1;     #um/min
    k_AGG := 1E-6; #L/min
    n_NUC := 1;
    n_CG := 1;
    n_AGG := 1;

END

INITIAL
#Initial condition for differential variables
WITHIN MSMPR DO
    CONCENTRATION_Mg = 2500;  #uM
    CONCENTRATION_N = 2500;   #uM
    CONCENTRATION_P = 2500;   #uM
    CONCENTRATION_Cl = 5000;  #uM
    CONCENTRATION_Na = 2500;  #uM
    VOL = 1;                  #L

#Unseeded reactor
N = 0;

```

```

#Seeded reactor. Currently commented out. The initial numbers are not
#important for continous simulations to steady state, however it
#becomes very important for batch and fed-batch simulations
{N(1) = 277719.16*1E-0;
N(2) = 72184.01*1E-0;
N(3) = 90943.19*1E-0;
N(4) = 114576.52*1E-0;
N(5) = 144349.89*1E-0;
N(6) = 181857.61*1E-0;
N(7) = 229107.39*1E-0;
N(8) = 288627.3*1E-0;
N(9) = 363600.16*1E-0;
N(10) = 458032.2*1E-0;
N(11) = 576964.8*1E-0;
N(12) = 726740.44*1E-0;
N(13) = 915334.44*1E-0;
N(14) = 1152771.4*1E-0;
N(15) = 1451642.9*1E-0;
N(16) = 1827752.8*1E-0;
N(17) = 2300916.5*1E-0;
N(18) = 2895948*1E-0;
N(19) = 3643869.2*1E-0;
N(20) = 4583385*1E-0;
N(21:NEQ) = 0;}

#The initial moments are calculated from the intial PSD
MOM(1) = SIGMA(N); #ZEROTH MOMENT
MOM(2) = SIGMA(LINT*N); #FIRST MOMENT
MOM(3) = SIGMA((LINT^2)*N); #SECOND MOMENT
MOM(4) = SIGMA((LINT^3)*N); #THIRD MOMENT

MOLES_STRUVITE = ((MOM(4)*RHO*Kv*VOL)/MW)*1E-15; #Moles of struvite
(mol)
END

SOLUTIONPARAMETERS
REPORTINGINTERVAL := 1;

#The index reduction is used for fixed pH simulations. The pH can be fixed
#so long as the NaOH fed to the reactor is free to change to adjust the pH
#to the fixed value. This is how the effects of pH control are examined.
#Currently it is commented out because the flow of NaOH is set and the pH
#is allowed to change accordingly.
#INDEXREDUCTION := ON; #Turn on for fixed pH simulations

SCHEDULE
#This determines how long the simulation will run for. Currently it is set
#to run for 10 residence times (TAU = 12.5min, simulation time = 125 mins)
CONTINUE FOR 125 #mins

```

```

#Process for running the stochastic simulations
UNIT
MonteCarlo AS STOCHASTIC

SET
#The number of simulations is set to 100. Because of memory allocation
#issues it is not possible to have many more simulations. However the
#sequence section of this entity can be used to reset the stochastic
#variables and re-allocate memory allowing a much greater number of
#simulation to be performed.
MonteCarlo.NoSimulations := 100;

EQUATION
#The following equations are the same as those in the deterministic model
#the equations are nested inside to WITHIN statements, one applies to this
#stochastic or MonteCarlo entity and the other is for the deterministic
#entity where each individual simulation is carried out.
WITHIN MonteCarlo DO
  FOR i := 1 TO NoSimulations DO
    WITHIN SimulationPB(i) DO
      Bo = k_NUC*(SimulationT(i).SI)^n_NUC;
      Go = k_CG*(SimulationT(i).SI)^n_CG;
      BETAo = k_AGG*(SimulationT(i).SI)^n_AGG;

      SimulationT(i).C_T_Mg = CONCENTRATION_Mg;
      SimulationT(i).C_T_NH4 = CONCENTRATION_N;
      SimulationT(i).C_T_PO4 = CONCENTRATION_P;

      SimulationT(i).C_Na = CONCENTRATION_Na;
      SimulationT(i).C_Cl = CONCENTRATION_Cl;
    END
  END
END

ASSIGN
#The variable assignments are the same as the determinsitc model except for
#the stochastic variables. In all cases they are uniformly distributed
#between +/- 10% of the deterministic value.
WITHIN MonteCarlo DO
  FOR i := 1 TO NoSimulations DO
    WITHIN SimulationPB(i) DO
      FLOW_MAP_IN := 0.07; ##L/min
      FLOW_NaOH_IN := 0.01; #L/min
      CONCENTRATION_Mg_IN := 5000; #uM
      CONCENTRATION_N_IN := UNIFORM(4500,5500); #5000;uM
      CONCENTRATION_P_IN := UNIFORM(4500,5500); #5000;uM
      CONCENTRATION_NaOH_IN := 40000; #uM
      N_IN := 0;

      # Kinetic parameters as stochastically determined #
      k_AGG :=UNIFORM(0.9E-6,1.1E-6); #1E-6;
      k_CG := UNIFORM(0.9,1.1); #1;
      k_NUC := UNIFORM(900000,1.1E6); #1E6;
      n_NUC := 1;
      n_CG := 1;
      n_AGG := 1;
    END
  END
END

```

```

        #For simulations where pH is controlled uncomment the following
        #ling and comment out FLOW_NaOH_IN (line 43)
        #SimulationT(i).pH := 8;
    END
END
END

INITIAL
WITHIN MonteCarlo DO
    FOR i := 1 TO NoSimulations DO
        WITHIN SimulationPB(i) DO
            CONCENTRATION_Mg = 2500;
            CONCENTRATION_N = 2500;
            CONCENTRATION_P = 2500;
            CONCENTRATION_Cl = 2500;
            CONCENTRATION_Na = 2500;
            VOL = 1;
            N = 0;

            MOM(1) = SIGMA(N); #ZEROTH MOMENT
            MOM(2) = SIGMA(LINT*N); #FIRST MOMENT
            MOM(3) = SIGMA((LINT^2)*N); #SECOND MOMENT
            MOM(4) = SIGMA((LINT^3)*N); #THIRD MOMENT

            MOLES_STRUVITE = ((MOM(4)*RHO*Kv*VOL)/MW)*1E-15; #Moles of
struvite (mol)
        END
    END
END

SOLUTIONPARAMETERS
REPORTINGINTERVAL := 125;
#INDEXREDUCTION := ON; #Turn on for fixed pH simulations

SCHEDULE #Operating Procedure
SEQUENCE
    CONTINUE FOR 125

    #The RESET command can be used in the sequence section to increase the
    #number of stochastic simulations possible. Only one reset is shown here
    #resulting in a total of 200 simulations. For more simulations just copy
    #and paste the code below as many times as desired.

    # RESET 1 #
    RESET
        WITHIN MonteCarlo DO
            FOR i := 1 TO NoSimulations DO
                WITHIN SimulationPB(i) DO
                    k_AGG := UNIFORM(0.9E-6,1.1E-6);
                    k_CG := UNIFORM(0.9,1.1);
                    k_NUC := UNIFORM(900000,1.1E6);
                    CONCENTRATION_N_IN := UNIFORM(4500,5500);
                    CONCENTRATION_P_IN := UNIFORM(4500,5500);
                END #Within SimulationPB(i)
            END #For loop
        END #Withen MonteCarlo
    END #Reset

```

CONTINUE FOR 125

#Parameter estimation entity showing the experiments used in the estimation, the parameters to be estimated plus the initial guess and upper and lower bounds.

EXPERIMENTS

SI04_Nineteenth_October1
SI04_Nineteenth_October2
SI04_Thirtyith_September
SI04_Twenty ninth_September1
SI04_Twenty ninth_September2
SI04_Twenty sixth_October
SI05_Eighteenth_October1
SI05_Eighteenth_October2
SI05_Fifteenth_September
SI05_Twenty eighth_September
SI05_Twenty sixth_October
SI05_Twenty third_September
SI075_Thirtyith_September_1

ESTIMATE

MSMPR.k_AGG
1.0E-7 : 1.0E-8 : 9.0E-6

ESTIMATE

MSMPR.k_CG
1.0 : 0.5 : 15.0

ESTIMATE

MSMPR.k_NUC
8.5E7 : 1.0E7 : 9.0E8

ESTIMATE

MSMPR.n_AGG
4.0 : 1.0 : 10.0

ESTIMATE

MSMPR.n_CG
2.0 : 1.0 : 6.0

ESTIMATE

MSMPR.n_NUC
3.0 : 1.0 : 5.0

Appendix C - Raw Data

The raw data used to perform the parameter estimation in Chapter 7 is presented in the “Experiments Performed” entities used in gPROMS.

```
# SI04_19/10/10a
PROCESS MSMPR

INITIAL_CONDITION
MSMPR.N(1) 5000000.0
MSMPR.N(2) 5000000.0
MSMPR.N(3) 5000000.0
MSMPR.N(4) 5000000.0
MSMPR.N(5) 5000000.0
MSMPR.N(6) 5000000.0
MSMPR.N(7) 5000000.0
MSMPR.N(8) 5000000.0
MSMPR.N(9) 5000000.0
MSMPR.N(10) 5000000.0
MSMPR.N(11) 5000000.0
MSMPR.N(12) 5000000.0
MSMPR.N(13) 5000000.0
MSMPR.N(14) 5000000.0
MSMPR.N(15) 5000000.0
MSMPR.N(16) 5000000.0
MSMPR.N(17) 5000000.0
MSMPR.N(18) 5000000.0
MSMPR.N(19) 5000000.0
MSMPR.N(20) 5000000.0
MSMPR.N(21) 5000000.0
MSMPR.N(22) 5000000.0
MSMPR.N(23) 5000000.0
MSMPR.N(24) 3935333.333
MSMPR.N(25) 2762333.333
MSMPR.N(26) 2001000.0
MSMPR.N(27) 1810666.667
MSMPR.N(28) 1888000.0
MSMPR.N(29) 2498000.0
MSMPR.N(30) 3819000.0
MSMPR.N(31) 4883333.333
MSMPR.N(32) 4448333.333
MSMPR.N(33) 1231333.333
MSMPR.N(34) 54333.33333
MSMPR.N(35) 15666.66667
MSMPR.N(36) 0.0
MSMPR.N(37) 0.0
Thermo.V_NaOH_added 0.0085

SENSOR
MSMPR.N(24)
CONSTANT_VARIANCE (10000.0)

SENSOR
```

MSMPR.N(25)
CONSTANT_VARIANCE (10000.0)

SENSOR

MSMPR.N(26)
CONSTANT_VARIANCE (10000.0)

SENSOR

MSMPR.N(27)
CONSTANT_VARIANCE (10000.0)

SENSOR

MSMPR.N(28)
CONSTANT_VARIANCE (10000.0)

SENSOR

MSMPR.N(29)
CONSTANT_VARIANCE (10000.0)

SENSOR

MSMPR.N(30)
CONSTANT_VARIANCE (10000.0)

SENSOR

MSMPR.N(31)
CONSTANT_VARIANCE (10000.0)

SENSOR

MSMPR.N(32)
CONSTANT_VARIANCE (10000.0)

SENSOR

MSMPR.N(33)
CONSTANT_VARIANCE (10000.0)

SENSOR

MSMPR.N(34)
CONSTANT_VARIANCE (10000.0)

SENSOR

MSMPR.N(35)
CONSTANT_VARIANCE (10000.0)

SENSOR

MSMPR.N(36)
CONSTANT_VARIANCE (10000.0)

SENSOR

MSMPR.N(37)
CONSTANT_VARIANCE (10000.0)

SENSOR

THERMO.pH
CONSTANT_VARIANCE (0.05)

MEASURE

MSMPR.N(24)

0.0	3935333.333
3.0	3069000.0
10.0	3038000.0
20.0	2502000.0
35.0	2890333.333
60.0	2746666.667
120.0	2700000.0

MEASURE

MSMPR.N(25)

0.0	2762333.333
3.0	2082666.667
10.0	1946333.333
20.0	1523000.0
35.0	1670666.667
60.0	1690000.0
120.0	1188000.0

MEASURE

MSMPR.N(26)

0.0	2001000.0
3.0	1569666.667
10.0	1437666.667
20.0	1239000.0
35.0	1154000.0
60.0	967666.6667
120.0	1181000.0

MEASURE

MSMPR.N(27)

0.0	1810666.667
3.0	1359666.667
10.0	1192333.333
20.0	1010333.333
35.0	909000.0
60.0	1002000.0
120.0	1087666.667

MEASURE

MSMPR.N(28)

0.0	1888000.0
3.0	1558000.0
10.0	1115000.0
20.0	983000.0
35.0	955666.6667
60.0	905333.3333
120.0	944333.3333

MEASURE

MSMPR.N(29)

0.0	2498000.0
3.0	1884000.0
10.0	1243000.0
20.0	1025666.667
35.0	983000.0
60.0	1037000.0
120.0	967333.3333

MEASURE

MSMPR.N(30)

0.0	3819000.0
3.0	2645666.667
10.0	1911333.333
20.0	1422000.0
35.0	1433666.667
60.0	1208000.0
120.0	1305666.667

MEASURE

MSMPR.N(31)

0.0	4883333.333
3.0	3974666.667
10.0	2898000.0
20.0	2331333.333
35.0	1903333.333
60.0	1779333.333
120.0	1755666.667

MEASURE

MSMPR.N(32)

0.0	4448333.333
3.0	4681666.667
10.0	4161000.0
20.0	3434666.667
35.0	3345000.0
60.0	2995333.333
120.0	3007333.333

MEASURE

MSMPR.N(33)

0.0	1231333.333
3.0	2568000.0
10.0	3422666.667
20.0	3632333.333
35.0	3998000.0
60.0	4001666.667
120.0	3826333.333

MEASURE

MSMPR.N(34)

0.0	54333.33333
3.0	337666.6667
10.0	1056666.667
20.0	2090000.0
35.0	2090000.0
60.0	2603000.0
120.0	2921666.667

MEASURE

MSMPR.N(35)

0.0	15666.66667
3.0	31000.0
10.0	58333.33333
20.0	291333.3333

35.0	291333.3333
60.0	392666.6667
120.0	458666.6667

MEASURE

MSMPR.N(36)

0.0	0.0
3.0	0.0
10.0	4000.0
20.0	15666.66667
35.0	15666.66667
60.0	11666.66667
120.0	27333.33333

MEASURE

MSMPR.N(37)

0.0	0.0
3.0	0.0
10.0	0.0
20.0	0.0
35.0	0.0
60.0	0.0
120.0	0.0

MEASURE

THERMO.pH

0.0	7.48
3.0	7.46
10.0	7.43
20.0	7.41
35.0	7.38
60.0	7.36
120.0	7.33

SI04_19/10/10b
PROCESS MSMPR

INITIAL_CONDITION

MSMPR.N(1) 5000000.0
MSMPR.N(2) 5000000.0
MSMPR.N(3) 5000000.0
MSMPR.N(4) 5000000.0
MSMPR.N(5) 5000000.0
MSMPR.N(6) 5000000.0
MSMPR.N(7) 5000000.0
MSMPR.N(8) 5000000.0
MSMPR.N(9) 5000000.0
MSMPR.N(10) 5000000.0
MSMPR.N(11) 5000000.0
MSMPR.N(12) 5000000.0
MSMPR.N(13) 5000000.0
MSMPR.N(14) 5000000.0
MSMPR.N(15) 5000000.0
MSMPR.N(16) 5000000.0
MSMPR.N(17) 5000000.0
MSMPR.N(18) 5000000.0
MSMPR.N(19) 5000000.0
MSMPR.N(20) 5000000.0
MSMPR.N(21) 5000000.0
MSMPR.N(22) 5000000.0
MSMPR.N(23) 5000000.0
MSMPR.N(24) 2323333.333
MSMPR.N(25) 2505666.667
MSMPR.N(26) 2315666.667
MSMPR.N(27) 2766333.333
MSMPR.N(28) 2894000.0
MSMPR.N(29) 3796000.0
MSMPR.N(30) 5229000.0
MSMPR.N(31) 5380666.667
MSMPR.N(32) 3970666.667
MSMPR.N(33) 1099333.333
MSMPR.N(34) 140000.0
MSMPR.N(35) 27333.33333
MSMPR.N(36) 8000.0
MSMPR.N(37) 0.0
Thermo.V_NaOH_added 0.0085

MEASURE

MSMPR.N(24)
0.0 2323333.333
3.0 1919333.333
10.0 1686000.0
20.0 2253000.0
35.0 2280666.667
60.0 1624000.0
120.0 1818333.333

MEASURE

MSMPR.N(25)
0.0 2505666.667
3.0 2004666.667

10.0	1538333.333
20.0	1662666.667
35.0	1635666.667
60.0	1332666.667
120.0	1177000.0

MEASURE

MSMPR.N(26)

0.0	2315666.667
3.0	1896000.0
10.0	1643333.333
20.0	1534666.667
35.0	1418000.0
60.0	1091666.667
120.0	947666.6667

MEASURE

MSMPR.N(27)

0.0	2766333.333
3.0	1927000.0
10.0	1546333.333
20.0	1491666.667
35.0	1231333.333
60.0	1060666.667
120.0	1037333.333

MEASURE

MSMPR.N(28)

0.0	2894000.0
3.0	2191000.0
10.0	1662666.667
20.0	1348333.333
35.0	1173333.333
60.0	909333.3333
120.0	909333.3333

MEASURE

MSMPR.N(29)

0.0	3796000.0
3.0	2583666.667
10.0	1946666.667
20.0	1596666.667
35.0	1387333.333
60.0	1235333.333
120.0	1088000.0

MEASURE

MSMPR.N(30)

0.0	5229000.0
3.0	3593666.667
10.0	2719666.667
20.0	1997000.0
35.0	1732666.667
60.0	1546000.0
120.0	1301333.333

MEASURE

MSMPR.N(31)

0.0	5380666.667
3.0	4689333.333
10.0	3733666.667
20.0	2898333.333
35.0	2285333.333
60.0	2152333.333
120.0	2020000.0

MEASURE

MSMPR.N(32)

0.0	3970666.667
3.0	4367000.0
10.0	4184333.333
20.0	3679333.333
35.0	3585666.667
60.0	3193666.667
120.0	2878666.667

MEASURE

MSMPR.N(33)

0.0	1099333.333
3.0	2024000.0
10.0	3081000.0
20.0	3286333.333
35.0	3617000.0
60.0	3353000.0
120.0	3469333.333

MEASURE

MSMPR.N(34)

0.0	140000.0
3.0	311000.0
10.0	777000.0
20.0	1165333.333
35.0	1651000.0
60.0	1962000.0
120.0	1981333.333

MEASURE

MSMPR.N(35)

0.0	27333.33333
3.0	27333.33333
10.0	31333.33333
20.0	85666.66667
35.0	209666.6667
60.0	283666.6667
120.0	353666.6667

MEASURE

MSMPR.N(36)

0.0	8000.0
3.0	11666.66667
10.0	8000.0
20.0	8000.0
35.0	0.0
60.0	7666.666667

120.0 15666.66667

MEASURE

MSMPR.N(37)

0.0	0.0
3.0	0.0
10.0	0.0
20.0	0.0
35.0	0.0
60.0	0.0
120.0	0.0

MEASURE

THERMO.pH

0.0	7.45
3.0	7.44
10.0	7.42
20.0	7.4
35.0	7.38
60.0	7.36
120.0	7.33

SI04_30/09/10
PROCESS MSMPR

INITIAL_CONDITION

MSMPR.N(1) 5000000.0
MSMPR.N(2) 5000000.0
MSMPR.N(3) 5000000.0
MSMPR.N(4) 5000000.0
MSMPR.N(5) 5000000.0
MSMPR.N(6) 5000000.0
MSMPR.N(7) 5000000.0
MSMPR.N(8) 5000000.0
MSMPR.N(9) 5000000.0
MSMPR.N(10) 5000000.0
MSMPR.N(11) 5000000.0
MSMPR.N(12) 5000000.0
MSMPR.N(13) 5000000.0
MSMPR.N(14) 5000000.0
MSMPR.N(15) 5000000.0
MSMPR.N(16) 5000000.0
MSMPR.N(17) 5000000.0
MSMPR.N(18) 5000000.0
MSMPR.N(19) 5000000.0
MSMPR.N(20) 5000000.0
MSMPR.N(21) 5000000.0
MSMPR.N(22) 5000000.0
MSMPR.N(23) 5000000.0
MSMPR.N(24) 8586333.333
MSMPR.N(25) 5723000.0
MSMPR.N(26) 4899333.333
MSMPR.N(27) 4463666.667
MSMPR.N(28) 4596000.0
MSMPR.N(29) 5866666.667
MSMPR.N(30) 7078666.667
MSMPR.N(31) 6818000.0
MSMPR.N(32) 2711666.667
MSMPR.N(33) 287333.3333
MSMPR.N(34) 35000.0
MSMPR.N(35) 31000.0
MSMPR.N(36) 11666.66667
MSMPR.N(37) 0.0
Thermo.V_NaOH_added 0.0085

MEASURE

MSMPR.N(24)
0.0 8586333.333
5.0 1.490733333E7
10.0 1.4895E7
20.0 1.465066667E7
35.0 1.6663E7
60.0 1.095233333E7
120.0 2.536166667E7

MEASURE

MSMPR.N(25)
0.0 5723000.0
5.0 9868000.0

10.0	9538000.0
20.0	8865666.667
35.0	1.0043E7
60.0	5023333.333
120.0	5046666.667

MEASURE

MSMPR.N(26)

0.0	4899333.333
5.0	7343000.0
10.0	6080000.0
20.0	6266666.667
35.0	6476333.333
60.0	3333333.333
120.0	3551000.0

MEASURE

MSMPR.N(27)

0.0	4463666.667
5.0	4631333.333
10.0	4281000.0
20.0	3725666.667
35.0	3757000.0
60.0	2362000.0
120.0	2622333.333

MEASURE

MSMPR.N(28)

0.0	4596000.0
5.0	3523666.667
10.0	2762666.667
20.0	2509333.333
35.0	2867333.333
60.0	1927000.0
120.0	2055333.333

MEASURE

MSMPR.N(29)

0.0	5866666.667
5.0	3655666.667
10.0	2774000.0
20.0	2327000.0
35.0	2194666.667
60.0	2035666.667
120.0	2292000.0

MEASURE

MSMPR.N(30)

0.0	7078666.667
5.0	4992333.333
10.0	3663666.667
20.0	2789666.667
35.0	2381666.667
60.0	2455333.333
120.0	2847666.667

MEASURE

MSMPR.N(31)

0.0	6818000.0
5.0	6507666.667
10.0	5509000.0
20.0	4203666.667
35.0	4075666.667
60.0	3609000.0
120.0	3652000.0

MEASURE

MSMPR.N(32)

0.0	2711666.667
5.0	6080000.0
10.0	6313333.333
20.0	5664333.333
35.0	5365333.333
60.0	5206000.0
120.0	5128333.333

MEASURE

MSMPR.N(33)

0.0	287333.3333
5.0	1814333.333
10.0	3111666.667
20.0	4491000.0
35.0	4895000.0
60.0	5406000.0
120.0	4695000.0

MEASURE

MSMPR.N(34)

0.0	35000.0
5.0	109000.0
10.0	361333.3333
20.0	808333.3333
35.0	1301333.333
60.0	1744333.333
120.0	1698000.0

MEASURE

MSMPR.N(35)

0.0	31000.0
5.0	7666.666667
10.0	15666.66667
20.0	38666.66667
35.0	62333.33333
60.0	97333.33333
120.0	140333.3333

MEASURE

MSMPR.N(36)

0.0	11666.66667
5.0	12000.0
10.0	0.0
20.0	4000.0
35.0	4000.0
60.0	23333.33333

120.0 8000.0

MEASURE

MSMPR.N(37)

0.0	0.0
5.0	0.0
10.0	0.0
20.0	0.0
35.0	0.0
60.0	0.0
120.0	0.0

MEASURE

THERMO.pH

0.0	7.49
5.0	7.48
10.0	7.46
20.0	7.44
35.0	7.42
60.0	7.4
120.0	7.38

SI04_29/09/10a

PROCESS MSMPR

INITIAL_CONDITION

MSMPR.N(1) 5000000.0
MSMPR.N(2) 5000000.0
MSMPR.N(3) 5000000.0
MSMPR.N(4) 5000000.0
MSMPR.N(5) 5000000.0
MSMPR.N(6) 5000000.0
MSMPR.N(7) 5000000.0
MSMPR.N(8) 5000000.0
MSMPR.N(9) 5000000.0
MSMPR.N(10) 5000000.0
MSMPR.N(11) 5000000.0
MSMPR.N(12) 5000000.0
MSMPR.N(13) 5000000.0
MSMPR.N(14) 5000000.0
MSMPR.N(15) 5000000.0
MSMPR.N(16) 5000000.0
MSMPR.N(17) 5000000.0
MSMPR.N(18) 5000000.0
MSMPR.N(19) 5000000.0
MSMPR.N(20) 5000000.0
MSMPR.N(21) 5000000.0
MSMPR.N(22) 5000000.0
MSMPR.N(23) 5000000.0
MSMPR.N(24) 5082000.0
MSMPR.N(25) 4759333.333
MSMPR.N(26) 4102333.333
MSMPR.N(27) 4071333.333
MSMPR.N(28) 4499000.0
MSMPR.N(29) 5975000.0
MSMPR.N(30) 7238000.0
MSMPR.N(31) 6662666.667
MSMPR.N(32) 2859333.333
MSMPR.N(33) 353666.6667
MSMPR.N(34) 27000.0
MSMPR.N(35) 0.0
MSMPR.N(36) 0.0
MSMPR.N(37) 0.0
Thermo.V_NaOH_added 0.0085

MEASURE

MSMPR.N(24)
0.0 5082000.0
3.0 6241500.0
10.0 6876666.667
20.0 6216000.0
35.0 1.016333333E7
60.0 6932000.0
110.0 1.841825E7

MEASURE

MSMPR.N(25)
0.0 4759333.333
3.0 3607500.0

10.0	2560333.333
20.0	2346666.667
35.0	4654333.333
60.0	2462500.0
110.0	1.04345E7

MEASURE

MSMPR.N(26)

0.0	4102333.333
3.0	2972000.0
10.0	2319333.333
20.0	2094333.333
35.0	3415000.0
60.0	2031000.0
110.0	7080500.0

MEASURE

MSMPR.N(27)

0.0	4071333.333
3.0	3024500.0
10.0	2140666.667
20.0	1884000.0
35.0	2443666.667
60.0	1803750.0
110.0	4373500.0

MEASURE

MSMPR.N(28)

0.0	4499000.0
3.0	2954500.0
10.0	2366000.0
20.0	1841666.667
35.0	2183333.333
60.0	1605500.0
110.0	2940000.0

MEASURE

MSMPR.N(29)

0.0	5975000.0
3.0	3980000.0
10.0	2572000.0
20.0	2311666.667
35.0	2144666.667
60.0	2060000.0
110.0	2494250.0

MEASURE

MSMPR.N(30)

0.0	7238000.0
3.0	5478000.0
10.0	3928000.0
20.0	2991333.333
35.0	2843666.667
60.0	2529250.0
110.0	2937250.0

MEASURE

MSMPR.N(31)
0.0 6662666.667
3.0 6253000.0
10.0 5571000.0
20.0 4429000.0
35.0 4254000.0
60.0 3683000.0
110.0 3834500.0

MEASURE
MSMPR.N(32)
0.0 2859333.333
3.0 4982500.0
10.0 6352000.0
20.0 5925000.0
35.0 5583000.0
60.0 4909750.0
110.0 5282750.0

MEASURE
MSMPR.N(33)
0.0 353666.6667
3.0 1148000.0
10.0 2906000.0
20.0 3811333.333
35.0 4386333.333
60.0 4545750.0
110.0 4592000.0

MEASURE
MSMPR.N(34)
0.0 27000.0
3.0 58000.0
10.0 256333.3333
20.0 610000.0
35.0 909000.0
60.0 1270500.0
110.0 1591000.0

MEASURE
MSMPR.N(35)
0.0 0.0
3.0 6000.0
10.0 4000.0
20.0 31333.33333
35.0 62333.33333
60.0 64000.0
110.0 128250.0

MEASURE
MSMPR.N(36)
0.0 0.0
3.0 0.0
10.0 0.0
20.0 4000.0
35.0 0.0
60.0 0.0

110.0 3000.0

MEASURE

MSMPR.N(37)

0.0	0.0
3.0	0.0
10.0	0.0
20.0	0.0
35.0	0.0
60.0	0.0
110.0	0.0

MEASURE

THERMO.pH

0.0	7.49
3.0	7.48
10.0	7.46
20.0	7.44
35.0	7.42
60.0	7.4
110.0	7.38

SI04_29/09/10b
PROCESS MSMPR

INITIAL_CONDITION

MSMPR.N(1) 5000000.0
MSMPR.N(2) 5000000.0
MSMPR.N(3) 5000000.0
MSMPR.N(4) 5000000.0
MSMPR.N(5) 5000000.0
MSMPR.N(6) 5000000.0
MSMPR.N(7) 5000000.0
MSMPR.N(8) 5000000.0
MSMPR.N(9) 5000000.0
MSMPR.N(10) 5000000.0
MSMPR.N(11) 5000000.0
MSMPR.N(12) 5000000.0
MSMPR.N(13) 5000000.0
MSMPR.N(14) 5000000.0
MSMPR.N(15) 5000000.0
MSMPR.N(16) 5000000.0
MSMPR.N(17) 5000000.0
MSMPR.N(18) 5000000.0
MSMPR.N(19) 5000000.0
MSMPR.N(20) 5000000.0
MSMPR.N(21) 5000000.0
MSMPR.N(22) 5000000.0
MSMPR.N(23) 5000000.0
MSMPR.N(24) 7319000.0
MSMPR.N(25) 4957000.0
MSMPR.N(26) 4215333.333
MSMPR.N(27) 3935333.333
MSMPR.N(28) 4638333.333
MSMPR.N(29) 5660333.333
MSMPR.N(30) 7381333.333
MSMPR.N(31) 6880333.333
MSMPR.N(32) 3236333.333
MSMPR.N(33) 668333.3333
MSMPR.N(34) 388333.3333
MSMPR.N(35) 35000.0
MSMPR.N(36) 7666.666667
MSMPR.N(37) 0.0
Thermo.V_NaOH_added 0.0085

MEASURE

MSMPR.N(24)
0.0 7319000.0
3.0 8294666.667
10.0 8177666.667
20.0 8889000.0
35.0 8768333.333
60.0 8415000.0
120.0 9646666.667

MEASURE

MSMPR.N(25)
0.0 4957000.0
3.0 4312333.333

10.0	3259666.667
20.0	3469000.0
35.0	3120000.0
60.0	3030333.333
120.0	3621000.0

MEASURE

MSMPR.N(26)

0.0	4215333.333
3.0	3729333.333
10.0	2719666.667
20.0	2560333.333
35.0	2564000.0
60.0	2121333.333
120.0	2602666.667

MEASURE

MSMPR.N(27)

0.0	3935333.333
3.0	3069333.333
10.0	2342666.667
20.0	2140666.667
35.0	1930000.0
60.0	1965666.667
120.0	2167666.667

MEASURE

MSMPR.N(28)

0.0	4638333.333
3.0	3190000.0
10.0	2455333.333
20.0	2144666.667
35.0	1977333.333
60.0	2036000.0
120.0	2031666.667

MEASURE

MSMPR.N(29)

0.0	5660333.333
3.0	4130000.0
10.0	3158333.333
20.0	2568333.333
35.0	2319666.667
60.0	2338666.667
120.0	2397000.0

MEASURE

MSMPR.N(30)

0.0	7381333.333
3.0	5680000.0
10.0	4825333.333
20.0	3527666.667
35.0	3282666.667
60.0	3123333.333
120.0	3314000.0

MEASURE

MSMPR.N(31)
0.0 6880333.333
3.0 6993000.0
10.0 6091666.667
20.0 5124333.333
35.0 4755666.667
60.0 4534000.0
120.0 4599666.667

MEASURE

MSMPR.N(32)
0.0 3236333.333
3.0 5555666.667
10.0 6499666.667
20.0 6406666.667
35.0 6344333.333
60.0 5711333.333
120.0 5392666.667

MEASURE

MSMPR.N(33)
0.0 668333.3333
3.0 1348000.0
10.0 2591333.333
20.0 3683000.0
35.0 4293000.0
60.0 4098333.333
120.0 4130000.0

MEASURE

MSMPR.N(34)
0.0 388333.3333
3.0 73666.66667
10.0 396333.3333
20.0 489333.3333
35.0 765333.3333
60.0 1010000.0
120.0 1429333.333

MEASURE

MSMPR.N(35)
0.0 35000.0
3.0 27000.0
10.0 23333.33333
20.0 19333.33333
35.0 19333.33333
60.0 54333.33333
120.0 97000.0

MEASURE

MSMPR.N(36)
0.0 7666.666667
3.0 0.0
10.0 4000.0
20.0 4000.0
35.0 4000.0
60.0 7666.666667

120.0 4000.0

MEASURE

MSMPR.N(37)

0.0	0.0
3.0	0.0
10.0	0.0
20.0	0.0
35.0	0.0
60.0	0.0
120.0	0.0

MEASURE

THERMO.pH

0.0	7.49
3.0	7.48
10.0	7.46
20.0	7.44
35.0	7.42
60.0	7.4
120.0	7.38

SI04_26/10/10

PROCESS MSMPR

INITIAL_CONDITION

MSMPR.N(1) 5000000.0
MSMPR.N(2) 5000000.0
MSMPR.N(3) 5000000.0
MSMPR.N(4) 5000000.0
MSMPR.N(5) 5000000.0
MSMPR.N(6) 5000000.0
MSMPR.N(7) 5000000.0
MSMPR.N(8) 5000000.0
MSMPR.N(9) 5000000.0
MSMPR.N(10) 5000000.0
MSMPR.N(11) 5000000.0
MSMPR.N(12) 5000000.0
MSMPR.N(13) 5000000.0
MSMPR.N(14) 5000000.0
MSMPR.N(15) 5000000.0
MSMPR.N(16) 5000000.0
MSMPR.N(17) 5000000.0
MSMPR.N(18) 5000000.0
MSMPR.N(19) 5000000.0
MSMPR.N(20) 5000000.0
MSMPR.N(21) 5000000.0
MSMPR.N(22) 5000000.0
MSMPR.N(23) 5000000.0
MSMPR.N(24) 5000000.0
MSMPR.N(25) 4192000.0
MSMPR.N(26) 4032666.667
MSMPR.N(27) 4693333.333
MSMPR.N(28) 6150000.0
MSMPR.N(29) 8485000.0
MSMPR.N(30) 9794333.333
MSMPR.N(31) 8096333.333
MSMPR.N(32) 2944666.667
MSMPR.N(33) 489666.6667
MSMPR.N(34) 186666.6667
MSMPR.N(35) 19333.33333
MSMPR.N(36) 15666.66667
MSMPR.N(37) 0.0
Thermo.V_NaOH_added 0.0085

MEASURE

MSMPR.N(25)
0.0 4192000.0
3.0 2428000.0
10.0 2475000.0
20.0 1969666.667
35.0 1962000.0
60.0 1958000.0
120.0 2063000.0

MEASURE

MSMPR.N(26)
0.0 4032666.667
3.0 2964333.333

10.0	2498333.333
20.0	1934666.667
35.0	1795000.0
60.0	1880333.333
120.0	1787000.0

MEASURE

MSMPR.N(27)

0.0	4693333.333
3.0	3593666.667
10.0	2711666.667
20.0	2389333.333
35.0	2276666.667
60.0	2074666.667
120.0	2001000.0

MEASURE

MSMPR.N(28)

0.0	6150000.0
3.0	4751333.333
10.0	3702666.667
20.0	2813000.0
35.0	3030333.333
60.0	2688333.333
120.0	2517333.333

MEASURE

MSMPR.N(29)

0.0	8485000.0
3.0	6888333.333
10.0	5509000.0
20.0	4126000.0
35.0	4126000.0
60.0	3815333.333
120.0	3411000.0

MEASURE

MSMPR.N(30)

0.0	9794333.333
3.0	9518333.333
10.0	7509666.667
20.0	6729000.0
35.0	5874000.0
60.0	5489666.667
120.0	5089333.333

MEASURE

MSMPR.N(31)

0.0	8096333.333
3.0	1.001166667E7
10.0	9930333.333
20.0	8656000.0
35.0	8127666.667
60.0	7618333.333
120.0	6868666.667

MEASURE

MSMPR.N(32)
0.0 2944666.667
3.0 4996333.333
10.0 7094333.333
20.0 8135333.333
35.0 8011000.0
60.0 8271333.333
120.0 7933000.0

MEASURE

MSMPR.N(33)
0.0 489666.6667
3.0 761333.3333
10.0 1666666.667
20.0 2544666.667
35.0 3582000.0
60.0 4413333.333
120.0 4335666.667

MEASURE

MSMPR.N(34)
0.0 186666.6667
3.0 89333.33333
10.0 132333.3333
20.0 198333.3333
35.0 376666.6667
60.0 509000.0
120.0 625333.3333

MEASURE

MSMPR.N(35)
0.0 19333.33333
3.0 11666.66667
10.0 19666.66667
20.0 19333.33333
35.0 19666.66667
60.0 15666.66667
120.0 27333.33333

MEASURE

MSMPR.N(36)
0.0 15666.66667
3.0 0.0
10.0 0.0
20.0 0.0
35.0 15666.66667
60.0 7666.666667
120.0 0.0

MEASURE

MSMPR.N(37)
0.0 0.0
3.0 0.0
10.0 0.0
20.0 0.0
35.0 0.0
60.0 0.0

120.0 0.0

MEASURE

THERMO.C_T_Mg

0.0	5105.0
3.0	5070.0
10.0	5002.0
20.0	4929.0
35.0	4909.0
60.0	4805.0
120.0	4831.0

MEASURE

THERMO.pH

0.0	7.49
3.0	7.47
10.0	7.44
20.0	7.41
35.0	7.39
60.0	7.37
120.0	7.34

SI05_18/10/10a

PROCESS MSMPR

INITIAL_CONDITION

MSMPR.N(1) 5000000.0
MSMPR.N(2) 5000000.0
MSMPR.N(3) 5000000.0
MSMPR.N(4) 5000000.0
MSMPR.N(5) 5000000.0
MSMPR.N(6) 5000000.0
MSMPR.N(7) 5000000.0
MSMPR.N(8) 5000000.0
MSMPR.N(9) 5000000.0
MSMPR.N(10) 5000000.0
MSMPR.N(11) 5000000.0
MSMPR.N(12) 5000000.0
MSMPR.N(13) 5000000.0
MSMPR.N(14) 5000000.0
MSMPR.N(15) 5000000.0
MSMPR.N(16) 5000000.0
MSMPR.N(17) 5000000.0
MSMPR.N(18) 5000000.0
MSMPR.N(19) 5000000.0
MSMPR.N(20) 5000000.0
MSMPR.N(21) 5000000.0
MSMPR.N(22) 5000000.0
MSMPR.N(23) 5000000.0
MSMPR.N(24) 2175666.667
MSMPR.N(25) 1713333.333
MSMPR.N(26) 2545000.0
MSMPR.N(27) 2405000.0
MSMPR.N(28) 2525333.333
MSMPR.N(29) 3349333.333
MSMPR.N(30) 3819333.333
MSMPR.N(31) 4732000.0
MSMPR.N(32) 4378333.333
MSMPR.N(33) 1600333.333
MSMPR.N(34) 124333.3333
MSMPR.N(35) 23333.33333
MSMPR.N(36) 0.0
MSMPR.N(37) 0.0
Thermo.V_NaOH_added 0.009

MEASURE

MSMPR.N(24)
0.0 2175666.667
3.0 2739000.0
6.0 2265000.0
12.0 1896000.0

MEASURE

MSMPR.N(25)
0.0 1713333.333
3.0 1849333.333
6.0 1624000.0
12.0 1456666.667

MEASURE

MSMPR.N(26)

0.0	2545000.0
3.0	2486666.667
6.0	2164000.0
12.0	2001000.0

MEASURE

MSMPR.N(27)

0.0	2405000.0
3.0	2303666.667
6.0	1938666.667
12.0	1810666.667

MEASURE

MSMPR.N(28)

0.0	2525333.333
3.0	1841666.667
6.0	1791000.0
12.0	1476333.333

MEASURE

MSMPR.N(29)

0.0	3349333.333
3.0	1911333.333
6.0	1725000.0
12.0	1767666.667

MEASURE

MSMPR.N(30)

0.0	3819333.333
3.0	2261333.333
6.0	1849333.333
12.0	1476333.333

MEASURE

MSMPR.N(31)

0.0	4732000.0
3.0	2785666.667
6.0	1985333.333
12.0	1367666.667

MEASURE

MSMPR.N(32)

0.0	4378333.333
3.0	3415000.0
6.0	2799000.0
12.0	1845333.333

MEASURE

MSMPR.N(33)

0.0	1600333.333
3.0	3582000.0
6.0	3294666.667
12.0	2432000.0

MEASURE

MSMPR.N(34)

0.0	124333.3333
3.0	1476666.667
6.0	2548666.667
12.0	3112000.0

MEASURE

MSMPR.N(35)

0.0	23333.33333
3.0	89333.33333
6.0	485666.6667
12.0	1173333.333

MEASURE

MSMPR.N(36)

0.0	0.0
3.0	8000.0
6.0	11666.66667
12.0	58333.33333

MEASURE

MSMPR.N(37)

0.0	0.0
3.0	0.0
6.0	0.0
12.0	0.0

MEASURE

THERMO.pH

0.0	7.64
3.0	7.62
6.0	7.59
12.0	7.56

SI05_18/10/10b

PROCESS MSMPR

INITIAL_CONDITION

MSMPR.N(1) 5000000.0
MSMPR.N(2) 5000000.0
MSMPR.N(3) 5000000.0
MSMPR.N(4) 5000000.0
MSMPR.N(5) 5000000.0
MSMPR.N(6) 5000000.0
MSMPR.N(7) 5000000.0
MSMPR.N(8) 5000000.0
MSMPR.N(9) 5000000.0
MSMPR.N(10) 5000000.0
MSMPR.N(11) 5000000.0
MSMPR.N(12) 5000000.0
MSMPR.N(13) 5000000.0
MSMPR.N(14) 5000000.0
MSMPR.N(15) 5000000.0
MSMPR.N(16) 5000000.0
MSMPR.N(17) 5000000.0
MSMPR.N(18) 5000000.0
MSMPR.N(19) 5000000.0
MSMPR.N(20) 5000000.0
MSMPR.N(21) 5000000.0
MSMPR.N(22) 5000000.0
MSMPR.N(23) 5000000.0
MSMPR.N(24) 2665000.0
MSMPR.N(25) 2436000.0
MSMPR.N(26) 2521666.667
MSMPR.N(27) 2618666.667
MSMPR.N(28) 3076666.667
MSMPR.N(29) 3714000.0
MSMPR.N(30) 4860000.0
MSMPR.N(31) 4522000.0
MSMPR.N(32) 1534666.667
MSMPR.N(33) 225333.3333
MSMPR.N(34) 11666.66667
MSMPR.N(35) 15666.66667
MSMPR.N(36) 0.0
MSMPR.N(37) 0.0
Thermo.V_NaOH_added 0.009

MEASURE

MSMPR.N(25)
0.0 2665000.0
3.0 2801000.0
8.0 2406500.0
12.0 3164000.0

MEASURE

MSMPR.N(26)
0.0 2436000.0
3.0 2478666.667
8.0 1882500.0
12.0 2535000.0

MEASURE

MSMPR.N(27)

0.0	2521666.667
3.0	1900000.0
8.0	1660500.0
12.0	1958000.0

MEASURE

MSMPR.N(28)

0.0	2618666.667
3.0	2148333.333
8.0	1579000.0
12.0	1894000.0

MEASURE

MSMPR.N(29)

0.0	3076666.667
3.0	2004333.333
8.0	1760000.0
12.0	2103500.0

MEASURE

MSMPR.N(30)

0.0	3714000.0
3.0	2463000.0
8.0	1835500.0
12.0	2418500.0

MEASURE

MSMPR.N(31)

0.0	4860000.0
3.0	2785333.333
8.0	2383500.0
12.0	2476500.0

MEASURE

MSMPR.N(32)

0.0	4522000.0
3.0	3695000.0
8.0	3024500.0
12.0	2750500.0

MEASURE

MSMPR.N(33)

0.0	1534666.667
3.0	3477000.0
8.0	3432500.0
12.0	3578000.0

MEASURE

MSMPR.N(34)

0.0	225333.3333
3.0	1383000.0
8.0	2832500.0
12.0	3514000.0

MEASURE

MSMPR.N(35)

0.0	11666.66667
3.0	97333.33333
8.0	699500.0
12.0	1393000.0

MEASURE

MSMPR.N(36)

0.0	15666.66667
3.0	27000.0
8.0	70000.0
12.0	198500.0

MEASURE

MSMPR.N(37)

0.0	0.0
3.0	0.0
8.0	0.0
12.0	0.0

MEASURE

THERMO.pH

0.0	7.62
3.0	7.6
8.0	7.56
12.0	7.54

SI05_15/09/10

PROCESS MSMPR

INITIAL_CONDITION

MSMPR.N(1) 5000000.0
MSMPR.N(2) 5000000.0
MSMPR.N(3) 5000000.0
MSMPR.N(4) 5000000.0
MSMPR.N(5) 5000000.0
MSMPR.N(6) 5000000.0
MSMPR.N(7) 5000000.0
MSMPR.N(8) 5000000.0
MSMPR.N(9) 5000000.0
MSMPR.N(10) 5000000.0
MSMPR.N(11) 5000000.0
MSMPR.N(12) 5000000.0
MSMPR.N(13) 5000000.0
MSMPR.N(14) 5000000.0
MSMPR.N(15) 5000000.0
MSMPR.N(16) 5000000.0
MSMPR.N(17) 5000000.0
MSMPR.N(18) 5000000.0
MSMPR.N(19) 5000000.0
MSMPR.N(20) 5000000.0
MSMPR.N(21) 5000000.0
MSMPR.N(22) 5000000.0
MSMPR.N(23) 5000000.0
MSMPR.N(24) 3605333.333
MSMPR.N(25) 3737333.333
MSMPR.N(26) 3881000.0
MSMPR.N(27) 4355000.0
MSMPR.N(28) 5521000.0
MSMPR.N(29) 6853000.0
MSMPR.N(30) 7676666.667
MSMPR.N(31) 6134666.667
MSMPR.N(32) 1678333.333
MSMPR.N(33) 163333.3333
MSMPR.N(34) 38666.66667
MSMPR.N(35) 0.0
MSMPR.N(36) 4000.0
MSMPR.N(37) 0.0
Thermo.V_NaOH_added 0.009

MEASURE

MSMPR.N(24)
0.0 3605333.333
3.0 4673666.667
6.0 5777000.0
10.0 6870500.0

MEASURE

MSMPR.N(25)
0.0 3737333.333
3.0 2925333.333
6.0 4114333.333
10.0 2861500.0

MEASURE

MSMPR.N(26)

0.0	3881000.0
3.0	2770333.333
6.0	2882666.667
10.0	1917000.0

MEASURE

MSMPR.N(27)

0.0	4355000.0
3.0	2680666.667
6.0	2665333.333
10.0	1579500.0

MEASURE

MSMPR.N(28)

0.0	5521000.0
3.0	2727000.0
6.0	2435666.667
10.0	1363500.0

MEASURE

MSMPR.N(29)

0.0	6853000.0
3.0	3259666.667
6.0	2443666.667
10.0	1497500.0

MEASURE

MSMPR.N(30)

0.0	7676666.667
3.0	4180666.667
6.0	2774000.0
10.0	1730500.0

MEASURE

MSMPR.N(31)

0.0	6134666.667
3.0	5069666.667
6.0	3500333.333
10.0	2436000.0

MEASURE

MSMPR.N(32)

0.0	1678333.333
3.0	4654000.0
6.0	4025000.0
10.0	3677000.0

MEASURE

MSMPR.N(33)

0.0	163333.3333
3.0	2117333.333
6.0	3298666.667
10.0	4044000.0

MEASURE

MSMPR.N(34)

0.0	38666.66667
3.0	279666.6667
6.0	1045333.333
10.0	1975500.0

MEASURE

MSMPR.N(35)

0.0	0.0
3.0	38666.66667
6.0	66333.33333
10.0	262000.0

MEASURE

MSMPR.N(36)

0.0	4000.0
3.0	4000.0
6.0	7666.666667
10.0	6000.0

MEASURE

MSMPR.N(37)

0.0	0.0
3.0	0.0
6.0	0.0
10.0	0.0

MEASURE

THERMO.pH

0.0	7.68
3.0	7.64
6.0	7.6
10.0	7.56

SI05_28/09/10

PROCESS MSMPR

INITIAL_CONDITION

MSMPR.N(1) 5000000.0
MSMPR.N(2) 5000000.0
MSMPR.N(3) 5000000.0
MSMPR.N(4) 5000000.0
MSMPR.N(5) 5000000.0
MSMPR.N(6) 5000000.0
MSMPR.N(7) 5000000.0
MSMPR.N(8) 5000000.0
MSMPR.N(9) 5000000.0
MSMPR.N(10) 5000000.0
MSMPR.N(11) 5000000.0
MSMPR.N(12) 5000000.0
MSMPR.N(13) 5000000.0
MSMPR.N(14) 5000000.0
MSMPR.N(15) 5000000.0
MSMPR.N(16) 5000000.0
MSMPR.N(17) 5000000.0
MSMPR.N(18) 5000000.0
MSMPR.N(19) 5000000.0
MSMPR.N(20) 5000000.0
MSMPR.N(21) 5000000.0
MSMPR.N(22) 5000000.0
MSMPR.N(23) 5000000.0
MSMPR.N(24) 2665000.0
MSMPR.N(25) 3138333.333
MSMPR.N(26) 3349000.0
MSMPR.N(27) 3279333.333
MSMPR.N(28) 3769333.333
MSMPR.N(29) 4938000.0
MSMPR.N(30) 6309333.333
MSMPR.N(31) 6519000.0
MSMPR.N(32) 4102666.667
MSMPR.N(33) 610000.0
MSMPR.N(34) 39000.0
MSMPR.N(35) 19333.33333
MSMPR.N(36) 0.0
MSMPR.N(37) 0.0
Thermo.V_NaOH_added 0.009

MEASURE

MSMPR.N(25)
0.0 3138333.333
3.0 2944000.0
7.0 2058333.333
10.0 1795000.0
15.0 1989000.0

MEASURE

MSMPR.N(26)
0.0 3349000.0
3.0 2628000.0
7.0 2004666.667
10.0 1585000.0

15.0 1686000.0

MEASURE

MSMPR.N(27)

0.0 3279333.333
3.0 2430000.0
7.0 1597000.0
10.0 1591000.0
15.0 1196666.667

MEASURE

MSMPR.N(28)

0.0 3769333.333
3.0 2360000.0
7.0 1321000.0
10.0 1095500.0
15.0 944000.0

MEASURE

MSMPR.N(29)

0.0 4938000.0
3.0 2395000.0
7.0 1383000.0
10.0 1194500.0
15.0 1018000.0

MEASURE

MSMPR.N(30)

0.0 6309333.333
3.0 3129500.0
7.0 1756000.0
10.0 1451000.0
15.0 1344333.333

MEASURE

MSMPR.N(31)

0.0 6519000.0
3.0 4277500.0
7.0 2696333.333
10.0 2243500.0
15.0 1864666.667

MEASURE

MSMPR.N(32)

0.0 4102666.667
3.0 5769000.0
7.0 4390333.333
10.0 3660000.0
15.0 3011000.0

MEASURE

MSMPR.N(33)

0.0 610000.0
3.0 3706000.0
7.0 4895333.333
10.0 4551000.0
15.0 4646666.667

MEASURE

MSMPR.N(34)

0.0	39000.0
3.0	740500.0
7.0	1958000.0
10.0	2465000.0
15.0	2984000.0

MEASURE

MSMPR.N(35)

0.0	19333.33333
3.0	70000.0
7.0	186666.6667
10.0	297000.0
15.0	369000.0

MEASURE

MSMPR.N(36)

0.0	0.0
3.0	6000.0
7.0	8000.0
10.0	12000.0
15.0	15666.66667

MEASURE

MSMPR.N(37)

0.0	0.0
3.0	0.0
7.0	0.0
10.0	0.0
15.0	0.0

MEASURE

THERMO.pH

0.0	7.66
3.0	7.6
7.0	7.54
10.0	7.52
15.0	7.5

SI05_26/10/10
PROCESS MSMPR

INITIAL_CONDITION

MSMPR.N(1) 5000000.0
MSMPR.N(2) 5000000.0
MSMPR.N(3) 5000000.0
MSMPR.N(4) 5000000.0
MSMPR.N(5) 5000000.0
MSMPR.N(6) 5000000.0
MSMPR.N(7) 5000000.0
MSMPR.N(8) 5000000.0
MSMPR.N(9) 5000000.0
MSMPR.N(10) 5000000.0
MSMPR.N(11) 5000000.0
MSMPR.N(12) 5000000.0
MSMPR.N(13) 5000000.0
MSMPR.N(14) 5000000.0
MSMPR.N(15) 5000000.0
MSMPR.N(16) 5000000.0
MSMPR.N(17) 5000000.0
MSMPR.N(18) 5000000.0
MSMPR.N(19) 5000000.0
MSMPR.N(20) 5000000.0
MSMPR.N(21) 5000000.0
MSMPR.N(22) 5000000.0
MSMPR.N(23) 5000000.0
MSMPR.N(24) 5000000.0
MSMPR.N(25) 8422666.667
MSMPR.N(26) 6643666.667
MSMPR.N(27) 5668333.333
MSMPR.N(28) 5956000.0
MSMPR.N(29) 8283000.0
MSMPR.N(30) 9763333.333
MSMPR.N(31) 8842333.333
MSMPR.N(32) 3601333.333
MSMPR.N(33) 357333.3333
MSMPR.N(34) 69666.66667
MSMPR.N(35) 31000.0
MSMPR.N(36) 0.0
MSMPR.N(37) 0.0
Thermo.V_NaOH_added 0.009

MEASURE

MSMPR.N(26)
0.0 6643666.667
3.0 2886666.667
6.0 4514666.667
10.0 5101333.333
15.0 2919500.0

MEASURE

MSMPR.N(27)
0.0 5668333.333
3.0 2517666.667
6.0 2894333.333
10.0 3333333.333

15.0 2069000.0

MEASURE

MSMPR.N(28)

0.0 5956000.0
3.0 2684666.667
6.0 2789333.333
10.0 2443666.667
15.0 1515000.0

MEASURE

MSMPR.N(29)

0.0 8283000.0
3.0 3772333.333
6.0 2774000.0
10.0 2284333.333
15.0 1620000.0

MEASURE

MSMPR.N(30)

0.0 9763333.333
3.0 5229333.333
6.0 3562666.667
10.0 2700333.333
15.0 2068500.0

MEASURE

MSMPR.N(31)

0.0 8842333.333
3.0 7230333.333
6.0 5485666.667
10.0 3679000.0
15.0 3572500.0

MEASURE

MSMPR.N(32)

0.0 3601333.333
3.0 7397000.0
6.0 7404666.667
10.0 6115000.0
15.0 5810000.0

MEASURE

MSMPR.N(33)

0.0 357333.3333
3.0 2844000.0
6.0 4732333.333
10.0 5613666.667
15.0 6049000.0

MEASURE

MSMPR.N(34)

0.0 69666.66667
3.0 268333.3333
6.0 866333.3333
10.0 1406666.667
15.0 1993000.0

MEASURE

MSMPR.N(35)

0.0	31000.0
3.0	19333.33333
6.0	42666.66667
10.0	81666.66667
15.0	140500.0

MEASURE

MSMPR.N(36)

0.0	0.0
3.0	7666.66667
6.0	11666.66667
10.0	4000.0
15.0	6000.0

MEASURE

MSMPR.N(37)

0.0	0.0
3.0	0.0
6.0	0.0
10.0	0.0
15.0	0.0

MEASURE

THERMO.C_T_Mg

0.0	4849.0
3.0	4527.0
6.0	4761.0
10.0	4706.0
15.0	4704.0

MEASURE

THERMO.pH

0.0	7.65
3.0	7.58
6.0	7.54
10.0	7.5
15.0	7.48

SI05_23/09/10
PROCESS MSMPR

INITIAL_CONDITION

MSMPR.N(1) 5000000.0
MSMPR.N(2) 5000000.0
MSMPR.N(3) 5000000.0
MSMPR.N(4) 5000000.0
MSMPR.N(5) 5000000.0
MSMPR.N(6) 5000000.0
MSMPR.N(7) 5000000.0
MSMPR.N(8) 5000000.0
MSMPR.N(9) 5000000.0
MSMPR.N(10) 5000000.0
MSMPR.N(11) 5000000.0
MSMPR.N(12) 5000000.0
MSMPR.N(13) 5000000.0
MSMPR.N(14) 5000000.0
MSMPR.N(15) 5000000.0
MSMPR.N(16) 5000000.0
MSMPR.N(17) 5000000.0
MSMPR.N(18) 5000000.0
MSMPR.N(19) 5000000.0
MSMPR.N(20) 5000000.0
MSMPR.N(21) 5000000.0
MSMPR.N(22) 5000000.0
MSMPR.N(23) 5000000.0
MSMPR.N(24) 1.850833333E7
MSMPR.N(25) 1.621233333E7
MSMPR.N(26) 1.179866667E7
MSMPR.N(27) 7479000.0
MSMPR.N(28) 4561333.333
MSMPR.N(29) 3764666.667
MSMPR.N(30) 4530000.0
MSMPR.N(31) 5392666.667
MSMPR.N(32) 2769333.333
MSMPR.N(33) 392666.6667
MSMPR.N(34) 97333.33333
MSMPR.N(35) 27333.33333
MSMPR.N(36) 7666.666667
MSMPR.N(37) 0.0
Thermo.V_NaOH_added 0.009

MEASURE

MSMPR.N(24)
0.0 1.850833333E7
3.0 4063666.667
6.0 3945000.0
10.0 5190333.333
15.0 5408000.0

MEASURE

MSMPR.N(25)
0.0 1.621233333E7
3.0 2945000.0
6.0 2535000.0
10.0 2004666.667

15.0 2716000.0

MEASURE

MSMPR.N(26)

0.0 1.179866667E7
3.0 2714000.0
6.0 2313500.0
10.0 1996666.667
15.0 2180000.0

MEASURE

MSMPR.N(27)

0.0 7479000.0
3.0 2300000.0
6.0 1946500.0
10.0 1534666.667
15.0 1585000.0

MEASURE

MSMPR.N(28)

0.0 4561333.333
3.0 2354333.333
6.0 1795000.0
10.0 1460666.667
15.0 1550000.0

MEASURE

MSMPR.N(29)

0.0 3764666.667
3.0 2133333.333
6.0 1742500.0
10.0 1550000.0
15.0 1166000.0

MEASURE

MSMPR.N(30)

0.0 4530000.0
3.0 2568000.0
6.0 1894000.0
10.0 1523000.0
15.0 1317000.0

MEASURE

MSMPR.N(31)

0.0 5392666.667
3.0 3671333.333
6.0 2628000.0
10.0 2067000.0
15.0 1504000.0

MEASURE

MSMPR.N(32)

0.0 2769333.333
3.0 4557333.333
6.0 3508500.0
10.0 2917666.667
15.0 2389000.0

MEASURE

MSMPR.N(33)

0.0	392666.6667
3.0	2443666.667
6.0	3648000.0
10.0	3815000.0
15.0	3194000.0

MEASURE

MSMPR.N(34)

0.0	97333.33333
3.0	307000.0
6.0	1189000.0
10.0	2043666.667
15.0	2471000.0

MEASURE

MSMPR.N(35)

0.0	27333.33333
3.0	19666.66667
6.0	111000.0
10.0	287333.3333
15.0	478000.0

MEASURE

MSMPR.N(36)

0.0	7666.666667
3.0	19666.66667
6.0	6000.0
10.0	15666.66667
15.0	12000.0

MEASURE

MSMPR.N(37)

0.0	0.0
3.0	0.0
6.0	0.0
10.0	0.0
15.0	0.0

MEASURE

THERMO.pH

0.0	7.64
3.0	7.6
6.0	7.56
10.0	7.53
15.0	7.5

SI075_30/09/10

PROCESS MSMPR

INITIAL_CONDITION

MSMPR.N(1) 5000000.0
MSMPR.N(2) 5000000.0
MSMPR.N(3) 5000000.0
MSMPR.N(4) 5000000.0
MSMPR.N(5) 5000000.0
MSMPR.N(6) 5000000.0
MSMPR.N(7) 5000000.0
MSMPR.N(8) 5000000.0
MSMPR.N(9) 5000000.0
MSMPR.N(10) 5000000.0
MSMPR.N(11) 5000000.0
MSMPR.N(12) 5000000.0
MSMPR.N(13) 5000000.0
MSMPR.N(14) 5000000.0
MSMPR.N(15) 5000000.0
MSMPR.N(16) 5000000.0
MSMPR.N(17) 5000000.0
MSMPR.N(18) 5000000.0
MSMPR.N(19) 5000000.0
MSMPR.N(20) 5000000.0
MSMPR.N(21) 5000000.0
MSMPR.N(22) 5000000.0
MSMPR.N(23) 5000000.0
MSMPR.N(24) 5000000.0
MSMPR.N(25) 6472333.333
MSMPR.N(26) 3178000.0
MSMPR.N(27) 3150666.667
MSMPR.N(28) 3562333.333
MSMPR.N(29) 4701000.0
MSMPR.N(30) 6103333.333
MSMPR.N(31) 6962333.333
MSMPR.N(32) 3986000.0
MSMPR.N(33) 3912333.333
MSMPR.N(34) 341666.6667
MSMPR.N(35) 35000.0
MSMPR.N(36) 8000.0
MSMPR.N(37) 0.0
Thermo.V_NaOH_added 0.0095

MEASURE

MSMPR.N(25)
0.0 6472333.333
3.0 2591000.0
6.0 2708000.0

MEASURE

MSMPR.N(26)
0.0 3178000.0
3.0 2253333.333
6.0 1748333.333

MEASURE

MSMPR.N(27)

0.0 3150666.667
3.0 1868666.667
6.0 1460666.667

MEASURE

MSMPR.N(28)
0.0 3562333.333
3.0 1930666.667
6.0 1076333.333

MEASURE

MSMPR.N(29)
0.0 4701000.0
3.0 1895666.667
6.0 1107333.333

MEASURE

MSMPR.N(30)
0.0 6103333.333
3.0 2183333.333
6.0 1150000.0

MEASURE

MSMPR.N(31)
0.0 6962333.333
3.0 2661333.333
6.0 1379333.333

MEASURE

MSMPR.N(32)
0.0 3986000.0
3.0 3850000.0
6.0 1896000.0

MEASURE

MSMPR.N(33)
0.0 3912333.333
3.0 4157000.0
6.0 3341000.0

MEASURE

MSMPR.N(34)
0.0 341666.6667
3.0 1977333.333
6.0 2634000.0

MEASURE

MSMPR.N(35)
0.0 35000.0
3.0 159333.3333
6.0 749666.6667

MEASURE

MSMPR.N(36)
0.0 8000.0
3.0 4000.0
6.0 31000.0

MEASURE

MSMPR.N(37)

0.0 0.0

3.0 0.0

6.0 0.0

MEASURE

THERMO.pH

0.0 7.8

1.0 7.76

2.0 7.73

3.0 7.71

4.0 7.67

5.0 7.66

6.0 7.63

8.0 7.6

10.0 7.58

15.0 7.54

Appendix E - Experimental Procedure

Introduction

This experimental procedure is written explicitly for the work done at *Suranaree University of Technology* as part of my PhD research. However, the experimental conditions and procedures could be modified for the purposes of different research aims.

Aim

These experiments aimed to determine the particle size distribution (PSD) dynamically during the batch crystallization of struvite. These PSDs could then be used to determine kinetic parameters for struvite nucleation, crystal growth and aggregation.

Equipment

This will be separated into the equipment required for the crystallization experiment, PSD analysis and reactants required.

Equipment for the crystallization experiment:

- 1 x1L beaker with four PVC baffles (to be used as the crystallizer)
- 3 x 20-30mL beakers (to be used to pipette stock solutions)
- 3 x 10mL pipettes (one graduated, two volumetric)
- 1 x1L volumetric flask
- Distilled water wash bottle (or higher quality water)
- pH probe and meter
- Thermometer (or a pH probe and meter with Automatic Temperature Correction)
- Computer (or pen and paper if the pH meter does not log data)

- Magnetic stirrer and stirrer bar

Equipment for the PSD analysis:

- Beckman Coulter Mastersizer 4 (the procedure may need to be changed for a different particle sizer)
- 1 x 100 μ m aperture tube
- 1 x 250mL beaker (for sample)
- Wash bottle (to be filled with electrolyte)
- 1 x 250mL measuring cylinder (200mL or 150mL would also suffice)
- 1 x 30mL beaker (to take sample from crystallizer)
- 1 x volumetric flask stopper (to displace a constant volume from the sample beaker)

Reactants required:

- Magnesium Chloride ($\text{MgCl}_2 \cdot 7\text{H}_2\text{O}$)
- Ammonium Dihydrogen Phosphate ($\text{NH}_4\text{H}_2\text{PO}_4$)
- Sodium Hydroxide (NaOH)
- Hydrochloric Acid (HCl)
- Solid Struvite ($\text{MgNH}_4\text{PO}_4 \cdot 6\text{H}_2\text{O}$)
- Beckman Coulter ISOTON 2 electrolyte
- pH 7 and pH 10 buffers
- 10 μ m latex calibration beads
- Distilled or higher quality water

Experimental Procedure

This will be split into three sections; stock solutions, crystallization and sampling and analysis.

Stock Solutions

There are five stock solutions that will be required to perform the experiments:

- 0.5M Magnesium Chloride
- 0.5M Ammonium Dihydrogen Phosphate
- 0.5M Sodium Hydroxide
- 1M Hydrochloric Acid
- ISOTON 2 saturated with struvite

It is assumed that it is within the skills of the reader to make these stock solutions without details except for the saturated ISOTON 2 which will be elaborated upon here. NOTE: the 1M HCl is only used to clean glassware in between experiments so its preparation does not have to be accurate, all other solutions should be prepared with pipettes and volumetric flasks.

Before making the saturated ISOTON 2 you must have solid struvite. The solid struvite is made by the following procedure:

1. Prepare 1L of 0.005M struvite solution as per the procedure in the crystallization section
2. Add 10mL of 0.5M NaOH
3. Leave the solution the crystallize for at least 30 minutes
4. Filter. Gravity filtration with any fine grade filter paper is ok, it will take about 15-20 minutes to filter 1L of solution, vacuum filtration can be used to speed up the process.
5. Dry and store the struvite.
6. Repeat the process until enough struvite has been stockpiled. The amount of struvite required will depend heavily of how many experiments you plan to do and how often you used fresh electrolyte and recycled electrolyte.

This current procedure is incredibly wasteful as there is still enough solute in the filtrate to make more struvite. However, it is of the utmost importance that struvite is the only solid phase and this procedure has been shown to produce struvite using X-Ray Diffraction (XRD) techniques. If the procedure was to be modified to make it less wasteful then XRD would have to be used to ensure the product was struvite and not a combination of other phases.

Once the solid struvite has been prepared the electrolyte can be saturated. The saturated electrolyte is made with the following procedure:

1. Place a container with unsaturated electrolyte on a magnetic stirrer.
2. Add one teaspoon of solid struvite for every one litre of electrolyte.
3. Leave the solution for 6 hours or overnight and check the electrolyte. If the electrolyte is saturated the whole solution will appear cloudy, if the electrolyte is not yet saturated it will appear clear with individual struvite aggregates in suspension.
4. Once the electrolyte is saturated vacuum filter at $0.45\mu\text{m}$ or smaller. The electrolyte is now ready to be used in the PSD analysis.

The ISOTON 2 electrolyte is a specialised reactant that must be purchased from Beckman Coulter and is quite expensive, to conserve electrolyte it may be recycled after each experiment. It is good practice to re-saturate the electrolyte if you are recycling it, this is because distilled water left in the coulter counter from cleaning can affect the electrolyte. A lot less struvite will be required to re-saturate recycled electrolyte.

There is also the stock seed solution. This needs to have a very high solids concentration so that a small volume can be added to the crystalliser during the experiments but still have a sufficient particle concentration to be analysed by the coulter counter.

1. Prepare 1L of 0.005M struvite solution as per the procedure in the crystallization section.
2. Add 10mL of 0.5M NaOH.
3. Leave the solution to crystallise for 6 hours or overnight.
4. Allow the solution to settle.
5. Decant the solution so there is 100mL left. I used a 50mL pipette to pipette the clear solution until 100mL was left.
6. Pour the seed solution into a sealable bottle and place the seed solution on a magnetic stirrer to keep them suspended.
7. Repeat the process until there is enough seeds for all your experiments.

Crystallisation Experiments

1. Pour between 15-20mL of the 0.5M Magnesium Chloride stock solution and 0.5M Ammonium Dihydrogen Phosphate stock solution into beakers to pipette from.
2. Rinse the 10mL volumetric pipettes with a small volume of stock solution, once rinsed pipette 10mL of the stock solutions from the beaker into the 1L volumetric flask.
3. Fill the 1L volumetric flask to the mark with distilled water and then transfer to the crystalliser.
4. Calibrate the pH probe, if the probe and meter do not have ATC capabilities then manually adjust the temperature in the pH meter, if the pH meter does not have a temperature setting then record the temperature so you can convert the pH reading later with the Nernst Equation.
5. Place the pH probe in the crystalliser and begin mixing the solution. The degree of stirring should be sufficient to constantly disturb the free surface of the solution. Record the setting of the magnetic stirrer as the hydrodynamics must be constant in all experiments.
6. If the pH meter has data logging capability begin logging pH data.

7. Pour between 15-20mL of the 0.5M Sodium Hydroxide stock solution into a beaker to pipette from.
8. Rinse the 10mL graduated pipette with a small volume of stock solution, once rinsed, pipette the desired concentration of Sodium Hydroxide into the reactor. There are three volumes of Sodium Hydroxide that can be added for these experiments; 10mL for stockpiling solid struvite, 9mL for the SI = 0.5 experiments and 8.5mL for the SI = 0.4 experiments.
9. Add 10mL of the seed solution to the crystalliser.
10. Take samples and perform PSD analysis, see the sampling and analysis section for details.
11. Filter the struvite to be kept for making saturated electrolyte.
12. Fill the crystalliser with tap water and 20-30mL of 1M HCl and place the pH probe in the solution to dissolve any residual struvite.
13. Repeat the process for the desired number of experiments.

NOTE: The pH probe only needs to be calibrated daily; if you are performing multiple experiments in one day then you do not need to calibrate it for every experiment. Fresh stock solutions should be used for every experiment, if the solutions are left open to the atmosphere evaporation will change the concentration enough to reduce the repeatability of the pH response.

Sampling and Analysis

1. Turn on the coulter counter and get it ready for measurements (read the instruction manual thoroughly before doing any analysis).
2. The coulter counter must be calibrated for the ISOTON 2 saturated with struvite; this only has to be done once but is very important. If you are using recycled electrolyte the coulter counter must be validated as the recycled electrolyte can have slightly different properties. If you are using fresh electrolyte validation is not required.

3. Set the coulter counter to perform three runs for each sample,
4. Pour 140mL of electrolyte into the 250mL beaker.
5. Place the 30mL sampling beaker into the crystalliser so it is full.
6. Plunge the volumetric flask stopper into the beaker to displace a constant volume of liquid. You will need to determine the volume of liquid left in the beaker; repeat the filling and plunging sampling method with tap water 10-20 times to determine your sample volume, at SUT my sample volume was 29 ± 0.5 mL.
7. Pour the sample into the 250mL beaker containing the 140mL of electrolyte.
8. Analyse the sample.
9. Repeat this procedure until the experiment is over

There are two experiments that the sampling and analysis happens for; $SI = 0.5$ and $SI = 0.4$. The sampling times for the two experiments are shown below in Table 1.

Table 1: Sampling times for the two experimental conditions

SI = 0.4	SI = 0.5
0 minutes	0 minutes
3 minutes	3 minutes
10 minutes	6 minutes
20 minutes	10 minutes
35 minutes	15 minutes
60 minutes	
120 minutes	

The sampling and analysis procedure should take 3 minutes if everything goes well. If the samples cannot be taken at these specific times then record the time at which it was taken and perform the analysis, these results will still be useful. There will be issues with aperture blockage during the $SI = 0.5$ experiment, if this happens click the “unblock aperture” icon and try again. Two runs for one sample will suffice if the aperture blockage is preventing you from getting three complete runs. If you cannot get two complete runs due to aperture blockage then this is the end of the experiment, stop the current experiment and try again.